In Pursuit of Alternatives to Poly(ethylene glycol) as Protein-Repellent but Cell-Adhesive Surface Coatings for Biomaterials

Dissertation

zur Erlangung des Doktorgrades
der Naturwissenschaften (Dr. rer. nat.)
der Fakultät für Chemie und Pharmazie
der Universität Regensburg

vorgelegt von
Jutta Lehnfeld
aus Burglengenfeld
2021

Die Arbeit wurde angeleitet von:	Apl. Prof. Dr. Rainer Müller
Promotionsgesuch eingereicht am:	26. März 2021
Kolloquiumstermin:	21. Juni 2021
Prüfungsausschuss:	Apl. Prof. Dr. Rainer Müller
	Prof. Dr. Hubert Motschmann
	Prof. Dr. Joachim Wegener
Vorsitzende:	Apl. Prof. Dr. Miriam Breunig

Science is a quest for understanding.
— Jocelyn Bell Burnell

Preface and Acknowledgement

This PhD thesis was carried out at the Department of Physical and Theoretical Chemistry at the University of Regensburg under the supervision of Apl. Prof. Dr. Rainer Müller. The practical work was performed between November 2016 and September 2020 at the aforementioned department, except for the following measurements. The summarized presentation of physicochemical characteristics and quantitative protein adsorption on self-assembled monolayers with varying functional groups also includes data that was obtained at the University of Regensburg but was measured by numerous interns over a period of several years. Significant contributions to the results were made by Michael Überreiter, Jakob Asenbauer, Andreas Eidt and Ulrike Vogl. In addition to that, XPS experiments were conducted at the Physics Department at the University of Regensburg by Dr. Matthias Kronseder. Qualitative protein adsorption was investigated at the Department of Oral Biology at the State University of New York (Buffalo, NY, USA) by various interns under the supervision of Prof. Dr. Stefan Ruhl. Our cooperation partners at the Department of Cell Biology of the Rostock University Medical Center, Martina Grüning and Dr. Susanne Stählke, performed streaming current as well as all cell experiments.

This thesis was made possible by the financial support of two scholarships, the chemistry fond fellowship ("Chemiefonds-Stipendium") of the Chemical Industry Fund ("Fonds der Chemischen Industrie" (FCI)) as well as the scholarship ("Promotionsaschluss-Stipendium") of the Bavarian State Ministry of Science and the Arts within the Bavarian program for the advancement of women in science ("Bayerisches Programm zur Realisierung der Chancengleichheit für Frauen in Forschung und Lehre").

This PhD thesis could not have been accomplished without the support, encouragement and aid of the following people and institutions I would like to thank in the following:

First and foremost, I want to thank my supervisor Apl. Prof. Dr. Rainer Müller, who offered me this highly fascinating research topic at the boundary between organic chemistry, physical chemistry, biology and medicine. It was an enriching experience to gain insight into many different fields of research and institutions. I am very thankful for his advice and profound knowledge, which guided me in the process of my thesis.

Likewise, I want to express my gratitude to Prof. Dr. Werner Kunz and Prof. Dr. Richard Buchner for providing me the provinces and instrumentation which were necessary for accomplishing this work.

Furthermore, I owe my gratitude to Dr. Matthias Kronseder, Martina Grüning and Dr. Susanne Stählke for performing numerous measurements as well as for the interesting and fruitful discussions.

My special thanks go to the various interns who did their internship, bachelor thesis or teacher's thesis under my supervision. Thank you Jonas Blahnik, Dominik Dollinger, Alina Scheklaukov, Verena Huber, Florian Kerkel, Andreas Jungwirth, Fiona Kappaun and Friederike Reinhoff for contributing to the research! Additionally, I want to acknowledge the efforts of previous interns, Michael Überreiter, Jakob Asenbauer and Ulrike Vogl, whose results helped complete this thesis. At this point, I also would like to thank Gudrun Deigele for her excellent technical assistance as well as many diverting conversations.

A big thank you goes to my colleagues at the Institute of Physical and Theoretical Chemistry, both for providing a helping hand if necessary as well as for the numerous chats, conversations and get-togethers, which made the days at the university more enjoyable. Besides, I would like to thank Franz and Felix for their thorough proof-reading.

Last but not least, I want to sincerely thank my family, friends and – most of all – my partner Franz for their unconditional love and support. This work would not have been possible without their confidence and encouragement. Thank you!

Abstract

Biomaterials are indispensable in health care. They are used in a plethora of applications, whenever the function of an organ or tissue needs to be supported, restored or replaced temporarily or permanently. The fate of any device interacting with the human body strongly depends on the amount and composition of the initially adsorbed protein layer. It governs, for instance, bacterial adhesion, potentially leading to a bacterial infection, and tissue cell attachment, allowing for successful tissue integration of an implant.

As protein adsorption is the first step in a cascade of interactions between biomaterials and living organisms, it is crucial to further understand how it is influenced by the biomaterial surface. Thus, this PhD thesis focuses on the investigation of surface properties and their effect on biological systems, pursuing two goals: Firstly, the research was aimed at developing a deeper understanding how protein adsorption is related to macroscopically determined surface characteristics. In addition to that, it was sought to develop novel surface modifications, which ideally combine protein-repellent with cell-adhesive properties for later application in dental or orthopedic implants. To this purpose, a large variety of surface modifications has been developed or synthesized according to previously published procedures. Immobilization of functionalizations was performed on a variety of appropriate model systems using silane chemistry.

The research of this thesis will be divided into four parts, all sharing a similar structure. At first, the successful synthesis of the respective surface coatings was confirmed via X-ray photoelectron spectroscopy (XPS), infrared (IR) spectroscopy and water contact angle measurements. In addition to that, fundamental physicochemical properties of the surface modifications were characterized: The surface free energy (SFE) and dynamic wetting behavior were analyzed via static contact angle measurements or tensiometry respectively. The zeta potential of the surface functionalizations was derived from electrophoresis or streaming current measurements. Furthermore, the interaction of those surface modifications with biological systems was investigated, including the quantitative or qualitative analysis of protein adsorption or the study of initial cell adhesion.

In the first chapter, protein adsorption was investigated on a variety of self-assembled monolayers (SAMs) with different terminal functional groups. Covering a broad range of surface wettabilities, SFEs and zeta potentials, the surfaces' properties were shown to

substantially influence qualitative and quantitative protein adsorption from the biofluids human saliva and human serum. Whereas some single proteins, most prominently lysozyme, clearly followed basic physicochemical rules in their adsorption behavior, no such dependence could be observed for the majority of proteins. The amounts and compositions of the adsorbed protein layers were clearly shaped by the characteristics of the surface, but no simple relations between surface properties and protein adsorption could be revealed.

The second chapter focuses on a group of surface modifications, which are related to the chemistry of the poly(amido amine) (PAMAM) dendrimer. Those six surface coatings all possessed terminal and inner amine groups, but they differed with respect to the presence or absence of inner amide groups and with respect to their structure, being either short-chained oligomers, linear polymers or dendrimers. These functionalizations all exhibited a moderately hydrophilic behavior, but they differed significantly in their electrokinetic behavior due to large differences in their amine group density. Protein adsorption from single protein solutions as well as from human saliva and fetal bovine serum (FBS) was found to be strongly governed by the zeta potential. Both linear polymers, characterized by their flexibility and hydrophilicity, exhibited protein-repellent behavior.

In addition to the PAMAM-derived coatings, further surface modifications with osmolyte motifs were developed, inspired by their unique protein-stabilizing function in nature. Immobilization of sulfobetaine or amine oxide groups led to hydrophilic surface coatings with negative zeta potentials under physiological conditions. The amine oxide modification, based on the osmolyte trimethylamine N-oxide (TMAO), exhibited excellent protein-repellency. A surface modification with terminal proline groups could not be performed completely successful, but some preliminary results were obtained.

In the last chapter, three amine-based modifications, representing the three different structural motifs, were immobilized on titanium substrates for cell experiments, analyzing the behavior, i.e. spreading, morphology, actin cytoskeleton and cell cycle, of osteoblastic MG-63 cells up to 24 h. In general, large differences in cell behavior were observed after 1 h of cultivation, which almost vanished after 24 h of cultivation. A drastically increased initial cell spreading was observed on the dendrimer coating, which was characterized by a large density of surface amine groups and a strongly positive zeta potential under physiological conditions. The linear polymer did not have a negative effect on the cell behavior despite its previously shown protein-repellency.

Contents

I Introduction **1**

II Fundamentals **7**

1 Biomaterial (Surfaces) – State of the Art **8**
1.1 Materials for Biomaterial Applications 9
1.2 Biomaterials in the Human Body 10

2 Self-Assembled Monolayers (SAMs) **12**
2.1 The Silane Molecule 12
2.2 Monolayer Formation 13
2.3 Stability 14
2.4 Surface Functionalities and Applications 15

3 Motifs of the Surface Modifications **17**
3.1 Dendrimers 17
3.1.1 Fundamental Information 17
3.1.2 Dendrimer Synthesis 18
3.1.3 Variety of Dendrimers 20
3.1.4 Properties 21
3.1.5 Examples of Dendrimer Application 25
3.2 Polymers 25
3.2.1 Poly(amido amine) Polymers 25
3.2.2 Poly(ethylene imine) Polymers 29
3.2.3 Polymers at Surfaces 31
3.3 Osmolytes 33
3.3.1 Fundamental Information 33
3.3.2 Properties of Osmolytes 34
3.3.3 Characteristics of Osmolyte Motifs Applied in this Thesis 36
3.3.4 Applications of Osmolytes 37

4 Proteins and Protein Adsorption **39**

4.1 Protein Properties and Stability . . . 39
4.1.1 Protein Folding and Stability . . . 39
4.1.2 Properties of Proteins Selected in this Thesis . . . 40
4.2 Protein Adsorption . . . 41
4.2.1 Protein Adsorption – A Widespread Phenomenon . . . 41
4.2.2 The Complexity of Protein Adsorption . . . 42
4.2.3 Thermodynamic Basics of Protein Adsorption . . . 42
4.2.4 Kinetics of Protein Adsorption . . . 43
4.2.5 Protein Adsorption – Rules of Thumb . . . 44
4.3 Protein-Repellent Surfaces . . . 45
4.3.1 Protein-Repellency – Rules of Thumb . . . 45
4.3.2 Overview over Protein-Repellent Surface Modifications . . . 46

5 Cell Adhesion 48
5.1 Osteoblasts as Models for Cell Experiments . . . 48
5.2 Cell-Surface Interactions . . . 49
5.2.1 Steps of Cell Adhesion . . . 49
5.2.2 Cell Adhesion via Specific Interactions . . . 50
5.2.3 Influence of Surface Properties on Cell-Surface Interactions . . . 51
5.3 Adhesion-Promoting Surfaces – State of the Art . . . 52

6 Surface Properties and their Characterization 54
6.1 Surface Composition – XPS . . . 54
6.2 Detection of Amine Groups – Sulfo-SDTB Assay and Chloranil Test . . 55
6.2.1 The Sulfo-SDTB Assay for Primary and Secondary Amine Groups 55
6.2.2 Qualitative Analysis of Tertiary Amines via the Chloranil Test . 55
6.3 Wettability – Contact Angle and SFE . . . 56
6.3.1 Static and Dynamic Contact Angles . . . 56
6.3.2 Dynamic Contact Angle Measurement . . . 57
6.3.3 Surface Free Energy (SFE) Calculation . . . 59
6.4 Surface Charge – Zeta Potential . . . 60
6.4.1 The Composition of the EDL . . . 61
6.4.2 Techniques for Zeta Potential Determination . . . 62
6.4.3 Electrophoresis . . . 62
6.4.4 Streaming Current Measurement . . . 64
6.4.5 Challenges in Zeta Potential Determination . . . 65
6.5 Quantitative and Qualitative Protein Adsorption . . . 66
6.5.1 Quantitative Protein Adsorption – BCA Assay . . . 66
6.5.2 Analysis of Qualitative Protein Adsorption . . . 66

6.6 Cell Behavior – Microscopic Techniques 70
6.6.1 Confocal Laser Scanning Microscopy 70
6.6.2 Fluorescent Labeling 72

III Experimental 75

7 Substrates and Materials 76
7.1 Substrates 76
7.1.1 Wafers 76
7.1.2 Silica Particles 76
7.2 Solvents and Reagents 77

8 Synthesis of the Poly(amido amine) Polymer 78

9 Synthesis of the Surface Modifications 79
9.1 Substrate Handling 79
9.1.1 General Remarks 79
9.1.2 Handling of Wafer Specimens 79
9.1.3 Handling of Particle Substrates 81
9.2 Substrate Oxidation 81
9.3 Immobilization of Self-Assembled Monolayers 82
9.3.1 SAM-CH_3 – Alkane Monolayer 83
9.3.2 SAM-CF_3 – Perfluorocarbon Monolayer 83
9.3.3 SAM-COOH – Monolayer with Carboxylic Acid Groups 84
9.3.4 SAM-Py – Monolayer with Pyridinium Groups 85
9.3.5 SAM-NH_2 – Monolayer with Primary Amine Groups 85
9.3.6 SAM-SO_3H – Monolayer with Sulfonic Acid Groups 87
9.3.7 SAM-PEG – Monolayer with Five Ethylene Glycol Units 87
9.3.8 TESPSA – Monolayer with Succinic Acid Anhydride Groups . . 88
9.3.9 SAM-NMe_2 – Monolayer with Tertiary Amine Groups 89
9.4 Synthesis of Oligomeric or Polymeric Amine-Terminated Surface Coatings 90
9.4.1 Immobilization of APD and PPI Dendrimers 90
9.4.2 Modification with the Linear PAMAM or PEI Polymer 91
9.4.3 Modification with the Amido Amine (AMAM) Oligomer 93
9.5 Synthesis of Osmolyte-Based Surface Modifications 94
9.5.1 Synthesis of a Sulfobetaine Surface Coating (DMAPS) 94
9.5.2 Formation of an Amine Oxide Monolayer (SAM-NO) 95
9.5.3 Immobilization of Proline 96

10 Analysis of Physicochemical Properties **97**
10.1 IR Spectroscopy . . . 97
10.2 X-Ray Photoelectron Spectroscopy (XPS) . . . 97
10.3 Sulfo-SDTB Assay . . . 97
10.4 Chloranil Test . . . 98
10.5 Static Contact Angle Measurements and SFE Calculation . . . 98
10.6 Measurement of Dynamic Contact Angles . . . 99
10.7 Electrokinetic Measurements . . . 99

11 Analysis of the Interaction of the Modifications with Proteins and Cells **101**
11.1 Testing Protein Adsorption . . . 101
11.1.1 Preparation of Protein Solutions . . . 101
11.1.2 Protein Quantification on Silica Beads . . . 102
11.1.3 Adsorption, Elution and Quantification of Proteins . . . 103
11.1.4 Qualitative Protein Adsorption . . . 104
11.2 Investigation of Cell Behavior . . . 107
11.2.1 Cell Cultivation and Sample Preparation . . . 107
11.2.2 Examination of Cell Morphology and Cell Spreading . . . 107
11.2.3 Analysis of the Actin Cytoskeleton . . . 108
11.2.4 Cell Cycle Analysis, Proliferation and Apoptosis . . . 108

12 Statistics **109**

IV Results and Discussion **111**

13 SAMs with Varying Terminal Functional Groups **115**
13.1 Verification of Successful Surface Coating . . . 116
13.1.1 Determination of the Chemical Composition via XPS . . . 116
13.1.2 Evaluation of IR Spectra . . . 117
13.2 Analysis of Physicochemical Properties . . . 119
13.2.1 Wettability and SFE . . . 119
13.2.2 Zeta Potential . . . 123
13.3 Quantitative and Qualitative Protein Adsorption . . . 126
13.3.1 Quantitative Protein Adsorption . . . 126
13.3.2 Qualitative Protein Adsorption . . . 137

14 Oligomeric and Polymeric Amine Group-Terminating Modifications **151**
14.1 Analysis of the PAMAM Polymer . . . 152

14.2 Verification of Successful Surface Coating . . . 155
14.2.1 Determination of the Chemical Composition via XPS . . . 155
14.2.2 Density of Amine Groups . . . 156
14.2.3 Analysis of IR Spectra . . . 158
14.3 Analysis of Physicochemical Properties . . . 160
14.3.1 Wettability and SFE . . . 160
14.3.2 Dynamic Contact Angles . . . 162
14.3.3 Zeta Potential . . . 168
14.4 Investigation of Protein Adsorption . . . 173
14.4.1 Overview . . . 173
14.4.2 Dependence of Protein Adsorption on Surface Properties . . . 175

15 Osmolyte-Based Functionalizations 182
15.1 Proline Immobilization – Considerations and Challenges . . . 183
15.2 Verification of Successful Surface Coating . . . 185
15.2.1 Determination of the Chemical Composition via XPS . . . 185
15.2.2 Analysis of Surface Amine Groups . . . 186
15.2.3 Analysis of IR Spectra . . . 187
15.3 Investigation of Physicochemical Properties . . . 189
15.3.1 Wettability and SFE . . . 189
15.3.2 Dynamic Wetting Behavior . . . 191
15.3.3 Zeta Potential . . . 194
15.4 Analysis of Protein Adsorption . . . 198

16 Results from Cell Experiments 202
16.1 Evaluation of Physicochemical Properties . . . 202
16.1.1 Verification of Successful Surface Modification via XPS . . . 202
16.1.2 Characterization of Wettability and SFE . . . 203
16.1.3 Zeta Potential of Functionalized Titanium Surfaces . . . 206
16.2 Analysis of Cell Biological Experiments . . . 209
16.2.1 Cell Spreading . . . 209
16.2.2 Cell Morphology . . . 210
16.2.3 The Actin Cytoskeleton . . . 212
16.2.4 Cell Cycle, Proliferation and Apoptosis . . . 213
16.2.5 Dependence of Cell Behavior on Surface Properties . . . 215

V Conclusion and Outlook **223**

VI Appendix **229**

Protein Adsorption on SAMs 230
Tensiometric Measurements 232
Protein Adsorption on Amine and Osmolyte Coatings 238
Protein Adsorption of HSA and Lysozyme 238
Dependence of Protein Adsorption on SFE 240
Cell Experiments 242
List of Abbreviations 250
List of Figures 253
List of Tables 265
Bibliography 268
List of Publications 301
Declaration/Eidesstattliche Erklärung 303

Part I

Introduction

Loss of function of a patient's tissue or organ may have many reasons because it can be the consequence of a trauma or injury, causing tissue damage, or the result of resection, for example of a tumor. In many cases, especially with respect to musculoskeletal joints, progressing wear may reduce the functionality of the joint with increasing age of the patient [1]. Biomaterials can often provide remedy as they allow the permanent replacement of the lost function or support the tissue temporarily, assisting in healing and function restoration [1, 2]. Hence, in the past decades, a plethora of different biomaterials for transient and permanent applications in differing tissues has been developed, such as contact lenses and cochlear implants, wound sutures and urinary catheters, dental implants, joint prostheses and artificial heart valves (see Figure I.1) [1, 2].

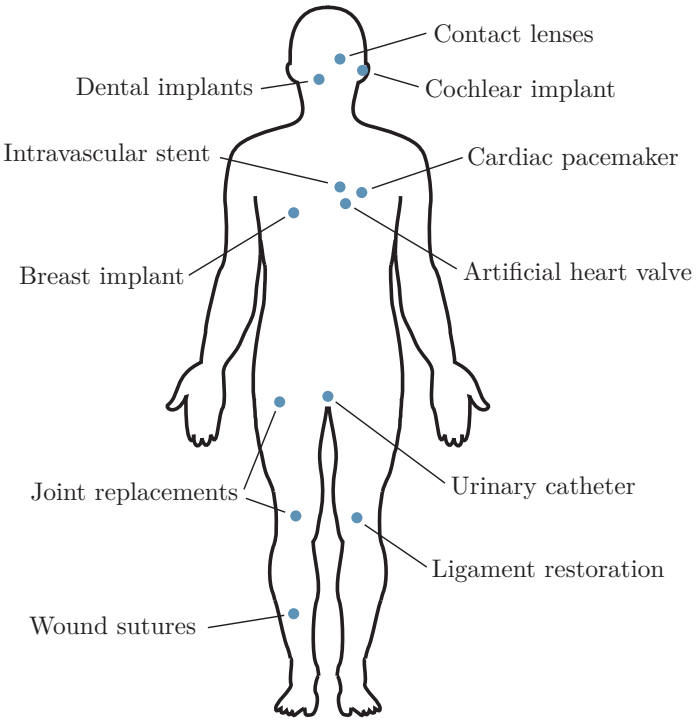

Figure I.1: Examples of the application of various biomaterials in the human body [1–3].

These materials, however, have usually been chosen according to their bulk properties, which are supposed to match the characteristics of the replaced tissue and allow optimal performance of the biomaterial. For contact lenses, for instance, poly(2-hydroxyethyl methacrylate) (pHEMA) is utilized due to its transparency, softness and wettability [4]. In joint replacements, titanium is the material of choice due to its excellent load-bearing properties and its corrosion resistance [5]. The polymer polyethylene terephthalate (PET) is used for ligament reconstruction because of its capability to withstand the mechanical strain [6].

Problems, however, can arise from adverse interactions of the biomaterial surface with its environment. Certain surface properties can, for example, induce hemolysis and trigger blood coagulation [2, 7]. Attachment of bacteria can lead to a bacterial infection and biofilm formation with potentially life-threatening consequences [8, 9]. For implants, which require successful tissue integration, implant rejection and encapsulation severely reduce the biomaterial's functionality [5, 9].
The aforementioned processes are strongly mediated by the initial adsorption of proteins, occurring immediately after biomaterial implantation [9–12]. Therefore, it is crucial to shed light on the influence of the surface properties of a biomaterial on protein adsorption and, by this means, control or direct blood compatibility, bacterial adhesion and tissue integration. This PhD thesis is thus dedicated to the investigation and improvement of the surface properties of titanium-based materials, which can be used as dental implants or parts of joint replacements. In the scope of the thesis, two different objectives were pursued. Due to the adverse effects of unspecific protein adsorption, it was investigated if and how it can be related to macroscopically measurable physicochemical surface properties. In addition to that, novel surface modifications were engineered, which were aimed at combining protein-repellency with enhanced cell adhesion and improved tissue integration.

To that purpose, surface modifications were prepared on substrates of varying geometry, allowing for different analysis techniques. In addition to titanium, silicon and silica-based materials were used as model substrates. Starting from initial functionalization via silane chemistry, different surface modifications were immobilized, which can be divided into three groups (see Figure I.2).
The first group consists of self-assembled monolayers (SAMs) with different functional end groups, which cover a broad range of wettabilities, surface free energies and zeta potentials. The second was inspired by the poly(amido amine) (PAMAM) dendrimer, which has been extensively studied at the work group by Verena Katzur [13] and Andreas Schneider. This family of amine-based surface modifications, studied in this thesis, also exhibits terminal as well as inner amine groups and some of them also inner amide groups, comparable to the PAMAM dendrimer. They, however, possess different structures and were immobilized as short-chained oligomers, linear polymers and dendrimers. In the third group, the structural motifs were derived from osmolytes, namely taurine, trimethylamine N-oxide (TMAO) and proline, with the aim of developing non-fouling surface coatings via increasing protein stability near the surface [14].

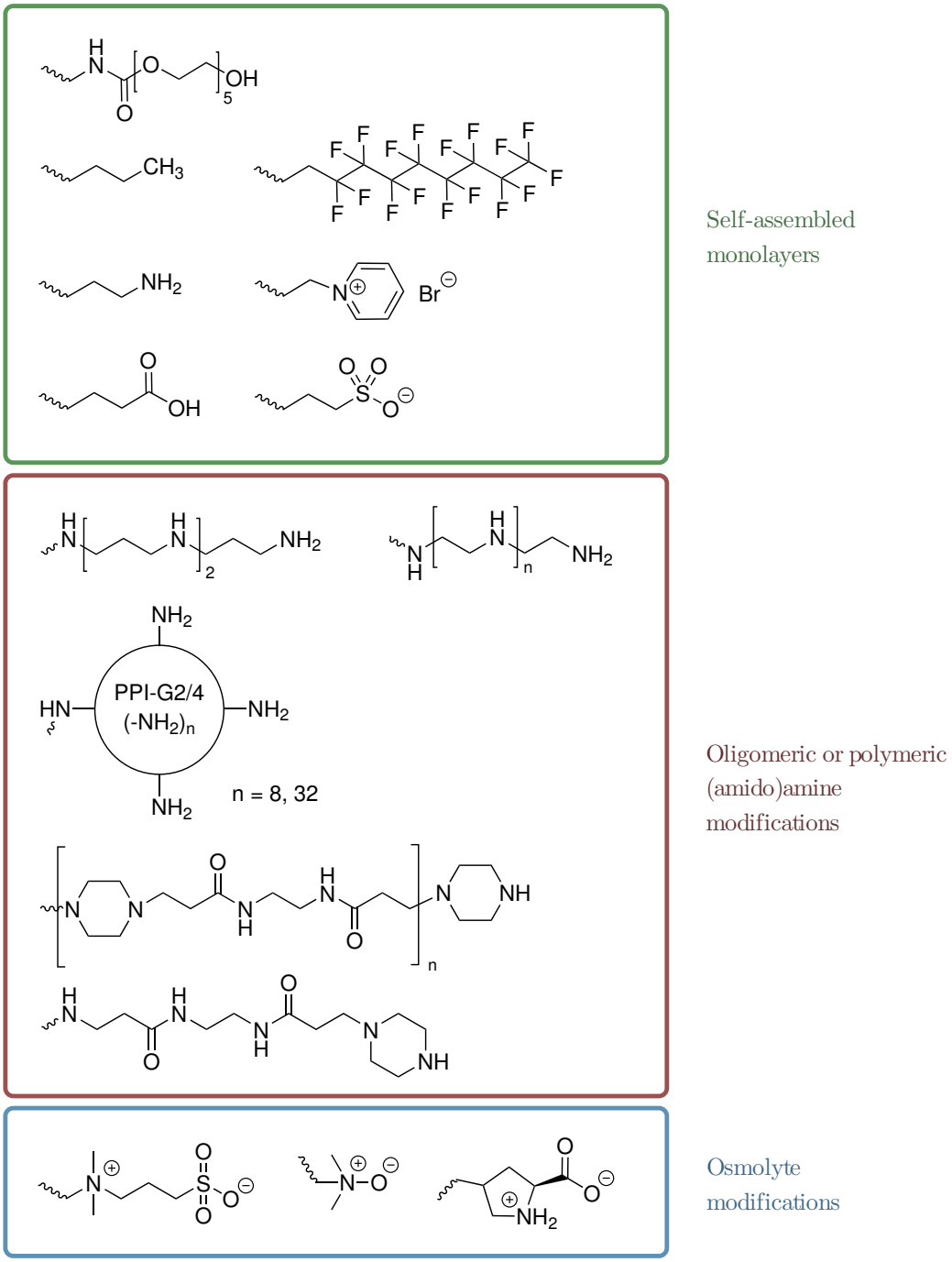

Figure I.2: Overview of the structural motifs of the self-assembled monolayers with varying terminal functional groups, oligomeric or polymeric (amido)amine-based modifications (bearing inner secondary or tertiary amines as well as partially amide groups in combination with terminal primary or secondary amine groups) and the osmolyte modifications (based on taurine, TMAO and proline).

This small library of surface coatings was thoroughly analyzed in order to test for synthesis success as well as to characterize main physicochemical properties. In addition to X-ray photoelectron spectroscopy (XPS), infrared (IR) spectroscopy as well as an amine group-quantifying assay (sulfo-SDTB assay, only on coatings with amine groups), the wetting and electrokinetic properties of the coatings were assessed with contact angle or zeta potential measurements respectively. The (non)-fouling behavior was tested via protein adsorption experiments with the physiological fluids human saliva, fetal bovine serum (FBS) and human serum. For the group of SAMs with varying end groups, quantitative protein adsorption was analyzed with the bicinchoninic acid (BCA) assay, whereas the qualitative composition of the adsorbed protein layers was assessed via sodium dodecyl sulfate polyacrylamide gel electrophoresis (SDS-PAGE) and western blot. For the amine and osmolyte-derived surface coatings, quantitative protein adsorption was tested both from single model proteins (human serum albumin (HSA) and lysozyme) as well as with complex physiological fluids (whole human saliva and FBS). Cell adhesion and proliferation of osteoblast-like cells was studied on selected amine-based surface modifications.

The PhD thesis was performed at the Institute of Physical and Theoretical Chemistry at the University of Regensburg. Here, the surface modifications as well as most of the physicochemical analyses were carried out. The first group of surface modifications, the self-assembled monolayers, was studied over a broad range of time, including the work of various interns as well as of Verena Katzur. Thus, partial results have been published before [13, 15–21]. The various physicochemical properties, published and unpublished, were still summarized in this work in order to discuss their influence on qualitative protein adsorption. These measurements (SDS-PAGE and western blot) were performed at the Department of Oral Biology at the State University of New York at Buffalo (Buffalo, NY, USA) by various interns under the supervision of Prof. Dr. Stefan Ruhl. In contrast to that, amine and osmolyte-based surface modifications were synthesized and analyzed in the scope of this PhD thesis. Here, also some results for the amine modifications are included that were obtained in the preceding master's thesis [22]. In cooperation with other researchers, X-ray photoelectron spectra were recorded at the Physics Department of the University of Regensburg by Dr. Matthias Kronseder and the streaming current experiments were measured by Martina Grüning or Dr. Susanne Stähnke at the Department of Cell Biology at the Rostock University Medical Center (Rostock, Germany). Quantification of the protein adsorption was performed at the University of Regensburg (SAMs, amine and osmolyte modifications) and the Department of Oral Biology in Buffalo (only SAMs), whereas the cell studies were carried out by Dr. Susanne Stähnke (Rostock University Medical Center, Rostock, Germany).

Part II

Fundamentals

1 Biomaterial (Surfaces) – State of the Art

In the following section, a short introduction to biomaterials, their properties, applications, but also drawbacks will be given to provide for the further introduction to surface modification and analysis.
A general definition of biomaterials was released by the NIH Consensus Development Conference on the Clinical Applications of Biomaterials 1982, defining the term as [23]

"any substance, other than a drug, or combination of substances, synthetic or natural in origin, which can be used for any period of time, as a whole or as a part of a system which treats, augments, or replaces any tissue, organ or function of the body."

In other words, biomaterials are used to fabricate medical devices, disposables and implants, which are applied, for example, in medicine, dentistry, surgery and healthcare and are meant to reliably fulfill their function without intolerable side effects [2, 24]. In order to do so, biomaterials have to meet a variety of requirements.
Although the demands vary strongly, depending on the intended purpose of the material, some general requirements are usually summarized as "biocompatibility" [3, 15, 23]. In the past, this term has mainly been defined for implants and summarized the requirements for biological safety in a list of "no-conditions" [3, 15, 23]. In this original definition, material inertia was desired. Biomaterials were supposed to be, for example, non-toxic, non-thrombogenic, non-carcinogenic and non-allergenic [3, 23]. This insufficient definition, however, has been extended. Biomaterials are now intended to exhibit biofunctionality and elicit an appropriate host response in the respective application situation [3, 15]. This very general concept has been described more precisely for long-term implants by Williams [3] as

"the ability of the device to perform its intended function, with the desired degree of incorporation in the host, without eliciting any undesirable local or systemic effects in that host."

In this context, the success of an implant depends on a large variety of parameters, among them the biocompatibility of the biomaterial, which itself is governed by its bulk and surface properties, but also the health status of the patient, the expertise of the surgeon as well as the absence or presence of microorganisms [2, 3].

1.1 Materials for Biomaterial Applications

In line with the large variety of applications (see Part I Introduction), a plethora of materials is applied in biomaterial science, which are usually selected according to their bulk properties. They can be divided into four major groups, which are summarized in Table 1.1 [2]:

Table 1.1: Summary of the major classes of biomaterials, examples and applications [2].

Material class	Examples	Applications
Metals	Stainless steel, Co-Cr alloys, Ti (alloys)	Joint replacements, bone plates/screws, dental root implants
Polymers	Nylon, polyester, silicone rubber, polyacrylates	Contact lenses, hip socket, sutures
Ceramics	Calcium phosphates, alumina zirconia	Orthopedic and dental implants
Composites	Wire- or fiber-reinforced bone cement	Dental resin, bone cement

Among these materials, titanium and its alloys will be presented in more detail as this PhD thesis was dedicated to the functionalization of titanium-based biomaterials. Titanium itself as well as the alloy Ti6Al4V are currently the off-the-shelf materials for orthopedic and dental applications, such as joint replacements, spinal fixation devices, dental implants, crowns and bridges [5]. These materials are broadly applied for load-bearing applications because they possess mechanical properties which are closest to those of bone tissue among the group of metallic materials [5]. In addition to that, titanium and its alloys are characterized by their corrosion-resistance and their biocompatibility [5]. The latter two properties are the consequence of the passivation of titanium via spontaneous formation of a thin (roughly 8 nm), strongly adhering oxide (TiO_2) layer [25, 26]. Usually good osseointegration is observed for those materials, i.e. the bone and the implant surface exhibit functional and structural interaction, but this process can also fail, leading to implant rejection and fibrous tissue encapsulation [5, 25]. The oxide surface, which is negatively charged under physiological conditions, can also be problematic in blood-contacting applications due to its ability to initiate blood coagulation [27]. In order to minimize those negative effects of titanium-based implants, their surfaces are usually modified [5].

1.2 Biomaterials in the Human Body

In order to evaluate to which purpose and how the surfaces of biomaterials can be functionalized, one must shortly consider how the surface of an implant interacts with its environment. The description in the following will mostly be directed to implants in contact with bone.
The implantation of a biomaterial in the human body is followed by the rapid adsorption of proteins. The amount, composition and structure of this protein layer then govern all further processes [7, 8, 10, 28]. Among those are the interaction with the immune system and with the human blood, which can possibly lead to adverse effects, such as thrombus formation [5, 7, 8].

The most important aspect of biomaterial-host interactions of implant materials is probably the "race for the surface", i.e. the competition between bacteria and tissue cells for surface space [9]. If the adhesion of tissue cells is successful, that is the tissue cells "win the race", the implant can be integrated into the surrounding tissue, e.g. the bone, and is "defended" against the bacteria. The colonization of the biomaterial surface with bacteria, however, can lead to a biomaterial-centered infection [1, 9]. Bacteria adhering to a surface usually secret exopolymers and thus develop a biofilm, then being less targetable by antibiotics and the immune system of the host [8]. Those microbial infections are very often chronic or recurring, often requiring implant replacement and increasing patient mortality [1, 8]. The mechanism of protein adsorption as well as cell adhesion have been part of this thesis and will thus be presented in more detail in the sections 4 and 5. The interaction of biomaterial surfaces with bacteria was not the topic of this thesis and will therefore not be examined further. Comprehensive summaries of those processes can be found in literature (for example [1, 8, 9]).

In order to obtain the desired interaction between the biomaterial and the host, modification of the material surface is often required. Here, the purpose of the biomaterial also determines the target surface properties [1]. Temporary devices, such as urinary catheters or contact lenses, are designed to be non-adhesive and withstand bacterial infection [1]. In contrast to that, permanent implants are tailored to support the adhesion of tissue cells, both to prevent the colonization of bacteria as well as to ensure proper tissue integration [1]. With respect to titanium-based implant materials for dental and orthopedic applications, surface coatings are supposed to direct protein adsorption, resist bacterial adhesion and promote bone cell adhesion and osseointegration [5, 9, 29].

A huge variety of methods has been developed and tested for titanium-based implants, such as physical treatments, modifying surface roughness [30], inorganic coatings (calcium phosphate or bioactive glass) [5] or organic coatings, such as modification with proteins (e.g. extracellular matrix proteins) [25] or synthetic polymers [31]. Fundamental information about the modifications used in this thesis, i.e. the initial silanization of the substrates as well as the molecules used for surface functionalization, will thus now be presented in the following.

2 Self-Assembled Monolayers (SAMs)

As this thesis is based on the synthesis of surface coatings via initial formation of self-assembled monolayers, the following section is dedicated to a summary of fundamental information about silane self-assembled monolayers. The following pages present an overview over their history, silane and monolayer synthesis as well as their properties with respect to stability and functionality, closing with a survey of some applications. Generally speaking, a self-assembled monolayer is a very thin, two-dimensional, highly ordered assembly, spontaneously formed on surfaces via chemisorption and completely determining the surface properties [32–34]. This behavior was first observed by the work group of Zisman, who discovered and investigated the formation of oleophobic films via adsorption of mainly long-chained alcohols on metal substrates [35]. Only very little research, however, was conducted until 1980, when the first organosilane monolayers were synthesized. Soon after, the term self-assembled monolayer (SAM) was proposed for the first time [32, 36]. Since then, a huge variety of monolayer types has been investigated. Among the less prevalent ones are, for example, the assembly of fatty acids on metals, alkyl chains on silicon or organophosphonates on silicon or titanium. The most important types, however, are SAMs of organosulfur compounds on metals (mainly alkanethiols on gold) and organosilane monolayers on hydroxylated surfaces, as applied in this thesis [33, 37].

2.1 The Silane Molecule

The silane molecules themselves comprise three different parts and can be described with a generalized formula of $X_3Si\text{-}(CH_2)_n\text{-}R$. The head group consists of a silicon atom that is connected to three leaving groups X (chloride -Cl, methoxy $-OCH_3$ or ethoxy $-OCH_2CH_3$). This group is responsible for the anchoring of the silane molecule on the substrate via formation of a chemical bond. The backbone connects the head group with the terminal group R and usually consists of an alkane chain ($-(CH_2)_n-$). Van der Waals interactions between neighboring silane molecules provide stability and promote the formation of an ordered SAM. The terminal group (surface group) R introduces functionality and thus determines the properties of the monolayer and the surface [37–39].
In order to prepare trichlorosilanes, mainly three synthesis routes have been developed in the past, which are depicted in Figure 2.1.

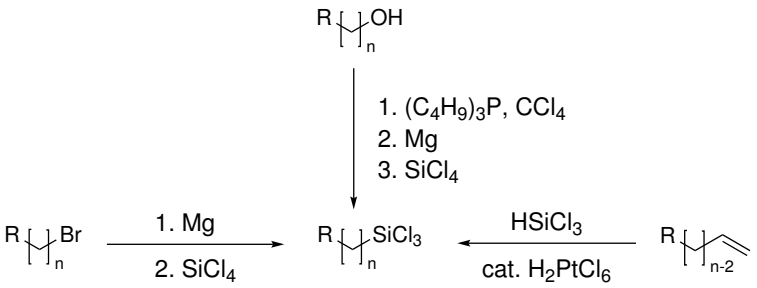

Figure 2.1: Schematic illustration of the synthesis of trichlorosilanes, as described in literature [40–42].

Netzer et al. described the first synthetic route for the preparation of trichlorosilanes from the corresponding alcohols. The hydroxyl group was at first exchanged by a chloride group that was subsequently activated with Mg and reacted with $SiCl_4$ [42]. Several years later, further synthetic strategies were used. In order to obtain silane molecules with a terminal vinyl group, a bromine substituted precursor was converted into a Grignard reagent and reacted with $SiCl_4$. For other silanes, $HSiCl_3$ was added to the double bond of the precursor in a Pt-catalyzed hydrosilylation reaction [41].

2.2 Monolayer Formation

The formation of monolayers via assembly of silane molecules is a very complex process, which is still under debate in some aspects. In general, SAMs can be formed from solution or vapor on a variety of (hydroxylated) surfaces, such as silicon oxide, quartz, glass, mica, aluminum oxide, titanium, tin-doped indium oxide (ITO), zinc selenide and gold [33, 37, 43]. This immobilization process is influenced by a variety of parameters, such as the presence of water, solvent and temperature, which will not all be discussed here in detail [32, 33]. Water, however, plays a predominant role as no or defective monolayers are obtained in complete absence of water. If the water content is too high, though, polymerization of silane molecules already occurs in solution, leading to the accumulation of polysiloxane on the surface [32, 33]. It has been concluded that traces of water are necessary in order to form well-ordered monolayers. A first explanation for that was given by Sagiv in 1980 [36]. He proposed that an adsorbed water layer on the surface of the hydroxylated substrate is responsible for the hydrolysis of the silane headgroups into reactive silanol groups. These groups subsequently react with surface silanol groups and with neighboring silanol groups via condensation reactions, forming a two-dimensional polysiloxane network [32, 36, 39].

This concept, however, had to be reconsidered after new contradictory results. Finklea et al., for example, were able to obtain monolayers on gold substrate lacking hydroxyl groups and Silberzan et al. showed that coating of substrates with silane SAMs caused

reduced surface roughness. This led to the hypothesis that silane SAMs consist of silane molecules which are mainly connected among each other via siloxane bonds and only possess few linkages to the underlying surface [44, 45].

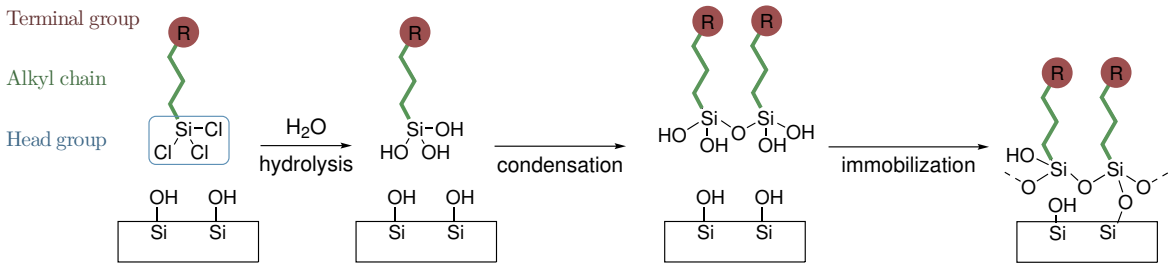

Figure 2.2: Scheme of the formation of a monolayer of silane molecules via self-assembly on a hydroxylated silicon surface, as suggested by Finklea et al. and Silberzan et al. [44, 45]. The silane molecules form a two-dimensional network and are immobilized on the surface via few Si-O-Si linkages [45].

Apart from the water content, other parameters also influence the monolayer formation crucially. Regarding solvent choice, for example, toluene and other aromatic solvents were found to lead to dense monolayers quickly. With respect to the impact of the reaction temperature, a threshold temperature has been identified. Above that temperature, no regular monolayer is assembled because the condensation reaction of silane molecules in solution is favored over the self-assembly at the solid-liquid interface [32, 33].

2.3 Stability

Silane self-assembled monolayers are in general more stable than, for example, thiol monolayers due to their covalent crosslinking [32, 40, 46]. This can especially be observed with respect to the thermal stability as Chandekar et al. showed that higher temperatures were required for the degradation of silane SAMs compared to different thiol SAMs [47]. Here, they could also demonstrate that the stability of a silane SAM depends on the type of the terminal functional group. Amine-terminated surfaces were found to degrade at temperatures 100 °C lower than those required for the degradation of perfluorinated SAMs (350 °C) in air [47]. Bhairamadgi et al. observed that temperatures of 433 °C were necessary to obtain 10% desorption of a octadecyl monolayer under ultrahigh vacuum conditions [46]. Thermal stability was still found to be good under oxidative conditions as no mass loss of octadecyl SAMs was measured for temperatures below 200 °C in air [48]. Regarding different chemical influences, silane SAMs are stable towards organic solvents, water and detergent solution [32]. Both Wasserman et al. and Bhairamadgi et al. observed increased instability under basic conditions, compared to solutions of acidic or neutral pH. A tetradecyl monolayer, for instance, was not damaged by immersion in a 0.1 N hydrochloric acid for at least 40 h, but almost immediate

monolayer degredation was observed with 0.1 N NaOH solution (50% loss in 80 min) due to cleavage of siloxane bonds [41, 46]. Also in this case, SAM stability varied with functionality of the end group as well as with the length of the alkane chain as Wang et al. found 3-aminopropyl SAMs to be significantly less stable towards hydrolysis in saline solution than alkane SAMs or amine SAMs with -$(CH_2)_{11}$- backbone [49].

2.4 Surface Functionalities and Applications

Different chemical functionalities, exposed by a self-assembled monolayer, can either be introduced with the silane molecules or via chemical reactions after SAM formation. In the first case, functionalized silane molecules have to be used. In many cases, though, this is not possible because the terminal group of the silane molecule interferes with the silane head group and the self-assembly process, preventing the formation of an ordered self-assembled monolayer [32, 38]. Especially polar groups, such as carboxylic acid, hydroxyl or amine groups, are incompatible with the silane head group [32, 38, 41]. Alternatively, SAMs with usually non-polar precursor groups are immobilized, which can then be modified via a wide range of chemical reactions. The transfer of a chemical reaction from the solution to a monolayer system, however, is challenging as various requirements have to be met [38, 41, 50].

First of all, the chosen reactions must not damage the underlying siloxane network. Thus, basic conditions, for instance, cannot be applied [41]. In general, functionalizations are ideally performed under mild conditions, i.e. at room temperature and atmospheric pressure [51]. In addition, modification reactions are required to give high yields and ideally quantitative conversion as removal of unconverted groups is not possible [38, 51]. Yet, this is not easily accomplished because reactions are often impeded by the crowded situation at the surface, causing, for example, sterical hindrance, charge repulsion or altered acidities and basicities [38, 43, 50]. At last, no catalysts should be necessary and no by-products, especially solid ones, should be formed. These are hard, sometimes even impossible to remove from the surface, especially because classical workup techniques, e.g. chromatography and distillation, cannot be applied [38, 51]. After immobilization and modification, analysis of the surface coatings poses another challenge as only very small numbers of functional groups in a layer of a few nanometers have to be characterized. Additionally, common analytical tools, such as nuclear magnetic resonance (NMR) spectroscopy or mass spectrometry (MS), are mainly attuned to pure substances or solutions. Thus, different techniques (e.g. contact angle measurements) or adapted methods (in case of e.g. IR spectroscopy) have to be applied and combined [32, 43].

Despite these limitations, a broad scope both of silane functionalities as well as modification reactions is available. The scope of compatible functional groups comprises, apart from alkanes and perfluorinated alkanes, for instance vinyl groups, bromo, sulfanyl and cyanide functionalities as well as epoxy and poly(ethylene glycol) (PEG) moieties [32, 40]. With regard to applicable modification reactions, a short overview will be given, sorting the reactions by type. At first, nucleophilic substitutions are an important tool in surface functionalization, especially starting from bromine-terminated SAMs. The bromine atom can be replaced, e.g. with azides (N_3^-), thiocyanates (SCN^-) or sulfides (S^{2-}), and further modified in oxidation or reduction reactions [32, 38]. Particularly the reduction of azide-terminated surfaces with lithium aluminum hydride ($LiAlH_4$), leading to a monolayer with terminal primary amine groups (-NH_2), is of importance [52]. Furthermore, click reactions meet the majority of the previously stated requirements and are thus often applied on surfaces. This group comprises, for example, Michael addition and Diels-Alder reaction, but the most important one is the Huisgen 1,3-dipolar cycloaddition between an azide and an alkyne, for the first time presented by Lummerstorfer et al. [34, 40, 51]. In addition, oxidations and reductions are often used [32, 40]. The most relevant among them probably is the conversion of terminal vinyl groups into carboxylic acid groups, as already described e.g. by Wasserman et al. in 1989 [41]. Functional groups, such as amine, hydroxyl or carboxylic acid groups, can then again be used for the immobilization of further reagents. Common procedures include esterification, amidation or urethane formation [40, 43].
Several of these reactions have been applied to immobilize macromolecules on surfaces, such as polymers [40], cyclodextrins [38], biomolecules (mainly DNA and proteins) [32], metal complexes [38] and fluorophores [34].
The range of surface modifications can even be extended by the introduction of further spatial structuring, for example via formation of mixed, multifunctional SAMs [32, 40], gradients [34], multilayers [32, 38] and patterning [32, 40].

The versatility of silane self-assembled monolayers, allowing, for example, control over surface properties, such as wettability, as well as their stability have given rise to the development of numerous applications. They have initially been applied as adhesion promoters on glass [32, 53] but are also, for instance, used as lubricants [32], for the study of interfacial phenomena [34], to control the interaction with proteins in non-fouling coatings [37] and to study cell adhesion [38]. Self-assembled monolayers are also investigated in the development of nanometer scale electronics, namely molecular electronics [39]. In addition to that, they have gained significance in sensoring applications, e.g. as fluorescence sensors [32], as part of lab-on-a-chip systems [40] and in biological microarrays, especially DNA chips [43].

3 Motifs of the Surface Modifications

3.1 Dendrimers

In this thesis, the initially assembled monolayers were modified with a variety of molecules, among them poly(propylene imine) (PPI) dendrimers of two different generations. As dendrimers represent a very interesting but rather uncommon type of molecules, a short introduction will be presented in the following. Here, both a general overview, concerning, for example, dendrimer synthesis, types and applications, as well as specific information about PPI dendrimers and their properties will be given.

3.1.1 Fundamental Information

Generally speaking, dendrimers are a class of synthetic macromolecules. They differ strongly from irregularly branched polymers as they are characterized by their highly ordered and regularly branched radial geometry and their monodispersity, which is obtained via a step-wise synthesis of branched segments emanating from a core molecule [54–56]. Their structure, resembling the architecture of tree branches, is also reflected in the name dendrimer, which is composed of the Greek words "dendros" (tree) and "meros" (meaning part).
Dendrimers are a comparably young group of macromolecules. They were first described in 1978 when the group of Vögtle presented an iterative synthesis of a dendritic polyamine structure [57]. An actual dendrimer synthesis including comprehensive analysis was not published until 1985 when Tomalia et al. were able to synthesize poly(amido amine) (PAMAM) dendrimers [58]. The class of dendrimers, however, did not receive much attention before the 1990s. In this decade, a novel synthetic route was described by Fréchet et al. for the preparation of poly(aryl ether) dendrimers [59] and the synthesis of Vögtle was completed by Mühlhaupt and Meijer, leading to PPI dendrimers [60, 61]. Since then, the variety of dendrimer designs and intended applications has increased drastically [55].

Despite their diversity with respect to their chemical motifs, dendrimers share a variety of unique structural and architectural elements, which will be explained in the following (see also Figure 3.1).
At the center of the dendrimer is the core, from which the dendrimer branches originate. The core moiety is rather shielded from the environment (depending on the dendrimer size), leading to the formation of a microenvironment, which can differ strongly from the surrounding medium.

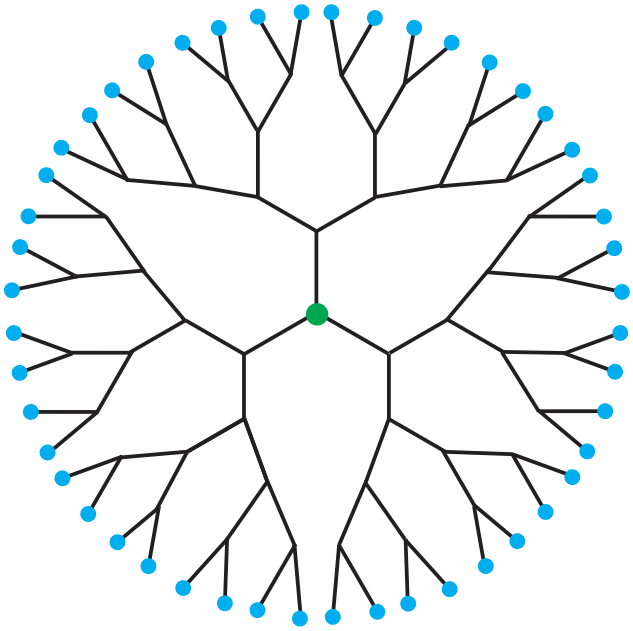

Figure 3.1: Schematic depiction of a dendrimer of generation 4 with a three-branched core.

Connected to the core are the so-called dendrons, the main building blocks of a dendrimer. Their number is equal to the multiplicity of the core structure. The size of the dendrons and thus of the dendrimer as a total is usually defined as the dendrimer generation G. It is given by the number of branching points that can be counted along a branch from the core to the dendrimer surface. Intermediate structures during dendrimer synthesis are often labeled as half-generations (e.g. G2.5), the core itself is labeled as generation zero (G0). The branches of the dendrons comprise the dendrimer shell and connect the core to the terminal groups. These are often also referred to as end or – less accurate – surface groups and their number increases exponentially with dendrimer generation, leading to the formation of a multivalent surface [55, 56, 62].

3.1.2 Dendrimer Synthesis

The unique geometry of dendrimers also requires special synthesis procedures. In general, two different routes can be distinguished, both of which share some characteristics, such as the step-wise construction of the macromolecules by iterative steps (see Figure 3.2) [55].
For the divergent synthesis method, the dendrimer is built up starting from the core moiety generation by generation in a step-wise manner. To that purpose, new branching points are generated by coupling of the monomers to the current end groups, followed by an activation step, which creates new reactive sites for the next coupling step [55, 62].

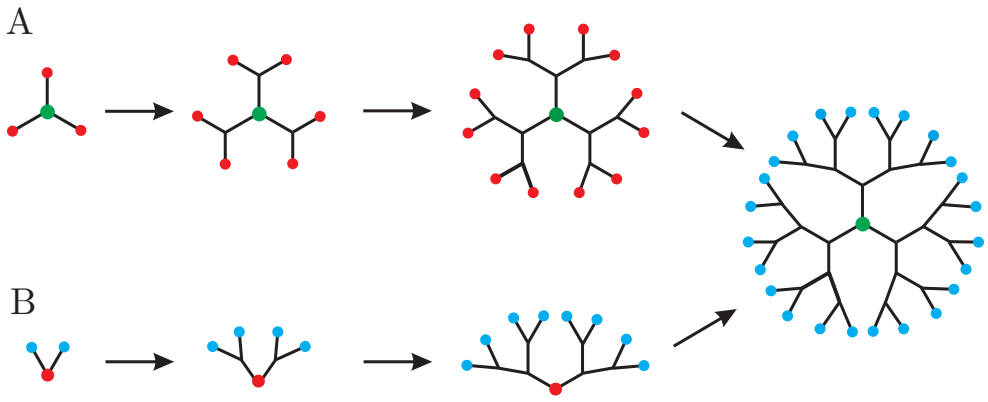

Figure 3.2: Comparison of the dendrimer synthesis via (A) divergent or (B) convergent approach [62]. The terminal functional groups are depicted in blue, reactive sites in red. The core moiety is colored in green.

This reaction procedure is utilized for the most common dendrimer family, the PAMAM dendrimers, as well as for PPI dendrimers (see Figure 3.3), which were used in this thesis [62]. In the latter case, 1,4-diaminobutane (DAB) or ammonia serves as a core molecule, which is alkylated with acrylonitrile in a Michael reaction. After that, the terminal nitrile groups are reduced to primary amine groups via heterogeneously catalyzed hydrogenation, thus being able to react with acrylonitrile in the next coupling step [60, 61].
This reaction method, however, suffers from two major disadvantages. At first, both the dendrimer size as well as the number of terminal groups rise exponentially with dendrimer generation. Thus, complete conversion of the end groups without unwanted side reactions requires high yield reactions and large excesses of reagents, yet still leading to defects in the product. In addition to that, the removal of such flawed products from perfect dendrimers is difficult as well because they only differ marginally in molecular weight as well as physical and chemical properties [55, 62].

These obstacles have been overcome by the introduction of the convergent synthesis route for the formation of poly(aryl ether) dendrimers by Fréchet [59]. In this case, construction of the dendrimer is performed in the opposite direction, beginning at the future terminal groups. These are coupled together in a series of coupling and activation steps, until dendrons of the desired size are obtained, which can be immobilized on a core moiety in the final step [55, 62]. This procedure does not only eliminate the disadvantages of the divergent approach but also increases the versatility of available dendrimers because different types of dendrons can be combined in one dendrimer, or functional but sensitive core molecules can be introduced [55, 62].

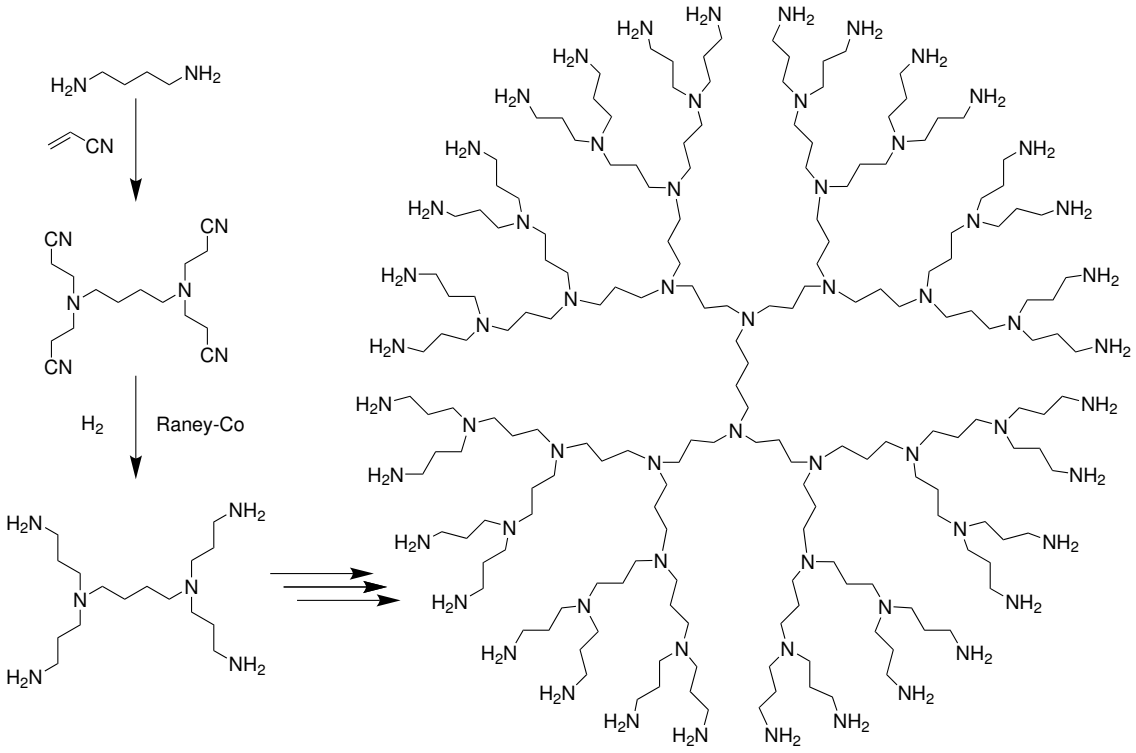

Figure 3.3: Scheme of the synthesis of a PPI dendrimer of generation 1 (PPI-G1) via Michael addition of acrylonitrile, followed by catalyzed hydrogenation [61]. Repeating these reaction steps leads to the formation of a PPI dendrimer of generation 4 (PPI-G4) [62].

Beyond these two methods, other synthesis techniques have emerged as well. Attempts have been made, for example, to construct dendrimers via self-assembly [62] or to create high-generation dendrimers via accelerated approaches, attaching, for instance, convergently grown dendrons to a divergently produced branched core [55].

3.1.3 Variety of Dendrimers

The extensive research on dendrimers in the last three decades also led to the development of a large variety of dendrimers, which cannot be summarized in the scope of this chapter. Yet, a short overview of the classes and types of dendrimers shall be given, more detailed information can be found in literature [54–56, 62–70].
As mentioned previously, the core moieties of dendrimers can be varied. Especially the convergent synthesis route offers the possibility to introduce complex structures, such as fullerenes or porphyrins, and even functional molecules, such as fluorophores, photochemically responsive structures or redox-active cores [55].
Besides that, the building blocks of the dendrimer branches can be derived from organic chemistry and comprise not only poly(amido amine) or poly(propylene imine) units but also poly(aryl alkyne), poly(alkyl ester) or polyphenylene groups as well as hydrocarbon structures [55, 62]. In addition to that, a broad scope of heteroatom-containing

dendrimers [63] or metallodendrimers [67] has been developed as well. Dendrimers can also be derived from biological structures and consist of or contain DNA fragments [62], saccharides [65] or peptides [68].
Further diversity can be obtained by creating dendritic copolymers, which represent a combination of different dendritic structures, for instance via coupling of different dendrons to a core molecule [55]. An enormous range of structures can be obtained via (postsynthetic) modification of the terminal groups, which very often alters the overall properties of the dendrimer completely [55, 66].
Dendrimers can even aggregate into larger structures, assemble into dimers [62] or form liquid crystalline phases [54]. In addition to that, dendritic structures can be combined with linear polymers, forming linear-dendritic copolymers, such as dendrigrafts [55, 62].

3.1.4 Properties

As a consequence of their unique structure, dendrimers also possess a variety of interesting properties, which often differ strongly from analogous linear polymers. Many of these differences can be explained with the branched dendrimer structure and the dominating effect of the large number of terminal functional groups, which increases exponentially with the dendrimer generation [55]. In comparison to linear polymers, dendrimers are more compact, monodisperse and roughly globular macromolecules with comparably low intrinsic viscosities and increased, tunable solubilities [55, 62]. Among the most important features of dendrimers are their acid-base properties (if they are polyelectrolytes), their conformational behavior, their ability to participate in host-guest complexes and their interaction with living organism, namely bacteria and eucaryotic cells. As characteristics of dendrimers can vary as greatly as their structural diversity, the following section will mainly be focused on PPI dendrimers.

At first, the protonation behavior of PPI dendrimers has to be discussed as it influences a variety of other properties as well. It was found that the protonation of PPI dendrimers is rather similar to the behavior of linear polyelectrolytes as in both cases only short-range interactions between ionizable moieties along the carbon chain have to be considered by approximation [71, 72]. Different experimental techniques, namely potentiometric titration as well as natural abundance ^{15}N-NMR spectroscopy, revealed a two-step protonation behavior in an "onion-like", i.e. alternating pattern [71, 72]. Starting at high pH values, all "odd" shells are protonated at approximately pH 10, which include the primary amines at the dendrimer surface and the tertiary amine groups in every second dendrimer layer. The remaining amine groups in "even" shells are not protonated until pH 6 is reached. Thus, an intermediate plateau can be observed at which 2/3 of the ionizable groups of the PPI dendrimer are charged [71, 72].

Regarding dendrimer conformation, some more general remarks have to be made. The first models on that topic were published by De Gennes and Hervet in 1983 [62]. Their calculations led to the conclusion that PAMAM dendrimers possess elongated branches, resulting in a hollow dendrimer core and a dense dendrimer surface crowded with terminal groups [54, 62]. Many other simulations, e.g. based on the kinetic growth model and performed by Lescanec and Muthukumar [73], however, gave opposite results.

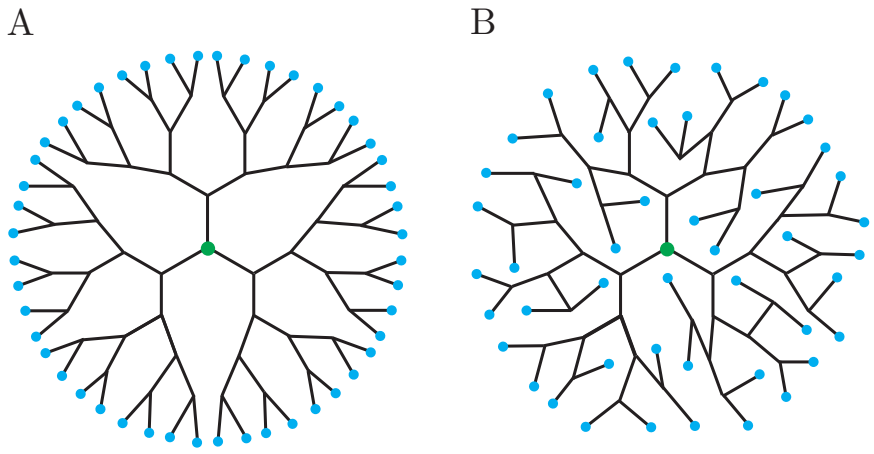

Figure 3.4: Dendrimer conformation in solution according to (A) the "dense shell" model by De Gennes or (B) with backfolding of dendrimer branches.

They predicted a compact dendrimer core and a radially decreasing density due to the backfolding of dendrimer branches [54]. The actual conformational behavior of a dendrimer thus depends on the interplay of entropy, favoring a more disordered structure with backfolding, and various enthalpic contributions. Strong interactions of surface groups with inner functionalities promote backfolding as well, whereas strong non-covalent bonds among surface groups favor a dense De Gennes-like structure [54, 62]. Thus, the conformational behavior of a dendrimer depends strongly on the structure and the functional moieties of the dendrimer itself but also on parameters of the surrounding fluid, such as the type of solvent, the ionic strength and the pH [62].
The first detailed studies for PPI dendrimers up to generation 5 were performed by Scherrenberg et al. in 1998 [74]. Via small-angle neutron scattering (SANS) and viscosimetry, they found that the dendrimer size increases as $M^{1/3}$. Additionally performed molecular dynamics simulations agreed with the experimental data and led to the result that PPI dendrimers are rather flexible molecules, exhibiting backfolding and thus a homogeneous radial density. Their conformation, therefore, does not represent a dense core nor a dense shell behavior [74].

A clear dependence of the dendrimer conformation on the solvent properties can be observed. In general, increased backfolding is present in a "bad", i.e. poorly solvating solvent [62]. This correlation was confirmed in NMR studies of PPI dendrimers, where increased intramolecular interactions and thus enhanced backfolding were found for the apolar solvent benzene. In chloroform, in contrast, interactions between solvent and dendrimer branches are possible, leading to a more extended dendrimer structure [75].

The conformation of ionizable dendrimers, such as the PPI dendrimer, is also strongly influenced by the solvent pH and its ionic strength. Various studies using molecular dynamics simulations have dealt with the pH dependence of PPI dendrimer size and structure in the past years [76, 77]. As explained previously, PPI dendrimers are non-protonated at high pH values ($\geq$ pH 10), whereas partial or complete protonation of the amine groups is observed at neutral pH (pH 7) or low pH ($\leq$ pH 4). Thus, at neutral or low pH electrostatic repulsion between the positively charged amine groups leads to a more extended structure with elongated branches and a globular shape. A more compact structure, i.e. a smaller radius of gyration, is observed at high pH values, where no charges and thus no Coulomb repulsion are present [76, 77]. This conformational behavior is reflected in the radial density profiles. At high pH values, a denser core is formed due to increased backfolding. The opposite situation of a dense shell structure is obtained for medium and low pH values. In this case, the reduced backfolding due to electrostatic repulsion is possibly enhanced by increased hydrogen bonding between amine groups, water and counterions [76, 77]. The data obtained for the density profiles of water and chloride counterions can be included into that conformational picture. At low and neutral pH, a more open and less compact dendrimer structure is accompanied by more pronounced water penetration. In addition to that, more chloride ions can be found in the dendrimer interior at low than at medium pH because under these conditions the charge density of the dendrimer is higher as well [76, 77]. Comparing these results to the other class of important polyelectrolyte dendrimers, the PAMAM dendrimers, in general less backfolding is observed for PPI dendrimers, which probably is the consequence of their shorter and thus less flexible branches [77].
The additional effect of high ionic strengths on dendrimer conformation was studied by Welch and Muthukumar [78]. Their simulations of a polyelectrolyte dendrimer led to the result that a compact, dense-core structure is obtained at high ionic strength due to charge screening, which resembles the backfolded conformation obtained at high pH values [62, 78].

As mentioned in the previous section, dendrimers in general and PPI dendrimers in particular are able to possess a conformation with a hollow core structure and a dense, compact shell under certain conditions [54]. So, these cavities can be used to entrap molecules of appropriate size and properties. PPI dendrimers in particular can be used to encapsulate hydrophobic molecules as they possess a nonpolar inner microenvironment [76]. This formation of stable guest-host complexes was first proved by Jansen et al. in 1994 [79]. Via modification of the terminal amine groups of PPI dendrimers with *tert*-butyloxycarbonyl (Boc)-protected amino acids, a stable compact dendrimer shell was obtained. Hydrophobic dye molecules, such as Rose bengal, were incorporated permanently into the dendrimer cavities, if present during the conversion of the amine end groups [79]. This observation gave rise to the use of dendrimer host-guest complexes in a variety of applications and will be reviewed below.

The last important aspect of dendrimer properties is their interaction with biological systems, namely bacteria and eucaryotic cells. Regarding their behavior towards eucaryotic cells, dendrimers with terminal amine groups, such as PAMAM and PPI dendrimers, which are positively charged under physiological conditions, exhibit cytotoxicity, which is not observed for molecules with neutral or negatively charged functionalities. This is probably the consequence of their strong interaction with negatively charged cell membranes and it can be reduced by conversion of the terminal groups into neutral or anionic groups [56, 80]. Such diminished cytotoxicity in *in vitro* studies was, for example, observed by Felczak et al., who examined the impact of PPI-G4 dendrimers without, with 25% and with 100% maltose end groups on various cell lines [81]. In their study, IC_{50} values in the micromolar range were observed for unmodified dendrimers, whereas cell viability was already drastically increased with a conversion of 25% of the end groups [81]. Similar results were obtained by Ziemba et al. in *in vivo* experiments, where PPI dendrimers with 0% and 25% sugar moieties exhibited acute toxicity in rats. No toxicity was observed for dendrimers with complete end group conversion. Noteworthy, however, is the observation that no permanent damages and full recovery were observed if dendrimers were no longer administered [80]. Despite their cytotoxic behavior, PPI dendrimers exhibited promising antimicrobial properties in various experiments. Felczak et al. found that unmodified PPI dendrimers showed good antimicrobial activities against gram-positive bacteria and yeast, which can cause a variety of clinically relevant infections [81]. Dendrimers whose end groups were modified with quaternary ammonium moieties showed potent antibacterial properties, even against the gram-negative *Escherichia coli* bacteria [82].

3.1.5 Examples of Dendrimer Application

Due to their special properties, dendrimers are used for a variety of purposes. Their applications thereby usually make use of their multivalency, e.g. for solubility modulation or ligand fixation, and/or their ability to encapsulate molecules in host-guest complexes [56, 66]. As a vast variety of different dendrimers has been developed in the last decades (see above), the scope of possible applications is similarly broad. In the majority of the studies, dendrimers are utilized in the medical field. They are applied in imaging techniques, e.g. as MRI contrast agents [83], as intrinsically antiviral or antibacterial compounds themselves [56, 64] and in vaccines [84]. Most attention, however, was received for their use in drug and gene delivery, e.g. in order to deliver anti-cancer drugs in a controlled manner to tumor cells [85] or to transfect plasmid DNA into cells effectively [86]. In addition to the application in the biomedical context, dendrimer-based systems are developed in catalysis, for example as dendrimer-encapsulated nanoparticles (DENs) [87]. This way advantages of homogeneous (e.g. high selectivity) and heterogeneous catalysis, such as their recyclability, can be combined [54, 87].

3.2 Polymers

As linear polymers as well as their behavior are more commonly known than dendrimers, no general introduction to their properties will be given. Instead, only the two polymer classes applied in this thesis, namely poly(amido amine)s as well as poly(ethylene imine)s, especially in their linear form, will be introduced. At last, some relevant information about the immobilization of polymers on surfaces as well as the properties of such surface-tethered polymers will be provided.

3.2.1 Poly(amido amine) Polymers

Poly(amido amine)s are a large family of synthetic polymers available with a huge variety of functionalities and, therefore, strongly varying properties [88]. They, however, share common functional motifs in the polymer backbone, the eponymous amide and amine groups, as well as their synthesis route via polyaddition of amines with bisacrylamides [88]. In order to differentiate these linear polymers from their hyperbranched analogs, very often different abbreviations are chosen in literature. Whereas the linear poly(amido amine)s are termed as PAAs, the acronym PAMAM is usually used for hyperbranched or dendritic poly(amido amine)s [88, 89]. As the polymer in this thesis was specifically designed to present a linear mimic of the PAMAM dendrimer, it was labeled PAMAM polymer and was addressed correspondingly throughout this thesis. The polymer class as a whole, however, will be summarized as PAAs.

Polymer Synthesis

PAAs are in general synthesized via stepwise aza-Michael reaction of bisacrylamides with suitable amines. For linear polymers, primary amines or secondary diamines can be chosen (see Figure 3.5), whereas primary diamines form crosslinked resins [88].

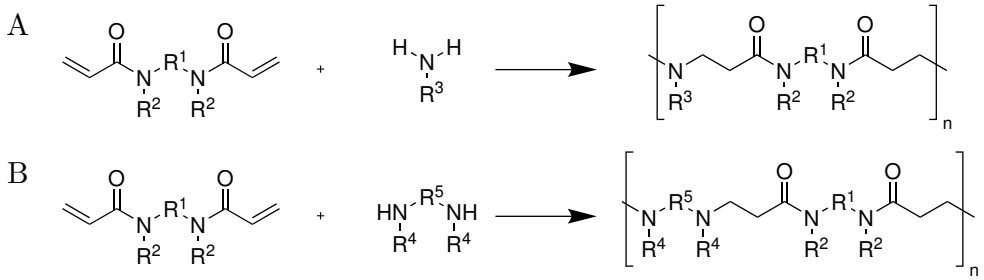

Figure 3.5: Synthesis of linear PAA polymers from bisacrylamides and (A) primary amines or (B) secondary diamines [88].

Table 3.1: Examples of residues tolerable in PAA synthesis [88]. The blue circle depicts the nitrogen atom(s), the moieties are linked to.

Residue	Available moieties
R^1	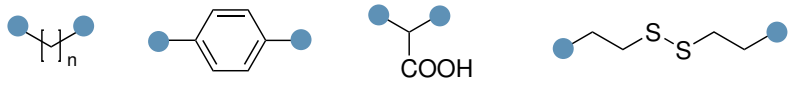
R^2	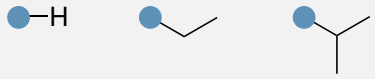
R^3	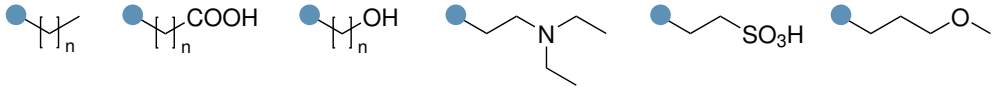
R^4	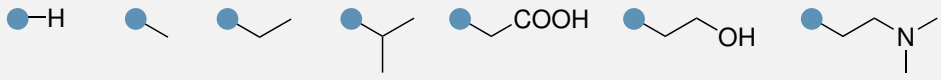
R^5	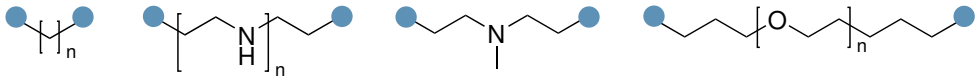

The synthesis procedures are in general characterized by their simplicity because the polymerization can be carried out at room temperature in water (or other protic solvents) without a catalyst [88, 90]. The polyaddition reaction tolerates a large variety of functional moieties, such as hydroxyl, carboxylic acid, ether or tertiary amine groups (see Table 3.1), enabling the synthesis of highly functionalized polymers [88, 90]. The resulting polymers can easily be employed as macromonomers in block or graft copolymers because their end groups can be tailored by using stoichiometric excess of one monomer during the polyaddition reaction [88, 90]. Thus, linear PAAs can furthermore be crosslinked to form hydrogels or can be immobilized on surfaces [88].

Properties of PAA Polymers

PAAs obtained via step-wise polyaddition usually exhibit an average molecular weight ($\overline{M}_n$) between 5000 and 30 000 g mol^{-1} as well as a polydispersity index of approximately 2 [88]. They all swell or dissolve in water, with many of them also being soluble in other polar solvents, such as lower alcohols or dimethyl sulfoxide [88].
Possessing protonable amine groups, PAAs exhibit unique protonation properties among the group of polyelectrolytes. Acid-base dissociation equilibria of polyelectrolytes can usually not be described by "real" dissociation constants but only by "apparent" dissociation constants, which depend on the protonation degree of the entire polymer and may thus differ drastically from the constants of analogous low-weight molecules [88, 90]. Most PAAs do not behave as typical electrolytes as distinct basicity constants can be determined for each kind of ionizable group of the polymer chain, which are in good agreement with the constants of the respective low-weight amine molecules [88, 90]. For the first amine group of the polymer backbone, usually a pK_a value between 7.25 and 8.25 is determined. A second amine group (in polymers from secondary diamines) usually possesses a pK_a value in a broad range between 3.25 and 7.5 [90]. The independent protonation of the amine groups of the different repeating units can be explained with the large distance between them and the presence of two charge-screening amide groups between neighboring monomers [88].
This peculiar protonation behavior also has a direct influence on the polymer structure and conformation in solution and its dependence on the solution pH. PAA polymers are in general characterized by rather extended structures, which lead to large hydrodynamic volumes if compared to other polymers of similar molecular mass [88]. If the solution pH is lowered so that one or both amine groups of each repeating unit become protonated, the conformational freedom of the previously coiled polymer is restricted due to electrostatic repulsion and the polymer is forced to adapt a more open and rigid structure [88, 89]. As PAAs in general possess distinct protonation constants, these protonation steps can be accompanied by comparably sharp jumps in conformation and solution properties, such as viscosity [88].

Poly(amido amine) polymers have been observed to degrade in aqueous solution within days to weeks with the degradation rate depending on temperature, solution pH, concentration and structural features of the polymer itself [90, 91]. It was originally believed that this degradation occurs via hydrolytic cleavage of the amide groups and is catalyzed by the proximity of the tertiary amine groups in the polymer chain [90, 91]. Recent NMR studies of Arioli et al., however, revealed that the degradation actually occurs via retro-aza-Michael reaction and only marginally, if at all, via hydrolytic processes [91]. They studied a variety of different PAAs, the most stable among them

being the product of the polyaddition of N,N'-methylenebisacrylamide and 2-methylpiperazine. This polymer strongly resembles the one studied in this thesis and was shown to degrade approximately 10% within 100 days in aqueous solution at pH $\geq$ 7 [91].

With respect to the interaction of PAAs with cells, it has been observed that poly(amido amine) polymers are in general significantly less cytotoxic than other cationic polymers, such as poly-L-lysine or poly(ethylene imine), probably due to their lower charge density per repeating unit of the polymer [88–90]. The negligible cytotoxic effect of a polymer consisting of methylenebisacrylamide and dimethylethylenediamine monomers in comparison with a commercially available branched poly(ethylene imine) was, for example, proven by Almulathanon et al. in their research on the applicability of PAAs as vectors for gene transfection [92]. In addition to that, some PAAs have shown further interesting properties in biochemical research. Some representatives exhibit, for example, intrinsic antiviral, antimalarial or anti-metastatic properties [88, 90, 93]. These effects themselves are, however, usually rather weak and thus exploited in combination with appropriate therapeutics (see below).

Applications of PAAs

In the past years, poly(amido amine) polymers have gained increasing interest with respect to a plethora of applications, ranging from the preservation of ancient paper and the use as a flame retardant for cotton [94, 95] to the utilization in water purification via complexation of heavy metal ions [88] and a variety of biological applications.
PAAs have, for example, been explored as soluble carriers for imaging probes (e.g. in MRI contrasting agents) [88] or for antimalarial, anticancer or antiviral therapeutics [88, 89, 93]. They have gained even more attention as non-viral vectors for intracellular delivery and gene transfection [88, 92, 96]. PAAs combine good complexation and transfection properties with low cytotoxicity and thus prove themselves as potential alternatives to established non-viral vectors, such as poly(ethylene imine) [88, 90, 92, 96].
Poly(amido amine) polymers have also been investigated as crosslinked hydrogels or part of block and graft copolymers. Reinforced hydrogels have successfully been applied in tissue engineering for the osteoinduction of osteoblast precursor cells [97]. Special amphoteric PAAs, which combine biodegradable, biocompatible as well as cell-adhesive properties, have been tested as guidance structure for peripheral nerve regeneration in rats [98]. Frequently, the heparin-adsorbing ability of several PAAs was utilized for materials in blood-contacting applications as, for example, copolymers containing PAA and poly(methyl methacrylate) (PMMA) exhibited non-thrombogenic properties after pre-heparinization [88, 99].

3.2.2 Poly(ethylene imine) Polymers

In contrast to the large and diverse family of the poly(amido amine)s, the group of poly(ethylene imine) (PEI) polymers is considerably smaller. In the following, the focus will be on the synthesis, properties and applications of linear PEIs, but some important examples of branched PEIs will also be included in the overview.

Synthesis of PEI Polymers

The synthesis of a linear PEI polymer is not straightforward. In contrast to that, the preparation of branched poly(ethylene imine)s can easily be performed via cationic ring-opening polymerization of aziridine, but in this way no linear polymer can be obtained [100, 101]. Substitution of the nitrogen atom of aziridine does not solve this issue as branching can still occur. Additionally, the cleavage of the nitrogen-bound side group can pose further problems as incomplete cleavage or undesired side reactions can prevent the formation of the desired product [100]. These obstacles are overcome by the development of a completely different synthetic route. This two-step procedure consists of a cationic ring-opening polymerization of 2-oxazoline, resulting in the N-acylated polymer, followed by alkaline or acidic hydrolysis [100]. In this manner, Tanaka et al. were able to obtain linear PEI polymers of high molecular weight (approximately 10 000 g mol^{-1}) via polymerization of 2-phenyl-2-oxazoline and subsequent acid-catalyzed debenzoylation [101].

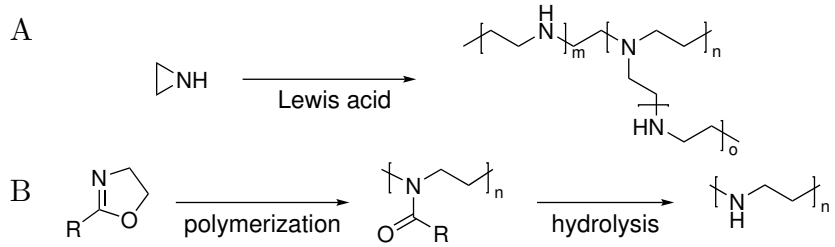

Figure 3.6: Synthesis of (A) a branched PEI polymer via ring-opening polymerization of aziridine and of (B) a linear PEI polymer via polymerization of 2-oxazolines and subsequent hydrolysis [100].

While this synthesis route provides a variety of advantages, such as the commercial availability of the monomers as well as the tolerance of the polymerization reaction towards a variety of functional groups, the comparably harsh conditions of the hydrolysis reaction are not compatible with many functional groups [100]. Therefore, post-hydrolysis functionalization is required, which is based on the conversion of the polymer's amine groups. However, these reactions might not be quantitative due to steric reasons [100].

Properties of Linear PEI Polymers

Regarding the properties of linear (and branched) PEI polymers, their protonation characteristics as well as their behavior towards living cells will be summarized briefly. In a linear PEI polymer, charged groups can be generated via protonation of the secondary amine groups in acidic media [102]. As all those ionizable groups are located along the polymer chain in rather close proximity, protonated groups influence the protonation of nearby ionizable sites via electrostatic interactions, i.e. the PEI polymer behaves as a "true" polyelectrolyte in contrast to the poly(amido amine) polymers [102, 103]. Potentiometric titrations of linear poly(ethylene imine)s thus resulted in titration curves ranging over roughly six pH units with a protonation degree of approximately 0.5 under physiological conditions (pH 7.4) [102]. Ziebarth and Wang obtained similar results from Monte Carlo simulations. From their calculations, a protonation degree of 55% can be expected under physiological conditions, with charged and uncharged amine groups being alternately located along the polymer chain [103].

The overall positive surface charge of PEI polymers under physiological conditions has a strong impact on its biocompatibility towards tissue cells as well as its interaction with bacteria. Generally speaking, PEI polymers can exhibit severely cytotoxic behavior as a consequence of their strong electrostatic interactions with negatively charged cell membranes [100]. Linear poly(ethylene imine)s have also been shown to be hemolytic [104]. These properties depend strongly on the structure and molecular weight of the polymer [100]. Cytotoxicity of linear PEIs was found to be usually lower than toxicity of analogous branched polymers and often tolerable in several biological applications [100, 105, 106].
Due to their positive charges at physiological pH, PEI polymers are also able to exhibit antimicrobial properties. Both linear and branched poly(ethylene imine)s displayed intrinsic antibacterial behavior towards, for example, *Staphylococcus aureus* and *Escherichia coli* [104, 106]. In a study with bacterial and mammalian model membranes, linear PEIs even exhibited selectivity towards bacterial membranes in comparison with mammalian membranes, qualifying them for biomedical applications [106].

Applications of Poly(ethylene imine) Polymers

Linear and branched PEI polymers are currently applied in a number of ways and fields. Apart from using the polymer itself in solution, it is often immobilized on surfaces, for instance on silicon wafers, via physisorption based on electrostatic interactions, for instance with the aim of preventing protein adsorption [107, 108]. Covalent grafting of PEI polymer chains is apparently of minor importance.

PEI polymers are furthermore often copolymerized or functionalized, e.g. via coupling of bioactive ligands. Here, especially the modification with PEG chains has gained significance due to the decreased cytotoxicity of the copolymer [100].
Branched and linear PEI polymers are established in some industrial applications, for example as flocculation aid in the paper industry or for ion complexation in waste water treatment [100]. In the past years, poly(ethylene imine)s have also been used as part of amine-silica adsorbents for CO_2 capture [109]. Recently, PEIs have gained significant attention in electrochemical applications, for instance in inverted polymer solar cells [110] or in Li-ion batteries [111].
Apart from wound dressings, which exploit the antimicrobial properties of PEIs [106], PEI polymers mainly have one purpose in biological applications: They serve as non-viral vectors for gene transfection [100]. Due to strong electrostatic interactions, PEI polymers can complex DNA or RNA, forming nano-sized particles, and protect the nucleic acids against degradation [100]. These DNA-PEI polyplexes show high cellular uptake as well as the release of the DNA into the cytoplasm [100]. Their excellent transfection efficiency, however, is accompanied by their intrinsic cytotoxicity [100]. Current research thus focuses on the reduction of the cytotoxic behavior of the polymers, while maintaining the transfection performance, for example via grafting of PEI with zwitterionic polymers [100, 112].
In summary, PEI polymers are significantly more important than other homologous amine polymers. The synthesis of poly(propylene imine) polymers via a ring-opening polymerization of azetidine has been described in literature significantly less often [113], the resulting branched and linear PPI polymers have been applied as CO_2 adsorbents [114, 115]. In contrast to that, no literature can be found for the synthesis of poly(butylene imine) polymers.

3.2.3 Polymers at Surfaces

As already mentioned in the previous sections, polymers are not only utilized in solution but are also grafted on surfaces for a variety of applications. Here, different immobilization techniques and resulting structures of the polymer layer can be observed. In order to avoid any lengthening, only linear homopolymers (such as the ones applied in this thesis) will be considered.
In order to attach a polymer on a surface, two fundamentally different techniques can be applied. At first, immobilization of the polymer chain can be achieved via physisorption. In this case, the polymer adsorbs on the surface via non-covalent forces, such as electrostatic interactions, van der Waals interactions or hydrogen bonding [116, 117]. This adsorption, however, is usually reversible, so that polymer desorption and displacement by other solution compounds might occur [116].

To avoid these drawbacks, polymers can be covalently immobilized on the surface, leading to coatings of improved stability and specific structure [118]. Here, an additional differentiation can be made between the "grafting to" and the "grafting from" approach [118]. The "grafting to" technique describes the immobilization of a pre-synthesized, end-functionalized polymer via reaction with appropriate reactive sites on the surface [116, 118]. This procedure is technically rather simple and allows polymer purification and analysis prior to the grafting [117, 118]. In general, however, only small amounts of immobilized polymer can be achieved as with increasing surface coverage diffusion of polymer chains to the surface is kinetically hindered and successively obstructs further film growth [116]. In the "grafting from" technique, these obstacles are overcome. The polymer film is synthesized via *in situ* polymerization at the surface, starting from surface-immobilized initiators [116, 118]. A huge variety of polymerization techniques has been adapted to this procedure and is available nowadays, which all allow the formation of dense polymer layers of controllable thickness [117, 118]. The only major disadvantage of this technique, however, remains the hindered analysis of the polymer itself as it must be cleaved from the surface for the determination of composition and molecular weight [117, 118]. For both techniques, the "grafting to" and the "grafting from" procedure, reactive surface groups are required. Among several other techniques, the formation of self-assembled monolayers has proven to be a valuable tool to achieve sufficiently densely packed reactive sites on the surface [119].

Depending on the immobilization procedure and the affinity of the polymer to the surface, different grafting densities, i.e. numbers of immobilized polymer chains per unit area, and resulting polymer conformations have to be differentiated [118].

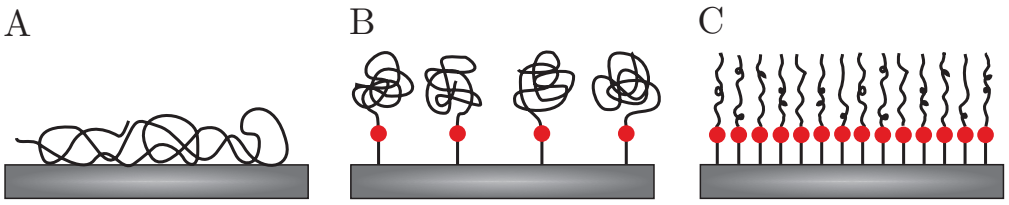

Figure 3.7: Schematic depiction of the three regimes of surface-immobilzed polyers: (A) pancake regime, (B) mushroom regime and (C) brush regime [120].

For physisorbed polymers, usually a surface layer in the pancake regime is observed instead of an end-on orientation of the polymer chains. Here, the polymer is bound to the surface in the so-called "trains", whereas the polymer ends, the tails, and the polymer segments between the trains, the loops, are not in contact with the surface and may extend into the solution [120]. Physisorbed polymers exhibit properties which are fundamentally different than those of swellable polymer brushes (see below) [118].

If the grafting density of a polymer without surface affinity is sufficiently low, i.e. the distance between grafting points is more than twice the polymer's radius of gyration, a polymer layer in the mushroom regime is obtained, which is usually the result of "grafting to" techniques [117, 118]. In this case, the distance between the polymer chains is comparably large. Hence, the polymers are immobilized in a random coil conformation identical to the bulk solution [121].
At higher grafting densities (if the grafting distance is smaller than twice the radius of gyration), an array of surface-attached polymer chains in close proximity is obtained, a so-called polymer brush [117, 118]. Such a dense packing of polymer chains can mainly be obtained via the "grafting from" approach [118]. In this case, the polymer conformation is strongly altered, compared to a random coil in solution, as the polymers are forced to adapt an elongated conformation in order to avoid unfavorable interactions with neighboring polymers [118]. The resulting entropic penalty has a strong influence on the properties of the protein layer, which differ considerably from those of the respective polymer in a random coil [117, 118]. Polymer brushes are often used to control the interactions of different species with the underlying surface [118]. Thus, they are, for instance, currently applied for the stabilization of nanoparticles, such as quantum dots, to modify the stationary phases of chromatographic columns or to improve the corrosion resistance of materials [117, 119]. They have also gained large attention in biological and biotechnical applications because the non-fouling properties of hydrophilic polymer brushes are exploited as coatings for biosensors, bioanalytical devices and implant materials [117].

3.3 Osmolytes

3.3.1 Fundamental Information

The term osmolyte comprises a variety of small molecules that are accumulated in high concentrations in cells being exposed to conditions threatening normal protein and cell functions [14, 122, 123]. These so-called cytoprotectants can be found in all types of organisms (ranging from bacteria and yeast to plants, marine animals and mammals) [123] and counteract a broad range of stresses, such as high osmolarity, cellular dehydration, temperature, hydrostatic pressure or presence of urea [14, 124]. All those environmental conditions would lead to protein denaturation in absence of osmolytes, reducing their functionality, and thus disturb intracellular processes [124].

The large number of different osmolytes can be divided into three major groups (see Figure 3.8). The first one (group A) consists of polyols and carbohydrates and contains molecules like glycerol and trehalose. The second (group B) contains amino acids

as well as their derivatives. Examples hereof are proline, glycine, ectoine and taurine. Molecules, such as trimethylamine N-oxide (TMAO) and glycine betaine, are included in the third group (group C), consisting of methylammonium and methylsulfonium compounds [14, 124]. All osmolytes have in common that they are usually small, organic, water-soluble molecules, which do not carry a net charge under physiological conditions [14, 125].

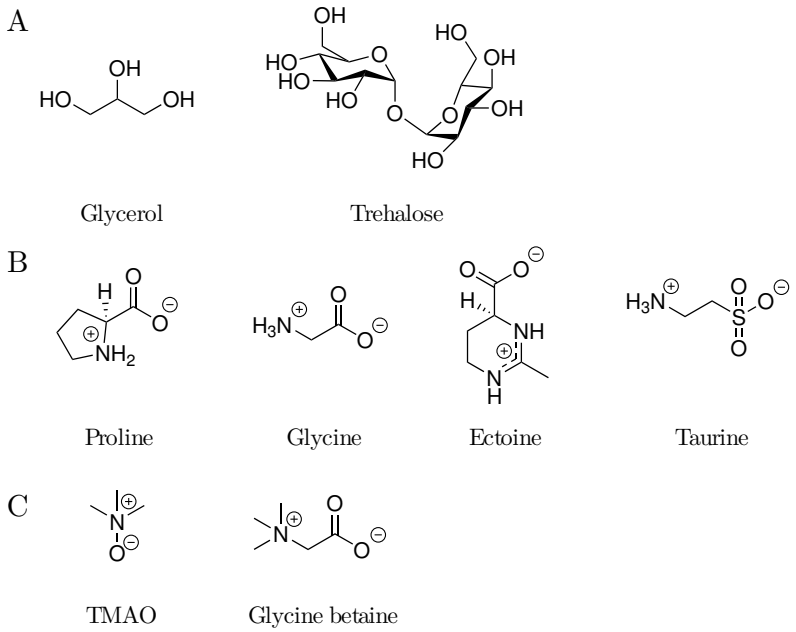

Figure 3.8: Survey of typical examples of the three main osmolyte categories: (A) polyols and carbohydrates, (B) amino acids and their derivatives and (C) methylammonium compounds, according to Yancey et al. [14].

3.3.2 Properties of Osmolytes

Regarding their properties and functions, three main aspects have to be distinguished when dealing with the effect of osmolytes on cellular processes and proteins in particular. At first, osmolytes stabilize proteins against denaturation [14] due to unfavorable interactions between the osmolyte and the protein backbone, the so-called osmophobic effect [126]. With the help of the thermodynamic cycle summarized in Figure 3.9, the effect of this preferential exclusion can be easily explained. As the peptide backbone is more exposed in a protein's denatured state, the denatured state is significantly more unfavorable in an osmolyte solution than the native conformation [126]. Thus, the transfer Gibbs energy of a denatured protein from water to an osmolyte solution ($\Delta G_{trans,D}$) is significantly more positive than the respective transfer Gibbs energy of the protein in native conformation ($\Delta G_{trans,N}$). As a consequence, the change in Gibbs energy that is related to the denaturation of the protein is more positive for the protein in osmolyte solution ($\Delta G_{den,O}$) than in pure water ($\Delta G_{den,W}$) [126].

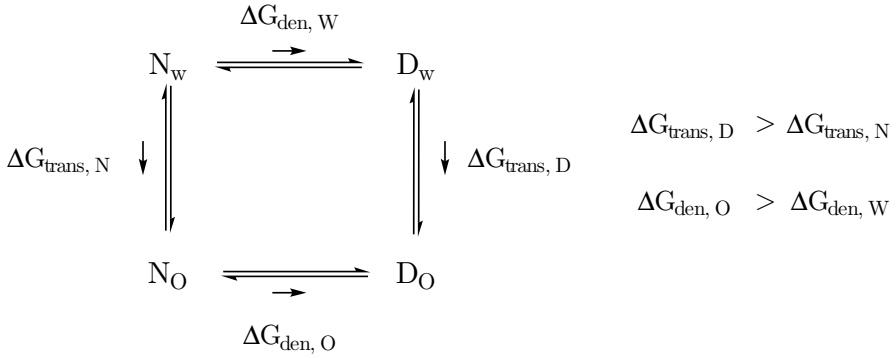

Figure 3.9: Thermodynamic cycle of the denaturation of a protein from its native conformation (N) into a denatured state (D) and its transfer from pure water (indicated by index W) to an osmolyte solution (indicated by index O). Transfer Gibbs energies are given as ΔG_{trans}, Gibbs free energies of the denaturation process are abbreviated as ΔG_{den}. The scheme was adopted from Bolen and Baskakov [126].

There is no unambiguous explanation why the protein backbone was chosen as the primary target in osmolyte evolution, but two explanations are possible. At first, the peptide backbone is a universal feature among proteins and also makes up for the largest portion of groups, which are exposed/buried upon protein denaturation/folding [126]. In addition, osmolytes targeting the protein backbone do not interfere with the driving forces of protein folding, such as electrostatic and hydrophobic interactions, which are mainly observed among the amino acids' side groups. Thus, osmolytes targeting the protein backbone usually do not disturb the folding of a protein into its native conformation [126].
Apart from the protection of proteins against denaturation, the further impact of osmolytes on protein conformation has also been observed in a variety of different situations. In absence of stress factors promoting protein denaturation, osmolytes have been reported to influence protein aggregation and to aid correct denatured or misfolded proteins in some cases. Thus, they are sometimes labeled as "chemical chaperones" [124–127].

In addition to these properties, osmolytes can be categorized as either compatible or counteracting [124]. The majority of osmolytes can be classified as compatible as, in contrast to, for example, inorganic salts or urea, they can be present at high concentrations in cells without perturbing protein function or other cellular processes [123, 124]. In contrast to that, some osmolytes, mainly methylammmonium-based molecules, can be labeled as counteracting osmolytes. These osmolytes have been found to increase protein stability and activity to such an extent that they can compensate the denaturing effect of urea in cells [14, 124]. If methylammonium-based osmolytes are present without a denaturing component, however, they seem to be able to "overstabilize" proteins, especially at high concentrations, and thus, for example, reduce enzyme activity [14].

The last aspect of osmolyte properties contradicts to some extent the concept of osmolytes as universal and interchangable protein stabilizers because some of these solutes seem to possess certain additional and specific effects. [14]. These cytoprotective properties may include sulfide detoxification and antioxidative properties, provided, for example, by hypotaurine. Carbohydrate-based osmolytes may serve as energy storage after dormancy, whereas dimethylsulfoniopropionate (DMSP) may be stored in cells in order to repell predators [14]. These additional properties can serve as an explanation – in addition to availability via diet or metabolism – why osmolytes exist in such diversity and vary so strongly among different species.

In addition to classical osmolytes, exhibiting the features mentioned above, it has to be emphasized that often no clear demarcation is possible between osmolytes and other solutes. As mentioned above, urea is a strong denaturant and thus destabilizes proteins. Nevertheless, it is accumulated in high concentrations in marine elasmobranchs, together with methylammonium compounds, such as TMAO, to compensate the osmolarity of the surrounding sea water [128]. Arginine possesses ambivalent properties as well as it destabilizes proteins but prevents protein aggregation [124, 125].

3.3.3 Characteristics of Osmolyte Motifs Applied in this Thesis

From the large variety of osmolytes, three different structural motifs have been used for surface modifications in the scope of this thesis. At first, the DMAPS coating, a self-assembled monolayer with a terminal sulfobetaine group, belongs to the family of betaines but is also closely related to taurine, which carries a sulfonic acid group as well [14]. The name of the betaine family of structurally related zwitterionic molecules is derived from N,N,N-trimethyl glycine, which was isolated from sugar beet and named "betaine" in the 1860s [129]. Betaine itself can be found in every kingdom of life, taurine mainly appears in marine animals and some mammalian tissue [14, 123]. In general, betaines are highly polar zwitterionic molecules, which carry a permanent positive charge at their quaternary ammonium group [129, 130]. They can, however, differ with respect to the characteristics of their anionic group. Carboxybetaines, carrying a carboxylic acid group, show a pH-dependent protonation behavior as this group possesses a pK_a value between 2.3 and 4.5 (depending on the distance to the ammonioum group) [131]. In contrast, sulfobetaines always contain a deprotonated sulfonic acid group due to its pK_a value of approximately -9, making them neutral zwitterionic molecules over the complete pH range [131]. The difference in acidic groups also influences the hydration behavior. Although both zwitterionic structures are strongly hydrated, the sulfonic acid group is surrounded by more but less structured water molecules due to

its moderate charge density [132, 133]. Apart from their function as protein stabilizers, betaine, taurine and their derivatives have been found to fulfill a variety of additional functions, e.g. detoxifying disulfide, maintaining the redox balance and acting as antioxidants [14].

The self-assembled monolayer with terminal amine oxide groups is the derived from the osmolyte TMAO, which is found in mollusks and crustaceans, elasmobranches as well as mammalian kidney tissue [14, 123]. As mentioned before, it is especially present in deep-sea fish, counteracting high hydrostatic pressure, whereas in sharks TMAO and urea are found in an 1:2 ratio, compensating the high salt content of sea water [14, 123, 124]. TMAO is a weakly basic (pK_a of roughly 4.5 [134]) but highly polar and hydrophilic molecule, possessing a dipole moment of 5.01 D [135]. TMAO has been recognized as an osmolyte responsible for a strong enhancement of protein stability [14]. Hence, it may "force" modified and unfolded proteins into their native conformation, but it can also "overstablize" proteins and inhibit enzyme function [14, 126]. This behavior can possibly be explained by the strong interaction of TMAO with water, which was studied in *ab initio* calculations by Kocherbitov et al. [135]. They did not only obtain as a result that interactions between TMAO and water were stronger than among two water molecules, but they also observed that the interaction between water molecules near the osmolyte was enhanced due to charge transfer [135]. In contrast to that, however, no effect on hydrophobic interactions could be determined by Athawale et al. [122].

The last surface modification was synthesized via immobilization of the proteinogenic amino acid proline, which acts as an osmolyte in a variety of organisms as it can be found in bacteria, plants, mollusks and crustaceans [123, 124, 136]. Its carboxylic acid and amine group possess a pK_a value of 1.99 and 10.6 respectively. Thus, the whole proline molecule exhibits an isoelectric point at pH 6.3 [137] and is nearly neutral at physiological pH. Proline is among the most hydrophilic amino acids [138] and thus initiates strong hydrogen bonding of surrounding water [139]. Apart from being an osmolyte, proline can also enhance the activity of enzymes, assist in cellular homeostasis as well as act as an antioxidant and a signal molecule [136].

3.3.4 Applications of Osmolytes

Due to their unique and interesting properties, osmolytes have gained attention in various applications, whenever stabilization of proteins in their native conformation is required. Osmolytes have, for example, been applied in vaccine production and storage [140] as well as in encapsulation experiments [141]. Ectoine and hydroxyectoine were

shown to be able to reduce the aggregation of β-amyloid, the cause of Alzheimer's disease [142]. Osmolytes were also examined in context with proteins which were misfold due to genetic diseases, such as Machado-Joseph disease or cystic fibrosis. In these experiments, reduced protein aggregation or correct protein folding and increased protein activity were achieved via addition of osmolytes [143–145]. A large variety of studies has been conducted, focusing on the influence of osmolytes on protein adsorption, with osmolytes added to the solution or immobilized on the surface. Wendorf et al. and Evers et al. were able to show that adsorption of proteins, such as bovine ribonuclease A, was reduced in presence of, for example, glycerol or trehalose [146, 147]. Strongly reduced adsorption of lysozyme on alkane self-assembled monolayers was achieved by Anand et al. due to non-covalent adsorption of TMAO from solution [148]. With respect to surface-immobilized osmolyte structures, carboxybetaine and sulfobetaine motifs seem to be the most common ones. They have been studied as side groups of various copolymers and as end group modification of branched poly(ethylene imine) [149–152]. Here, some polymers exhibited excellent protein-repellent properties. Less research was performed with modifications based on different osmolyte motifs, however, some studies have been reported. Miyata et al. could prove decreasing fibrinogen and globulin adsorption with increasing content of monosaccharide side groups in the investigated copolymer films [153]. Studying adsorption of lysozyme and fibrinogen on SAMs, Dobrzanska et al. found reduced adsorption after conversion of terminal tertiary amine groups into amine oxide groups similar to TMAO for several surface modifications [154].

4 Proteins and Protein Adsorption

The following chapter introduces proteins and their behavior, starting at first with the properties of proteins in solution. In addition to that, basic information about the proteins or protein solutions tested in this thesis will be given in order to facilitate later discussion of the results of protein adsorption experiments. In the second part, the adsorption of proteins on solid surfaces will be reviewed, elaborating both the thermodynamic and kinetic basics of the underlying processes as well as deriving some "rules of thumb", at last presenting principles of protein-repellent surface coatings.

4.1 Protein Properties and Stability

4.1.1 Protein Folding and Stability

Proteins can be regarded as linear polymers consisting of around 22 differing amino acids, which are connected among each other via covalent amide bonds. As the side groups of the amino acids vary strongly in their properties, being e.g. hydrophobic, hydrophilic, acidic or basic, the complete protein is in most cases amphiphilic and amphoteric [24, 155]. The specific ordering of the amino acids in the polypeptide chain, the primary structure of the proteins, leads to the formation of specific local conformations, the secondary structures, mainly α-helices and β-pleated sheets. These conformations are stabilized by hydrogen bonds [24, 155]. The pre-structured segments arrange into a three-dimensional folded structure, the tertiary structure, via different driving forces, which will be described below. The spatial arrangement of the polypeptide chain defines the shape, turning it into a fibrillar or globular protein for instance, and the functionality of the protein by formation of active sites [24, 155]. At this point, is has to be mentioned shortly that several polypeptide chains (subunits) can be combined to a quaternary structure (stabilized via non-covalent and covalent interactions, like disulfide bonds) and proteins can be modified after translation, e.g. via glycosylation, increasing the incredible number and diversity of proteins even more [156, 157].

In an aqueous environment, a protein is folded into its native 3D arrangement if the change of the corresponding Gibbs energy $\Delta_{folding}G$ is negative. Here, mainly two opposing driving forces, both attributing to the system's entropy, have to be considered [155]. Protein folding is mainly favored due to the dehydration of the hydrophobic side groups, which can be hidden in the interior of the protein. This so-called hydrophobic effect leads to the release of water molecules, causing an increase in the system entropy. A compact spatial arrangement of the polypeptide chain, however,

reduces its conformational freedom and, hence, provides a negative contribution to the entropy [155]. In summary, proteins in aqueous solutions are only marginally stable with a standard Gibbs energy of unfolding of approximately 20–60 $\mathrm{kJ\,mol^{-1}}$ as the contributions to $\Delta_{folding}G$ almost compensate each other [155, 158].

4.1.2 Properties of Proteins Selected in this Thesis

From this plethora of proteins, two single proteins were selected for the adsorption experiments due to their opposing properties.
Human serum albumin (HSA) is a medium-sized protein (molecular weight 66.5 kDa), which possesses an isoelectric point (IEP) at pH 4.7 [26, 155]. Thus, HSA is negatively charged under physiological conditions (pH 7.4). In addition to that, it can be classified as a "soft" protein, possessing a comparably low internal stability [155]. The related bovine serum albumin (BSA) possesses a Gibbs energy of unfolding of only 18 $\mathrm{kJ\,mol^{-1}}$ [158]. Lyoszyme, on the other hand, belongs to the groups of "hard" proteins due to its comparably high structural stability (with a Gibbs energy of unfolding of 60 $\mathrm{kJ\,mol^{-1}}$) [155, 158]. It is a small protein (molecular weight 14.6 kDa) with an IEP at pH 11.1. Due to that, lysozyme is still positively charged at physiological pH [155].

In addition to these model proteins, three physiological fluids were tested, human saliva, fetal bovine serum (FBS) and human AB serum (HABS). Human saliva is a complex fluid, which serves a variety of purposes with the general aim of maintaining oral health, such as buffering, lubrication and antimicrobial protection [159]. It consists mainly of water (> 99%) and contains only small amounts of proteins (0.3%, approximately 1–2 $\mathrm{mg\,mL^{-1}}$) and other inorganic or trace substances (0.2%) [159]. Basic physicochemical parameters strongly depend on the saliva flow rate, but in general an approximately neutral pH (between pH 6.7 and 7.7) is observed. Ionic strength may vary between 40 and 90 $\mathrm{mmol\,L^{-1}}$, meaning it is a hypotonic fluid [160]. In the past years, more than 1000 proteins from whole saliva have been identified [159]. Among them are, for example, proline-rich proteins (PRPs), mucins (large glycoproteins ensuring lubrication), amylases and lipases (aiding digestion), cystatin (inhibiting cysteine proteinases), and histatins (possessing antimicrobial properties), to name only a few [159, 161–163]. Although the proteome of human saliva of course spans a wide range of molecular weights and isoelectric points, some information can be given. It has to be noted that almost half of the proteins (46%) weighs less than 40 kDa, and the proteins' IEPs range mainly between pH 4 and pH 8, i.e. many of them can be considered acidic [162].
FBS is harvested from unborn calves [164]. The blood serum is obtained after removal of clotting factors and possesses a high protein content between 32 and 42 $\mathrm{mg\,mL^{-1}}$, with

albumin being the most abundant component (approximately 2/3 of the total protein) [165, 166]. It is further characterized by a pH of 7.4 (range 7.2 to 7.6) and an ionic strength of approximately 150 mmol L^{-1} mainly due to the presence of sodium chloride [167]. In addition to the large number of proteins, FBS also comprises a variety of amino acids, carbohydrates and further components, such as lipids, fatty acids, vitamins, and growth factors [165]. It is frequently applied as a supplement for cell culturing purposes as it contains high levels of growth-stimulating factors in combination with low amounts of growth-inhibiting components [165].
HABS is obtained from human donors who possess the blood group AB because their blood serum does not contain ABO antibodies [168]. The serum, that is received after removal of fibrin clots from blood plasma, is characterized by a protein content that exceeds the protein amounts in FBS [168]. The total content of proteins in HABS ranges approximately between 54 and 57 mg mL^{-1} [168]. Similar to FBS, the most abundant ones are albumin with a concentration of roughly 37–38 mg mL^{-1} and immunoglobulin G (IgG), making up for 10–20% of plasma proteins [168, 169]. In addition to more than 1000 identified proteins, HABS also contains a variety of further components, such as electrolytes, lipids and urea, similar to the composition of FBS [168, 170].

4.2 Protein Adsorption

4.2.1 Protein Adsorption – A Widespread Phenomenon

Protein adsorption has been described as ubiquitous and complex by Nakanishi et al. [171]. It occurs in many different situations, often with adverse effects, is difficult to prevent and difficult to explain [172]. In all cases, adsorption of proteins occurs rapidly after a surface comes into contact with a protein solution, e.g. an implant with a body fluid like blood [173–175]. This initial protein layer mediates further processes, such as bacterial adhesion, biofilm formation, biofouling, cell-surface interactions and thrombus formation [28, 174–176]. The attachment of proteins on surfaces as well as these subsequent processes are undesirable in a variety of fields, such as the marine industry [176, 177], food industry [171, 177] and *in vitro* diagnostics [177, 178].
Unwanted protein adsorption is particularly problematic in the medical field. Consequences may be reduced efficacy of drug delivery systems [178, 179] or bacterial infections of temporary devices, such as catheters [177]. With respect to blood-contacting materials (e.g. artery stents or artificial heart valves), protein-surface interactions may lead to thrombus formation [158, 180]. Many adverse effects of protein adsorption have also been observed after insertion of implants, such as prosthetic devices. Here, it may lead to bacterial infection and biofilm formation or fibrosis and development of scar tissue instead of proper integration into the surrounding tissue [177, 178].

4.2.2 The Complexity of Protein Adsorption

Protein adsorption is very complicated as it depends on a multitude of parameters. Summarizing shortly, not only the characteristics of the protein and the surface but also the properties of the environment influence this process [24, 155, 172]. The various aspects, which have to be considered, are compiled in Table 4.1.

Table 4.1: Overview of the parameters influencing protein adsorption.

Protein(s)	Surface	Environment
Size/molecular weight [24, 172]	Topography/roughness [24, 173]	pH [172, 173]
Hydrophilicity/-phobicity [155]	Wettability/SFE [24, 155, 172]	Ionic strength [172, 173]
Electric charge (IEP) [181]	Electric charge [24, 155]	Temperature [172]
Structural stability [181]	Functional groups [24]	Buffer composition/ ion species [172, 182]
Shape/orientation [171, 172]		Presence of other solutes [146]
Bulk concentration [24, 171]		
Number/kinds of proteins in physiological solutions [172]		

In summary, it can be stated that each protein possesses a unique "personality", which of course has vital influence on its interaction with surfaces [172]. As these properties as well as environmental conditions cannot be changed in the surrounding of an implanted biomaterial, the implant surface itself has to be modified and adapted.

4.2.3 Thermodynamic Basics of Protein Adsorption

Describing the complex thermodynamics of protein adsorption, the Derjaguin-Landau-Verwey-Overbeek (DLVO) theory can be chosen as starting point. It explains the interactions between colloidal particles by means of the change of the Gibbs energy of the system $G(r)$, which comprises distance-dependent contributions from van der Waals interactions $G_{vdW}(r)$ and from electrostatic interactions $G_{el}(r)$ [183, 184]:

$$G(r) = G_{vdW}(r) + G_{el}(r) \tag{4.1}$$

Although the DLVO model is too simplistic for the complex situation of protein adsorption [184], some aspects remain valid. At first, protein adsorption occurs if the system's Gibbs energy decreases [24, 155]:

$$\Delta_{ads}G = \Delta_{ads}H - T\Delta_{ads}S < 0 \tag{4.2}$$

For the thermodynamic description of protein adsorption, the DLVO approach is extended and four different aspects are considered. In addition to van der Waals and electrostatic interactions, hydrophobic interactions as well as the effect of conformational changes of the protein have to be considered [24, 155, 158].

Van der Waals interactions are always present, i.e. also participate in protein adsorption. They are always attractive, short-ranged (decreasing with r^{-6}) and small, yet not negligible [158]. As in the DLVO theory, sign and amplitude of the electrostatic interactions strongly depend on the charges themselves but also on environmental parameters, such as ionic strength [184]. Starting from the Poisson equation and a Boltzmann distribution of the solvent ions, the strength of this interaction can be estimated [158]. As previously implied, the role of ions has to be considered as well as they may be incorporated or released during protein adsorption [155]. Hydrophobic interactions are a strong driving force of protein adsorption and often dominate the process [158, 181]. At hydrophobic surfaces, water molecules are poorly bonded and forced to adapt an ordered structure. Release of those water molecules thus results in an entropy gain of the system [155, 185]. The last major aspect of protein adsorption are conformational changes of the protein itself as the protein conformation associated with the minimum of free energy in solution is usually not identical to the conformation corresponding to the lowest free energy of the protein at the surface [172]. These structural changes are usually primarily observed in "soft" proteins and lead to an increase in the contact area between protein and surface, enhancing hydrophobic interactions [172, 181, 185]. The denaturation of the protein may be accompanied by a loss of secondary structure and thus a gain in rotational entropy [158, 172]. Yet, in no case, complete unfolding into an entirely loose structure is observed and the resulting increase in entropy is probably too small to be a major driving force of protein adsorption [155, 158].

4.2.4 Kinetics of Protein Adsorption

Although already shortly mentioned in the previous paragraph, the kinetics of protein adsorption will be inspected briefly. Simplifying this complex topic, two main steps can be distinguished: At first, the protein rapidly adsorbs to the surface in its native state and subsequently conformational changes can occur [24, 172]. This relaxation processes are slow compared to the rate of the initial attachment of the protein, leading to an irreversibly adsorbed protein layer in many cases [172, 185]. Thus, the adsorption process cannot be described with a Langmuir isotherm, although in many cases a saturation curve can be observed macroscopically [171]. Conformational changes as well as interactions among proteins, though, can lead to deviations, e.g. an overshooting [172]. Therefore, starting from a Langmuir approach, a huge number of increasingly

complicated models, such as the random sequential adsorption (RSA) model, have been developed in order to describe the kinetics of protein adsorption [172]. The real situation is even more complex because also lateral interactions among adsorbed proteins have to be considered [172]. Additionally, if not only the adsorption of a single protein but from a complex protein mixture is examined, the competitive adsorption is often characterized by a complex sequence of adsorption, exchange and relaxation, called the Vroman effect [24, 181, 186]. In a nutshell, the smaller, i.e. more mobile proteins appearing in higher concentrations adsorb at first and are successively replaced by larger proteins with higher surface affinity [24, 186, 187].

4.2.5 Protein Adsorption – Rules of Thumb

A lot of effort has been put into the attempt to condense the complex mechanism of protein adsorption described in previous chapters into easy principles, which can be used to analyze protein adsorption and to design protein-repellent surfaces. These guidelines are in all cases simplifications, which have to be applied carefully. The most important scheme has been provided by Norde [155, 181] and is summarized in Table 4.2.

Table 4.2: Scheme for the prediction of protein adsorption depending on substrate and protein properties, as proposed by Norde [181]. Blue color indicates protein adsorption under the given conditions.

			Protein			
			Soft		Hard	
		Charge	+	−	+	−
Surface	Hydrophobic	+				
		−				
	Hydrophilic	+				
		−				

Due to the dominant effect of hydrophobic interactions, all proteins are expected to adsorb to hydrophobic surfaces irrespective of protein stability and charges. On polar (hydrophilic) surfaces, differences can be observed between "hard" and "soft" proteins. Due to their lower structural stability, the latter ones can even adsorb to like-wise charged surfaces despite electrostatic repellency. "Hard" proteins, in contrast, only adsorb if an attractive electrostatic interaction is present [181]. At this point, one additional definition has to be introduced in order to differentiate between hydrophilic and hydrophobic surfaces. In the context of protein adsorption, the concept of "Berg's limit" was developed, which defines surfaces with water contact angles below 65° ($\Theta < 65°$) as hydrophilic and surfaces exhibiting water contact angles of more than 65° ($\Theta > 65°$) as hydrophobic [187].

4.3 Protein-Repellent Surfaces

4.3.1 Protein-Repellency – Rules of Thumb

In order to prevent protein adsorption thermodynamically, it must result in an increase in the system's Gibbs energy [24]. This can at first be achieved by unfavorable entropic contributions if the surface is modified with a flexible and swellable polymer (entropic model) [188]. An adsorbing protein leads to a compression of the polymer layer, causing steric repulsion. The protein is repelled because the restriction of polymer conformation as well as the osmotic pressure building up counteract protein adsorption [185, 189, 190]. The resistance towards protein adsorption here depends on many parameters, such as the chain length and flexibility, grafting density and layer thickness [10, 189, 191, 192].
With respect to the influence of enthalpic contributions, two different aspects have to be differentiated. At first, surfaces without net surface charges are advantageous as in this case no attractive electrostatic interactions between surface and protein can occur [190]. In addition, protein-repellency is observed for strongly hydrated surfaces (water barrier model). The strong interaction between the water molecules and the surface coating make the replacement of water by the protein unfavorable, resulting in a repulsive solvation force [188, 192, 193].

From these thermodynamic considerations, some general rules of thumb for the design of protein-repellent surface coatings can be derived. At first, polymer surface modifications with flexible chains can show resistance towards protein adsorption [190], yet the importance of chain flexibility is still under debate [189] and is not a prerequisite for protein-repellency [194]. The requirements regarding the chemical functionalities have been summarized in the so-called "Whitesides rules" [187, 195]. According to those guidelines, nonfouling surfaces are obtained if the coatings possess polar functional groups (i.e. are hydrophilic), exhibiting hydrogen bond acceptors, but lack hydrogen bond donors as well as net charges [195]. The third condition (no H-bond donors), however, is violated considerably often by protein-repellent coatings, such as polysaccharides or oligo(ethylene glycol)s with terminal hydroxyl groups [190, 196]. Nevertheless, it seems to be advantageous if the functional groups of the coating, which are able to form H-bonds, are primarily available to water molecules but not to the considerably larger protein. To ensure that when dealing with surface coatings with low packing density, it can be advantageous to "end-cap" groups, such as -OH or -NH_2 with methyl groups [196].

4.3.2 Overview over Protein-Repellent Surface Modifications

The "rules of thumb" for protein-repellency derived above were used to develop a plethora of coatings, which are supposed to be protein-repellent. The major group here consists of hydrophilic polymers without a net charge, with coatings based on poly(ethylene glycol) (PEG) or oligo(ethylene glycol) (OEG) building blocks as the most prominent species [197]. PEG or OEG coatings are often referred to as "gold standard" [187, 197] because they are considered to be biocompatible, non-toxic, anti-fouling and even withstand the adhesion of platelets [191]. So far, a variety of different geometries, such as oligomers, linear or branched polymers and copolymers, and immobilization techniques, for example covalent immobilization or graft polymerization, have been applied [177, 197–199]. This way, researchers could develop surface coatings that withstand the adsorption of proteins from various single protein solutions (such as lysozyme, albumin and insulin) completely [199] or almost completely suppress the adsorption of proteins from FBS ($< 1\,\mathrm{ng\,cm^{-2}}$)[178]. The reason for the excellent performance of PEG and OEG coatings is still not completely understood, but it seems to be explained with the general working principles of hydrophilic polymers: The protein-repellency can, therefore, be interpreted as a combination of a repulsive elastic force, induced via an entropy loss of the polymer chains upon protein attachment, and an osmotic penalty, caused by the removal of water from the hydration layer of ethylene glycol groups [177, 197]. Coatings based on PEG or OEG, however, are limited in *in vivo* applications due to a variety of adverse properties. At first, these modifications are not stable in the presence of oxygen, hence in most biological media, and tend to autoxidize, leading to a loss of their protein-repellent properties [177, 197, 200]. Further disadvantages have been found, such as the triggering of hypersensitivity or an immune response, caused by toxic metabolites from PEG degradation or by impurities from the coating synthesis [187, 197]. These drawbacks of PEG and OEG modifications have provoked considerable research on the development of alternate protein-repellent coatings.
Emanating from PEG, a variety of other uncharged and hydrophilic polymers has been explored as nonfouling surface modifications. Among these are, for example, poly(2-hydroxyethyl methacrylate) (pHEMA), polyglycerols, polysaccharides, poly(2-oxazoline)s (POxs) as well as peptides and peptoids [177, 190, 197].

Even more important than these are coatings based on zwitterionic polymers, mainly polybetaines, such as phosphobetaines, sulfobetaines and carboxybetaines [190, 197, 201]. The betaine functionalities can be obtained by combining the functional groups on the same branch (separated by a spacer) or the zwitterionic functionality is obtained via a 1:1 ratio of positively and negatively charged groups in the SAM or polymer

(polyampholytes) [190, 201, 202]. Their resistance towards protein adsorption is based on the electrostatically induced hydration, leading to the formation of a hydration shell, which is more stable than that of coatings without charges (e.g. PEG) [130, 201]. The best results with respect to protein-repellency are obtained if the IEP of the coating is close to pH 7.4 [202] and can even be increased by introduction of fluorinated side chains [151]. A major advantage of carboxybetaine modifications in particular over PEG coatings is the availability of multiple carboxylic acid groups throughout the polymer, which can be utilized for further modification, e.g. for the tethering of antibodies [201, 203].

A further group of protein-repellent surface coatings is derived from molecules that are excluded from the protein surface in the respective ternary system (water - protein - cosolute) [194]. This behavior is observed for kosmotropes and osmolytes, which are thus suitable building blocks for protein-repellent surfaces, resulting in surface coatings with motifs, such as betaines (see previous section), taurine, TMAO or saccharides [154, 177, 194, 204].

A completely different approach towards nonfouling surfaces was chosen with the formation of superhydrophobic coatings. These rough surfaces exhibit very high contact angles ($\Theta > 150°$) and possess very small polar and dispersive components of the surface free energy [205, 206]. These features lead to strongly reduced interactions (also van der Waals interactions) between the surface and approaching proteins, reducing protein adsorption [205, 206].

5 Cell Adhesion

As also the behavior of cells on the novel surface functionalizations has been examined at the Department of Cell Biology at the Rostock University Medical Center in the scope of this thesis, an introduction to cell-surface interactions will be presented in the following.

5.1 Osteoblasts as Models for Cell Experiments

As the research in this thesis is directed towards the development of surface functionalizations for bone-contacting applications, such as dental implants or joint replacements, the investigation of cell-surface interactions was limited to bone cells, namely osteoblasts. Bone tissue is characterized by the complex interplay of mainly two cell types with opposing functions: osteoblasts and osteoclasts [11]. Osteoblasts stem from mesenchymal progenitor cells and are responsible for bone mineralization via production of the osteoid, a collagen-rich matrix, and its subsequent calcification [11]. Thus, they are vital for bone remodeling as well as osseointegration of a biomaterial [11, 207]. Due to their special function, a variety of specific markers can be used to study osteoblast behavior, such as the secretion of collagen I or osteocalcin as well as the activity of alkaline phosphatase [11, 208].
Studying cell behavior *in vitro*, two options are available: primary cells or permanent cell lines [209, 210]. While primary osteoblasts obtained from a donor are certainly the ideal option, they are associated with a variety of practical problems and restrictions, such as their variance in behavior depending on donor and isolation method [207, 208]. Thus, in many cases, immortalized cell lines are used as they are commercially available, allow comparison of different studies, are easy to cultivate and possess a stable phenotype, but they do not completely represent the behavior of primary cells [207, 209, 210].
In this study, the osteoblast-like cell line MG-63 was used. It is derived from the osteosarcoma of a 14 year old male and has been shown to be stable over the passage range P5-P30 [207, 211]. MG-63 cells are suitable for studying several cell properties, such as cell adhesion and integrin subunit expression [211], however they proliferate faster than primary osteoblasts [209]. Thus, they are appropriate for the investigation of cell-surface interactions up to one day [207].

5.2 Cell-Surface Interactions

In order to present a focused overview of the interaction of cells, namely osteoblasts, with a biomaterial surface, a short survey of the different steps of the adhesion process will be provided. The decisive step, the cell adhesion via specific cell-surface interactions, will be discussed in more detail with respect to its mechanism but also its dependence on the characteristics of the substrate surface.

5.2.1 Steps of Cell Adhesion

The process of cell adhesion is vital to most cells, such as osteoblasts, as they are anchorage-dependent. Hence, without attachment to a substrate, the cells cannot survive and undergo anoikis, i.e. apoptosis caused by lacking surface adhesion [29, 212]. The establishment of this necessary cell-surface interaction is divided into several phases, which are characterized by different demands for surface properties and are of course depending on each other [213]. Initially, a cell approaching the surface can be attached via non-specific interactions. This rapid but reversible attachment process is governed by physicochemical interactions, such as electrostatic interactions, and thus is strongly influenced by the properties of the surface [11, 213]. An attached cell can undergo actual cell adhesion via formation of specific cell-surface interactions. This much slower and more complex step mediates further processes and involves many different biomolecules, most importantly extracellular adhesion proteins [11, 213].
The quality of the cell-surface interactions regulates further processes, at first cell spreading and migration, followed by cell proliferation and differentiation [11, 213]. Here, a non-linear relation between adhesion strength and cell behavior can be observed. As essential as proper cell adhesion is for cell proliferation, very strong cell-surface interactions may have adverse effects and lead to reduced proliferation and quiescence [212]. After establishing contact with the surface, the behavior of the cells on the substrate is defined by the quantity and quality of gene expression and protein synthesis, a process again dependent on surface characteristics [11]. As the cell adhesion process via specific interactions is the determining step in cell-surface interactions, this stage will be presented in more detail in section 5.2.2.

In the complete process of cell-surface interactions, the role of proteins is heavily debated among researchers. Proteins adsorb immediately on the surface of a biomaterial, as soon as it is in contact with a body fluid, such as blood [11, 12]. The qualitative and quantitative composition as well as bioactivity of this protein layer depends on the properties of the surface, such as wettability and charge [12, 214]. Here, especially the presence of adsorbed extracellular matrix (ECM) proteins, most importantly

fibronectin and vitronectin, has a huge impact on the cell adhesion [11, 12]. No consensus, however, can be found regarding the question how strong the influence of this initial protein adsorption is on cell-surface interactions in general. Some researchers claim that the protein layer "translates" the surface properties into a biological system and thus the cell response mainly depends on the features of this protein profile [12]. Others emphasize the effect of both protein precoating and surface properties [11]. It was found, for instance, that cells can also adhere to surfaces in absence of proteins in the surrounding medium if they are able to synthesize their own ECM proteins fast enough [215]. In summary, the mediating effect of the initial protein layer on cell adhesion has been proven in many studies, but physicochemical features of the surface may also have a direct impact on cell-surface interaction.

5.2.2 Cell Adhesion via Specific Interactions

At the heart of cell adhesion is the specific interaction of cell receptors with the extracellular matrix (ECM) [12]. The ECM proteins of bone consist of 90% collagenic proteins (mainly type I collagen) and 10% non-collagenic proteins, such as osteocalcin, osteonectin and fibronectin [213]. Among these ECM proteins, especially fibronectin and vitronectin have been found to strongly promote osteoblast adhesion *in vitro* [213]. It must be mentioned, though, that the ECM is a dynamic system, which is constantly altered, as the cells themselves are able to remove, synthesize, secret or crosslink ECM proteins [185, 213]. The cell-adhesive properties of fibronectin, vitronectin and other ECM proteins are based on their interaction with cell membrane receptors, such as the integrins [185, 213]. Recognition usually occurs at comparably small protein sites, consisting of up to five amino acids [185]. The most known cell-binding motif is the tripeptide RGD (Arg-Gly-Asp), e.g. found in fibronectin and vitronectin [12, 185, 213].

The integrins themselves, belonging to the larger family of adhesion molecules, are transmembrane heterodimers, which are comprised of two non-covalently associated subunits [213]. The combination of these subunits (among at least 16 different α and 8 β subunits) defines the specificity of the integrin receptor towards the different ligand proteins [213]. Integrins consist of a large extracellular domain, interacting with the RGD motif, a transmembrane domain, transmitting information, and a small intracellular component [213]. At the sites of ECM-integrin interaction, focal contacts can be formed, junctions with a distance of 10–15 nm between cell and substrate surface [213]. Whereas the receptors, such as integrin, are exposed on the exterior side, the intracellular domain of the receptor molecules is associated with a variety of proteins, such as talin, vinculin and paxillin (see Figure 5.1) [213]. With these proteins, integrins can interact with the actin cytoskeleton as mechanotransducers [213, 214].

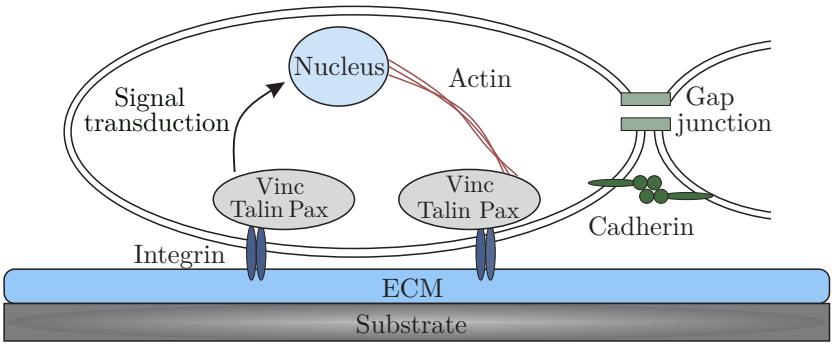

Figure 5.1: Scheme of the cell-cell and cell-surface interactions of a cell attached to a biomaterial substrate, according to [213]. ECM: Extracellular matrix, Pax: Paxillin, Vinc: Vincullin.

This way, cell spreading can promote cell proliferation not only via a biochemical intracellular signaling pathway but also via mechanical signal transduction [212]. Hence, the actin cytoskeleton itself is not only responsible for supporting the cell shape and adhesion in a passive manner, it also participates actively in modulating signal transduction, gene expression and cell function [213, 216]. The behavior of cells is strongly controlled by the cell-surface interactions, but it is also affected by soluble factors and cell-cell interactions [214]. Intercellular adhesion and communication is achieved via adherens junctions formed with cadherins as well as gap junctions [213].

5.2.3 Influence of Surface Properties on Cell-Surface Interactions

As described above, the interactions between a surface, adsorbed proteins as well as cells are rather complex [12, 213, 214]. Therefore, the following section will be focused on the impact of surface characteristics, directly or mediated via proteins, on cell attachment, adhesion and spreading, mainly omitting the effect on further processes.
Regarding physical parameters, surface roughness and topography on a micro- or nanoscale are known to affect cell behavior [214]. Both the scale as well as the spatial pattern seem to be relevant, although the effects are not completely understood yet [30, 212, 214]. Macroroughness ($> 100\,\mu m$) only seems to improve the anchorage of a bone-contacting implant in the surrounding tissue but not affect cell behavior [212]. In contrast to that, nanoscale roughness ($< 100\,nm$) mimics the roughness of natural bone (approximately 32 nm) and has been proven to support cell adhesion, growth and maturation [212, 217]. Contradictory results are obtained for surfaces with microroughness (between 1 and 100 µm) as both positive and negative effects on cell behavior have been reported [212]. In addition to that, substrate stiffness and mechanical load can be sensed by cells and influence, for example, cell adhesion and differentiation [212–214].

Furthermore, chemical properties affect cell-substrate interactions in a twofold way, either directly or via their influence on the amount, composition and conformation of adsorbed proteins, especially ECM proteins [12, 214]. At first, cells adhere preferentially to hydrophilic surfaces (contact angle $\Theta < 65°$), as a consequence of the adsorption of adhesion proteins [12, 213]. Preferential adsorption of vitronectin is observed for hydrophilic coatings, whereas fibronectin loses cell-adhesive functionality after adsorption to a hydrophobic surface [12]. Surface charge seems to affect cell adhesion both directly as well as indirectly. To begin with, positively charged surfaces facilitate initial cell attachment via attractive electrostatic interactions with the pericellular hyaluronan, a highly negatively charged glycosaminoglycan [31, 218]. Furthermore, the ECM protein fibronectin seems to adsorb preferentially to positively charged surfaces, promoting cell adhesion on them [12]. Not only surface hydrophilicity and charge influence cell behavior, but also the nature of the functional groups at the surface itself seems to have an effect on cell-substrate interactions as calcium phosphate coatings on implants have, for example, been shown to be osteoinductive [214].

One must exercise caution to transfer these results, mainly obtained from *in vitro* experiments, to the situation *in vivo* where the picture that is presented to the cells is possibly quite different. The main differences between laboratory experiments and the implantation site in terms of osteoblast environment are, for example, the presence of a fibrin network (due to blood clot formation) and the previous arrival of other cells, such as platelets and leukocytes, *in vivo* [12]. Thus, results from *in vitro* experiments cannot be simply translated to the *in vivo* situation, yet they provide valuable insight in the relation between surface characteristics and cell adhesion.

5.3 Adhesion-Promoting Surfaces – State of the Art

How a biomaterial surface is supposed to interact with cells, depends on its application. For dental implants and joint replacements, however, good osseointegration is a prerequisite for biofunctionality, requiring adhesion, proliferation and differentiation of bone cells on the material surface [12, 217].
In order to ensure that, two opposing approaches are available, either promoting the adsorption of supporting proteins and cells in an unspecific manner or immobilizing specific adhesion promoters [217].
The first procedure is usually based on the synthesis of hydrophilic and positively charged surfaces [212, 219] due to two different reasons. These surface properties do not only enhance the initial cell attachment due to attractive electrostatic interactions, but they also promote the adsorption of ECM proteins in an active conformation, as

described in section 5.2.3 [12, 31]. The best results were obtained for surfaces with amine groups as functional moieties, which were able to promote actin cytoskeleton formation, enhance cell function and upregulate the expression of osteoblast-specific genes [220, 221].

If cell attachment is desired, the immobilization of adhesion promoters is often necessary for surfaces with protein-repellent coatings (such as PEG or zwitterionic polymers) because these surfaces often also prevent cell adhesion [178, 203, 222]. The most straightforward approach is the covalent immobilization of ECM proteins, which support cell adhesion, such as collagen [25] or fibronectin [203]. This procedure, however, is associated with a variety of drawbacks. The protein may be changed in its conformation during the adsorption and thus provoke a foreign body response, or it may be subject to enzymatic degradation [25, 214]. Furthermore, isolation and purification of those proteins is rather costly [214].

Thus, in most cases, only short peptide domains are immobilized, which serve as binding sites for adhesion receptors such as integrin. Among those are the GFOGER peptide from collagen I or, most common, the tripeptide RGD [213, 222, 223].

6 Surface Properties and their Characterization

This last chapter of the fundamentals part is directed to the practical work. In the following, the basic principles behind the analysis techniques applied in this thesis will be explained.

6.1 Surface Composition – XPS

X-ray photoelectron spectroscopy (XPS), sometimes also called electron spectroscopy for chemical analysis (ESCA), is an experimental technique, which is broadly applied for the investigation of the elemental and chemical composition of a material surface [224, 225]. This method is based on the photoelectric effect, i.e. the sample is irradiated with usually monochromatic X-ray radiation under high vacuum conditions and the emitted core electrons are collected and analyzed. These electrons possess the following kinetic energy E_{kin} [224, 225]:

$$E_{kin} = h\nu - BE - \phi_s \tag{6.1}$$

The kinetic energy of the photoelectrons depends on the energy of the X-ray radiation ($h\nu$), the binding energy (BE) of the respective atomic orbital and the work function of the spectrometer ϕ_s [224]. In the corresponding spectrum, depicting the number of counted electrons per interval of kinetic energy, the peak positions provide qualitative information [224]. As each element is characterized by its specific set of binding energies, the different elements of the material surface can be identified [224]. Small deviations, so-called chemical shifts, are caused by the chemical state of the atoms and thus reflect the oxidation state or the functional group, the atom is part of [224, 225]. Quantitative information is gained from the peak height or area and can be used for the calculation of the surface composition [224].
It has to be mentioned here that XPS is a very surface-sensitive technique as the mean free path length of the emitted photoelectrons is very short [224]. Thus, XPS spectra only include information about the outer 10 nm of the material [224, 225], which makes XPS analysis a very useful tool in the investigation of surface coatings.

6.2 Detection of Amine Groups – Sulfo-SDTB Assay and Chloranil Test

6.2.1 The Sulfo-SDTB Assay for Primary and Secondary Amine Groups

The sulfo-SDTB assay, named after the sulfo-succinimidyl-4-O-(4,4'-dimethoxytrityl)-butyrate (sulfo-SDTB) molecule, was performed for the determination of the amounts of primary and secondary amine groups on surfaces.

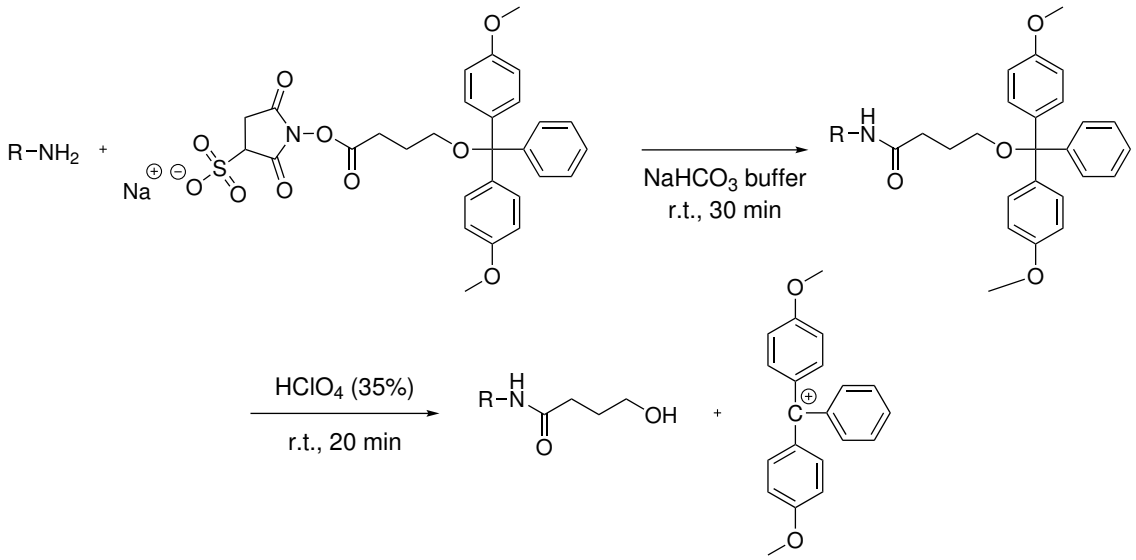

Figure 6.1: Scheme of the color-forming reaction during the sulfo-SDTB assay for amino group detection [226, 227].

Here, sulfo-SDTB molecules are bound to amine groups via formation of an amide bond under alkaline conditions. After removal of excess reagent, 4,4'-dimethyltrityl cations are released upon treatment with perchloric acid . These cations possess a molar extinction coefficient of $70\,000\,\mathrm{L\,mol^{-1}\,cm^{-1}}$ at 498 nm and can be quantified spectroscopically [226, 227].

6.2.2 Qualitative Analysis of Tertiary Amines via the Chloranil Test

As the sulfo-SDTB assay can only be used for the detection of primary and secondary amine groups, a different strategy is necessary to prove the presence of tertiary amine groups. In this case, the procedure was derived from the chloranil assay developed by Smith and Davis [228]. This assay can be used for the quantification of a variety of primary, secondary and tertiary amines in solution (aliphatic and aromatic) via formation of a strongly colored compound upon reaction with chloranil (tetrachloro-1,4-benzoquinone) (see Figure 6.2) [228].

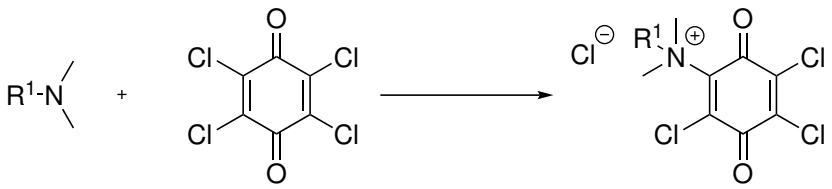

Figure 6.2: Scheme of the color-forming reaction in the chloranil assay via reaction of a tertiary amine with chloranil [228].

The reaction proceeds at room temperature in different organic solvents and leads to the development of a blue to purple color in usually less than one hour [228].

6.3 Wettability – Contact Angle and SFE

6.3.1 Static and Dynamic Contact Angles

If a small volume of liquid is brought into contact with a flat and solid surface, one of two possible scenarios can be observed: Either the liquid spreads completely over the surface or a stable droplet is formed on the solid surface [229]. This droplet is characterized by the contact angle Θ, which can be measured between the solid-liquid interface and the tangent at the three-phase boundary (solid-liquid-gas) (see Fig. 6.3) [230].

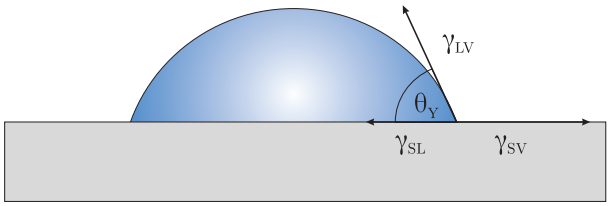

Figure 6.3: Static contact angle of a drop of liquid on an ideal surface in thermodynamic equilibrium, as described by Young's equation [230, 231].

For an ideal solid, the thermodynamic equilibrium can be described with Young's equation in terms of a balance between the interfacial tensions (solid-liquid γ_{SL}, liquid vapor γ_{LV}, solid-vapor γ_{SV}) (see equation 6.2) [230, 231]:

$$\gamma_{LV}\ cos\Theta_Y = \gamma_{SV} - \gamma_{SL} \tag{6.2}$$

This static equilibrium contact angle can be measured with a goniometer via the sessile drop technique [232]. According to the result obtained for measurements with pure water, surfaces can be categorized as hydrophilic ($\Theta < 90°$), hydrophobic ($\Theta > 90°$) or even superhydrophobic ($\Theta > 150°$) [230, 233]. In the context of protein adsorption, already contact angles above 65° ($\Theta > 65°$) are labeled as hydrophobic [187].

Young's equation, however, is only valid for ideal, i.e. smooth, homogeneous and rigid surfaces. In a real system, though, a single equilibrium angle Θ_Y cannot be measured [234]. Instead, stable contact angles Θ can be found in a certain range. Here, the advancing angle Θ_a, obtained at the newly formed three-phase boundary of the advancing droplet, constitutes an upper limit. The receding angle Θ_r is the lower limit and obtained if the droplet is retracted from the surface [229, 234]:

$$\Theta_r < \Theta_Y < \Theta_a \tag{6.3}$$

Yet, in many cases, the advancing angle Θ_a can be regarded as a good approximation for the equilibrium contact angle Θ_Y [231, 235]. In other calculations, the following relation between the equilibrium angle and the advancing and receding angle is proposed [236, 237]:

$$\Theta_Y = \frac{1}{2}\left(\Theta_a + \Theta_r\right) \tag{6.4}$$

The difference between advancing and receding angle is defined as contact angle hysteresis H [230]:

$$H = \Theta_a - \Theta_r \tag{6.5}$$

Contact angle hysteresis can be the consequence of a variety of causes, which can be divided into two groups. Surface roughness and chemical inhomogeneities as well as configuration changes lead to thermodynamic hysteresis, which is constant with time throughout the experiment. Dynamic processes, such as the swelling or deformation of the surface as well as adsorption and desorption processes, cause a time-dependent change in hysteresis and are thus attributed to kinetic hysteresis [229, 230, 236].

6.3.2 Dynamic Contact Angle Measurement

In order to measure dynamic contact angles, a huge variety of techniques is available, which determine contact angles either directly via optic methods or indirectly via force-based measurements. These methods comprise, for example, tilting plate, sessile drop, capillary rise and Wilhelmy balance technique [233]. As the latter one was applied in this thesis, it will be discussed in detail below. The Wilhelmy balance technique was first introduced by Ludwig Wilhelmy in 1863 [238] and it is based on the immersion of a regularly shaped sample in the probe liquid (see Figure 6.4) [230].

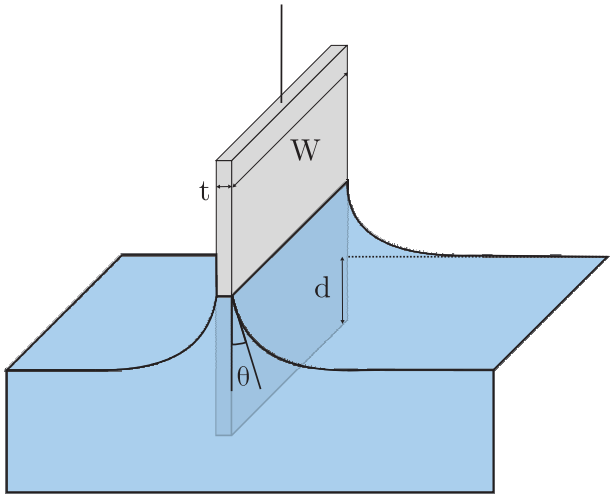

Figure 6.4: Graphic illustration of the Wilhelmy plate method [233] (W: width of the plate, t: thickness of the plate, d: immersion depth, Θ: contact angle).

The total force exerted on a rectangular sample, which is measured with an electrobalance, is described by the following equation [236]:

$$F = F_g + F_b + F_W = mg - \rho g t W d + L\gamma_{LV} \cos\Theta \tag{6.6}$$

Thus, the total force can be regarded as the sum of the gravitational force of the sample F_g, the counteracting buoyancy force F_b and the Wilhelmy force F_W. Here, m describes the mass of the plate, g the gravitational acceleration and ρ the density of the probe liquid. The dimensions of the sample are defined by its thickness t, width W and the resulting perimeter L ($L = 2t + 2W$) [236, 239].
Resetting of the balance before immersion into the liquid, leads to elimination of F_g, simplifying equation 6.6 to [236]:

$$F = F_b + F_W = -\rho g t W d + L\gamma_{LV} \cos\Theta \tag{6.7}$$

For the calculation of the advancing and receding contact angles Θ_a and Θ_r, force-immersion $F(d)$ cycles are recorded via repeating immersion and emersion of the sample in the probe liquid. The linear parts of the force-immersion lines are then extrapolated to zero immersion depth (d = 0) in order to eliminate the contribution of buoyancy. Advancing angles are obtained from immersion runs and receding angles from emersion runs [230, 236] of each Wilhelmy force loop. The contact angles can then by obtained via [230]:

$$\cos\Theta = \frac{F}{L\gamma_{LV}} \tag{6.8}$$

Compared to other techniques for the determination of dynamic contact angles, the Wilhelmy balance technique offers a variety of advantages. At first, it is a highly accurate, operator-independent method, which allows the study of dynamic processes as well if cycled measurements are performed. As a consequence of the instrumental geometry, the large volume of probe liquid reduces the risk of errors due to contamination of the liquid. In addition to that, one measurement itself contains averaged results as the complete perimeter of the sample is measured at once [230, 233, 240]. The requirements for the sample geometry, however, also represent the major drawback of this method. It is vital, that the sample possesses a regular shape and a known diameter as well as the same surface properties on all sides [240].

6.3.3 Surface Free Energy (SFE) Calculation

Measured contact angles can be utilized to obtain an estimation of the surface free energy (SFE) γ_{SV} of the solid. As it can be seen, though, from Young's equation (see equation 6.2), only the contact angle Θ and the surface tension of the liquid γ_{LV} are accessible via experiments [229, 241]. In order to obtain γ_{SV}, a relation between γ_{SV} and γ_{SL} has to be derived [231].
For that purpose, Fowkes introduced the approach to describe the surface tensions as sums of different components, which account for the different types of intermolecular forces [235]. This idea was continued by Owens and Wendt as well as van Oss, Chaudhury and Good, finally leading to the Lifshitz-van der Waals/acid-base (LW/AB) approach, which was used in this thesis and thus will be presented in detail [241]. In the LW/AB theory, surface tensions are split up in a Lifshitz-van der Waals component γ^{LW} and a component γ^{AB} summarizing hydrogen bond-based interactions [235, 241]. The first constituent γ^{LW} consists of dispersion (London), induction (Debye) and orientation (Keesom) interaction. The latter term comprises both electron acceptor, i.e. Lewis acid properties (γ^+) as well as electron donor, i.e. Lewis base properties (γ^-) [235, 241]:

$$\gamma = \gamma^{LW} + \gamma^{AB} = \gamma^{LW} + 2\sqrt{\gamma^+\gamma^-} \tag{6.9}$$

For an apolar substance, both γ^+ and γ^- are negligible. If only one term has to be considered, the substance is monopolar, for bipolar substances both terms are appreciable [235, 241].
Applying equation 6.9, the following expression can be derived for γ_{SL} [231, 241]:

$$\gamma_{SL} = \left(\sqrt{\gamma_{SV}^{LW}} - \sqrt{\gamma_{LV}^{LW}}\right)^2 + 2\left(\sqrt{\gamma_{SV}^+\gamma_{SV}^-} + \sqrt{\gamma_{LV}^+\gamma_{LV}^-} - \sqrt{\gamma_{SV}^+\gamma_{LV}^-} - \sqrt{\gamma_{SV}^-\gamma_{LV}^+}\right) \tag{6.10}$$

Introducing this expression into Young's equation (equation 6.2) leads to [235, 241]:

$$\gamma_{LV}\,(1 + cos\Theta) = 2\left(\sqrt{\gamma_{SV}^{LW}\gamma_{LV}^{LW}} + \sqrt{\gamma_{SV}^{+}\gamma_{LV}^{-}} + \sqrt{\gamma_{SV}^{-}\gamma_{LV}^{+}}\right) \tag{6.11}$$

In this case (determined case), measurements have to be performed with three different liquids with known surface tension components and the resulting set of three equations has to be solved in order to obtain γ_{SV}^{LW}, γ_{SV}^{+} and γ_{SV}^{-} [235, 241]. Attention has to be paid with respect to the choice of liquids. Ideally, one apolar and two monopolar liquids of opposite signs are used, but also measurements with one apolar liquid and two bipolar liquids were found to yield good results [241, 242].

At last, some general remarks have to be made with regard to the interpretation of the surface free energies, obtained from the aforementioned calculations. If very precise results are needed, more advanced analysis can be performed. Instead of data from measurements with three liquids, a larger set of contact angle data can be used for instance. In this "overdetermined" case, no exact solution can be found, but a set of surface free energy components can be determined, for which minimal deviations are obtained in all equations [242].
Additionally, a remark on the relation between the Lewis acid and Lewis base parameter (γ^+ and γ^-) is necessary. They were arbitrarily set to be equal for water ($\gamma_{H_2O}^{+} = \gamma_{H_2O}^{-}$) [235]. All other components γ^+ and γ^- originate from this definition and the resulting scale. Thus, comparisons can just be made among components of the same kind, i.e. either among acidic or basic components [242].
In summary, the determination of the surface free energy of a solid is far from trivial and depends on a variety of parameters, such as the nature of the measured contact angles, the choice of liquids and the model applied for calculation [241]. In any case, the obtained results should be dealt with care.

6.4 Surface Charge – Zeta Potential

Immersion of a solid in an electrolyte solution usually leads to the generation of a charged interface [243]. Processes responsible for charge formation are, for example, the adsorption or desorption of lattice ions, preferential adsorption of solutes or formation of charged surface groups (e.g. via dissociation) [243]. As electroneutrality of the complete system is required, the surface charge is compensated via accumulation of counterions from the solution in the liquid phase. The system, that is formed this way, is termed electric double layer (EDL), although it usually is far more complex than a simple double layer [243, 244].

6.4.1 The Composition of the EDL

The different layers of the EDL, the ion distribution and the corresponding potential for a negatively charged surface are depicted in Figure 6.5.

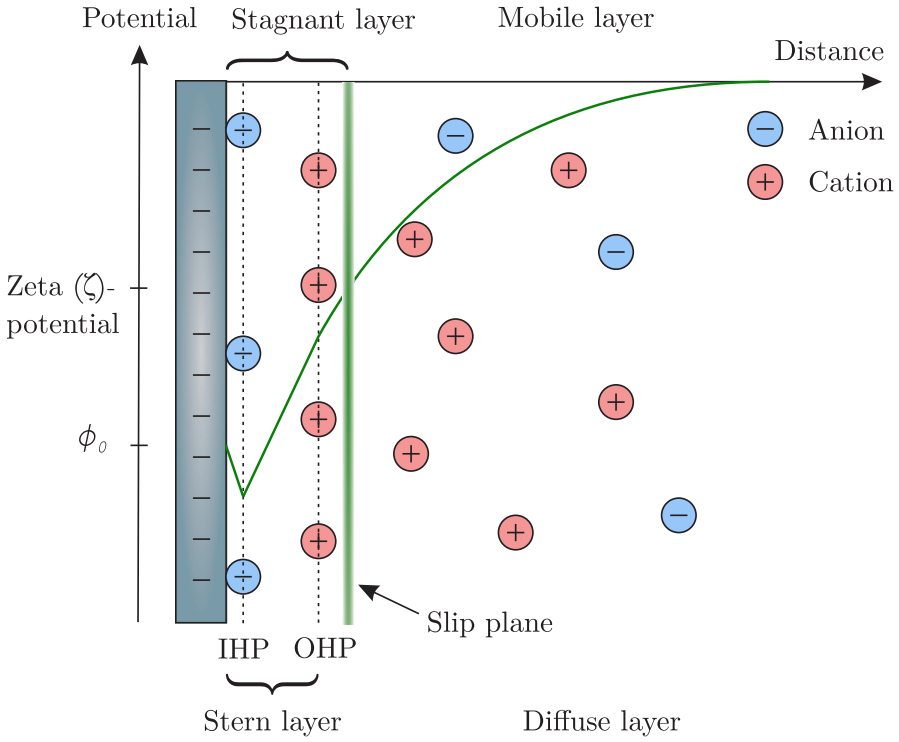

Figure 6.5: Schematic representation of the EDL and the corresponding potential $\phi(d)$ at a negatively charged surface, according to the Gouy-Chapman-Stern-Grahame model [243, 245]. IHP: inner Helmholtz plane; OHP: outer Helmholtz plane.

This schematic illustration describes the EDL according to the Gouy-Chapman-Stern-Grahame model [245], which comprises the following parts in the direction from the surface to the bulk solution.

The inner Helmholtz layer (IHL) is located between the surface and the inner Helmholtz plane (IHP). It requires a separate description as it is characterized by the specific adsorption of ions, usually anions, not only via Coulomb interactions but via their chemical affinity to the surface. Between the IHL, positioned at the center of these adsorbed ions, and the outer Helmholtz plane (OHP), hydrated counterions are rigidly adsorbed via electrostatic interactions (indifferent ions) and form the outer Helmholtz layer (OHL). The IHL and OHL together are often labeled as Stern layer and are characterized by a linear change of the potential ϕ with increasing distance d from the surface, starting at the surface potential ϕ_0. The OHP marks the boundary of the diffuse layer, which extends into the bulk solution and is characterized by mobile ions. Due to the opposing effects of Coulomb interactions and thermal motion, an exponential decay in counterion concentration is observed. Accordingly, the potential in the diffuse layer decreases exponentially as well and can be described with the Poisson-Boltzmann

equation [243, 245–247]. For further reading about the theoretical derivation of the distance-dependent potential, the reader is referred to literature (for example [248]). Starting from this quiescent situation, a tangential flow of liquid can be introduced. In this case, the diffuse layer containing the mobile ions is sheared off, while only a thin layer, the hydrodynamically stagnant layer, remains adhered to the surface. The boundary between the remaining stagnant layer and the removed layer is the (hydrodynamic) slip plane, the associated potential the zeta (ζ) potential. The slip plane is close to but usually does not coincide with the OHP, whose actual potential is not accessible experimentally [243, 245, 246]. Notwithstanding, the zeta potential is a key property of macroscopic surfaces as it can be determined with a variety of electrokinetic techniques and represents the quantity determining the electrostatic interactions with its environment [245, 246].

6.4.2 Techniques for Zeta Potential Determination

The zeta potential of a surface can be determined via a variety of techniques, which can be categorized according to their sample geometry and the driving force used for signal generation. In general, samples can either be macroscopic (and thus immobile) or mobile particles. Driving forces can either be an applied electrical field or a mechanical force (pressure, gravitation) [246, 249]. The methods resulting from the available combinations of geometry and driving force are summarized in Table 6.1.

Table 6.1: Summary of the main electrokinetic effects used for the determination of the zeta potential, distinguished according to the mobility of sample surface and the applied driving force [249].

		Charged surface	
		Stagnant	Mobile
Driving force	Electrical field	Electro-osmosis	Electrophoresis
	Mechanical driving force	Streaming current/potential	Sedimentation potential

As only electrophoresis and streaming current measurements (marked in blue in Table 6.1) were used in this thesis, only these techniques will be presented in the following.

6.4.3 Electrophoresis

If a charged colloidal particle is suspended in an electrolyte solution, application of an external electrical field initiates movement of the particle towards the electrode of opposite sign. Rapidly, a steady state between the accelerating force exerted by the electric field and the opposing Stokes friction is observed [243, 246, 249]. This way, the

electrophoretic mobility u_e, i.e. the particle velocity v_e divided by the applied electrical field E [246]

$$u_e = \frac{v_e}{E} \tag{6.12}$$

can be related to the zeta potential ζ of the particle. Here, different scenarios have to be distinguished, which differ in the particle size (expressed via the curvature radius a) and the thickness of the EDL, which can be decribed by the Debye length κ^{-1} [243, 249]. The Debye length κ^{-1} increases, e.g. with decreasing electrolyte concentration, and is defined as follows [243]:

$$\kappa^{-1} = \sqrt{\frac{\epsilon_r \epsilon_0 k_B T}{2 I e^2 N_A}} \tag{6.13}$$

Here, ϵ_0 describes the electric permittivity of vacuum, ϵ_r the relative permittivity of the electrolyte solution, k_B the Boltzmann constant, T the thermodynamic temperature, I the ionic strength of the electrolyte solution, e the elementary charge and N_A the Avogadro constant. If κa is small ($\kappa a < 1$, with a being the curvature radius), then the Hückel(-Onsager) equation is valid and the relation between electrophoretic mobility u_e and zeta potential ζ can be described as [246] (with the dynamic viscositiy of the liquid η):

$$u_e = \frac{2}{3} \frac{\epsilon_0 \epsilon_r}{\eta} \cdot \zeta \tag{6.14}$$

For $\kappa a \gg 1$ (usually $\kappa a > 20$) the Helmholtz-Smoluchowksi equation is valid [246]:

$$u_e = \frac{\epsilon_0 \epsilon_r}{\eta} \cdot \zeta \tag{6.15}$$

If κa is in an intermediate regime, the relation between u_e and the zeta potential can be described with Henry's formula [246]:

$$u_e = \frac{2}{3} \frac{\epsilon_0 \epsilon_r}{\eta} \cdot \zeta \cdot f_1(\kappa a) \tag{6.16}$$

with the function f_1 transitioning smoothly from 1.0 (for small κa) to 1.5 (for large κa) [246].
In this thesis, a 1:1 electrolyte (concentration $1\,\mathrm{mmol\,L^{-1}}$) was used. Thus, the following Debye length was estimated:

$$\kappa^{-1} = \sqrt{\frac{80 \cdot 8.85 \cdot 10^{-12}\,\mathrm{A\,s\,V^{-1}\,m^{-1}} \cdot 1.38 \cdot 10^{-23}\,\mathrm{V\,A\,s\,K^{-1}} \cdot 298\,\mathrm{K}}{2 \cdot 1\,\mathrm{mol\,m^{-3}} \cdot (1.60 \cdot 10^{-19}\,\mathrm{A\,s})^2 \cdot 6.02 \cdot 10^{23}\,\mathrm{mol^{-1}}}} \approx 9.7\,\mathrm{nm} \tag{6.17}$$

Taking into account the radius of the measured particles (500 nm), κa is approximately 50. Therefore, the Helmholtz-Smoluchowski equation (equation 6.15) can be applied for zeta potential calculation.
In this thesis, the zeta potential of charged, functionalized particles was determined via laser Doppler velocimetry. This technique relies of the detection of light, scattered by the moving particles, and the analysis of the resulting autocorrelation function [246]. It is broadly applicable as long as some basic requirements are fulfilled as the liquid phase has to be transparent and possess a refractive index different from the particles [246].

6.4.4 Streaming Current Measurement

For these measurements, the charged surface is stagnant and a tangential movement of the liquid phase is achieved via a pressure gradient [246]. A streaming current can then be obtained via measuring the electric current in direction of the fluid movement with an electrometer of low internal resistance. A streaming potential measurement can be carried out via detection of the built-up potential difference with an high-input impedance voltmeter [246, 250]. This technique is applicable for a variety of macroscopic surfaces in different geometries, such as capillaries, parallel-plate microchannels and fiber bundles, as long as these samples are chemically and mechanically stable under the experimental conditions [244, 246]. Thus, streaming current measurements have gained increasing popularity because many samples can easily be prepared on flat surfaces and can additionally be characterized with other analytical techniques (e.g. XPS, contact angle measurements) in this geometry [250].
For a microchannel setup with parallel plates (length L, width b, channel height h), the following relation between the measured streaming current I_{str} and the zeta potential ζ can be derived for a fixed pressure gradient Δp in the Helmholtz-Smoluchowksi regime [244, 246, 250]:

$$\zeta = -\frac{\eta}{\epsilon_0 \epsilon_r} \frac{I_{str}}{\Delta p} \frac{L}{hb} \tag{6.18}$$

From a streaming potential U_{str} measurement, the zeta potential can analogously be obtained via [246]:

$$\zeta = \frac{\eta}{\epsilon_0 \epsilon_r} \frac{U_{str}}{\Delta p} \cdot K_L \tag{6.19}$$

where K_L is the electrical conductivity of the bulk liquid [244, 246]. A more detailed derivation for streaming current and streaming potential measurements can be found in literature [244, 250].

6.4.5 Challenges in Zeta Potential Determination

In many cases, the calculation of the zeta potential of a sample from the measured quantity (such as the electrophoretic mobility or the streaming potential) is not as straightforward as it can be presumed from the equations presented above (equations 6.15, 6.18 and 6.19).

At first, in many cases, the surface conductivity K^{σ} has to be taken into account [244, 246, 250]. This excess quantity is the consequence of the accumulation of charged species in the EDL and thus may be significantly higher than the bulk conductivity K_L [244, 246, 250]. In order to avoid erroneous calculation of the zeta potential, the influence of the surface conductivity can be introduced in the respective equations via the so-called Dukhin number (see literature [246, 250]). The surface conductivity can only be neglected under certain circumstances, which include, for example, rather low values of the zeta potential and $\kappa a \gg 1$ [246].

In addition to that, measured samples are often non-ideal surfaces. The description of electrokinetic phenomena, though, relies on surfaces which are smooth (even at a molecular scale), non-porous, chemically homogeneous and rigid, i.e. they are not deformed under the applied shear [246]. These requirements are usually not met by real samples, such as hard particles with adsorbed polymer chains. Via application of the respective equations, a zeta potential can still be derived from the measured quantities, however, one should be aware that this "effective" zeta potential is probably only of practical value, but it does not reflect the actual electrostatic potential [246].

Summing up, the quantitative interpretation of the data obtained from electrokinetic experiments is often rather difficult and requires elaborate treatments. Without those, the calculated ζ-potentials must not be used for further thermodynamic calculations. The obtained values, however, can be used for the determination of the isoelectric point and serve as an estimation of the sign and magnitude of the electrostatic interactions [246].

6.5 Quantitative and Qualitative Protein Adsorption

6.5.1 Quantitative Protein Adsorption – BCA Assay

In order to quantify proteins, a variety of different techniques is available today, among them several colorimetric methods with different advantages and disadvantages [251]. The bicinchoninic acid (BCA) assay, used in this thesis, has gained major importance due to its insensitivity towards interference by most of the commonly used surfactants and buffer salts [251, 252].

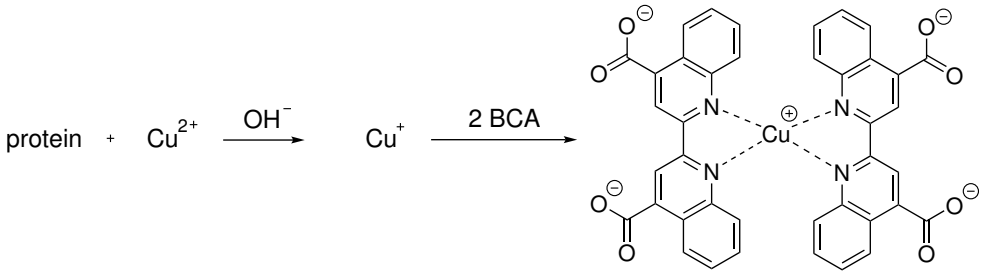

Figure 6.6: Illustration of the formation of the colored Cu^+-BCA complex [252]

Via the Biuret reaction, Cu^{2+} ions are reduced to Cu^+ ions under alkaline conditions in a redox reaction with the protein. These ions form a stable, water-soluble and purple complex with two molecules of BCA, which then strongly absorbs at 562 nm [251, 252].

6.5.2 Analysis of Qualitative Protein Adsorption

Adsorption of proteins from biofluids (saliva and serum) on SAMs with different functional groups was studied at the Department of Oral Biology at the State University of New York (Buffalo, NY, USA) via gel electrophoresis and subsequent western blotting. Thus, the basic concepts of these two methods will be summarized in the following.

Protein Separation – SDS-PAGE

In research, it is often necessary to separate proteins of a complex mixture according to certain properties. One of the most common techniques to do so is electrophoresis, which exploits the fact that proteins carry a net charge unless the pH is identical to their IEP [253, 254]. Thus, they are accelerated in an electric field [254] and, soon after, move with constant velocity due to the force balance between the electrical force F_e and the opposing friction force F_r [254]. Here, the mobility of the protein depends on its charge, size and shape [253]. Further factors influencing protein migration are, for instance, the composition of the buffer system (pH, ionic strength), the strength of the applied electrical field as well as the properties of the carrier system, e.g. its pore size [253, 254].

Among these electrophoretic separation techniques, the most common one is the gel electrophoresis with a polyacrylamide gel (PAGE), which is prepared via radical poly merization of acrylamide with a bifunctional linker (usually N,N'-methylenebisacrylamide) and catalyzed with N,N,N',N'-tetramethylethylenediamine (TEMED) and ammonium peroxodisulfate [253, 254]. Variation in the ratio between acrylamide and crosslinker allows control over the pore size of the gel [253, 254]. This way, also gels with a pore size gradient can be generated in order to separate proteins over a large range of molecular masses (e.g. 6–250 kDa) with improved resolution [254].

Performing a native gel electrophoresis, i.e. separating native proteins with intact secondary, tertiary and quaternary structure, the separation of the proteins depends on their charge, size and structure, complicating the analysis and interpretation of the results [254]. Separation by only one protein feature – their molecular weight – is achieved with the help of the detergent sodium dodecyl sulfate (SDS) [254]. This system was first described by Laemmli in 1970 for the separation of virus proteins [255]. In this case, proteins are denatured prior to separation when they are heated in the presence of SDS and a reducing agent, such as β-mercaptoethanol or dithiotreitol (DTT). This way, disulfide bridges are broken and the proteins lose their tertiary and quaternary structure [254]. As approximately 1.4 g SDS bind to 1.0 g of protein, overall negatively charged complexes are formed, overruling the intrinsic protein charge completely [254]. This leads to an approximately constant charge to mass ratio for all proteins, allowing separation only by protein molecular weight (see Figure 6.7) [254].

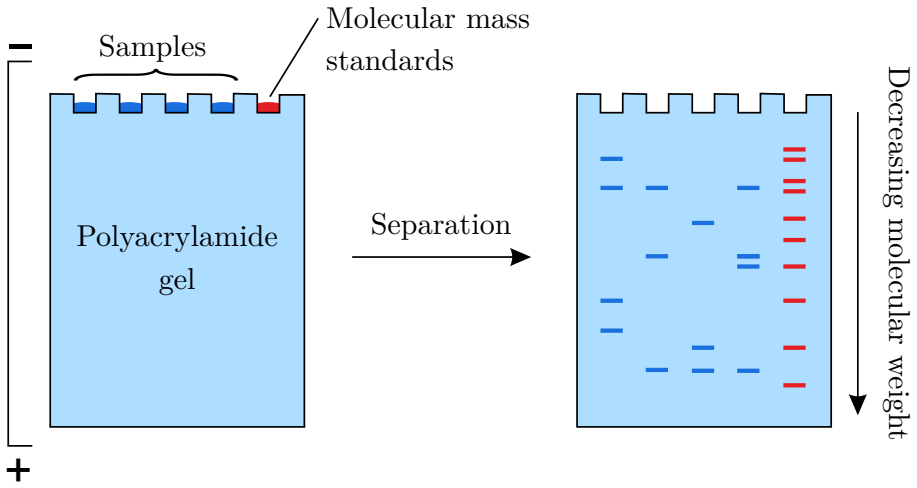

Figure 6.7: Schematic of a SDS-PAGE with a molecular weight standard (red) for the separation of proteins according to their molecular weight [254, 256].

Apart from the separation by molecular weight, proteins can also be separated by their isoelectric point via isoelectric focusing. Furthermore, SDS-PAGE and isoelectric focusing can be combined in a two-dimensional (2D)-electrophoresis [254].

After performing the electrophoresis, the separated proteins are usually visualized via staining in the gel. In most cases, the blue-colored sulfonated triphenylmethane dye Coomassie Brilliant Blue (CBB) is used, which interacts non-covalently with proteins via electrostatic interactions, namely with the basic amino acids arginine, lysine and histidine, as well as via hydrophobic interactions with aromatic side groups [257]. This staining techniques is easy to perform, but it also suffers from some disadvantages: It is rather time-consuming as several staining and destaining steps have to be performed and possesses only moderate sensitivity [254, 257]. This issue is overcome by the silver staining, which exhibits an approximately 10-100-fold higher sensitivity than the CBB staining [258]. In this method, Ag^+ ions are complexed by glutamic acid, cysteine and arginine, and subsequently reduced to elemental silver with formaldehyde [254]. Also fluorescent stains or negative staining, e.g. with the zinc/imidazole system, can be used [254]. In addition to that, it is possible to specifically stain proteins with post-translational modifications, such as phosphorylation or glycosylation [254, 257]. Glycoproteins are commonly visualized via the periodic acid-Schiff (PAS) stain [254, 257]. Here, vicinal hydroxyl groups are oxidized with periodic acid, the resulting aldehyde groups react with Schiff's reagent and generate red-colored protein bands [254, 257].

Protein Identification – Western Blot

After performing SDS-PAGE, the pattern of separated proteins can be stained via colorimetric or fluorescent methods [257]. In order to identify single proteins, however, the separated proteins are transferred onto a membrane (blotting) and subsequently visualized via immunostaining [256, 259].
This blotting technique for proteins was independently developed by three research groups around the year 1980 [256, 260]. It was named "western blot" in order to emphasize the resemblance to the Southern blot for the transfer of fractionated DNA [260, 261]. Since then, it has evolved into one of the most applied tools in protein characterization as it allows the identification and semi-quantitative analysis of single proteins from complex mixtures [256, 259, 260].
In the blotting step, the proteins are transferred from the separation gel onto a membrane [259]. As membrane materials usually nitrocellulose or polyvinylidene fluoride (PVDF) are chosen [256, 259]. The protein transfer can be achieved by diffusion or, in most cases, electrophoretically in an immersion or semi-dry method [256, 259]. In electroblotting, the membrane and the gel are placed next to each other between filter papers in a sandwich-like structure and the proteins are transferred via application of an electric field perpendicular to the gel surface (see Figure 6.8) [259]. As a result, an exact replica of the protein pattern of the gel is obtained [256].

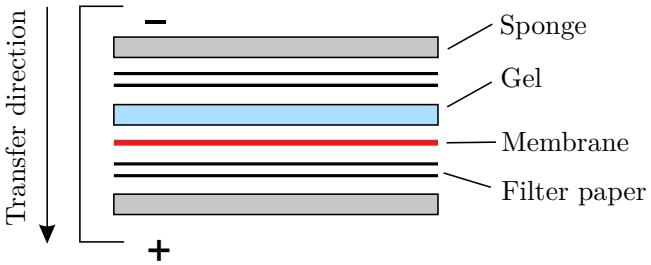

Figure 6.8: Scheme of the transfer of proteins onto a membrane via electroblotting (western blot) [256, 259].

After protein transfer, the visualization of the target proteins is usually achieved via indirect immunostaining. After checking for homogeneous transfer, the membrane is treated with protein solution (BSA or non-fat milk powder). This way, unspecific interactions of the antibodies with the membrane in the next step are prevented [256, 259]. After that, the membrane is incubated with the primary antibody, which binds to antigens of the protein of interest [256, 259]. Here, monoclonal or polyclonal antibodies can be used. The former, however, might suffer from the disadvantage that they do not bind to the protein if the target epitope is denatured and cannot be recognized by the antibody [256, 261]. After rinsing, the membrane is exposed to the labeled secondary antibody in the next step, which binds to the primary antibody [256, 259, 262]. Detection of the secondary antibody and thus the target protein is commonly achieved via chemiluminescene [256, 262]. Thereto, the secondary antibody is conjugated with the enzyme horseradish peroxidase (HRP), which catalyzes the oxidation of luminol in the presence of hydrogen peroxide [262]. The emitted light of the chemiluminscence can be recorded via a CCD camera or can be captured on a film (Figure 6.9) [262].

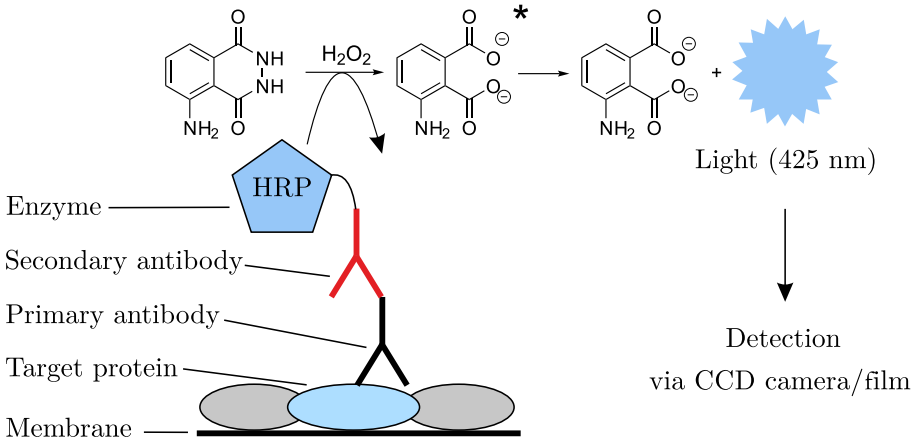

Figure 6.9: Schematic of the chemiluminescence reaction and its detection in the indirect western blot (HRP: horseradish peroxidase) [256, 262].

Alternatively, tagging of the secondary antibody with a fluorescent label is a frequently applied detection method, too. This technique is rapid, rather easy and has been applied in the analysis of adsorbed saliva or serum proteins presented in this thesis [256, 262].

6.6 Cell Behavior – Microscopic Techniques

In cooperation with the Department of Cell Biology at the Rostock University Medical Center, the behavior of osteoblastic cells was studied on selected surface modifications with different tools. In the scope of this thesis, not all of them can be introduced in the following. As confocal laser scanning microscopy may not be as familiar to the chemist as scanning electron microscopy (SEM), this technique as well as the required labeling procedures will be presented here.

6.6.1 Confocal Laser Scanning Microscopy

Confocal laser scanning microscopy (CLSM) is currently one of the most important techniques in biological research [263, 264]. This tool can be applied for the visualization of fixed or living tissue via labeling with fluorescent tags [264].
The development of this technique was motivated by the drawbacks of conventional wide-field fluorescence microscopy, in which the complete sample is illuminated at once. Here, not only light from the focal plane is recorded, but instead also out-of-focus fluorescence is detected. The resulting blurring of the image decreases image contrast and limits resolution, especially for thick samples [263, 264].
This problem has been solved in a confocal microscope, which only detects fluorescence from the plane of interest but not light from above and below via introduction of two aligned, i.e. confocal pinholes [263, 264]. The set-up of a confocal laser scanning microscope is depicted in Figure 6.10.

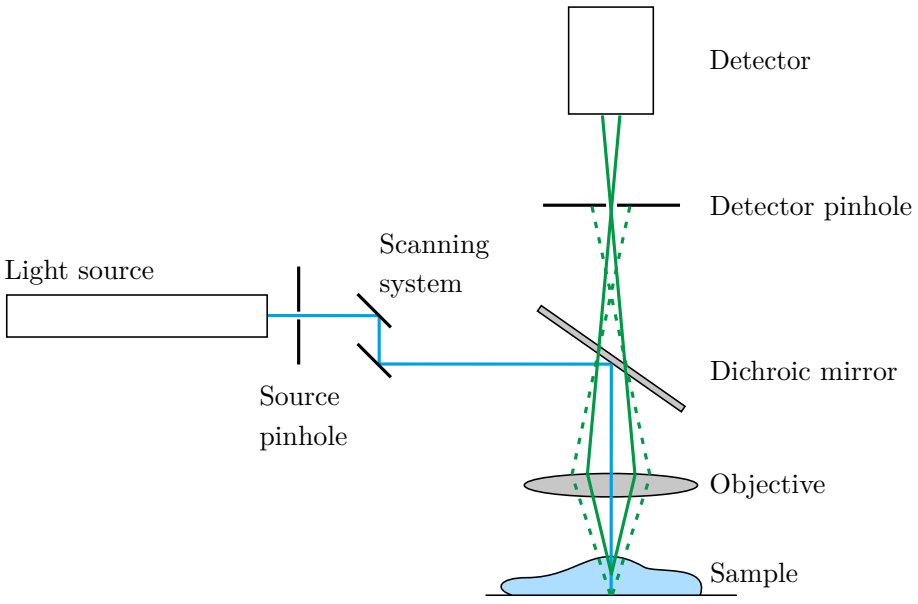

Figure 6.10: Schematic of a confocal laser scanning microscope [263, 264].

The light, necessary for the excitation of fluorescence in the sample, is generated by a light source and passed through a pinhole for point illumination [263, 264]. Today, usually lasers (or laser diodes) are used because they allow illumination of a small spot of the focal plane and good penetration into thicker samples [263]. The focused laser light then passes the scanner. Here, the excitation light is positioned via a galvanometer-driven mirror system or an acusto-optical device. Scanning across the stationary sample results in a complete image of the plane of interest [263, 264]. The light is then reflected by a dichroic mirror and focused on the sample by an objective [263, 264]. Here, objective properties, such as magnification, type of correction and numerical aperture, strongly influence the quality of the obtained image, e.g. its resolution, and therefore the objective must be chosen appropriately [263, 264]. Hitting the sample, the light beam excites fluorescence in the focal plane but also above and below it. This fluorescence light, possessing a higher wavelength, is able to pass the dichroic mirror and hits the second pinhole [263]. Only light emitted from the plane of interest can pass and no out-of-focus fluorescence light can reach the detector as this pinhole is in confocal alignment with the first pinhole [263, 264]. Passing the second pinhole, the in-plane fluorescence is usually detected with a photomultiplier tube (PMT) [263, 264].

In comparison with other techniques, CLSM possesses a variety of advantages and disadvantages. Compared to SEM, another common tool for cell imaging, CLSM needs less sample preparation and is non-invasive. Thus, it is suitable for imaging of living tissue. CLSM, however, yields images of significantly lower resolution [263]. Due to Abbé's limit, a resolution of 200 nm can be achieved in x-y direction, the vertical resolution (in z-direction) is only 400-500 nm [263, 264]. The complex confocal setup allows the imaging of three-dimensional samples ($< 100\,\mu m$), but it can also be the reason for significant signal loss [263]. Further disadvantages are the risk of photobleaching or phototoxicity (with living specimens) as well as the rather slow data acquisition (often approximately one frame per second) [263, 264].

As already indicated, these confocal laser scanning microscopes can not only be used for 2D imaging. Instead, time-lapse imaging as well as the acquisition of three-dimensional representations (or combinations thereof) are possible [264]. CLSM has also been combined with other techniques (correlative microscopy) or refined, leading to the development of multifocal or multiphoton microscopy [263, 264].

6.6.2 Fluorescent Labeling

In order to visualize organelles or structural elements of cells, a variety of fluorescent labels is nowadays available [264]. They all have to meet a variety of requirements, such as suitable excitation and emission wavelengths in combination with sufficient brightness (high absorption coefficient and high quantum yield) [265]. In addition to that, the fluorophores are, for instance, also supposed to be soluble in the respective solvent, stable, well-characterized and non-cytotoxic [265].

These demands are predominantly met by three types of fluorophore systems. The first group consists of molecule-based fluorophores, such as organic dyes and metal-ligand complexes [265]. Their optical properties as well as further characteristics, e.g. their solubility, can be tuned by functionalization via organic synthesis [265]. They are small and commercially available in broad variety but usually do not possess intrinsic affinity for the target (protein) [266]. In addition to molecular, also nanocrystalline systems (mainly quantum dots) can be applied [265]. They are characterized by favorable optical properties but suffer from a variety of disadvantages, such as their large size and their potential toxicity [265, 266]. The last and completely differing group consists of fluorescent proteins, the most prominent among them being the green fluorescent protein (GFP) [263, 266].

As already mentioned previously, fluorescent labels often lack affinity towards the intended target structure [266]. Thus, they are often attached to a carrier with specificity for the respective cell structure. In this context, immunolabeling is a frequently used technique for protein visualization [266]. As already described in the previous section for the western blot (see section 6.5.2), the protein of interest is at first targeted by a primary antibody, followed by the immobilization of a secondary antibody carrying the fluorophore [266]. Completely different is the principle of genetic targeting. Here, the DNA for a fluorescent protein or a genetic tag is transfected and expressed in the cell. The labeling is thus very precise and can be used for live-cell imaging [266].

In many cases, however, the dye-carrier system, e.g. a fluorophore-labeled antibody, is too large to be membrane permeable [266]. These techniques can thus not be used for the investigation of living cells but only for permeabilized cells [266]. Thereto, the cells are usually fixed and cross-linked (with formaldehyde or glutaraldehyde) and subsequently permeabilized with organic solvents or surfactants, such as 4-(1,1,3,3-tetramethylbutyl)phenyl-poly(ethylene glycol) (Triton X-100) [267]. For live-cell imaging different techniques, such as the expression of fluorescent proteins, must be used [263].

At last, the fluorophores used in this thesis, will be presented shortly. DAPI (4',6-diamidino-2-phenylindole) is commonly used for staining of nuclei. It binds to minor grooves of A-T rich sequences of double-stranded DNA, which leads to a shift in the absorption and emission spectra of DAPI as well as a more than 20-fold increase in quantum yield [268]. For the staining of the cytoskeleton, phalloidin-tetramethylrhodamine isothiocyanate (TRITC) is used. Phalloidin belongs to a group of fungal toxins, which consist of bicyclic heptapeptides [269]. It strongly binds to F-actin and its fluorescent derivatives can thus be used for staining of the actin filaments [269, 270]. As phalloidin is not able to penetrate intact cell membranes and disturbs cell dynamics via complexation of actin, it is usually not applied for live-cell imaging [270].

Part III

Experimental

7 Substrates and Materials

7.1 Substrates

The model substrates, used in this thesis, differed with respect to their geometry. This was necessary in order to enable analysis of the immobilized surface coatings with a variety of different techniques. Furthermore, in addition to silicon and silica-based materials, substrates with titanium surface were used for cell biological experiments as titanium and its alloys are suitable for biomaterials with bone contact [25]. In this way, a first step towards clinical application of the surface coatings was taken.
In the following, a short overview of the different substrate materials as well as their purpose in the scope of this thesis will be given.

7.1.1 Wafers

Silicon wafers in two different geometries were obtained from Si-Mat Silicon Materials (Kaufering, Germany) and cut by Disco Hi-Tec Europe GmbH (Kirchheim, Germany). Square, single-side polished wafers (n-type, phosphor-doped, thickness 650–700 µm, 5–25 Ω cm resistivity) with an edge length of 10 mm were utilized for static contact angle measurements, XPS and streaming current measurements. Double-side polished wafers with dimensions of 10 x 25 mm were needed for dynamic contact angle measurements. For cell biological investigations, titanium-sputtered silicon wafers were utilized. These substrates were of identical geometry as the single-side polished silicon wafers, i.e. 10 x 10 x 0.75 mm with one polished side, and were purchased from the Center for Microtechnologies (ZfM, University of Technology Chemnitz, Chemnitz, Germany).

7.1.2 Silica Particles

For colorimetric assays (sulfo-SDTB and BCA assay), non-porous, sintered silica beads were obtained from Brace GmbH (Alzenau, Germany). They possessed diameters between 250 and 315 µm, resulting in a specific surface area of $0.19\,m^2\,g^{-1}$.
For electrophoretic determination of the zeta potential, monodisperse silica spheres with a diameter of 1 µm were purchased from Micromod Partikeltechnologie GmbH (Rostock, Germany). These non-porous SiO_2 particles possessed a specific surface area of $2.80 \pm 0.04\,m^2\,g^{-1}$, as determined by adsorption measurements [13].

7.2 Solvents and Reagents

A variety of solvents and reagents was utilized in this thesis. Thus, not every single reagent will be stated separately. If not mentioned otherwise explicitly, reagents and solvents were purchased from Sigma-Aldrich Chemie GmbH (Taufkirchen, Germany), VWR International GmbH, Merck KGaA (both Darmstadt, Germany) or Fisher Scientific GmbH (Schwerte, Germany) in analytical grade (p.a.). Some reagents, which were used for more than one synthesis or analysis or required special pretreatment, will be listed below. Further chemicals are mentioned in the respective section.

- Sterile-filtrated water was obtained via purification by an ultrafiltration apparatus of Millipore Corp. (Billerica, MA, USA) and subsequent filtration with a bottle top vacuum filtration system with a 0.2 µm polyethersulfone membrane by VWR International GmbH (Darmstadt, Germany).
- Concentrated nitric acid (HNO_3, $\geq 65\%$) was obtained from Carl Roth GmbH + Co. KG (Karlsruhe, Germany). It was delivered and stored in glass bottles at all times in order to avoid substrate contamination.
- Molecular sieve (3 Å or 4 Å) was purchased from Carl Roth GmbH + Co. KG (Karlsruhe, Germany) and used to dry solvents, such as toluene, dimethyl sulfoxide (DMSO) or tetrahydrofuran (THF), by adding it to the stock solution or a Schlenk flask with the solvent. The solvents were kept under argon atmosphere and the content of remaining water was monitored by Karl Fischer titration.
- The silanes n-octyltrichlorosilane (97%), 1H,1H,2H,2H-perfluorodecyltrichlorosilane (97%), 7-octenyltrichlorosilane (95%, 10-30% isomers), 11-bromoundecyltrichlorosilane (95%), N-(triethoxy-silylpropyl)-O-poly(ethylene oxide) urethane (with 5 ethylene glycol units), 3-(triethoxy)propyl succinic acid anhydride (95%) and (3-N,N-dimethylaminopropyl)trimethoxysilane (97%) were obtained from abcr GmbH (Karlsruhe, Germany) and stored in a glovebox under nitrogen atmosphere.
- Pyridine (95%, from Sigma-Aldrich Chemie GmbH, Taufkirchen, Germany) was purified by drying over potassium hydroxide and subsequent distillation, as described previously [13]. It was stored in the stock solution bottle under argon atmosphere, equipped with 4 Å molecular sieve.
- N,N'-ethylenebisacrylamide (EBA, 96%) and anhydrous piperazine (99%) were obtained from abcr GmbH (Karlsruhe, Germany).
- Phosphate-buffered saline (PBS) solution was prepared by dissolving the respective buffer tablets from Sigma-Aldrich Chemie GmbH (Taufkirchen, Germany) in sterile-filtrated water (final composition 137 mmol L^{-1} NaCl, 2.7 mmol L^{-1} KCl, 10 mmol L^{-1} phosphate buffer, pH 7.4 at 25 °C).

8 Synthesis of the Poly(amido amine) Polymer

In contrast to the commercially available linear PEI polymer, a linear poly(amido amine) (PAMAM) polymer had to be synthesized in our work group. The procedure used was based on the protocol by Dey and Ray [99] and has already been described in the preceding master's thesis [22].

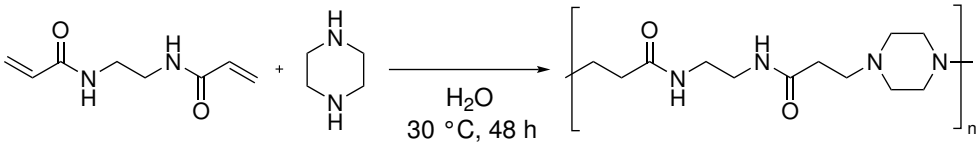

Figure 8.1: Synthesis of the linear PAMAM polymer from EBA and piperazine.

For the polymer synthesis, EBA as well as piperazine were dissolved in water in a 1:1 molar ratio under argon atmosphere. The reaction was performed for 48 h at 30 °C. After 43 h, a 20% molar excess of piperazine, dissolved in a minimal amount of water, was added in order to ensure piperazine end groups. After 48 h, the reaction mixture was poured into an excess of acetone, from which the polymer precipitated as a yellowish viscous substance. The crude product was filtered over a Büchner funnel and dried. In order to remove remaining starting material as well as low-weight oligomeric species, the polymer was dialyzed against water for 24 h, using a Spectra/Por® Float-A-Lyzer® G2 dialysis device (volume 10 mL, molecular weight cut-off 3500–5000 g mol^{-1}). The final product was obtained by freeze-drying over night at −40 °C, followed by drying in a desiccator under vacuum.

In order to confirm successful synthesis, the product was analyzed via diffuse reflectance infrared Fourier transform (DRIFT) spectroscopy, using a FT/IR-610 infrared spectrometer from Jasco International Co., Ltd. (Tokyo, Japan) in combination with an EasyDiff™ diffuse reflectance accessory from Pike Technologies Inc. (Madison, WI, USA). ^{1}H- and ^{13}C-NMR spectra in D_2O were recorded on an Advance 300 device from Bruker BioSpin GmbH (Rheinstetten, Germany). The polymer was further analyzed via high performance liquid chromatography (HPLC)-MS in the Central Analytics Services department of the University of Regensburg. Chromatography was carried out on a Poroshell 300-SB column by Agilent Technologies (Santa Clara, CA, USA) with isocratic elution (water/acetonitrile 95:5 (v/v)) und UV detection. The subsequent electrospray ionization (ESI)-MS was performed on a 6540 UHD Q-TOF MS system by Agilent Technologies.

9 Synthesis of the Surface Modifications

9.1 Substrate Handling

As this thesis deals with the synthesis and analysis of surface modifications, which are sensitive to contamination, careful handling of the substrates was required at all times. Appropriate procedures have been developed at the work group and have been described previously [13]. Nevertheless, the most relevant aspects of substrate handling will be summarized in the following, covering both general aspects as well as procedures specifically used for different substrate geometries.

9.1.1 General Remarks

In order to avoid adsorption of contaminants on the substrate surface from the surrounding air, substrates were handled unter protective argon atmosphere, unless otherwise stated. To that purpose, a large plastic basin (approximately 30 x 28 x 18 cm (L x W x H)) was flooded with argon and continuously refilled with a low stream of argon. Spoiling of the surfaces by surfactants and grease was prevented as well. Glassware was cleaned in an alkaline bath (40 g KOH L^{-1} isopropanol) for at least two days and subsequently neutralized by placing in an acid bath ($1\,mol\,L^{-1}$ HCl). No surfactant-based cleaners were utilized. If necessary, glassware was dried in an oven at 130 °C for at least 30 min and allowed to cool down to ambient temperature in the plastic basin under argon atmosphere. No grease was necessary because PTFE stopcocks were used instead of glass stopcocks and desiccators were equipped with rubber seals.
Contamination from solvents was prevented as well. Thereto, only sterile-filtrated water was used in substrate handling. For moisture sensitive modification steps, e.g. silanization or reaction with lithium aluminum hydride ($LiAlH_4$), solvents dried over molecular sieve were utilized.

9.1.2 Handling of Wafer Specimens

Transfer of wafers was achieved by forceps. Single-side polished wafers were only touched at the edges by metal forceps in order to avoid scratching of the polished wafer surface. In addition, attention had to be paid to always place wafers with their polished side facing up. Double-side polished wafers were moved using plastic forceps. As the wafers had to be touched on the polished surfaces, one of the shorter edges was equipped with a scratched marking. This part of the wafer was touched by the forceps, placed in the teflon holder etc., whereas the other side was measured in dynamic contact angle measurements.

Modification of wafers was either performed in bulk in appropriate glassware or individually in small snap vials with a total volume of approximately 7 mL. Whereas common glassware, such as petri dishes, could be used for silanization reactions at room temperature, special glass devices were necessary for the silanizations at elevated temperatures, as already previously described in the PhD thesis of Verena Katzur [13]. All devices are characterized by their flat bottom, are equipped with a Schlenk side arm (for protective atmosphere) and can be connected to a reflux condenser. For single-side polished wafers two glass devices of different sizes were available (see Figure 9.1). For the modification of double-side polished wafers, a glass device similar to the smaller one-piece device for single-side polished wafers was available. The respective cylindrical pot was equipped with a teflon holder which allows for mounting of up to 14 double-side polished wafers in an upright position.

Figure 9.1: Glass devices for the silanization of single-side polished wafers at elevated temperatures.

In snap vials, 0.8 to 1 mL or 6 mL of solution were used for single-side or double-side polished wafers respectively. For long reaction times, the snap vials were placed on a laboratory shaker. Removal of excess reagent or byproducts was achieved by varying numbers of rinsing cycles, which were performed in snap vials with the aforementioned solvent volumes. One rinsing cycle consisted of treatment of the vials in an ultrasonic bath for 3 min, followed by solvent exchange. The rinsing solution was removed with a Pasteur pipette and immediately replaced by fresh solvent. For drying, single-side polished wafers were placed in a petri or crystallizing dish, equipped with a filter paper. Double-side polished wafers were transferred to fresh snap vials. Specimens were dried in desiccators under vacuum, using a diaphragm or oil pump. For storage, wafers were placed in the wells of microwell plates and kept in desiccators under argon atmosphere.

9.1.3 Handling of Particle Substrates

Silica beads and silica spheres possessed a completely different geometry and thus had to be handled differently. Silica spheres and small amounts of silica beads were transferred as a suspension, using a Pasteur pipette. Larger amounts of beads were poured. In order to separate substrate and solution, centrifugation (3500 rpm for 4 min) was necessary for silica spheres. Silica beads, however, sedimented quickly. Thus, the supernatant solution could simply be decanted.
Modification of silica spheres and beads was performed in appropriate glassware. For spheres and large batches of silica beads, round bottom flasks were used, whereas for small batches of silica beads, glass tubes with screw caps were utilized. For reactions with a reaction time of at least two hours, the spheres or beads were placed on a laboratory shaker. For shorter reaction times, substrates and reaction solution were agitated more strongly with the help of a rotational apparatus or an overhead shaker.
Rinsing of the substrates consisted of decantation of the rinsing solution, addition of fresh solvent, resuspension of the particles by vortexing (especially in case of the silica spheres) and ultrasonication for 3 min. Rinsing was performed in tapered centrifuge tubes (silica spheres and small batches of silica beads) or round bottom flasks. If not mentioned otherwise, 1.5 mL solvent were needed per gram beads or 5 mL per 100 mg silica spheres, respectively.
In order to dry the substrates, solvent was at first removed with the help of a rotary evaporator and the particle substrates subsequently dried under vacuum. For storage, silica beads were transferred to snap vials, whereas silica spheres were kept in the 25 mL round bottom flasks they were dried in. Samples were stored under argon atmosphere at room temperature or, if necessary, in the refrigerator at $< 10\,^{\circ}\mathrm{C}$.

9.2 Substrate Oxidation

Prior to substrate silanization, the surfaces had to be cleaned in order to remove contaminants and particles, such as dust, and oxidized to obtain surface hydroxyl groups. As oxidizing agent usually strong acids or an oxygen plasma are used [32, 39]. In our work group, half-concentrated nitric acid (HNO_3, 38%, 1:1 (v/v)) was employed, which was obtained via dilution of concentrated nitric acid with sterile-filtrated water.
To that purpose, all types of wafers were cleaned by ultrasonication with acetone for 15 min. After that, the acetone was replaced with half-concentrated HNO_3 and the substrates were treated in an ultrasonic bath for 30 min before storing them at room temperature until usage. Here, silicon wafers had to be stored for at least two weeks, whereas titanium wafers were usually stored for one week. A storage time of two weeks was never exceeded for titanium wafers as this led to a loss of the titanium layer. Prior

to silanization, the acidic solution had to be removed from the wafer surface. For that reason, the wafers were firstly dipped into a water immersion bath and subsequently rinsed several times with water, until the pH of the supernatant solution reached at least pH 6. After that, the substrates were dried in a desiccator for 30 min to 1 h, using a diaphragm pump.
Silica beads were oxidized by suspending them in 1.5 mL HNO_3 per gram beads and treating them in an ultrasonic bath for 30 min. The particles then remained in the acidic solution at least over night. When needed, the nitric acid had to be removed via rinsing multiple times with sf-water, until the pH of the supernatant solution exceeded pH 5. The silica beads were filtered by means of a Büchner funnel, pre-dried under a faint stream of argon for 10 min and dried in a desiccator over night, using a diaphragm pump. The silica spheres were delivered in containers filled with inert gas. Thus, no cleaning or oxidation was necessary and the silica spheres could be used as received.

9.3 Immobilization of Self-Assembled Monolayers

The formation of self-assembled monolayers with silanes was always the initial surface modification. If necessary, further functionalization was then achieved via conversion of the terminal groups of the silane molecules or via immobilization of further reagents. Here, a variety of different self-assembled monolayers was synthesized in the scope of the thesis, which will be described in the following. The immobilization of amine group-bearing or osmolyte-derived molecules is then described in successive sections. Silanization reactions were always performed with substrates prepared according to the procedure described in the previous section.
As this silanization step was very sensitive to the presence and amount of water, special attention was paid to eliminating moisture. To that purpose, the aforementioned protocols, e.g. drying of glassware and solvents, were followed strictly and, in addition, the required silane solution was prepared in the N_2-glovebox and always handled under protective atmosphere (argon or N_2).
In contrast to common organic syntheses taking place in the liquid phase, special attention had to be paid to the amount of reagents used in surface reactions. An excess of reagent, e.g. silane, with respect to the available surface area had to be guaranteed. A detailed evaluation of the different situations was performed by Verena Katzur in her PhD thesis [13] and reactions were performed accordingly in this work. Thus, the calculations are not repeated here. If not mentioned otherwise, for the silanization of wafers, a 25 mmol L^{-1} solution in dry toluene was used, for silica particles a 50 mmol L^{-1} silane solution was applied. Silanization of silica beads was performed with 2 mL solution per gram beads, whereas an amount of 10 mL per 100 mg was used for silica spheres.

9.3.1 SAM-CH_3 – Alkane Monolayer

A simple alkane monolayer (SAM-CH_3) was achieved via immobilization of octyltrichlorosilane (see Figure 9.2), based on previously published protocols [21].

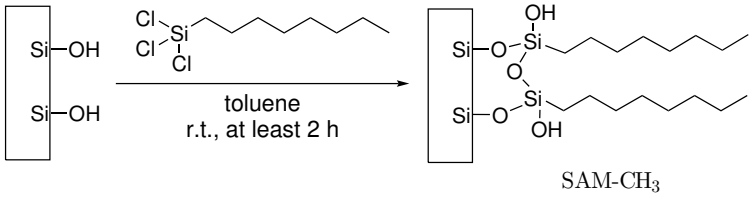

Figure 9.2: Reaction scheme of the formation of an alkane monolayer via silanization of a hydroxylated surface with octyltrichlorosilane.

The silanization reaction was performed for at least 2 h at room temperature under nitrogen or argon atmosphere. Wafers were subsequently dipped into a toluene immersion bath, rinsed twice with toluene and once with chloroform before drying. Excess silane was removed from silica particles with several washing steps with toluene (first three with anhydrous toluene) before drying them at the rotary evaporator (bath temperature 60 °C, pressure 300 to 95 mbar).

9.3.2 SAM-CF_3 – Perfluorocarbon Monolayer

The synthesis of a perfluorinated alkane SAM (SAM-CF_3) was performed analogously to the procedure described for the alkane monolayer and also derived from previously published procedures [21].

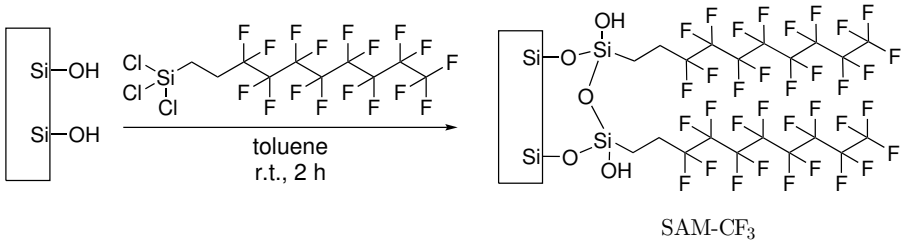

Figure 9.3: Reaction scheme of the immobilization of a trichlorosilane carrying a perfluorinated alkane chain on a hydroxylated surface.

The substrates were immersed into a solution of 1H,1H,2H,2H-perfluorodecyltrichlorosilane for 2 h at room temperature under argon or nitrogen atmosphere. Wafers were cleaned from excess silane by rinsing them twice with toluene and once with chloroform. Particle substrates were separated from the silane solution via filtration over a Büchner funnel (only silica beads), rinsed multiple times with toluene and subsequently dried at the rotary evaporator (bath temperature 60 °C, pressure 300 to 95 mbar).

9.3.3 SAM-COOH – Monolayer with Carboxylic Acid Groups

The formation of a 6-carboxyhexanylsiloxane monolayer (SAM-COOH) consisted of two steps, the immobilization of a monolayer with terminal alkene groups (SAM-CH=CH_2) and their oxidation to carboxylic acid groups with potassium permanganate ($KMnO_4$). The reaction procedure was derived from the protocol by Liu et al. [271] and had already been applied previously in our work group [18, 19].

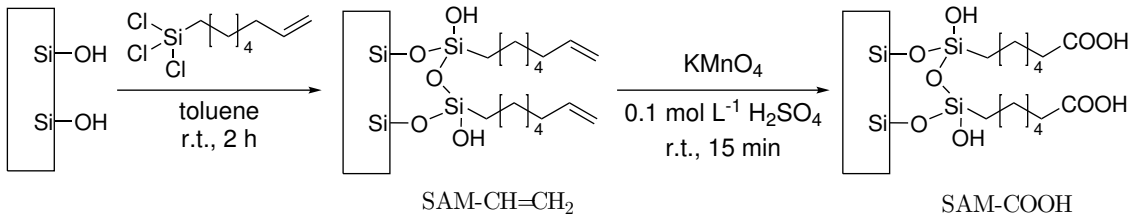

Figure 9.4: Schematic representation of the formation of a carboxylic acid-terminated SAM, via immobilization of an alkene-terminated SAM, followed by conversion of the olefine groups into carboxylic acid groups via oxidation with $KMnO_4$.

In the first step, the silane 7-octenyltrichlorosilane was immobilized on the substrates, forming an alkene-terminated SAM. To that purpose, substrates were treated with a silane solution in anhydrous toluene for 2 h at room temperature under nitrogen or argon atmosphere and exclusion of light. Wafers were subsequently dipped into a toluene immersion bath, rinsed twice with toluene and once with chloroform before drying. Excess silane was removed from silica beads with six washing steps with toluene (first three with anhydrous toluene). For silica spheres, four rinsing steps were required. Particle substrates were dried at the rotary evaporator (bath temperature 60 °C, pressure 300 to 95 mbar).

Oxidation of the terminal olefine groups was performed with a 25 mmol L^{-1} solution of $KMnO_4$ in 0.1 mol L^{-1} sulfuric acid (H_2SO_4) at room temperature. A reaction time of 15 min was not exceeded. For silica beads and spheres, again 2 mL per gram beads or 10 mL per 100 mg silica spheres were required. In order to remove excess $KMnO_4$ and reduce manganese oxide (MnO_2), wafers were rinsed once with 0.1 mol L^{-1} H_2SO_4, twice with 0.1 mol L^{-1} sodium hydrogen sulfite ($NaHSO_3$) solution, once with 0.1 mol L^{-1} HCl and several times with water until a neutral pH was reached.

Silica beads were separated quickly from the $KMnO_4$ solution by filtering over a Büchner funnel. The substrates were washed this way as well by rinsing four times with 0.1 mol L^{-1} H_2SO_4, four times with 0.2 mol L^{-1} $NaHSO_3$ solution, four times with 0.1 mol L^{-1} HCl and repeatedly with water, with portions of 1 mL per gram beads each. Silica spheres required two washing cycles with 0.1 mol L^{-1} H_2SO_4, two with 0.1 mol L^{-1} $NaHSO_3$ solution, one with 0.1 mol L^{-1} HCl and several with water before drying at the rotary evaporator (bath temperature 70 °C, pressure 250–95 mbar).

9.3.4 SAM-Py – Monolayer with Pyridinium Groups

The synthesis of a monolayer carrying pyridinium groups (SAM-Py) was achieved via a two-step procedure, consisting of the immobilization of a bromine-terminated monolayer (SAM-Br), followed by nucleophilic substitution of the bromine by pyridine, as it was described by Verena Katzur in her PhD thesis [13].

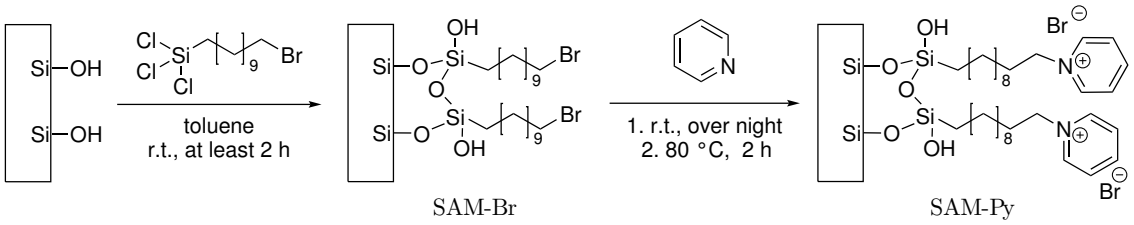

Figure 9.5: Schematic illustration of the synthesis of a pyridinium SAM, via immobilization of a bromine-terminated SAM, followed by substitution of the terminal bromine atom with pyridine.

At first, the bromine-terminated SAM was immobilized on the substrate surface via silanization with 11-bromoundecyltrichlorosilane for at least two hours at room temperature under exclusion of light. For wafers, excess silane was removed by rinsing twice with toluene and once with chloroform before drying. Silica particles were rinsed with toluene several times and once with pyridine. For contact angle measurements, workup of wafers consisted of three rinsing steps with toluene and one step with chloroform.
For the substitution of bromine by pyridinium groups, the substrates were immersed in pyridine at room temperature over night, completing the reaction the next day by heating to 80 °C for at least two hours. Subsequently, wafers were dipped into a methanol immersion bath and rinsed with methanol four times. Unbound pyridine was removed from particle substrates by rinsing multiple times with methanol before drying at the rotary evaporator (bath temperature 60 °C, pressure 400 mbar).

9.3.5 SAM-NH_2 – Monolayer with Primary Amine Groups

As ordered amine monolayers cannot be prepared directly from amine-substituted silanes [32], the three-step reaction procedure described here was applied.
It is based on the protocol by Balachander and Sukenik [52] and has been reported in previous publications of our work group [18, 19].
Initially a bromine-terminated SAM was immobilized on the substrate surface, as described in section 9.3.4. After rinsing with toluene, wafers were sonicated once, particle substrates at least twice with dry DMSO.

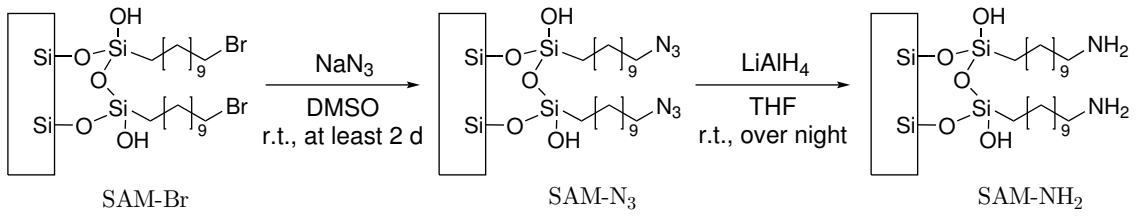

Figure 9.6: Schematic illustration of the synthesis of an amine-terminated SAM (SAM-NH_2), via substitution of the terminal bromine atom with an azide group, followed by the reduction with $LiAlH_4$.

The nucleophilic substitution was carried out with a 120 mmol L^{-1} (wafers), 240 mmol L^{-1} (beads) or 500 mmol L^{-1} (silica spheres) solution of sodium azide (NaN_3, purum, > 90%, Fluka, now part of Sigma-Aldrich Chemie GmbH, Taufkirchen, Germany) in anhydrous DMSO for at least two days at 25 °C. Subsequently, wafers were rinsed once with DMSO, dipped into a THF immersion bath and rinsed twice with THF prior to reduction with lithium aluminum hydride ($LiAlH_4$). Similarly, workup of particle substrates consisted of three washing steps with DMSO and five to six steps with THF. If substrates with terminal azide groups (SAM-N_3) were required for contact angle measurements or click chemistry, a different procedure was applied. After the substitution reaction, wafers were rinsed once with DMSO, dipped into a methanol immersion bath and rinsed multiple times with methanol. Silica beads were washed three times with DMSO and several times with methanol before drying at the rotary evaporator (bath temperature 30 °C, pressure 350 to 120 mbar).

In order to obtain self-assembled monolayers with terminal amine groups, reduction of the azide group of wafers was performed with a 90 mmol L^{-1} solution of $LiAlH_4$ in anhydrous THF over night at room temperature. For silica beads, a 200 mmol L^{-1} solution was used (2 mL per gram beads), silica spheres required a 500 mmol L^{-1} solution (10 mL per 100 mg). Remaining $LiAlH_4$ was removed from wafers by dipping them into an immersion bath containing 10% HCl, rinsing them once with 0.1 mol L^{-1} HCl and repeatedly with water until a neutral pH was reached. Due to the violent reaction of $LiAlH_4$ with water and acids under release of H_2, a different procedure was used for the workup of silica beads and spheres. Particle substrates were at first rinsed three times with anhydrous THF in order to remove the majority of the remaining $LiAlH_4$. Then, the beads were carefully washed with 0.1 mol L^{-1} HCl and several times with water until a neutral pH was reached. Silica spheres were rinsed once with 10% HCl, twice with 0.1 mol L^{-1} HCl and multiple times with water. Particle substrates were dried at the rotary evaporator (bath temperature 60 °C, pressure 200 to 50 mbar).

9.3.6 SAM-SO_3H – Monolayer with Sulfonic Acid Groups

A self-assembled monolayer carrying sulfonic acid groups (SAM-SO_3H) was prepared similar to the procedure described by Shyue et al. via a three-step synthesis [272] and was previously described by Verena Katzur in her PhD thesis [13].

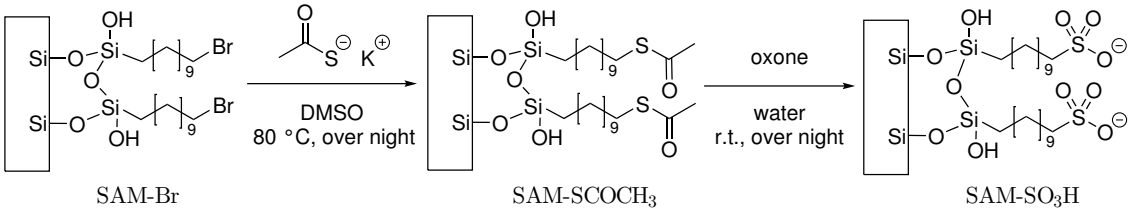

Figure 9.7: Scheme of the synthesis of a self-assembled monolayer with terminal sulfonic acid groups via formation of a thioester (SAM-$SCOCH_3$), followed by oxidation with oxone [272].

The first step of the synthesis route, the immobilization of a bromine-functionalized monolayer, was performed as described previously (see section 9.3.4). After rinsing with toluene, the substrates were sonicated once (wafer) or three times (particles) with dry DMSO. The substitution of the bromine group by thioacetate was performed with a $0.6\,\mathrm{mol\,L^{-1}}$ solution of potassium thioacetate in dry DMSO at 80 °C over night under exclusion of light. Subsequently, wafers were dipped into a water immersion bath and rinsed four times with water. Excess reagent was removed from particle substrates by rinsing twice with dry DMSO and multiple times with water. Conversion of the thioester groups into sulfonic acid groups was carried out with a saturated solution of oxone® ($2\,KHSO_5 \cdot KHSO_4 \cdot K_2SO_4$, Sigma-Aldrich Chemie GmbH, Taufkirchen, Germany) in sf-water over night at room temperature, followed by rinsing with water and drying.

9.3.7 SAM-PEG – Monolayer with Five Ethylene Glycol Units

In order to obtain a reference surface modification, substrates were functionalized with a silane containing five ethylene glycol units (SAM-PEG), similar to the previously published procedure [19, 21].

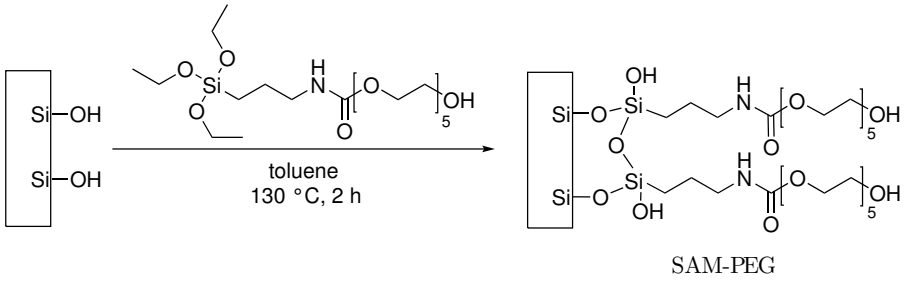

Figure 9.8: Schematic depiction of the immobilization of N-(triethoxysilylpropyl)-O-polyethylene oxide urethane for the formation of SAM-PEG.

Silanization was performed with a solution of N-(triethoxysilylpropyl)-O-polyethylene oxide urethane in dry toluene for 2 h at 130 °C. Wafers were rinsed twice with toluene und once with chloroform. Excess silane was removed from particle substrates by rinsing several times with toluene, followed by drying at the rotary evaporator (bath temperature 60 °C, pressure 150 to 90 mbar).

9.3.8 TESPSA – Monolayer with Succinic Acid Anhydride Groups

Self-assembled monolayers with terminal succinic acid anhydride groups (TESPSA) were prepared with the silane 3-(triethoxy)propyl succinic acid anhydride according to the previously published procedure [18, 20].

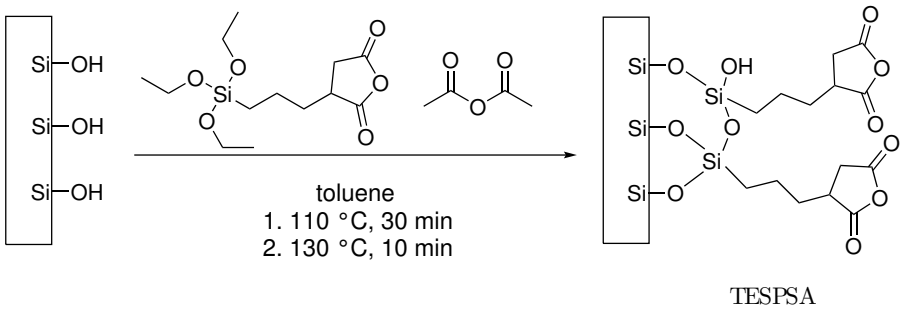

Figure 9.9: Reaction scheme of the immobilization of the silane 3-(triethoxy)propyl succinic acid anhydride on hydroxylated surfaces, leading to a SAM with terminal succinic acid anhydride groups (TESPSA).

The modification of wafers with succinic acid anhydride-terminated SAMs was carried out with a 1.56 mmol L^{-1} solution of silane in anhydrous toluene. In order to prevent the ring-opening of the anhydride ring via reaction with released ethoxy groups, three molar equivalents acetic acid anhydride (dried over 4 Å molecular sieve) were added to the solution (4.68 mmol L^{-1}). For silica beads, a toluene solution containing 25 mmol L^{-1} 3-(triethoxy)propyl succinic acid anhydride and 75 mmol L^{-1} acetic acid anhydride was used, for silica spheres 50 mmol L^{-1} and 150 mmol L^{-1} were needed, respectively. The silanization reaction was performed at elevated temperatures (30 min at 110 °C, followed by 10 min at 130 °C). Prior to further modification, wafers were dipped into a toluene immersion bath and rinsed twice with dry toluene. Wafers that needed to be isolated, e.g. for contact angle measurements, were rinsed an additional time with toluene and once with chloroform. Workup of silica beads consisted of four washing steps with dry toluene, whereas silica spheres were rinsed three times with anhydrous toluene.

9.3.9 SAM-NMe_2 – Monolayer with Tertiary Amine Groups

Self-assembled monolayers exposing tertiary amine groups (SAM-NMe_2) were obtained via silanization with (3-N,N-dimethylaminopropyl)trimethoxysilane. The procedure was similar to the one described in the previous secion (section 9.3.8).

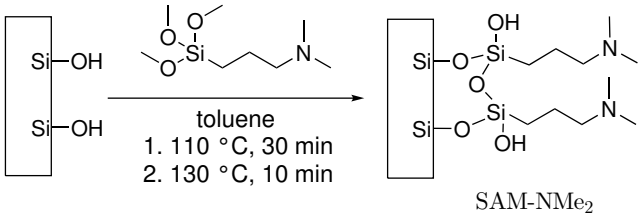

Figure 9.10: Schematic illustration of the synthesis of a self-assembled monolayer with tertiary amine moieties.

As for the synthesis of a TESPSA monolayer, silanization was carried out with a silane solution in dry toluene at elevated temperatures (30 min at 110 °C, followed by 10 min at 130 °C). After that, silicon wafers were dipped into an immersion bath with dry toluene, rinsed three times with dry toluene and once with chloroform. Silica beads were rinsed six times with toluene (first three rinsing steps with anhydrous toluene), whereas silica spheres required four washing steps. Subsequently, silica particles were dried at the rotary evaporator (bath temperature 60 °C, pressure 300 to 90 mbar).

9.4 Synthesis of Oligomeric or Polymeric Amine-Terminated Surface Coatings

Six different surface modifications with oligomers, linear polymers or dendrimers, possessing terminal amine groups, were synthesized and examined in this thesis with N,N'-bis(3-aminopropyl)-1,3-propanediamine (APD), an oligo(propylene imine), poly(propylene imine) dendrimers of generation 2 and 4 (PPI-G2 and PPI-G4), a linear poly(amido amine) (PAMAM) polymer, a linear poly(ethylene imine) (PEI) polymer and lastly an amido amine (AMAM) structure from EBA and piperazine. The immobilization reactions, described in the following, had been developed in the preceding master's thesis [22], have recently been published [273] and were carried out on all kinds of substrates (single-side and double-side polished wafers, silica beads, silica spheres).

9.4.1 Immobilization of APD and PPI Dendrimers

The TESPSA monolayer was used for the immobilization of APD (97%), which was purchased from abcr GmbH (Karlsruhe, Germany), and PPI dendrimers of generation 2 and 4 (PPI-G2 and PPI-G4 respectively), which were obtained from SyMO-Chem (Eindhoven, Netherlands).

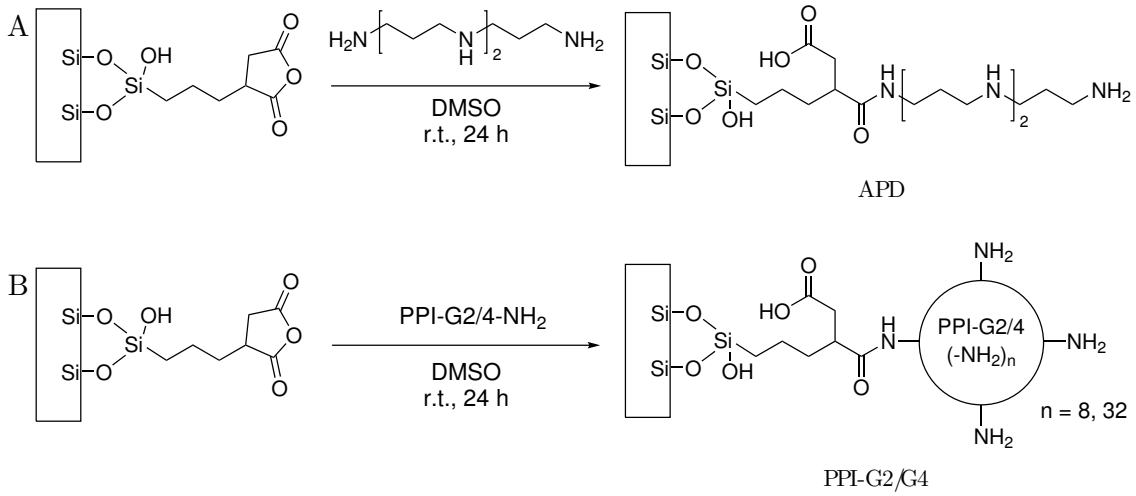

Figure 9.11: Schematic illustration of the immobilization of (A) APD and (B) PPI-G2 or PPI-G4 on TESPSA substrates via formation of an amide bond.

In all cases, the TESPSA-modified substrates were rinsed with dried DMSO in order to remove the toluene. For wafers and spheres, one rinsing step was sufficient, whereas silica beads were rinsed twice (1.25 mL per gram beads). Surface modification was then achieved via immersion of the substrates in a solution of the respective reagent in anhydrous DMSO for at least 24 h at 25 °C. For beads, 1.25 mL per gram beads were used, for silica spheres 5 mL per 100 mg. The concentrations are summarized in Table 9.1.

Table 9.1: Summary of the reagent concentrations for the immobilization of APD, PPI-G2 and PPI-G4 on TESPSA-functionalized substrates.

	Concentration of reagent solution [mmol L^{-1}]		
	APD	PPI-G2	PPI-G4
Wafer	100	5	0.5
Silica beads	200	50	5
Silica spheres	200	10	1

Single- and double-side polished wafers were rinsed once with DMSO, dipped into a methanol immersion bath and subsequently rinsed at least four times with methanol. Silica beads were rinsed once with DMSO (1.25 mL per gram), followed by multiple washing steps with methanol until the DMSO was removed completely. Silica spheres required six rinsing steps with methanol. Subsequently, particle substrates were dried at the rotary evaporator (bath temperature 30 °C, pressure 350 to 120 mbar).

9.4.2 Modification with the Linear PAMAM or PEI Polymer

The carboxylic acid-terminated self-assembled monolayer was utilized for the immobilization of both linear polymers, the PEI polymer (linear, molecular weight 25 000 g mol^{-1}), which was purchased from abcr GmbH (Karlsruhe, Germany), as well as the PAMAM polymer, which was synthesized in the scope of this thesis (see section 8). Immobilization on TESPSA surfaces (as described in the previous section) could not be performed because both polymers were insoluble in DMSO. They required the use of protic solvents, which lead to hydrolysis of the succinic anhydride ring of TESPSA.
In both cases, the immobilization procedure consisted of two steps, the conversion of the carboxylic acid groups into active esters and the covalent coupling of the polymers to the substrate surface.

In the first step, activation of the carboxylic acid groups was performed with a solution of N-(3-dimethylaminopropyl)-N'-ethylcarbodiimide (EDC) and N-hydroxysuccinimide (NHS) in a 0.1 mol L^{-1} 2-(N-morpholino)ethanesulfonic acid (MES) sodium salt buffer (pH adjusted to 5.4 with HCl, no salt added). For all wafer species and silica spheres (5 mL solution per 100 mg spheres), EDC and NHS concentrations of 100 mmol L^{-1} were chosen, whereas concentrations of 50 mmol L^{-1} (2 mL solution per gram beads) were used for silica beads. The reaction was performed for 2 h at room temperature.
After that, different procedures were needed for the immobilization of PAMAM and PEI polymer. In order to prepare wafers for the coating with PAMAM polymer, they were dipped into a MES buffer immersion bath, rinsed once with MES buffer, then

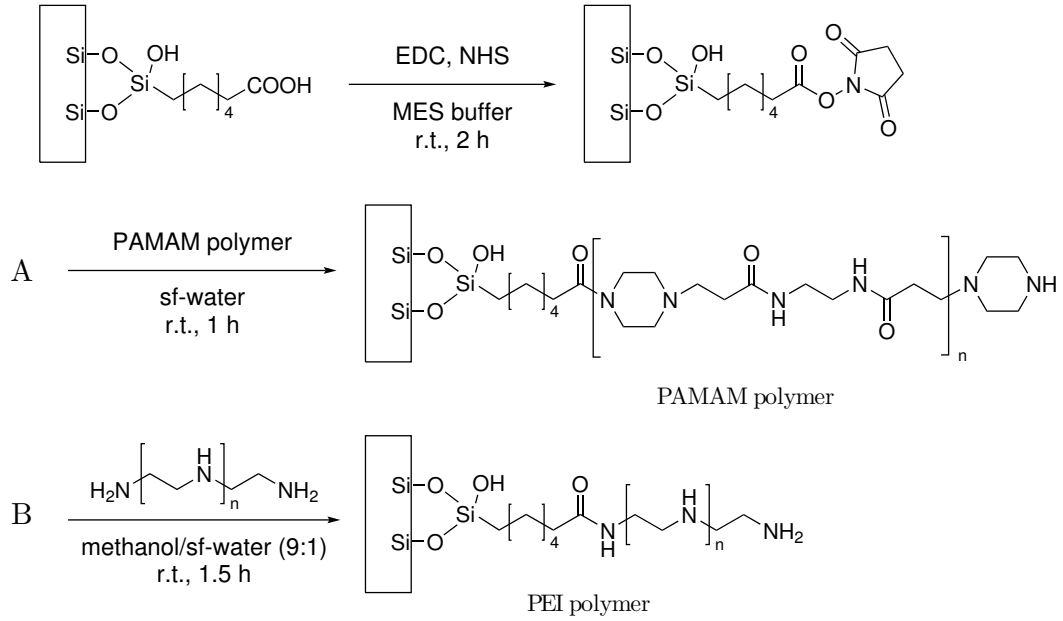

Figure 9.12: Scheme of the immobilization of the (A) PAMAM or (B) PEI polymer on SAM-COOH via formation of an active ester with EDC/NHS.

dipped into a sf-water immersion bath and subsequently rinsed twice with water. Silica beads were rinsed twice with MES buffer and four times with water, whereas silica spheres were rinsed once with MES buffer and twice with water. The immobilization of the PAMAM polymer was carried out with a $10\,\mathrm{mg\,mL^{-1}}$ solution in sf-water for 1 h at 25 °C. For silica beads, 2 mL solution per gram beads were used, whereas 5 mL solution per 100 mg spheres were needed. Workup of wafers included dipping the specimens into a water immersion bath, followed by rinsing them three times with water. From silica beads, unbound polymer was removed with six washing steps with water. Silica spheres were rinsed three times with water and once with methanol, before pre-drying at the rotary evaporator (bath temperature 30 °C, pressure 250 to 50 mbar).

The PEI polymer was insoluble in water. Thus, it was dissolved in a methanol/water mixture (9:1 v/v). This also required additional rinsing steps, compared to the immobilization of the PAMAM polymer. For all wafer substrates and silica spheres, an additional rinsing step with methanol was added after washing of the surfaces with active ester groups with water. Silica beads, however, were rinsed once with MES buffer, three times with water and twice with methanol. After that, the functionalization with PEI polymer was carried out with a solution of $10\,\mathrm{mg\,mL^{-1}}$ for 1.5 h at 25 °C, with the same volumes as used for the immobilization of the PAMAM polymer. Unbound PEI polymer was removed from wafers by dipping them into an immersion bath (with the methanol/water mixture) and rinsing them twice with the methanol/water mixture and once with methanol. Silica beads were rinsed three times with the solvent mixture and

three times with methanol, whereas silica spheres were worked up with three washing steps with the solvent mixture and one step with methanol. Particle substrates were then dried at the rotary evaporator (bath temperature 30 °C, pressure 250 to 95 mbar).

9.4.3 Modification with the Amido Amine (AMAM) Oligomer

The amine-terminated self-assembled monolayer was used as a base for the synthesis of a short-chained amido amine (AMAM) structure analogous to the PAMAM polymer. It consisted of the immobilization of EBA via an aza-Michael addition, followed by the coupling of piperazine.

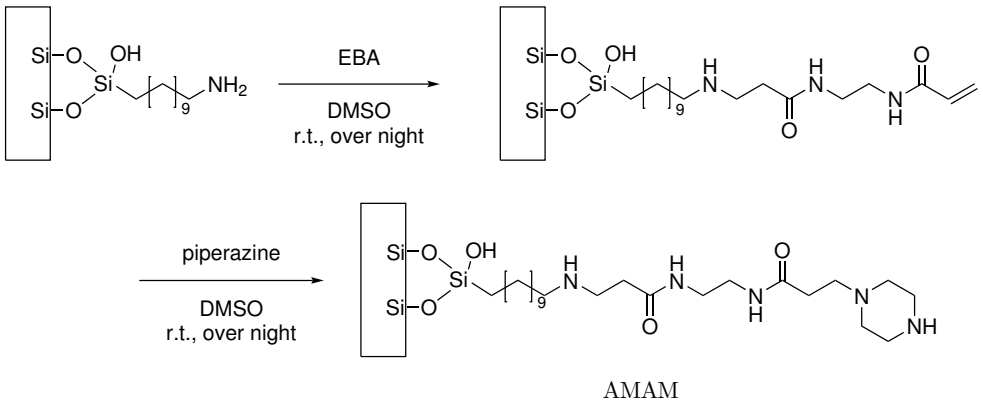

Figure 9.13: Schematic representation of the formation on an amido amine (AMAM) structure via aza-Michael coupling of EBA and piperazine.

The first reaction step was performed with a 200 mmol L^{-1} EBA solution in anhydrous DMSO over night at 25 °C. Unbound reagent was removed by rinsing with dry DMSO. For wafers, after dipping them into an immersion bath, three rinsing steps were sufficient, whereas for silica beads and spheres six or five washing steps were needed, respectively.

Immobilization of piperazine was then achied via reaction of the substrates with a 200 mmol L^{-1} solution of piperazine in dry DMSO over night at 25 °C. After that, wafers were dipped into a DMSO immersion bath, rinsed once with DMSO, then dipped into a methanol immersion bath and rinsed four times with methanol. The workup of silica beads comprised one washing step with DMSO, followed by multiple rinsing steps with methanol until the DMSO was removed completely. Silica spheres were rinsed six times with methanol. All particle substrates were then dried at the rotary evaporator (bath temperature 30 °C, pressure 350 to 100 mbar).

If wafers or silica beads were supposed to be isolated after the coupling of EBA, e.g. for contact angle measurements, they were at first rinsed once with DMSO after the reaction with EBA. Then, the substrates were rinsed multiple times with methanol until the DMSO was removed.

9.5 Synthesis of Osmolyte-Based Surface Modifications

In the following, the synthesis procedures for surface coatings based on osmolyte motifs will be presented. These functionalizations possess sulfobetaine or amine oxide end groups. In addition to that, several attempts were made to immobilize proline moieties on surfaces. Although some preliminary results were obtained, several obstacles occurred. These challenges as well as possible solutions will also be discussed in section 15.1.

9.5.1 Synthesis of a Sulfobetaine Surface Coating (DMAPS)

Sulfobetaine moieties were immobilized on SAM-NH_2 via an aza-Michael addition of 2-(N-3-sulfopropyl-N,N-dimethyl ammonium)ethyl methacrylate (95%, Sigma-Aldrich Chemie GmbH, Taufkirchen, Germany), an acrylate-substituted sulfobetaine. The reaction protocol was developed according to the conditions summarized in the review by Genest et al. and more explicitly described by Ranu and Banerjee [274, 275].

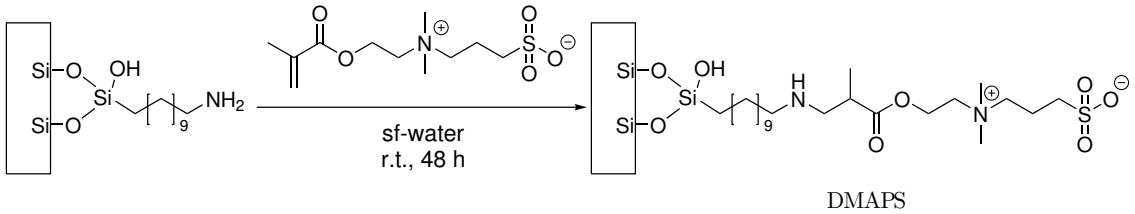

Figure 9.14: Schematic representation of the immobilization of the acrylate-substituted sulfobetaine on SAM-NH_2-functionalized substrates via aza-Michael reaction.

Immobilization of the sulfobetaine on wafers was performed with a 100 mmol L^{-1} solution in water for at least 48 h at 25 °C. After that, the specimens were dipped into a sf-water immersion bath and rinsed three times with water before drying. Silica particles were functionalized with a 200 mmol L^{-1} solution of the acrylate-substituted sulfobetaine in sf-water (2 mL per gram beads or 10 mL per 100 mg spheres respectively) for 48 h at room temperature, supported by an overhead shaker. Subsequently, the beads were rinsed six times with sf-water (2 mL per gram beads), filtered over a Büchner funnel and dried. Silica spheres were washed four times with water, once with methanol and dried at the rotary evaporator (bath temperature 30 °C, pressure 250 to 95 mbar).

9.5.2 Formation of an Amine Oxide Monolayer (SAM-NO)

Self-assembled monolayers with terminal amine oxide groups (SAM-NO) were generated from SAMs with terminal tertiary amine groups via oxidation. From the variety of oxidizing agents described in literature [276], 3-chloroperbenzoic acid (mCPBA, $\leq$ 77%, Sigma-Aldrich Chemie GmbH, Taufkirchen, Germany) was used.

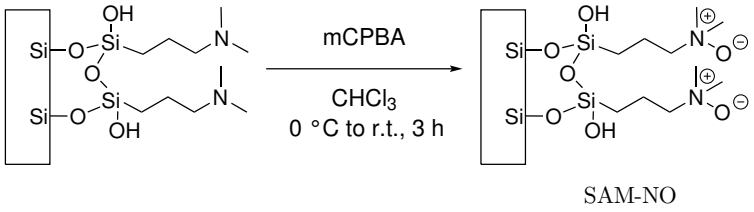

Figure 9.15: Schematic representation of the conversion of SAM-NMe_2 into an amine oxide monolayer via oxidation with mCPBA.

Commercially available mCPBA only contains approximately 75% mCPBA but also 3-chlorobenzoic acid and water to increase the stability of the reagent. Preparation of mCPBA was based on previously published protocols [277]. In order to purify mCPBA and remove 3-chlorobenzoic acid, the mixture was dissolved in chloroform and extracted three times with phosphate buffer (concentration 0.1 mol L^{-1}, pH 7.5). The resulting solution was used for the oxidation reaction.

The oxidizing reaction was performed according to the procedure of Craig and Purushothaman [278]. Oxidation of the terminal amine groups of wafers was carried out with a 100 mmol L^{-1} solution of mCPBA in chloroform. To that purpose, single-side polished wafers were placed in a crystallizing dish of appropriate diameter, double-side polished wafers were distributed into snap vials. After precooling in an ice bath, the mCPBA solution was added. The oxidation reaction was performed in the plastic basin under argon atmosphere for 3 h. The reaction temperature was kept at 0 °C for 1 h and then allowed to reach room temperature. After that, wafers were cleaned by dipping them in a chloroform immersion bath and rinsing them three times with chloroform.

For the reaction with silica particles (beads and spheres), a 200 mmol L^{-1} solution of mCPBA in chloroform was prepared and added to the particles in a precooled round bottom flask under argon atmosphere (2 mL per gram beads or 10 mL per 100 mg spheres respectively). The reaction was performed with the aforementioned temperature profile while stirring. For workup, beads were rinsed five times with chloroform (2 mL per gram beads). Silica spheres required six rinsing steps with chloroform, before drying at the rotary evaporator (bath temperature 25 °C, pressure 300 to 150 mbar).

Excess mCPBA was reduced via reaction with sodium thiosulfate ($Na_2S_2O_3$). In order to detect quantitative conversion, sodium iodide (NaI) was added, which led to a pink color of the chloroform solution as long as mCPBA was present.

9.5.3 Immobilization of Proline

The modification with proline was achieved via click reaction of an azide group-terminating SAM with Boc-(R)-4-(2-propynyl)-L-proline (≥ 96%, Sigma-Aldrich Chemie GmbH, Taufkirchen, Germany), an alkyne-substituted proline with a Boc protecting group, in a procedure similar to Prakash et al. and Himo et al. [279, 280]. In the second step, the Boc protecting group was removed via cleavage with trifluoroacetic acid. Here, the reaction protocol was derived from the ones by Blondelle and Houghten as well as Shendage et al. [281, 282]. The reaction, however, was only performed on beads and will be discussed in detail in section 15.1 with respect to success and further optimization.

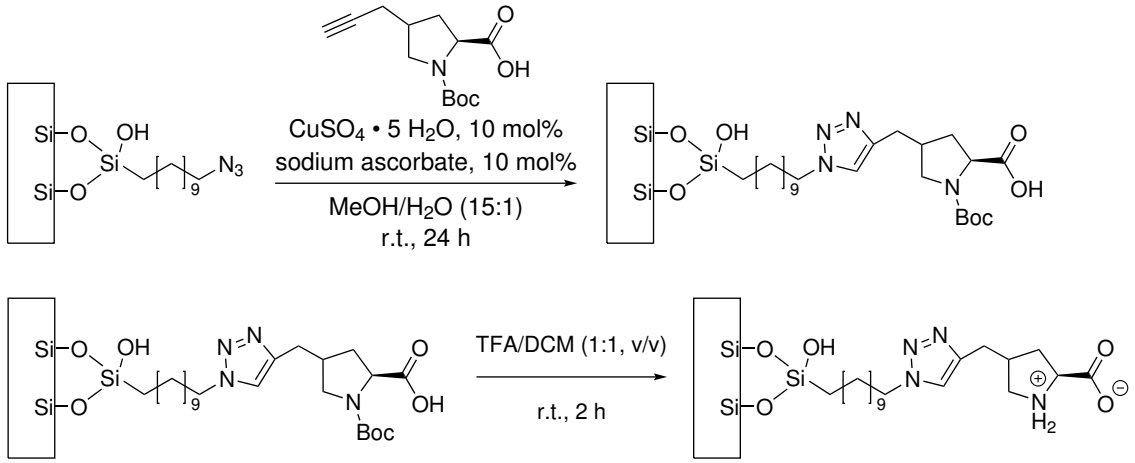

Figure 9.16: Scheme for the immobilization of N-Boc-protected proline via click reaction with an azide-terminated SAM, followed by deprotection with trifluoroacetic acid (TFA).

The click reaction was carried out with a 100 mmol L^{-1} solution of substituted proline in methanol, to which 10 mol-% of sodium ascorbate and 10 mol-% copper sulfate pentahydrate ($CuSO_4 \cdot 5\ H_2O$) (as aqueous solution) were added. The reaction was performed with 1.25 mL solution per gram beads for 24 h at room temperature. Upon preparation of the reaction solution, it was noticed that the initially cyan blue color of the solution changed to a greenish yellow, which then remained unchanged in the process of the reaction. Subsequently, the beads were rinsed four times with methanol until the supernatant solution was colorless and three times with water (2 mL solvent per gram beads each) before drying.

The removal of the Boc protecting group was carried out with trifluoroacetic acid (TFA) in dichloromethane (DCM) (1:1 v/v) for 2 h at room temperature (1.25 mL per gram beads). After that, the beads were rinsed three times with DCM (2 mL per gram beads) and dried at the rotary evaporator (bath temperature 30 °C, pressure 600 to 350 mbar). In order to remove the trifluoroacetate counterion, the beads were rinsed three times with a 50 mmol L^{-1} $NaHCO_3$ buffer (adjusted to pH 8) and finally four times with water (2 mL solvent per gram beads each) before drying.

10 Analysis of Physicochemical Properties

The different surface modifications, synthesized in this thesis, were analyzed with a variety of physicochemical techniques, which will be explained in the following section.

10.1 IR Spectroscopy

In order to confirm successful surface functionalization of silica spheres, diffuse reflectance infrared Fourier transform (DRIFT) spectra were recorded. A FT/IR-610 infrared spectrometer from Jasco International Co., Ltd. (Tokyo, Japan), equipped with an EasyDiff^{TM} diffuse reflectance accessory from Pike Technologies Inc. (Madison, WI, USA), was used. Unmodified spheres were used for background spectra.

10.2 X-Ray Photoelectron Spectroscopy (XPS)

The elemental composition of the surface coatings on wafers (single-side polished wafers with silicon or titanium surface) was determined with X-ray photoelectron spectroscopy. All measurements were carried out by Dr. Matthias Kronseder at the Physics Department of the University of Regensburg. Spectra were recorded with an electron spectrometer PHI 5700 of Physical Electronics Co. (Chanhassen, MN, USA), using monochromatic Al-Kα radiation (1486.6 eV).

10.3 Sulfo-SDTB Assay

In this thesis, the sulfo-SDTB assay was used to determine the density of primary and secondary surface amine groups of functionalized silica beads. It was based on the procedure by Gaur and Gupta as well as the instructions of the Pierce Chemical Company [226, 227] and applied for all amine- and osmolyte-based surface modifications, except for SAM-NMe_2 and SAM-NO as these surfaces do not exhibit the necessary primary or secondary amine groups (see section 10.4).
In the first step of the colorimetric assay, sulfo-SDTB (from bioWORLD, Dublin, OH, USA) was bound to the surfaces. To this purpose, 1 mL of the reagent solution of approximately 0.1 mol L^{-1} sulfo-SDTB in 50 mmol L^{-1} $NaHCO_3$ buffer (pH 8.5, 2 vol-% dimethylformamide (DMF)) was added to 50 $\pm$ 0.5 mg of beads in 2 mL Eppendorf reaction cups from Eppendorf AG (Hamburg, Germany) for each measurement. Immobilization was carried out for 30 min at 25 °C, mixing with an overhead shaker. In order to remove unbound sulfo-SDTB, four rinsing steps with 1 mL sf-water each were performed. Each rinsing step consisted of carefully aspirating the supernatant solution,

replacing it with 1 mL sf-water and mixing beads and rinsing solution with an overhead shaker for 5 min. After removing the last washing solution as quantitatively as possible, cleavage of the colored trityl cation was achieved by adding 1.5 mL half-concentrated perchloric acid ($HClO_4$, 35%) to each sample and mixing for 20 min at room temperature. If primary or secondary amine groups were present, the supernatant solution turned orange. Its absorbance at 495.6 nm was recorded with the Lambda 18 UV/Vis spectrophotometer by PerkinElmer (Waltham, MA, USA). Half-concentrated $HClO_4$ served as blank and reference.

10.4 Chloranil Test

As mentioned above, the sulfo-SDTB assay could not be applied to prove the successful conversion of the tertiary amine groups of the intermediate SAM-NMe_2 modification into amine oxide groups. Instead, a qualitative test, derived from the chloranil assay by Smith and Davis, was utilized [228]. In this assay, however, the reaction of chloranil with the tertiary amine leads to the formation of a colored compound in solution. In this thesis, the tertiary amines were immobilized on the substrate surface. Thus, the procedure could only be used for a qualitative detection of the presence or absence of tertiary amine groups by observing the coloring of the substrate surface. Here, only silica-based particulate substrates were used as they possess a white surface and a higher specific surface area and no XPS data was available for them.
The chloranil test was performed with a solution of 10 mmol L^{-1} chloranil in chloroform. 1 mL of the yellow solution was added to silica substrates with SAM-NMe_2 or SAM-NO coating in 2 mL Eppendorf reaction cups. After shaking, changes in color of the substrate surface were observed for up to one hour at room temperature.

10.5 Static Contact Angle Measurements and SFE Calculation

Static contact angle measurements were performed on single-side polished wafers via the sessile drop technique. Water contact angle measurements were both used for monitoring synthesis success as well as for the characterization of the wettability of the final surface modifications. To that purpose, sf-water droplets of 2.5 µL were deposited on the wafer surface with an automated dispenser from Hamilton Company (Reno, NV, USA). After an equilibrating time of 30 s, the resulting contact angle was measured with a P1 goniometer of Erna Inc. (Tokyo, Japan), which is equipped with a light microscope with back light. Two or at least three wafers were measured for synthesis monitoring or surface characterization respectively, with usually four measurements per wafer.

For the determination of the SFE of the surface modifications, static contact angle measurements with formamide ($\geq$ 99.5%, Sigma-Aldrich Chemie GmbH, Taufkirchen, Germany) and diiodomethane (99%, containing copper as stabilizer, Sigma-Aldrich Chemie GmbH, Taufkirchen, Germany) were conducted in addition to measurements with water. This way, the SFE could be calculated, applying the LW/AB approach [241].

10.6 Measurement of Dynamic Contact Angles

Tensiometric measurements were performed in order to obtain more detailed information about the dynamic wetting behavior of the surface modifications. To that purpose, dynamic contact angle measurements were conducted with double-side polished silicon wafers, using a K100 tensiometer from Krüss GmbH (Hamburg, Germany). Experiments were performed with sf-water (unbuffered, pH 5.5) as well as with PBS solution (total ionic strength 150 mmol L^{-1}, pH 7.4) at 25 °C. At first, the surface tension of the wetting liquid was determined via Wilhelmy plate technique, using a roughened platinum plate. After that, tensiometric experiments of the wafers were performed with ten immersion cycles per wafer with a maximum immersion depth of 12 mm and a progression speed of 10 mm min^{-1}. In order to extract advancing and receding contact angles, the linear parts of the force/length lines were extrapolated to zero immersion because no contribution of the wafer buoyancy has to be considered there and the respective contact angles could be calculated [236].

10.7 Electrokinetic Measurements

The zeta potential of the surface modifications was determined with two different techniques, requiring two different surface-functionalized substrate geometries. Modified silica spheres were necessary for electrophoretic measurements, conducted with a Zetasizer Nano ZS from Malvern Panalytical (Malvern, UK), whereas streaming current measurements of single-side polished wafers were carried out with a SurPass electrokinetic analyzer from Anton Paar GmbH (Graz, Austria), facilitated with an adjustable gap cell (length 20 mm, width 10 mm, gap height set to 100 µm). Streaming current measurements of amine or osmolyte-derived modifications were performed by Martina Grüning or Dr. Susanne Stählke at the Rostock University Medical Center.
For the electrophoretic experiments, spheres were suspended in 1 mmol L^{-1} KCl solution via sonication. After that, two different types of measurements have to be distinguished. For divergent measurements, pH was allowed to stabilize (usually at approximately pH 5.5) and was then increased or decreased stepwise. For consecutive

measurements, the starting pH was adjusted to pH 3 and raised stepwise in the course of the measurement. In both cases, zeta potential was measured in the range between pH 3 and pH 9 or 10 with steps of 0.5 pH units. An error of 0.05 pH units was accepted. pH adjustment was done with HCl and KOH solutions. Each time, an appropriate volume of the suspension was injected into the previously rinsed, disposable capillary cell (Malvern, UK) and measured at 25 °C, after an equilibrating time of 120 s. The Helmholtz-Smoluchowski equation was chosen for the calculation of the zeta potentials. Streaming current measurements were performed in a similar manner. As for the electrophoretic experiments, 1 mmol L^{-1} KCl solution was used, and HCl and NaOH or KOH solutions were needed for pH adjustment. If the streaming current measurements were only performed to confirm the IEP and determine the zeta potential at physiological conditions (for amine and osmolyte functionalizations), the pH range was reduced, with measurements being performed from pH 6.5 to pH 8.5/9.5.

11 Analysis of the Interaction of the Modifications with Proteins and Cells

11.1 Testing Protein Adsorption

11.1.1 Preparation of Protein Solutions

Protein adsorption on differently functionalized silica beads was tested with single protein solutions as well as complex physiological fluids. As model systems, solutions of HSA (lyophilized powder, $\geq$ 96%, Sigma-Aldrich Chemie GmbH, Taufkirchen, Germany) or lysozyme ($\geq$ 90%, Sigma-Aldrich Chemie GmbH, Taufkirchen, Germany) with various concentrations (1, 2, 5, 10, 25 and 50 mg mL^{-1}) were tested. As complex samples, FBS was purchased from PAN-Biotech GmbH (Aidenbach, Germany), whereas human male AB serum (HABS) was obtained from Valley Biomedical (Winchester, VA, USA).

In contrast to that, human saliva was collected and prepared within the work groups. For the quantification of protein on the surface of the silica beads, as it was performed in Regensburg, collection of human saliva was carried out according to the procedure described previously [19]. Stimulated whole saliva was obtained from four consenting individuals, chewing paraffin wax, and collected in sterilized 50 mL polypropylene Falcon tubes, cooled on ice. Removal of particles and bacteria was achieved by sterile-filtration with low-protein binding syringe filters (Acrodisc®, Supor® polyethersulfone membrane) of decreasing pore size (5 µm, 1.2 µm, 0.45 µm and 0.2 µm). After that, the saliva was pooled, aliquoted and stored at −18 °C until used. In that case, the saliva was thawed, sonicated and filtered once using a 1.2 µm syringe filter. FBS, which had been aliquoted previously and was stored at −18 °C as well, was handled identically (thawing, sonication, filtration with a 1.2 µm syringe filter).
For the qualitative protein adsorption experiments carried out at the Department of Oral Biology at the State University of New York (Buffalo, NY, USA), a different procedure was applied for saliva collection and preparation. Here, saliva was obtained from individual, consenting donors without stimulus and subsequently centrifuged at 7000 rpm for 15 min at 4 °C. After discarding the pellet, the clear supernatant was either used immediately or kept at 4 °C over night for usage the next day.

11.1.2 Protein Quantification on Silica Beads

In Regensburg, protein adsorption was examined by direct quantification of the adsorbed proteins on the functionalized silica beads via the BCA assay, according to the protocol described previously [19–21]. To that purpose, the bicinchoninic acid kit for protein determination from Sigma-Aldrich Chemie GmbH (Taufkirchen, Germany) was used, containing BCA solution, 4% (w/v) $CuSO_4 \cdot 5\ H_2O$ solution and $1\,mg\,mL^{-1}$ BSA reference solution. Unless otherwise stated, solutions and dilutions of proteins were always prepared with PBS solution (total ion content $150\,mmol\,L^{-1}$, pH 7.4). Both protein adsorption and the BCA analysis were performed in 2 mL reaction cups (Eppendorf, Germany or Brand, Germany). As no photometric end point is reached during the coloring reaction, a standard curve was run in duplicates with each assay.

Prior to adsorption onto functionalized substrates, the protein content of the biofluids was determined via BCA assay. For each thawed aliquot, two separate assays with appropriate dilutions of the physiological fluids (saliva undiluted, 1:2 and 1:5, FBS/HABS 1:40, 1:80 and 1:200) in triplicates were measured. For the standard curve, BSA solutions with concentrations of 1.0, 0.5, 0.25, 0.1, 0.05 and $0.01\,mg\,mL^{-1}$ were prepared via dilution of the BSA reference solution, which is part of the BCA kit. The assay was carried out without beads but otherwise identical to the procedure described below.

Protein Adsorption

Protein adsorption onto functionalized beads was performed for 60 min at room temperature by mixing beads and protein solution (4 mL per gram beads) by means of an overhead shaker. Unbound protein was removed by rinsing the beads five times with PBS buffer and once with sf-water (in both cases 4 mL liquid per gram beads). In each rinsing cycle, the supernatant solution was carefully aspirated from the beads with a pipette, replaced by fresh buffer or water, respectively, and the suspension was mixed for 5 min with an overhead shaker. After removal of the last washing solution, beads were dried under vacuum over night.

Analysis of the Amount of Adsorbed Protein

Analyzing the adsorbed amounts of HSA or lysozyme, one assay usually only consisted of the samples of different concentrations of one protein for one of the surface modifications. Thus, beads of the respective surface modification (without adsorbed protein) were used for the standard curve and the blanks. Regarding saliva, FBS and HABS, however, several modifications were measured in one assay. Therefore, oxidized but otherwise untreated beads were used for blanks and standard curve.

In all cases, preparation of the samples was performed while cooling the reaction cups in an ice bath. For the standard curve, 100 µL of the respective protein solution of known concentration were added to the cups, whereas 100 µL sf-water were added to blanks and samples in order to obtain identical total volumes. 1.4 mL of the BCA working solution (prepared according to the manufacturer's instructions) were added to all cups. Subsequently, the cups were placed in a water bath at 40 °C for 30 min, mixing beads and solution by turning them upside down in regular intervals, before placing them in an ice bath in order to stop the coloring reaction. The initially green BCA solution had turned violet in samples with protein. Extinction of the supernatant solution was measured at 562 nm with the Lambda 18 UV/Vis spectrophotometer by PerkinElmer (Waltham, MA, USA). The results of the standard curve were fitted with a second order polynomial. This way, the measured absorbance could be linked to the amount of protein in the samples and, taking into account the surface area of the beads, subsequently the mass of adsorbed protein per surface area was obtained.

11.1.3 Adsorption, Elution and Quantification of Proteins

For the experiments with human serum and saliva on self-assembled monolayers with different end groups, performed at the Department of Oral Biology at the State University of New York (Buffalo, NY, USA), a different procedure was chosen. Here, for adsorption of salivary proteins, 2.5 mL saliva per gram beads were mixed with the functionalized silica beads at 37 °C for 1 h under gentle rotation. Adsorption of serum proteins was performed with 1 mL HABS per gram beads at 37 °C for 10 min. Unbound proteins were removed by rinsing the beads three times with PBS buffer (pH 7.2, containing 0.05% NaN_3) before transferring them to a new vial and washing them another time.

After removal of residual water, using a pulled glass Pasteur pipette fitted to vacuum suction, proteins were desorbed from the beads' surface via boiling with 200 µL SDS solution (2% SDS in PBS buffer) per gram beads at 100 °C for 5 min. The eluate was transferred to an Eppendorf vial and stored at 4 °C for immediate use or frozen at −30 °C.

The protein content of HABS, saliva as well as the eluates was determined in 96 well microwell plates with the BCA assay, using the Pierce BCA Assay Kit from Thermo Fisher Scientific (Waltham, MA, USA). BSA was used as standard, all measurements were performed in duplicates. In each well, 10 µL protein solution were incubated with 200 µL BCA working solution for 30 min at 37 °C. Measurement of the absorption at 562 nm was carried out with a Synergy HT multi-detection microplate reader by BioTek Instruments, Inc. (Winooski, VT, USA). Protein concentration was calculated with the software Gen5.200.

11.1.4 Qualitative Protein Adsorption

On SAMs with different functional groups, qualitative protein adsorption was studied at the Department of Oral Biology at the State University of New York (Buffalo, NY, USA) via SDS-PAGE and western blotting.

Protein Separation via SDS-PAGE

In order to analyze the protein eluates, the serum or saliva proteins were at first separated via SDS-PAGE, similar to previously published protocols [283, 284]. To that purpose, appropriate dilutions of protein solutions were prepared with Tris-glycine SDS sample buffer, consisting of 2.5 g SDS, 0.606 g tris(hydroxymethyl)aminomethane (Tris) base and 2 mg bromophenol blue in 10 mL 70% glycerol solution. In order to break the proteins' disulfide bonds, β-mercaptoethanol was added to each sample (final concentration 2.5%), which was then heated to 100 °C for 10 min. Equal volumes of eluates (15 µL per lane for CBB/PAS stain, 20 µL for immunoblots) were separated on an 8–16% pre-cast Tris-glycine gel (Life Technologies, Carlsbad, CA, USA) for 90 min at 130 V. Precision Plus Protein™ All Blue Prestained Protein Standards (Bio-Rad Laboratories Inc., Hercules, CA, USA) were used as a molecular weight ladder.

Protein Staining after Separation

After separating the salivary or serum proteins via SDS-PAGE, the proteins were visualized via two different procedures, staining with CBB and with the periodic acid-Schiff (PAS) stain.

Coomassie Brilliant Blue (CBB) was used to visualize all proteins. To that purpose, the gels are soaked in the CBB staining solution, consisting of 1 g L^{-1} CBB (Bio-Rad, Hercules, CA, USA) in a 40% ethanol/10% acetic acid solution (v/v), for at least 3 h on an orbital shaker. Destaining of the gel was achieved by rinsing three times with the same solvent mixture (40% ethanol/10% acetic acid by volume) for 30 min each. After fixation of the gel in 1% acetic acid for 30 min, the stained gel was scanned.

Subsequently, the gel was also treated with the PAS stain for the visualization of glycoproteins. The gels were prepared by soaking in 10% acetic acid for at least 2 h at room temperature. Glycoproteins were then oxidized for 1–2 h at 4 °C with a 5 g L^{-1} periodic acid solution. Residual periodic acid was removed by several rinsing steps with decreasing concentrations of sodium arsenite ($NaAsO_2$) in 5% acetic acid (5 g L^{-1} $NaAsO_2$, 1 g L^{-1} $NaAsO_2$). After a final rinsing step with 5% acetic acid, the oxidized glycoproteins were stained via soaking in Schiff's reagent for 3 h to over night in the dark. The solution was prepared by dissolving 2.5 g basic fuchsin and 5 g sodium metabisulfite in a mixture of 500 mL water (with 5% acetic acid) and 50 mL 1 mol L^{-1} HCl.

Imaging of stained gels was carried out using a flat-bed scanner ImageScanner III from GE Healthcare (Amersham, UK) in the transparent mode.

Western Blot Analysis

For immunoblotting, proteins were transferred onto a nitrocellulose membrane after SDS-PAGE. The transfer was achieved via a Trans-Blot Turbo Blotting System by Bio-Rad (Hercules, CA, USA) (1.3 A, 25 V, 7 min). The membrane was then washed with Tris-buffered saline solution (TBS, 150 mmol L^{-1} NaCl, 20 mmol L^{-1} Tris-HCl, 0.02% NaN_3, pH 7.4) for 5 min. Blocking of unoccupied membrane surface was achieved by soaking the membrane in blocking solution, containing 2% milk in TBS-T (TBS with 0.1% Tween 20) for 1 h. Subsequently, the primary antibody was immobilized via incubation of the membranes with appropriate dilutions of the respective antibody (see Table 11.1) in blocking solution for 1 h at room temperature or 4 °C over night, before washing them three times with TBS-T buffer. The binding of the fluorophore-tagged secondary antibody (see Table 11.2) was achieved by soaking the membranes in a solution of the respective antibody in blocking solution for 1 h at room temperature. Membranes were then washed three times with TBS-T buffer and dried on a filter paper in the dark for 30 min. Membranes were scanned with a Typhoon 9400 fluorescence scanner by GE Healthcare (Amersham, UK).

Table 11.1: Survey of the primary antibodies used in immunostaining of salivary or serum proteins after separation via SDS-PAGE.

	Protein	Antibody type	Dilution	Supplier
Primary antibodies saliva	Lysozyme	Anti-human lysozyme C (E-5) mouse monoclonal antibody	1:200	Santa Cruz Biotechnology Inc. (Dallas, TX, USA)
	Cystatin	Anti-human cystatin rabbit polyclonal antibody	1:500	Gift from Dr. Molakala Reddy (University of Buffalo)
	ZAG	Anti-human zinc-α_2-glycoprotein rabbit polyclonal antibody	1:1000	BioVendor (Asheville, NC, USA)
	IgG FC	Anti-human IgG goat polyclonal antibody, Fc fragment specific	1:1000	Jackson ImmunoResearch (West Grove, PA, USA)
	Amylase	Anti-human amylase rabbit polyclonal IgG	1:1000	Calbiochem, EMD Biosciences Inc. (La Jolla, CA, USA)
	IgA HC	Anti-human IgA rabbit polyclonal IgG	1:1000	DakoCytomation (Glostrup, Denmark)
	MUC7	Anti-human MUC7 mouse monoclonal antibody (4D2-1D7)	1:1000	Abcam Inc. (Cambridge, MA, USA)
	DMBT1	Anti-human GP340 mouse monoclonal antibody (1G4)	1:500	Thermo Fisher Scientific (Rockford, IL, USA)
Primary antibodies serum	IgG F(ab')$_2$	Anti-human IgG goat polyclonal IgG, Fab fragment specific	1:1000	Jackson ImmunoResearch (West Grove, PA, USA)
	IgA HC	Anti-human IgA rabbit polyclonal IgG	1:1000	DakoCytomation (Glostrup, Denmark)
	ZAG	Anti-human zinc-α_2-glycoprotein rabbit polyclonal antibody	1:1000	BioVendor (Asheville, NC, USA)
	Albumin	Anti-human albumin chicken polyclonal IgY++ (IgG)	1:500	Abcam Inc. (Cambridge, MA, USA)
	Fibronectin	Anti-human fibronectin rabbit polyclonal IgG	1:1000	Abcam Inc. (Cambridge, MA, USA)

Table 11.2: Survey of the fluorescently labeled secondary antibodies used in immunostaining of salivary or serum proteins after separation via SDS-PAGE.

Antibody	Used for	Dilution	Supplier
Alexa Fluor 488 goat anti-mouse IgG	Lysozyme, MUC7, DMBT1	1:1000	Life Technologies Corp. (Eugene, OR, USA)
Alexa Fluor 488 goat anti-rabbit IgG	Cystatin, ZAG, amylase, IgA HC, fibronectin	1:1000	Life Technologies Corp. (Eugene, OR, USA)
Alexa Fluor 488 chicken anti-goat IgG	IgG Fc, IgG F(ab')$_2$	1:1000	Life Technologies Corp. (Eugene, OR, USA)
Alexa Fluor 488 donkey-α-chicken IgY++ (IgG)	Albumin	1:500	Jackson ImmunoResearch (West Grove, PA, USA)

11.2 Investigation of Cell Behavior

All cell experiments were performed at the Department of Cell Biology of the Rostock University Medical Center and were carried out by Dr. Susanne Stählke. The procedures have already been published in detail [20] and only the essential steps will be summarized in the following. Experiments were performed with single-side polished wafers with a titanium surface.

11.2.1 Cell Cultivation and Sample Preparation

For all experiments, the human osteoblast-like cell line MG-63 (American Type Culture Collection ATCC®, CRL-1427™, Manassas, VA, USA) was used. Cells were cultured in Dulbecco's modified Eagle's medium (DMEM) (Life Technologies GmbH, Darmstadt, Germany), containing 10% fetal calf serum (Biochrom FBS Superior, Merck KGaA, Darmstadt, Germany) and 1% gentamicin (Ratiopharm GmbH, Ulm, Germany), under standard conditions (temperature 37 °C, 5% CO_2/95% air).
Prior to cell experiments, unmodified titanium wafers were sterilized in 70% ethanol for 10 min, then rinsed with PBS. Modified titanium wafers were rinsed with PBS and preconditioned via incubation in medium with FBS for 1–3 h before storing in PBS buffer. Suspended MG-63 osteoblasts were then seeded on the surfaces and cultivated for 1 h or 24 h (40 000 cells/wafer for cell spreading and morphology after 1 h, 30 000 cells/wafer for cell spreading and morphology after 24 h and 50 000 cells/wafer for cell cycle analysis).

11.2.2 Examination of Cell Morphology and Cell Spreading

Morphology of the cells after cultivation on functionalized titanium wafers for 1 h or 24 h was investigated via field emission SEM. To that purpose, cells were fixed with 2.5% glutaraldehyde, dehydrated through an acetone concentration series and dried in a critical point dryer (EmiTech K850, Quorum Technologies Ltd, Lewes, UK). After sputtering the cells with gold, cells were imaged via field emission SEM (Merlin VP compact, Carl Zeiss AG, Oberkochen, Germany), using an acceleration voltage of 5 kV [20]. In order to evaluate cell spreading, cell areas (in μm^2) were determined from the obtained SEM images. To that purpose, the cell area of 40 cells per sample was measured with the software ImageJ 1.48a (Wayne Rasband, National Institutes of Health, USA).

11.2.3 Analysis of the Actin Cytoskeleton

For the examination of the actin cytoskeleton of cells on the differently functionalized substrates, cells were cultivated on the wafers for 1 h or 24 h and subsequently fixed with 4% paraformaldehyde. Permeability of the cell membranes was achieved by a treatment with 0.1% Triton X-100, followed by the staining of the F-actin with $0.1\,\mathrm{mg\,mL^{-1}}$ phalloidin-TRITC. Images were obtained from cells embedded in mounting medium Fluoroshield™ (Sigma-Aldrich Chemie GmbH, Taufkirchen, Germany, contains DAPI for staining of the nuclei) with the inverted confocal laser scanning microscope LSM780 (Carl Zeiss Microscopy GmbH, Jena, Germany), which was equipped with a helium-neon laser (excitation wave length 543 nm) and a 63x oil immersion objective. The software ZEN 2011 (ZEN 2011 SP4, black edition, Carl Zeiss, Carl Zeiss Microscopy GmbH) was used.

11.2.4 Cell Cycle Analysis, Proliferation and Apoptosis

Cell cycle analysis was performed with a flow cytometer (FACSCalibur, Becton Dickinson, BD Biosciences, San Jose, CA, USA) equipped with an argon ion laser (excitation wavelength 488 nm) via determination of the relative DNA content. To that purpose, cells were cultivated on modified wafer substrates for 24 h before detaching the cells by trypsinization in order to obtain suspended cells. Washing media were collected for the determination of apoptotic cells. After fixation and permeabilization of the cells with 70% ethanol at −20 °C over night, RNA was removed via treatment with RNAse (ribonuclease A, from bovine pancrease) before staining the DNA with propidium iodide (PI). From the data of the flow cytometric measurement (software CellQuest™ Pro, BD Biosciences), the percentage of proliferative and apoptotic cells was calculated as well (software ModFIT LT 3.0, BD Biosciences).

12 Statistics

Unless otherwise stated, results are provided as medians. The 25% and 75% quartiles are given as range (in brackets in tables) or error bars (in figures). The following numbers of samples were used. For XPS spectra, at least two wafers were measured ($n \geq 2$). The amine group density was calculated from at least two independent experiments with three replicates each ($n \geq 6$) for each surface coating, except for SAM-N_3 and proline ($n = 3$). Surface wettability and SFE were determined from contact angles measured on at least four wafers per liquid (usually four drops per wafer, $n \geq 16$). Dynamic contact angle measurements were carried out with six wafers for each surface modification ($n = 6$). Regarding the zeta potential, electrophoresis data was obtained from at least two measurements at each pH value, each consisting of two measurements in triplicates ($n \geq 12$). For each surface modification, three streaming current measurements were performed ($n = 3$). For the analysis of quantitative protein adsorption on the surfaces, BCA assays were carried out in at least two independent experiments with three replicates each ($n \geq 6$). Protein quantification from the eluates was performed at least three times for each surface and biofluid ($n \geq 3$). Cell spreading was determined from the cell area of 40 cells for each modification and incubation time. Cell cycle analysis was performed with two independent experiments with two technical replicates each. For protein adsorption and cell experiments, pairwise comparisons were performed with the Mann-Whitney-U-Test with considered p values of < 0.05 (software IBM SPSS Statistics 25, IBM, Armonk, NY, USA).

Part IV

Results and Discussion

Before the results of this PhD thesis are presented, analyzed and discussed in the following chapters, two tables are given in order to make the discussion more comprehensible. The first one (Table IV.1) summarizes which substrate was used for which analysis technique, whereas the second one (Table IV.2) gives an overview which surface properties were studied for each individual modification.

Table IV.1: Overview of the use of different substrate geometries for the various analysis techniques.

Substrate type	Analysis via
Single-side polished silicon wafer	XPS, static contact angle measurements (and SFE), streaming current measurements
Double-side polished silicon wafer	Tensiometry, static contact angle measurements
Titanium wafer	XPS, static contact angle measurements (and SFE), streaming current measurements, cell experiments
Silica beads	Sulfo-SDTB assay, protein adsorption
Silica spheres	IR spectroscopy, electrophoresis

In Table IV.2 it also is indicated where results from the master's thesis or previous publications of the work group are included for comparison or broader discussion. Data is available if cells are filled with a check mark (✓). A check mark in brackets means that experiments could only be performed partially. No experiments have been carried out in cases where cells are marked with a cross (✗). Results from measurements during the master's thesis are displayed when cells are indicated with the letter **M**.

Table IV.2: Survey of the investigated surface modifications and applied analytical techniques, presented in this PhD thesis.

Surface coating	Analytical Technique										
	XPS	IR spectroscopy	Sulfo-SDTB assay	Contact Angle	SFE	Tensiometry	Electrophoresis	Streaming current	BCA assay	SDS-PAGE + western blot	Cell experiments
SAM-PEG	✓[a]	✓	✗	✓	✓	✗	✗	✓[a]	✓[a]	✓	✗
SAM-CH_3	✓[a]	✓	✗	✓	✓	✗	✗	✓[a]	✓[a]	✓	✗
SAM-CF_3	✓[a]	✓	✗	✓	✓	✗	✗	✓	✓[a]	✓	✗
SAM-NH_2	✓	✓[a]	✓[b]	✓	✓	✗	✗	✓[a]	✓[a]	✓	✗
SAM-Py	✓	✓[a]	✗	✓	✓	✗	✗	✓	✓[a]	✓	✗
SAM-COOH	✓[a]	✓[a]	✓[b]	✓	✓	✗	✗	✓[a]	✓[a]	✓	✗
SAM-SO_3H	✓[a]	✓	✗	✓	✓	✗	✗	✓[a]	✓	✓	✗
APD	✓	**M**	✓[b]	✓[b]	✓[b]	✓	**M**	(✓)[c]	✓	✗	✓
PPI-G2	✓	**M**	✓[b]	✓[b]	✓[b]	✓	**M**	✓	✓	✗	✗
PPI-G4	✓	**M**	✓[b]	✓[b]	✓[b]	✓	**M**	✓	✓	✗	✓
PAMAM polymer	✓	✓	✓[b]	✓[b]	✓[b]	✓	✓	✗	✓	✗	✗
PEI polymer	✓	✓	✓[b]	✓[b]	✓[b]	✓	✓	✓	✓	✗	✓
AMAM	✓	**M**	✓[b]	✓[b]	✓[b]	✓	**M**	✗	✓	✗	✗
DMAPS	✓	✓	✓	✓	✓	✓	✓	✓	✓	✗	✗
SAM-NMe_2	✓	✓	✗[d]	✓	✓	✓	✓	✗	✓	✗	✗
SAM-NO	✓	✓	✗[d]	✓	✓	✓	✓	✗	✓	✗	✗
Proline	✗	✗	✓	✗	✗	✗	✗	✗	(✓)	✗	✗

[a] Data has previously been published at least partially [13, 15, 16, 18, 19, 21].

[b] Results from the PhD thesis were combined with data from the preceding master's thesis [22].

[c] Streaming current measurements were only performed on titanium wafers.

[d] Instead, synthesis success was qualitatively checked via the chloranil test.

The large number of investigated surface functionalizations and applied analysis techniques also necessitates structuring and dividing of the obtained results. Thus, the surface modifications will be split up into three major groups, as already indicated in Table IV.2. These groups are the self-assembled monolayers with different functional groups, the oligomeric or polymeric amine group-bearing modifications (namely APD, PPI-G2, PPI-G4, PEI polymer, PAMAM polymer and AMAM) and the osmolyte-derived coatings (DMAPS, SAM-NO and proline) with their precursors. Results for these groups will be presented separately and subdivided further. At first, the data that verifies successful surface modification (XPS, IR spectroscopy, sulfo-SDTB assay) will be presented. After that, the investigated surface functionalizations are analyzed in detail with respect to their wetting behavior, their surface free energy as well as their zeta potential. At last, the results from protein adsorption experiments as well as their relation with surface properties will be discussed for each group of modifications. The last separate chapter will consist of the analysis of the results for titanium wafers, which were obtained from physicochemical analysis as well as from cell experiments at the Department of Cell Biology of the Rostock University Medical Center.

13 SAMs with Varying Terminal Functional Groups

In order to develop novel protein-repellent surface coatings, it is vital to gain a detailed understanding of how protein adsorption depends on the quantitatively measurable physicochemical properties of the surface. To that purpose, this first chapter will summarize the properties of a variety of self-assembled monolayers with different end groups (see Figure 13.1) and examine how these characteristics affect protein adsorption from human saliva and serum quantitatively and qualitatively. The investigated surface modifications exhibit a broad range of different surface properties. They are hydrophobic (SAM-CH_3, SAM-CF_3), hydrophilic (SAM-PEG), permanently charged (SAM-Py, SAM-SO_3H) or exhibit a pH-dependent protonation behavior (SAM-NH_2, SAM-COOH).

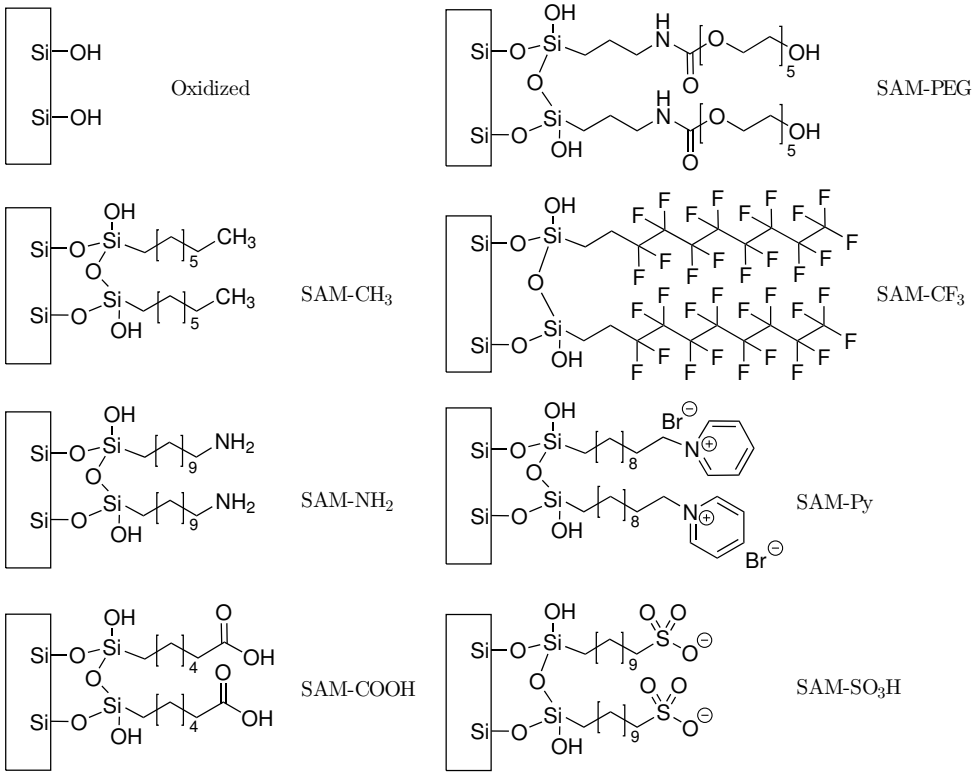

Figure 13.1: Overview of the examined SAMs with different functional groups as well as their abbreviated name.

In order to present a comprehensive overview, data will be summarized that was acquired over a large period of time with the help of many interns. Significant contributions to the results were made by Michael Überreiter, Jakob Asenbauer, Andreas Eidt and Ulrike Vogl. Data on physicochemical properties has partially been included in previous publications as well as in the of PhD thesis of Verena Katzur [13, 15–21]. The results for quantitative and qualitative protein adsorption, together with a summary of the measured surface characteristics, have recently been submitted for publication.

13.1 Verification of Successful Surface Coating

13.1.1 Determination of the Chemical Composition via XPS

The successful immobilization of the self-assembled monolayers on wafers was routinely verified by XPS. The results are summarized in Table 13.1 and have already been published previously for the most part [13, 15, 16, 18, 21].

Table 13.1: Chemical composition of self-assembled monolayers with different terminal functional groups, determined via XPS.

Surface modification	Elemental composition [at-%]				
	Si	C	O	N	Other
Oxidized	44	17	32	1	
SAM-PEG[a,b]	37	21	40	2	
SAM-CH_3[a]	43	17	39	0	
SAM-CF_3[a,b]	18	18	17	0	F: 50
SAM-Br[c,d]	41	30	28	0	Br: 1
SAM-N_3[c,d]	38	30	29	3	Br: 0
SAM-NH_2	35	34	28	2	
SAM-Py	32	44	26	1	Br: 0
SAM-CH=CH_2[c,d]	43	28	29	0	
SAM-COOH[c,d]	41	26	33	0	
SAM-$SCOCH_3$[d]	8	74	15	0	S: 4
SAM-SO_3H[d]	5	61	25	1	S: 5

[a] Elemental composition was published in Schweikl et al. [15].
[b] XPS data was previously published in Mueller et al. [16, 21].
[c] XPS data was previously published in Katzur et al. [18].
[d] XPS data was part of the PhD thesis of Verena Katzur [13].

In comparison with the oxidized but unfunctionalized wafers, successful silanization is confirmed by a decrease in the silicon content and accompanied by an increase in the carbon content due to the immobilization of the alkane backbone, observable for all surface modifications. The synthesis of the monolayer SAM-PEG can additionally be confirmed by the increase in oxygen and nitrogen, which is caused by the introduction of urethane and ethylene glycol groups. The synthesis of a perfluorinated surface coating is easily verified by a fluorine content of 50 at-% on the functionalized surface. The XPS spectra of the remaining surface modifications are best compared to the data of the intermediate SAMs (see Table 13.1). On both SAM-NH_2 and SAM-Py, no bromine

but nitrogen can be detected, meaning the substitution of the terminal bromine of the intermediate SAM by azide or pyridine was successful [13, 18]. The reduction of the azide group to the primary amine groups cannot be proven with this method. It is, however, confirmed by the results of IR spectroscopy, contact angle measurements and the sulfo-SDTB assay (see section 14.2.2). The successful conversion of SAM-$CH{=}CH_2$ to SAM-COOH leads to an increased oxygen as well as decreased carbon content due to the cleavage of carbon dioxide during the oxidation with $KMnO_4$ [13, 18]. The monolayer bearing terminal sulfonic acid groups (SAM-SO_3H) is characterized by the presence of sulfur but also by the increase in oxygen content compared to the intermediate thioester (SAM-$SCOCH_3$), a result of the oxidation with oxone [13].

13.1.2 Evaluation of IR Spectra

On particulate substrates, no XPS analysis was performed. Instead, the immobilization of self-assembled monolayers with the desired end groups was investigated with DRIFT spectroscopy. The obtained IR spectra have partially been published in the PhD thesis of Verena Katzur (SAM-NH_2, SAM-Py, and SAM-COOH) [13].
The IR spectra are summarized in Figure 13.2. All modifications share a negative band at approximately $3740\,cm^{-1}$. This is the consequence of the reduced silanol group density after silanization and thus proves successful surface coating [285]. At least two signals in the range between 3000 and $2800\,cm^{-1}$ can be attributed to the asymmetric and symmetric C-H stretching vibration of the -CH_2- units of the SAM backbone of all coatings [285]. Most surface functionalizations (with exception of SAM-CF_3) also exhibit a broad band at approximately $1250\,cm^{-1}$ with a shoulder at $1090\,cm^{-1}$. This signal cannot be assigned unambiguously but is probably composed of contributions from C-C skeletal vibrations, Si-O-Si vibrations and Si-CH_2-R vibrations [285]. In the IR spectrum of SAM-CF_3, instead a broad vibration band around $1340\,cm^{-1}$ is observed, which is related to the C-F stretching vibrations of the perfluoroalkane chain [285]. The surface coating with ethylene glycol units (SAM-PEG) carries three different types of functionalities, a urethane group, five ether units as well as the terminal hydroxyl group, which can be attributed to additional vibrational bands of the IR spectrum. The O-H stretching vibration of the hydroxyl group is probably responsible for the broad band observable around $3400\,cm^{-1}$ [285]. The signal at $1725\,cm^{-1}$ is related to the C=O stretching vibration of the urethane group. The asymmetric and symmetric C-O-C stretching vibration of the ether groups probably do no only contribute to the signal at $1095\,cm^{-1}$, but they also cause the additional band at $960\,cm^{-1}$ [285].
Regarding the remaining modifications with charged or ionizable groups, the discussion of their IR spectra will be kept short (for details see [13, 18]). For the sulfonic acid SAM, successful synthesis cannot be confirmed unambiguously, although the asymmetric and

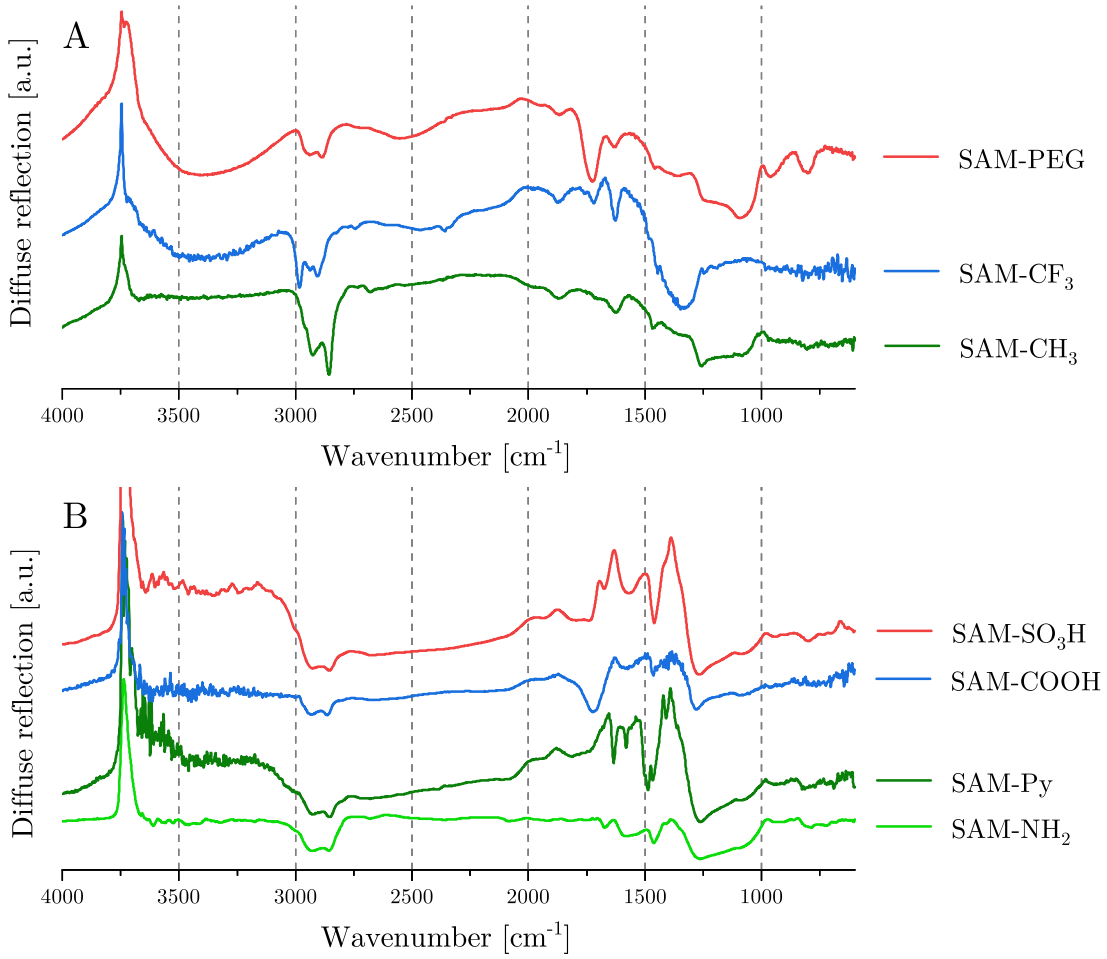

Figure 13.2: IR spectra of self-assembled monolayers with (A) non-ionizable and (B) ionizable functional groups, recorded via DRIFT spectroscopy. The IR spectra have partially been published by Verena Katzur in her PhD thesis [13].

symmetric vibration of the sulfonic acid groups may contribute to the bands at 1260 and 1070 cm^{-1} [13, 285]. The oxidation of the vinylic SAM (SAM-CH=CH_2) to SAM-COOH can be proven in two ways: At first, no band of vinylic C-H stretching vibrations can be identified above 3000 cm^{-1}. Instead, the signal at 1725 cm^{-1} can be attributed to the C=O stretching vibration of the carboxylic acid group [13, 18, 285]. The IR spectrum of SAM-Py exhibits several characteristic bands at 1635, 1580 and 1485/1465 cm^{-1}, which are caused by C=N and C=C stretching vibrations of the pyridinium ring as well as by C-H deformation vibrations of the aliphatic -$(CH_2)_n$- chain [13, 285]. At last, the successful formation of an amine-terminated SAM (SAM-NH_2) from SAM-N_3 can be confirmed via the disappearance of the characteristic band of the azide group in the region between 2200 and 2000 cm^{-1} as well as the appearance of N-H deformation vibrations at 1585 and 1460 cm^{-1} [13, 18, 285].

In summary, the formation of the desired SAMs can both be confirmed on planar silicon wafers and on particulate silica substrates for most modifications.

13.2 Analysis of Physicochemical Properties

Two vital surface properties were analyzed for all self-assembled monolayers: their wetting behavior as well as their electrokinetic behavior. As expected from the diversity of functional groups, a broad range of contact angles, surface free energies and zeta potentials was obtained.

13.2.1 Wettability and SFE

Both the hydrophilicity and the SFE of the different self-assembled monolayers were derived from static contact angle measurements via the sessile drop technique. The surface wettability was assessed via the water contact angle, for the calculation of the SFE additional contact angle measurements were carried out with formamide and diiodomethane. As water contact angles have been measured routinely, and therefore data has been collected continuously, similar contact angles have been published multiple times [13, 15–18, 20, 21]. The wettability, however, of all seven surface modifications, has not yet been compared comprehensively. Therefore, all water contact angles from the different self-assembled monolayers as well as intermediate modifications are summarized in Table 13.2 and Figure 13.3. The contact angles with formamide and diiodomethane for the calculation of the SFE (and its components) are added in Table 13.2 as well.

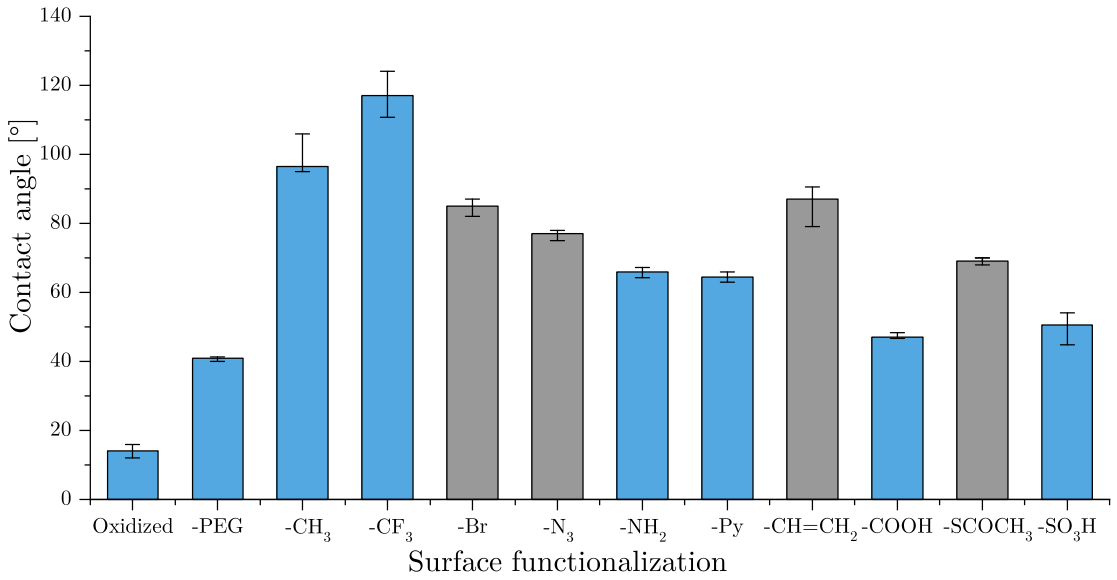

Figure 13.3: Water contact angles of self-assembled monolayers and intermediate SAMs as a measure of the modifications' wettability.

Table 13.2: Static contact angles (with water, formamide and diiodomethane) of self-assembled monolayers with different end groups and their precursor SAMs. Similar water conact angles have previously been published [13, 15–18, 20, 21].

Surface modification	Contact angle [°]		
	Water	Formamide	Diiodomethane
Oxidized	14 (12-16)	10 (6-12)	37 (33-42)
SAM-PEG	41 (40-41)	27 (26-28)	33 (32-35)
SAM-CH_3	97 (95-106)	81 (78-87)	66 (62-68)
SAM-CF_3	117 (111-124)	98 (96-102)	93 (91-96)
SAM-Br	85 (82-87)		
SAM-N_3	77 (75-78)		
SAM-NH_2	66 (64-67)	44 (44-44)	39 (36-42)
SAM-Py	65 (63-66)	39 (37-39)	40 (39-42)
SAM-CH=CH_2	87 (79-91)		
SAM-COOH	47 (47-48)	20 (17-27)	37 (35-39)
SAM-$SCOCH_3$	69 (68-70)		
SAM-SO_3H	51 (45-54)	24 (22-26)	44 (42-46)

As it can be seen from Figure 13.3, the surface modifications cover a large range of wettabilities due to their different functional groups. The most hydrophilic behavior is observed for the uncoated, oxidized wafer substrates, exhibiting a water contact angle of 14°. These results are identical or similar to previously published data of our work group [13, 15–18, 20, 21] but slightly higher than literature data, where complete wetting (contact angle 0°) was observed [56].

Similar water contact angles between 41° and 51° are observed for SAM-PEG as well as the surface modifications with a negative charge, SAM-COOH and SAM-SO_3H, as published previously [13, 15–18, 21]. The hydrophilic properties of these surface coatings agree well with literature. Janssen et al., for example, measured a water contact angle of 35.8° for a self-assembled monolayer carrying six to nine ethylene glycol units [286]. The data obtained for SAM-COOH also matches the water contact angle data in literature (48.3° [271], advancing angle 46° [272]). For this surface modification, also a significant decrease in the contact angle in comparison with the intermediate SAM-CH=CH_2 again confirms the successful oxidation reaction. The wettability of the sulfonate monolayer SAM-SO_3H is significantly higher than of the intermediate SAM-$SCOCH_3$. Yet, the hydrophilicity is is lower, i.e. the contact angle higher than measured by other researchers (advancing angle 32° [272], advancing angle 15° [287]).

Thus, one might assume that the oxidation reaction of the thioacetate groups was not quantitative, as proposed by Verena Katzur in her PhD thesis [13].
Both modifications with positive charges, SAM-NH_2 and SAM-Py, exhibit water contact angles of approximately 65° and are thus positioned at the border between hydrophobic and hydrophilic behavior [187]. Both modifications show a significant decrease in their contact angle with regard to the respective precursor (SAM-N_3 with 77° for SAM-NH_2 and SAM-Br with 85° for SAM-Py), indicating the successful conversion of the end groups. The wettability of amine-functionalized surfaces is in good accordance with literature data (advancing angle 70° [272], 68° [288]). For a pyridinium-terminated surface coating, only very limited literature data is available. Müller et al., however, measured lower contact angles (51°, 54°) for modifications with a terminal pyridinium and an inner ester group [289].
The remaining two self-assembled monolayers, SAM-CH_3 and SAM-CF_3, are characterized by their high water contact angles of 97° or 117° respectively, i.e. their hydrophobicity. For both modifications, these results are in accordance both with previously published results of our work group [15–17, 21] but also with literature data as Janssen et al. obtained a contact angle of 98.2° for an alkyl SAM with a C-18 chain and an angle of 109.6° for a perfluorinated monolayer [286].

From the static contact angles with water, formamide and diiodomethane, the surface free energy of the surface modifications was calculated according to the LW/AB approach. Previously published SFE data for oxidized wafers, SAM-NH_2 and SAM-COOH [18, 20] was obtained from different contact angles and performed with the approach of Owens, Wendt, Rabel and Kaelble. Hence, slightly deviating results were obtained. In this work, calculations were performed according to Shalel-Levanon and Marmur [241]. To that purpose, the following components of the surface tensions of the three liquids were used (see Table 13.3).

Table 13.3: Surface tensions γ as well as their components γ^{LW}, γ^+ and γ^- of water, formamide and diiodomethane for the SFE calculation, summarized by Kwok [290].

	Surface tension (components) [mN m^{-1}]			
	γ	γ^{LW}	γ^+	γ^-
Water	72.8	21.8	25.5	25.5
Formamide	58	39	2.28	39.6
Diiodomethane	50.8	50.8	0	0

The resulting SFE components and total surface free energies are depicted in Figure 13.4. One notices at first glance that – similar to the water contact angles – the surface free energies vary greatly among the different modifications.

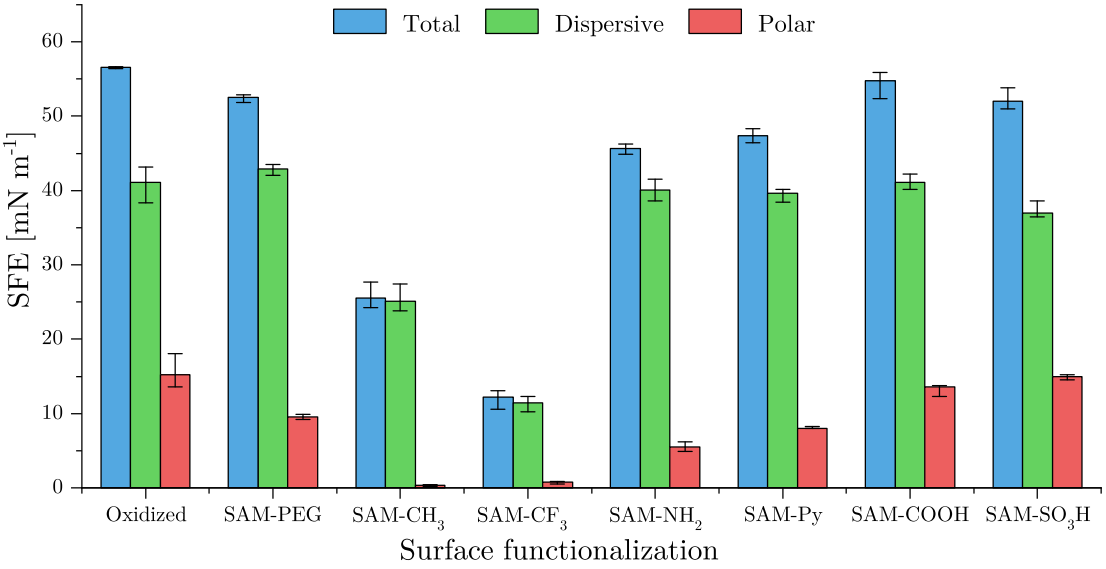

Figure 13.4: SFE as well as its polar and dispersive component of self-assembled monolayers with varying functional end groups, calculated according to the LW/AB approach.

The highest surface free energy and highest polar component (56.5 and 15.2 mN m^{-1}) is obtained for the oxidized and unmodified wafer substrates, which is rather similar to results previously published by our group [20]. Surface free energies that are only slightly lower ($\approx$ 52–55 mN m^{-1}) are obtained for the hydrophilic surface modifications SAM-PEG, SAM-COOH and SAM-SO_3H. Both modifications with acidic groups possess also very high polar SFE components (13.6–15 mN m^{-1}), whereas the polar component of the ethylene glycol coating is significantly lower (9.5 mN m^{-1}). A similar picture presents itself for the cationic modifications SAM-NH_2 and SAM-Py. As for the water contact angles, they share very similar total surface free energies of approximately 46 mN m^{-1}, they differ, however, with regard to their polar SFE components. The ionic coating SAM-Py exhibits a higher polar component of 8.0 mN m^{-1} than the amine coating SAM-NH_2 (5.5 mN m^{-1}). The results for the modifications SAM-NH_2 and SAM-COOH are in good agreement with previously published data [18], although the Owens-Wendt approach was chosen here for the SFE calculation. The remaining two modifications, SAM-CH_3 and SAM-CF_3, again differ from the other coatings as they are characterized by very low surface free energies of 25.4 mN m^{-1} and 12.2 mN m^{-1} and very small polar contributions $<$ 1 mN m^{-1}. These total SFEs were similarly obtained by Janssen et al. (23.5 and 13.5 mN m^{-1} respectively), applying the approach of Owens, Wendt, Rabel and Kaelble [286].

In summary, the surface modifications carrying very different functional groups exhibit a broad range of wettabilites and, hence, surface free energies as expected. Thus, they are suitable for studying the influence of wetting properties on protein adsorption.

13.2.2 Zeta Potential

In addition to the hydrophilicity and the surface free energy, also the zeta potential of the coatings was examined via streaming current measurements of functionalized wafers. The surface modifications of this chapter have mainly been investigated in the scope of the PhD thesis of Verena Katzur where they have been studied thoroughly. Hence, the zeta potential curves of oxidized wafers as well as SAM-PEG, SAM-CH_3, SAM-NH_2, SAM-COOH and SAM-SO_3H are not shown here because they are available in previous publications [13, 18, 19]. The zeta potential curves of the remaining two modifications, SAM-CF_3 and SAM-Py, are shown in Figure 13.5.
The zeta potential curves were used to determine the isoelectric points as well as the zeta potentials at the pH of the physiological fluids studied in protein adsorption experiments (HABS: pH 7.4, saliva: pH 8.3, see Table 13.4).

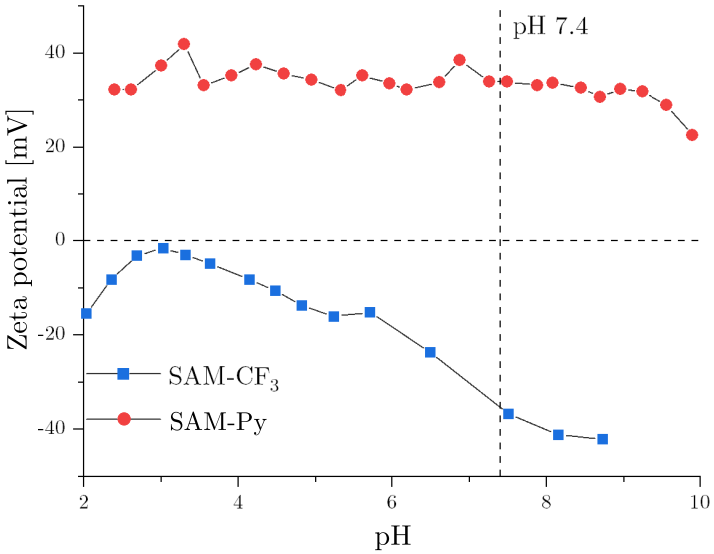

Figure 13.5: Zeta potential of wafer substrates functionalized with a perfluoroalkane SAM (SAM-CF_3) or with pyridinium groups (SAM-Py).

The oxidized but unfunctionalized surface is characterized by a low IEP at pH 2.8 and a strongly negative zeta potential under physiological conditions ($< -105\,\text{mV}$) [13, 18, 19] because negative charges are present on the wafer surface due to the dissociation of surface silanol groups [291].
The surface coatings without ionizable groups, SAM-PEG, SAM-CH_3 and SAM-CF_3, all show very similar electrokinetic properties, which do not differ strongly from the unfunctionalized silicon surface. Here, low IEPs in the range between pH 3 and pH 4 are observed, which correspond to negative zeta potentials (-35 to $-90\,\text{mV}$) at pH 7.4 or 8.3 respectively [13, 19]. These results are in accordance with literature as an isoelectric point below pH 4 for a methyl group-terminated SAM was also observed by Shyue et al., whereas Chan et al. obtained an IEP of 4.3 for an OEG surface coating [272, 292].

Table 13.4: Isoelectric point and zeta potential at pH 7.4 and pH 8.3, obtained from streaming current measurements of wafers with functionalized self-assembled monolayers.

Surface Coating	IEP	ζ-potential [mV]	
		At pH 7.4	At pH 8.3
Oxidized[a,b,c]	2.8	−105	−125
SAM-PEG[a]	3.2	−70	−75
SAM-CH_3[a]	3.8	−80	−90
SAM-CF_3	-	−35	−40
SAM-NH_2[a,b]	7.1	−3	−20
SAM-Py	-	+35	+35
SAM-COOH[a,b,c]	-	−25	−35
SAM-SO_3H[a]	-	−120	−125

[a] Data is derived from zeta potential curves presented by Verena Katzur in her PhD thesis [13].

[b] The data has previously been published in Eichler et al. [19].

[c] The results have been previously been published by Katzur et al. [18].

A completely different situation can be observed for the group of ionic coatings. The zeta potentials cover a large range from −120 mV to +40 mV and exhibit completely different isoelectric points. A differentiation can be made between the surfaces bearing positive charges (SAM-NH_2, SAM-Py) and the surfaces with negative charges (SAM-COOH, SAM-SO_3H).

Among the cationic coatings, the surface with terminal pyridinium groups always carries positive charges, irrespective of the pH. Hence, a rather similar positive zeta potential between +30 mV and +40 mV is observed in the range between pH 2 and pH 10, and no isoelectric point can be determined. This behavior is rather similar to the electrokinetic properties of a self-assembled monolayer with positively charged quaternary ammonium groups, which was examined by Shyue et al. [272], but it contradicts the results Verena Katzur presented in her PhD thesis [13]. In her work, the pyridinium coating unexpectedly exhibited an IEP of 5.1 and negative zeta potentials under physiological conditions, which was explained by a low number of immobilized pyridinium groups, smaller than the number of remaining surface silanol groups [13]. In comparison to these early studies, the modification procedure has been improved significantly, and thus the density of immobilized groups has probably been increased, resulting in higher zeta potentials seen in this thesis. A different situation can be seen

for SAM-NH_2 because the protonation and, therefore, the charge of these groups depend on the pH of the surrounding solution. Thus, the zeta potential decreases with increasing pH, corresponding to an IEP at pH 7.1 and a slightly negative zeta potential at pH 7.4 and pH 8.3 [13, 18, 19], similar to the zeta potential curve measured by Shyue et al. [272].

Regarding the anionic surface coatings SAM-COOH and SAM-SO_3H, some differences can be observed. Having a look at the surface with carboxylic acid groups at first, the respective zeta potential curve approaches 0 mV at approximately pH 3, although no actual isoelectric point can be determined, as also observed by Shyue et al. [272]. The corresponding zeta potential at physiological conditions is negative (−25 mV or −35 mV respectively) [18, 19]. Deviating from their behavior in solution (pK_a of roughly 4.8 [131]), surface-immobilized carboxylic groups exhibit a gradual deprotonation, starting roughly at pH 3 and being completed at pH 11, which corresponds to an effective pK_a between 6 and 9, depending on the degree of deprotonation [293]. In contrast, a different behavior is observed for SAM-SO_3H. Sulfonic acid groups act as a very strong acid in solution (pK_a −9 [131]) and they retain moderately acidic properties, even if they are immobilized in a self-assembled monolayer. Here, they exhibit a pK_a of roughly 2 and are fully deprotonated at pH 5 [272]. This is reflected by the decrease of the zeta potential at low pH values, which reaches a plateau at roughly pH 5, when the deprotonation of the sulfonic acid groups is complete. The resulting surface does not exhibit an IEP and carries a strongly negative charge (−120 mV) at physiological conditions [13].

13.3 Quantitative and Qualitative Protein Adsorption

Following physicochemical characterization, adsorption of salivary and serum proteins was studied both quantitatively as well as qualitatively. Quantification was performed with the BCA assay in two different ways. In Regensburg, the amount of adsorbed proteins was determined on the silica beads, whereas in Buffalo the adsorbed mass was calculated from the protein concentration of the eluates after desorption of the proteins from the surface. Protein adsorption studies on SAMs with saliva or FBS have previously been published by our work group, applying either the BCA assay [19, 21] or other quantification techniques [16, 17, 19, 21]. A comprehensive set of results for all modifications, except SAM-CF_3 and SAM-SO_3H, was presented by Verena Katzur in her PhD thesis [13]. No data has yet been published for human serum. In addition to the BCA assay, SDS-PAGE and western blotting were used in Buffalo to identify the composition of the protein layers on the different surface modifications. The results of quantitative and qualitative protein adsorption, together with the characterization of the surface modifications, have recently been submitted for publication.

Prior to all experiments, the protein content of the physiological fluids was determined with the BCA assay. A total protein content of 0.91 (0.86–0.96) $\mathrm{mg\,mL^{-1}}$ was obtained for pooled saliva. The median protein concentration of saliva from individual donors, as used for qualitative protein adsorption, was determined as 1.08 (0.90–1.30) $\mathrm{mg\,mL^{-1}}$. For FBS, a protein content of 36.1 (35.0–37.8) $\mathrm{mg\,mL^{-1}}$ was measured. These results are in accordance with literature [159, 165]. The protein content of human serum was quantified as 48.3 (45.1–55.2) $\mathrm{mg\,mL^{-1}}$ and thus slightly lower than data found in literature [168]. The saliva samples possessed a pH of 8.3 ± 0.1, the pH value of the FBS samples was 7.7 ± 0.1. For human serum, a pH of 7.4 was reported in literature [294].

13.3.1 Quantitative Protein Adsorption

Adsorption of proteins from whole human saliva was determined on the surfaces or in solution after desorption of the proteins from the surface (see Figure 13.6).
As can be seen, the results for both methods mostly resemble each other. In both cases, strong protein adsorption is observed on SAM-NH_2 and SAM-SO_3H ($\approx$ 40–50 $\mathrm{ng\,cm^{-2}}$). Medium protein adsorption ($\approx$ 25–35 $\mathrm{ng\,cm^{-2}}$) is measured for oxidized substrates as well as SAM-Py and SAM-COOH, whereas low protein fouling is obtained for SAM-CH_3 and SAM-CF_3 ($< 20\,\mathrm{ng\,cm^{-2}}$). For the SAM-PEG coating, however, large discrepancies are observed between the small amount measured on the surface (non-fouling surface) and the considerably larger protein amounts measured in solution after protein desorption (similar to the amount on SAM-Py).

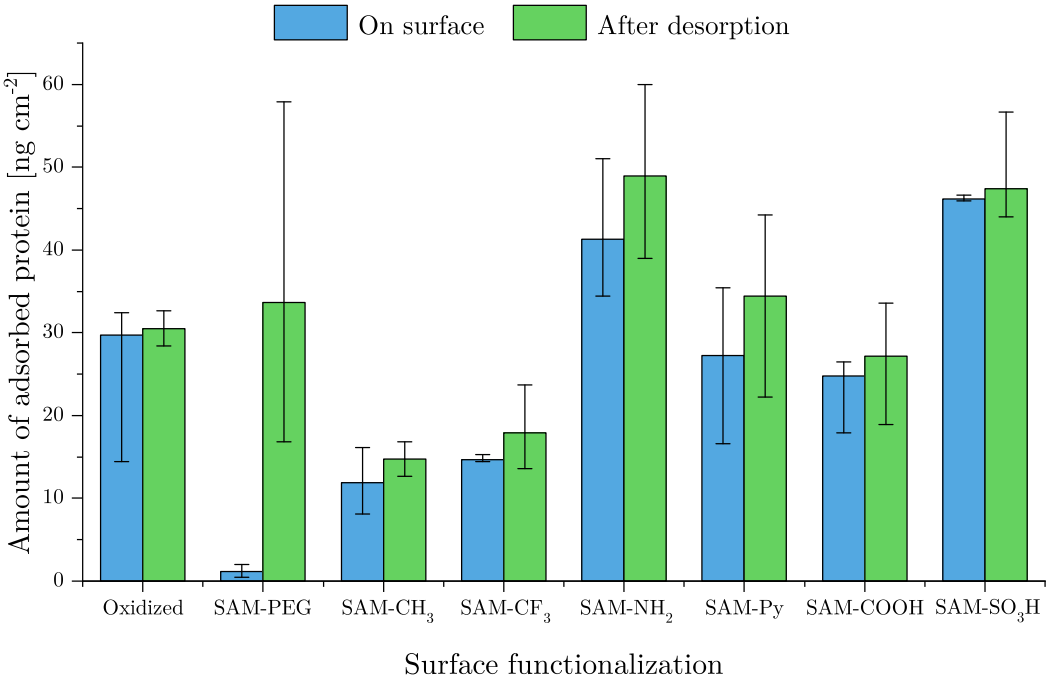

Figure 13.6: Amount of adsorbed protein from whole human saliva on SAMs with different end groups. Protein quantification was performed with the BCA assay, either on the substrate surface or after protein desorption. Results have partially been published previously [13, 17, 19, 21]. For improved clarity, the results of the Mann-Whitney-U test are not included in the figure but will be summarized here. Comparing the results of the BCA assay on the surface, all pairwise comparisons among adsorbed proteins showed significance except for the following: oxidized – SAM-CF_3/SAM-Py/SAM-COOH, SAM-CH_3 – SAM-CF_3, SAM-NH_2 – SAM-SO_3H and SAM-Py – SAM-COOH. For the protein amounts determined from the eluate, $^*p < 0.05$ was only obtained for: oxidized – SAM-CH_3/SAM-NH_2/SAM-SO_3H, SAM-CH_3 – SAM-NH_2/SAM-Py/SAM-COOH/SAM-SO_3H, SAM-CF_3 – SAM-NH_2/SAM-SO_3H, SAM-Py – SAM-SO_3H and SAM-COOH – SAM-SO_3H.

A similar situation is observed for the adsorption of serum proteins from either HABS or FBS (only determined on the surface), as shown in Figure 13.7.
From FBS, proteins seem to adhere strongly to oxidized and sulfonated surfaces (roughly 400 ng cm^{-2} on the surfaces), whereas little adsorption is observed on SAM-PEG, SAM-CH_3, SAM-CF_3 and SAM-COOH (< 50 ng cm^{-2}). Intermediate protein amounts are measured on SAM-NH_2 and SAM-Py (160–200 ng cm^{-2}).
In comparison to the results for saliva, large differences can be observed between the determined amounts of human serum proteins on the surfaces and after desorption. Quantification on the surfaces reveals large amounts of adsorbed proteins (> 400 ng cm^{-2}) on oxidized substrates, SAM-NH_2, SAM-Py and SAM-SO_3H, whereas protein-repellency (< 50 ng cm^{-2}) is observed for SAM-PEG, SAM-CH_3, SAM-CF_3 and SAM-COOH.

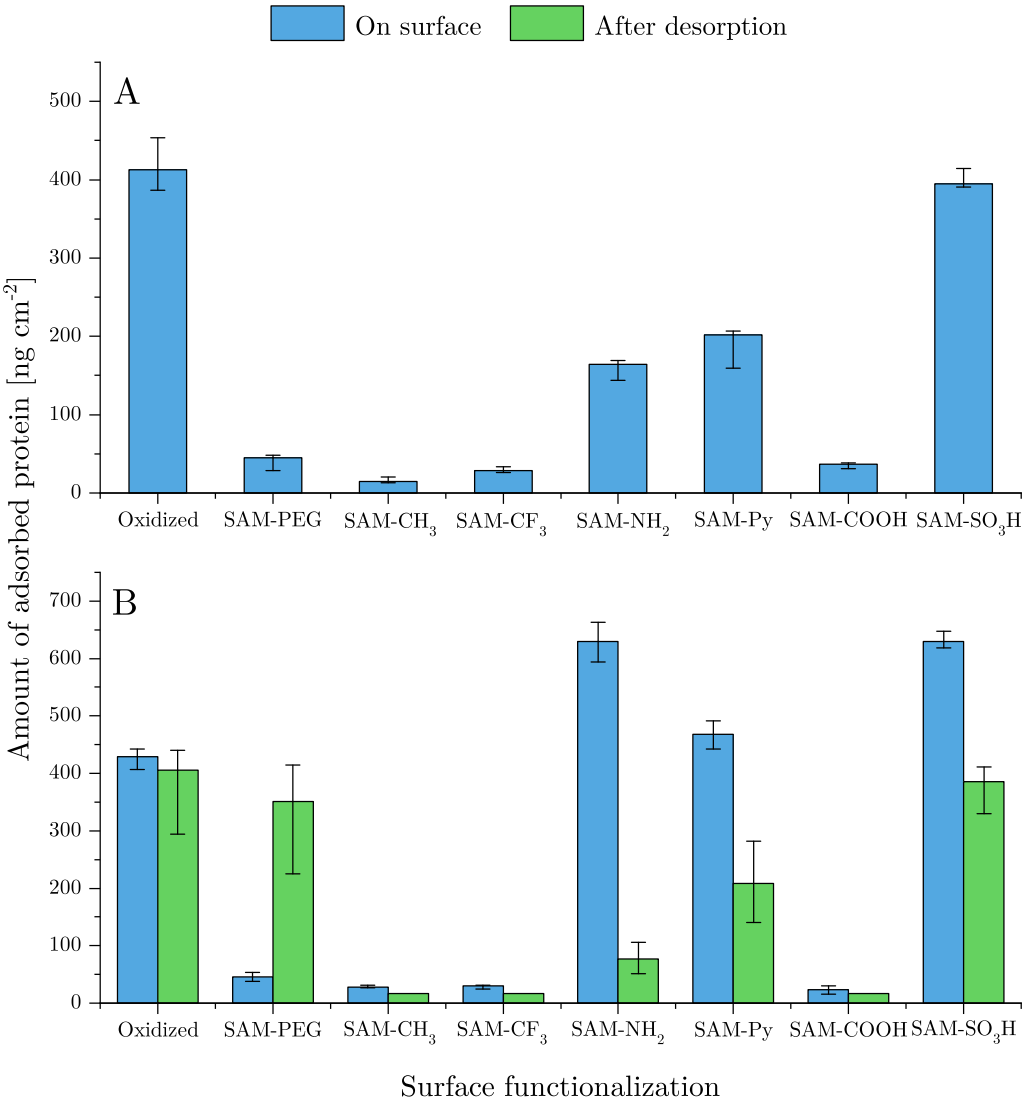

Figure 13.7: Amount of adsorbed protein from HABS or FBS on SAMs with different end groups. Protein quantification was performed with the BCA assay, either on the substrate surface or after protein desorption. Results for (A) FBS (only on surface) and (B) HABS are displayed. Data for FBS has partially been published previously [13, 16, 17, 21]. For improved clarity, the results of the Mann-Whitney-U test are not included in the figure as most pairwise comparisons of different surface modifications for the same protein solution showed significance for the protein amounts on the surface. Exceptions for FBS are: oxidized – SAM-SO_3H and SAM-NH_2 – SAM-Py. For HABS (on surface), p-values ≥ 0.05 were obtained for oxidized – SAM-Py, SAM-CH_3 – SAM-CF_3, SAM-CH_3 – SAM-COOH, SAM-CF_3 – SAM-COOH and SAM-NH_2 – SAM-SO_3H. In contrast to that, for the protein amounts determined in the eluates $^*p < 0.05$ was obtained for: oxidized – SAM-CH_3/SAM-CF_3/SAM-NH_2/SAM-COOH, SAM-PEG – SAM-CH_3/SAM-COOH, SAM-CH_3 – SAM-NH_2/SAM-Py/SAM-SO_3H, SAM-CF_3 – SAM-NH_2, SAM-NH_2 – SAM-COOH, SAM-Py – SAM-COOH and SAM-COOH – SAM-SO_2H.

In general, stronger protein adsorption occurs from FBS than from saliva as well as from HABS than from FBS due to the large differences in protein content [159, 168]. Performing a BCA assay with the solution obtained after protein desorption, protein amounts comparable to the ones measured on the surface are observed for oxidized substrates as well as SAM-CH_3, SAM-CF_3 and SAM-COOH. Larger protein amounts, however, are measured on SAM-PEG, a situation similar to the results obtained for the adhesion of salivary proteins. In contrast to that, significantly smaller serum protein amounts are quantified for SAM-NH_2, SAM-Py and SAM-SO_3H in solution after SDS treatment.

Comparison of the Chosen Quantification Methods

For the adsorption of proteins from the human biofluids saliva and serum, protein quantification was performed in two ways, determining the amounts of adsorbed proteins directly on the surface or via the protein concentration of the eluate after protein desorption. Doing so, rather similar results are obtained for the majority of surface modifications and protein solutions, but in some cases discrepancies are observed.

As mentioned previously, significantly larger amounts of adsorbed proteins are determined on SAM-PEG in protein eluates than on the surface for both biofluids. Supposedly, the reason for these differences cannot be found in the different analysis procedures but in the differing conditions of the protein adsorption experiments. Strong protein adsorption is observed if the adsorption experiments were performed at 37 °C in contrast to 25 °C. In the past years, several researchers have found evidence of temperature-dependent changes in the properties of OEG or PEG surfaces. Schoch et al. found that the thickness of PEG brushes decreases with increasing temperature in the range between 5 °C to 35 °C [295]. The group of Leckband was able to show that PEG coatings could switch from a protein-repelling to a protein-adhesive behavior with increasing temperature [296, 297]. At 35 °C for example, spontaneous adhesion between streptavidin and PEG chains with approximately 45 ethylene oxide units was observed [297]. Increased adsorption of lysozyme and fibrinogen at higher temperatures was also measured by Li et al. [298]. They explained the loss in protein-repellency with the decreased hydration of PEG at higher temperatures, expressed in the lower number of hydrogen bonds [298]. Therefore, it is recommendable to repeat the protein adsorption experiments with PEG at different temperatures with the same method in order to confirm this hypothesis.

In addition to that, differences in the determined amounts of serum proteins between the two quantification procedures are observed for SAM-Py, SAM-NH_2 and SAM-SO_3H, but here the opposite trend is seen. Lower amounts of proteins are quantified in the eluates after protein desorption. The discrepancy observed here cannot be explained by differences in the quantification procedure. In both cases, the same colorimetric assay, the BCA assay, was applied. The presence of SDS in the eluate is not expected to influence the result of the assay either as the surfactant can be tolerated up to a concentration of 5% [251]. Variations in the quantification procedure, however, can be found in the protocol used for protein adsorption as well as in the desorption step. One might assume at first that the lower protein amounts determined in eluates can be the result of non-quantitative protein desorption. Regarding the elutability of adsorbed proteins, mixed results have been obtained by other researchers. Von Baeckmann et al., for instance, observed complete removal of proteins from amino-functionalized nanoparticles in contrast to incomplete desorption from surfaces with thiol or epoxy groups because there, proteins could be covalently linked to the surfaces [299]. In contrast to that, many other studies found non-quantitative desorption of adsorbed proteins for different hydrophilic surfaces, even without covalent linkage of the protein [300–302]. The use of various surfaces, adsorption procedures as well as desorption protocols, however, makes comparisons difficult. At last, it might be worth considering the possibility that the protein desorption itself is complete, but smaller amounts of protein, however, have adsorbed in the first place due to the higher temperature. Further experiments are recommendable to clarify this issue.

Dependence of Protein Adsorption on Surface Properties

It is interesting to examine whether the amount of adsorbed proteins can be put into relation with some of the measured surface characteristics, such as the surface wettability, surface free energy or zeta potential. A similar analysis is also performed for the amine-based modifications in section 14.4.2, therefore, some parallels can be found.

Having a look at the influence of surface wettability on protein adsorption (see Figure 13.8), no correlation can be found. Both hydrophobic SAMs (SAM-CH_3 and SAM-CF_3) exhibit rather low protein adsorption, whereas very differing results are obtained for the group of hydrophilic modifications, mainly adsorbing larger amounts of protein. This result is unexpected as increased protein adsorption is usually observed on hydrophobic surfaces. The relation between surface wettability and protein attachment has been the subject of multiple studies, investigating the behavior of single proteins. In their atomic force microscopy (AFM) studies, Xu and Siedlecki as well as Sethuraman et al. observed a step-wise pattern with stronger protein adhesion on more hydrophobic

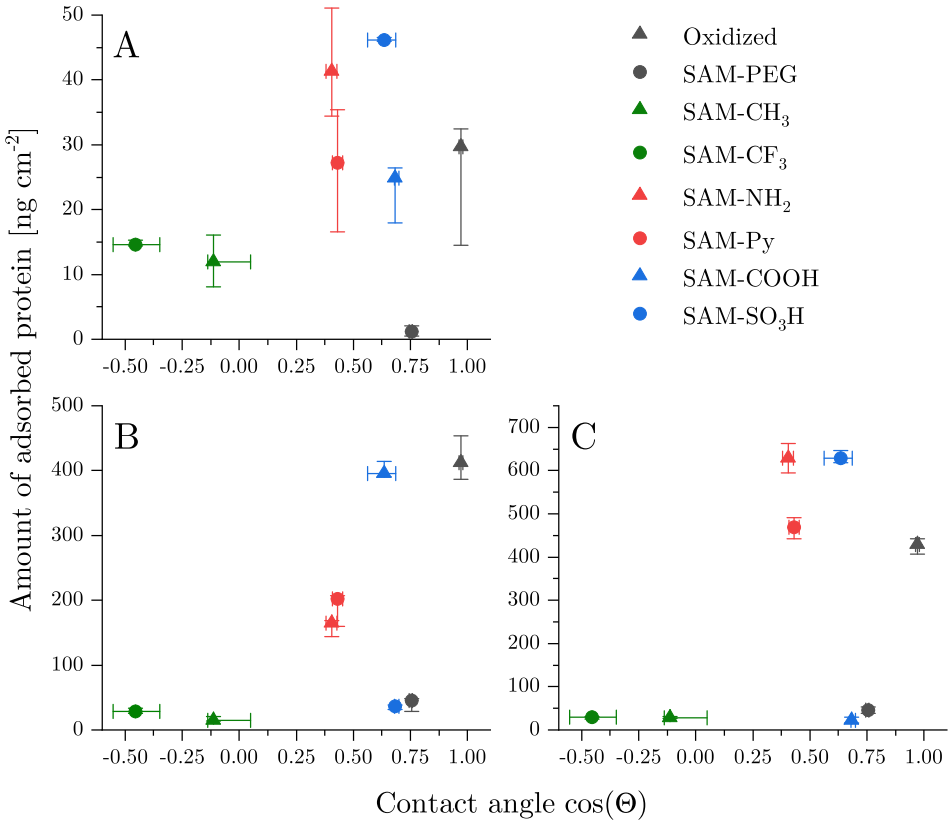

Figure 13.8: Dependence of the protein adsorption from (A) saliva or (B) FBS as well as (C) HABS on the hydrophilicity of the self-assembled monolayers, as determined via the static contact angle Θ. Protein adsorption was determined on the surfaces via BCA assay.

surfaces (contact angle approximately > 65°) [193, 303]. Their research also included serum or saliva proteins, such as albumin, immunoglobulin and lysozyme [193, 303]. Similarly, Sigal et al. found that protein adsorption on self-assembled monolayers with different functional groups and thus wettabilities decreased with increasing surface wettability, measuring the water contact angle under cyclooctane [304]. Here, small proteins were found to follow this rule more strictly than larger proteins, which also adsorbed to less hydrophobic surfaces to a low extent [304]. It has to be mentioned, though, that in some studies, no correlation was detected [305]. In contrast to the abundance of literature on the adsorption from single protein solutions, a lot less data is available on the adsorption of proteins from the complex biofluids serum and saliva. They, however, seem to confirm the trends seen for single protein solutions. For saliva, for instance, an analogous behavior, i.e. higher protein adsorption on hydrophobic surfaces, was obtained by Lindh et al. and Vassilakos et al. [306, 307]. Visalakshan et al. measured the largest amount of proteins from human serum on a substrate that was functionalized via plasma polymerization and carried hydrophobic octadiene groups [308].

For the surfaces' SFE (and components therof), no correlation is obtained with protein adsorption either, as it can be seen in the figures in the appendix (Figures VI.1, VI.2 and VI.3). As for the surface wettability, detailed studies were conducted using single protein solutions. They, however, gave mixed and sometimes contradictory results. Michiardi et al., for example, found a linear increase in HSA adsorption with the polar component of the SFE [309]. De Bartolo et al. observed enhanced adsorption of albumin, fibrinogen and immunoglobulin G (IgG) with an increasing Lewis base component of the SFE γ^-, whereas no correlation for the adsorption of HSA was obtained by Miyata et al. [153, 310]. The latter, however, measured smaller amounts of fibrinogen and globulin on surfaces with higher SFE and a larger polar component [153]. For complex protein solutions, less data is available in literature. Comelles et al. observed less adsorption of serum proteins on low energy surfaces after incubation of different polymer surfaces with cell medium containing 10% FBS [311]. This observation is in accordance with the protein-repellency that is observed for the low energy coatings SAM-CH_3 and SAM-CF_3. No literature regarding the relation between protein adsorption from saliva and the SFE could be found.

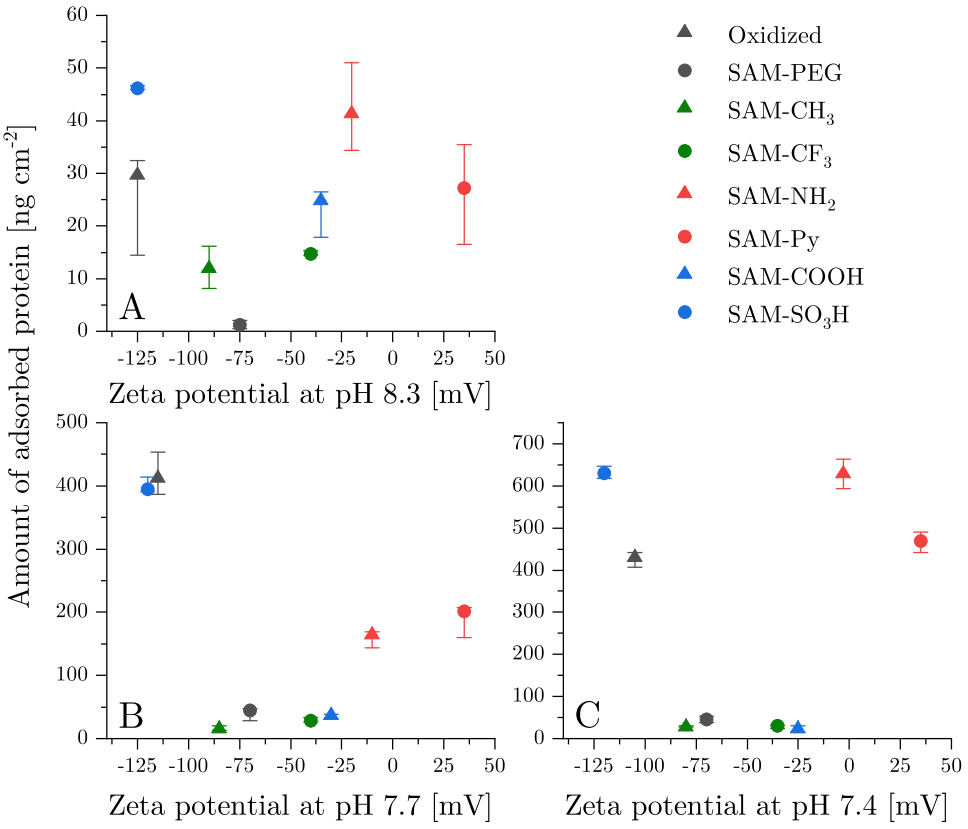

Figure 13.9: Dependence of the protein adsorption from (A) saliva or (B) FBS as well as (C) HABS on the zeta potential of the self-assembled monolayers at the pH of the respective protein solution. Protein adsorption was determined on the surfaces via BCA assay.

Having a look at Figure 13.9, the surface zeta potential does not correlate with the adsorption of salivary proteins. For the adsorption from human serum and FBS, however, minimized protein adsorption can be observed for moderately negatively charged surfaces (roughly -25 to -90 mV). As for the influence of surface wettability on protein behavior, extensive literature is available on experiments with single proteins [28, 219, 312]. Here, protein adsorption can usually be explained with attractive or repulsive electrostatic interactions between the surface and the protein. These observations will be discussed in more detail in section 14.4.2. Significantly less research has been performed with protein mixtures or physiological fluids. Similar to the results presented in this thesis, Lück et al. also obtained the least adsorption of plasma proteins on latex particles with a slightly negatively charged and hydrophilic surface coating [313]. El-Ghannam et al. observed a reduced amount of serum proteins on bioactive glass surfaces with a zeta potential of approximately -40 mV [314]. In contrast to that, PAMAM dendrimers with differing end groups, which exhibited different electrokinetic behavior, did not show strongly differing adsorption of serum proteins from FBS [20]. No detailed information could be found for the adsorption of salivary proteins. As the salivary proteome comprises a large number of proteins with different IEPs, adsorption can be expected regardless of the surface charge. A large portion of those proteins, however, possesses an IEP between pH 4 and pH 8 [162]. Thus, many of them are negatively charged under physiological conditions and can be attracted to positively charged surfaces. Yet, in the current study, strong adsorption was also observed on the negatively charged oxidized substrates and SAM-SO_3H.

Performance of the Different Surface Modifications

In the previous section, the relation between the amount of adsorbed protein and some physicochemical features of the SAMs was examined. Here, almost no or no correlation could be found. Searching for an explanation, the performance of some of the SAMs, which exhibited properties surprising at first glance, will be evaluated in more detail. At first, it is unexpected that large amounts of protein are found on oxidized silicon substrates despite their hydrophilicity. In literature, an inconsistent situation is observed. Studying the effect of PEG chain density on protein adsorption from human serum, Dalsin et al. also measured large amounts of proteins on unmodified TiO_2 substrates ($\approx 350\,\mathrm{ng\,cm^{-2}}$) [315]. In contrast to that, Rezwan et al. found that almost no BSA, the main component of serum [165], adsorbed on negatively charged silica particles [28]. They, however, detected large amounts of lysozyme and were able to show that the protein attachment was clearly ruled by electrostatic interactions between protein and surface [28]. Similarly, Bellion et al. measured roughly twice as much lysozyme than amylase or BSA on oxidized silicon wafers with silicon dioxide surface layers [183].

The sulfonate self-assembled monolayer shows a rather similar behavior. This modification is characterized by its moderately hydrophilic behavior (contact angle roughly 50°) and a strongly negative zeta potential under physiological conditions (approximately −120 mV). On this coating, strong adsorption of salivary or serum proteins was measured in this thesis. Similar to the literature about unfunctionalized silica or titanium oxide substrates, several other studies found strong adsorption of lysozyme on sulfonate surfaces. Holmlin et al., for instance, observed strong adsorption of lysozyme and fibrinogen on sulfonate SAMs [202]. Meder at al. measured large amounts of lysozyme and trypsin, both positively charged under the conditions of the adsorption experiments, on colloidal alumina particles with sulfonate groups [316]. In contrast to that, almost no negatively charged albumin adhered to this surface [316]. A nonwoven fabric with -SO_3H groups was even used for the specific binding of lysozyme by Kim et al. [317], whereas functionalization of graphene oxide with sulfonate groups was used to obtain membranes which are nonfouling to BSA by Ayyaru and Ahn [318].

It is surprising to see that a completely opposite behavior is observed for the carboxylic acid monolayer SAM-COOH. This moderately hydrophilic surface (contact angle 47°) carries surface groups which can be deprotonated as well and thus possesses a negative zeta potential at physiological conditions (≈ -30 mV). Whereas moderate protein adsorption of salivary proteins is observed, this coating is highly resistant towards protein adsorption from human or bovine serum. These findings cannot be confirmed by the results of other researchers. Hasan et al., for instance, examined the separate and competitive adsorption of the serum proteins BSA, IgG and fibrinogen on silane SAMs with different functional groups [319]. They did not only observe that more albumin or IgG adsorbed on SAM-COOH than on unmodified or amine-functionalized substrates in experiments with single protein solutions, but they also found enhanced adsorption from binary protein mixtures (350–400 ng cm^{-2}) [319]. Gessner et al. studied the quantitative and qualitative adsorption of proteins from human serum on latex nanoparticles with different end groups, among them carboxylic acid (-COOH), sulfonate (-SO_3^-) and sulfate (-SO_4^-). They quantified similar amounts of total protein on all three surfaces, yet the composition of the protein corona was different. Large amounts of albumin and IgG were detected on SAM-COOH, whereas the adsorption of apolipoprotein H was strongly enhanced on the sulfonated surface [179].

In summary, oxidized, carboxylated and sulfonated surfaces are all hydrophilic and bear deprotonable groups, which generate an overall negative zeta potential. They differ, however, in the acidity of the surface groups and thus in the magnitude of the zeta potential. While SAM-COOH is characterized by its low to moderate protein adsorption,

large amounts of proteins were quantified on oxidized substrates and SAM-SO_3H. No explanation could be found in literature. It can, however, be assumed that the electrostatic interactions between proteins and the more negatively charged surfaces possess a longer range and are stronger, leading to the accumulation of larger amounts of adsorbed proteins.

Another unexpected result of the protein adsorption experiments is the protein-repelling behavior of the hydrophobic coatings SAM-CH_3 and SAM-CF_3, which is contradictory to many other studies. As mentioned before, Sethuraman et al. as well as Xu and Siedlecki reported stronger adhesion of various proteins on more hydrophobic surfaces (contact angle $\Theta > 65°$) [193, 303]. Decreasing HSA adsorption with increasing surface hydrophilicity in mixed monolayers was also observed by Martins et al. [320].
It must not be omitted, however, that some researchers detected differing results. Müller et al., for example, reported lower adsorption of serum proteins on hydrocarbon and fluorocarbon surfaces than on oxidized substrates or specimens with PEG modification [16]. Lower albumin and fibrinogen attachment on these two surface coatings in comparison with a hydroxylated surface was also observed by Wertz and Santore [321]. They explained this observation with the different spreading behavior of the proteins on both surfaces. On hydrophobic surfaces, extensive and quick spreading occurs. Thus, each protein occupies a larger surface area and less protein mass can be adsorbed per surface area [321]. It has to be questioned whether this explanation for lower surface coverage, leading still to approximately $200\,\mathrm{ng\,cm^{-2}}$, is applicable to the results of this study, where almost complete protein-repellency is observed.

Instead, two further explanation attempts have to be considered. At first, it should be taken into account that the proteins adsorbed to the hydrophobic surfaces are maybe strongly denatured. If this was the case, it may be possible that they are not recognized in immunostaining (see following section) and are not detected in the BCA assay either. This, however, is highly unlikely. "Soft" proteins have indeed been shown to undergo structural changes and partially lose their secondary structure [158, 172]. Hasan et al., for example, observed a reduction in the β-sheet content and an increase in random coil structures for adsorbed fibrinogen and immunoglobulin, which was more pronounced on hydrophobic substrates [319]. Yet, the denatured protein is very likely to be detected via the BCA assay due to two reasons. At first, adsorbed proteins do not lose their secondary structure completely [158, 172] and, more importantly, the BCA assay is expected to also detect denatured proteins. Studies revealed the disturbing effects of detergents and reducing agents on the BCA assay [322]. These chemicals, however, were definitely not present in the quantification experiments performed in Regensburg,

with the proteins still attached to the surface. Further experiments by Cortés-Ríos et al. led to enhanced absorption in the BCA assay if the proteins were denatured by pretreatment with a detergent [323]. Thus, lacking sensitivity of the BCA assay towards denatured proteins can be excluded as a reason for the low protein adsorption measured on SAM-CH_3 and SAM-CF_3.

The second hypothesis cannot be proven in the scope of this thesis but requires further measurements. It is based on the fact that the analysis of physicochemical characteristics was performed on different substrate geometries throughout this work. The XPS as well as static contact angle measurements were carried out on planar silicon wafers which possess a flat surface on a microscale and nanoscale in AFM measurements (see section 16.1.2). On SEM images of silica beads, however, a rough surfaces exhibiting bumps in a size regime $\leq 1\,\mu m$ can be seen (see Figure 13.10). Thus, the assumption can be made that the hydrophobic SAM-CH_3 and especially the SAM-CF_3 coating behave as superhydrophobic coatings on those beads.

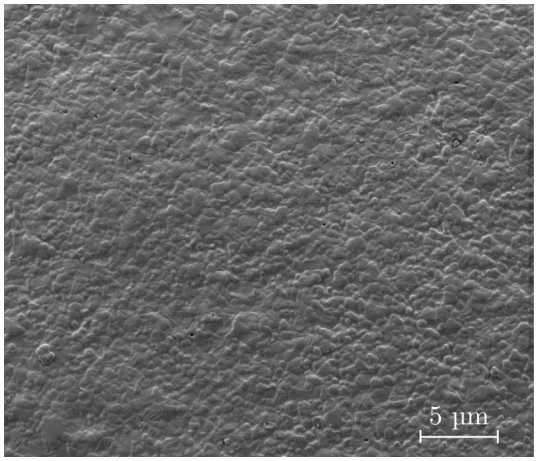

Figure 13.10: Surface topography of silica beads, as obtained from SEM images.

As mentioned previously, superhydrophobic surfaces are characterized by their high water contact angles ($> 150°$). Ideally, they exhibit very low surface free energies (both polar and dispersive components) and can thus additionally be labeled as lipophobic [151, 177, 206]. These surfaces can be prepared by combining low SFE materials, mainly fluorocarbons, with an appropriate surface topography or roughness, which may mimic naturally occurring non-fouling materials, such as shark skin or lotus leafs [177, 205, 206, 233, 324]. Therefore, these materials do not only exhibit strongly reduced interactions with water but also with hydrophobic surfaces due to decreased van der Waals interactions [205, 206]. Such surfaces have been applied successfully in protein-repellent coatings. Kumar et al., for example, were able to synthesize rough fluorocarbon polymer coatings, which showed reduced adsorption of the model proteins ovalbumin, HSA and

fibrinogen [324]. Wang and Zuilhof combined nanostructured silicon surfaces with fluoropolymer brushes and obtained surface coatings repellent towards BSA and 10% blood plasma [325]. The hydrocarbon and fluorocarbon coatings studied in this thesis already exhibit hydrophobic properties on flat surfaces with contact angles of 97° and 117° respectively. A rather high contact angle with diiodomethane is also observed, especially for the SAM-CF_3 surface (93°), i.e. this surface can also be described as lipophobic. If these properties are enhanced by the rough surface of the silica particles, then superhydrophobic surfaces are obtained, which repel proteins. In order to prove this assumption, more detailed characterization of the particles' surface as well as the resulting apparent contact angles and SFEs is required.

13.3.2 Qualitative Protein Adsorption

In order to understand the results of the qualitative protein adsorption, the data obtained from SDS-PAGE and western blot will be analyzed in the following.

Adsorption Pattern of Salivary Proteins

Regarding the adsorption of salivary proteins, strongly differing protein patterns can be observed among the various surface modifications. The bands obtained after staining are depicted in Figure 13.11 and the extracted information is summarized in Table 13.5.

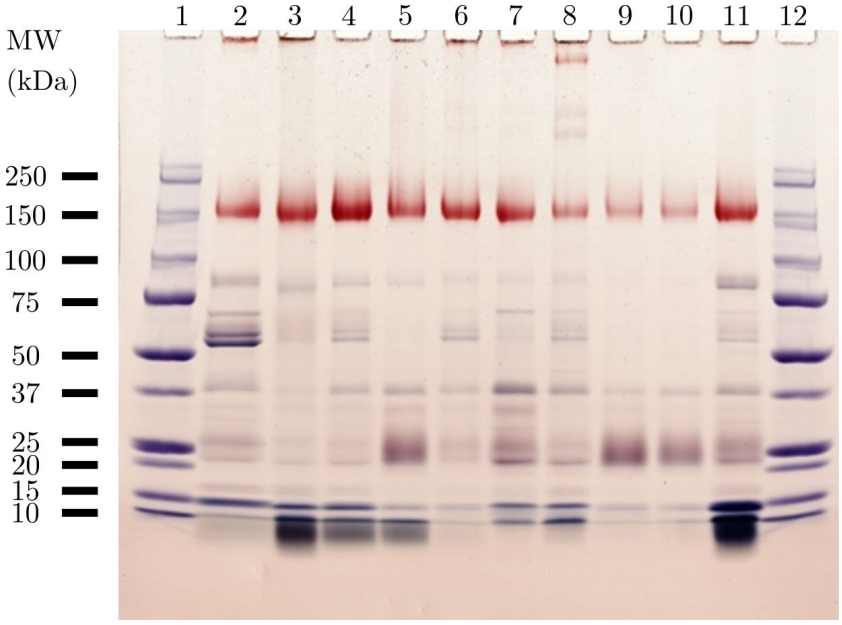

Figure 13.11: Representative stained gel after SDS-PAGE of the proteins adsorbed to (3) unmodified beads, (4) oxidized beads, (5) SAM-COOH, (6) SAM-PEG, (7) SAM-NH_2, (8) SAM-Py, (9) SAM-CH_3, (10) SAM-CF_3 and (11) SAM-SO_3H. Whole saliva (2) as well as a molecular weight standard (1, 12) are included for reference. Strongly glycosylated proteins appear in red, proteins with little or no glycosylation are stained blue.

As it can be seen there, almost no proteins with molecular weights $\leq$ 15 kDa are found on SAM-CH_3, SAM-CF_3 or SAM-PEG. The bands for oxidized substrates, SAM-NH_2, SAM-Py and SAM-COOH are more intense in color, whereas very pronounced bands are obtained for unmodified beads and SAM-SO_3H. A strongly differing situation presents itself for the bands in the range between 20–25 kDa. Here, weakly colored bands are observed for unmodified and oxidized beads as well as SAM-PEG. In contrast, strong protein accumulation, leading to the formation of smeared bands, is detected for SAM-CH_3, SAM-CF_3 and SAM-COOH. A very defined band at roughly 37 kDa is visible for all surface modifications, being more pronounced on modifications with charged groups (SAM-NH_2, SAM-Py, SAM-COOH and SAM-SO_3H).

Table 13.5: Summarized analysis of the bands obtained on the stained gel after SDS-PAGE of proteins, adsorbed from human saliva onto SAMs with different functional groups. The following situations are differentiated here: no band detected (✖), band weakly visible (●), band similar to reference lane with saliva (✚), medium or strong accumulation with respect to whole saliva as reference (✚✚ and ✚✚✚).

MW	Surface Modifications								
[kDa]	Unm.	Ox.	-PEG	-CH_3	-CF_3	-NH_2	-Py	-COOH	-SO_3H
150	✚	✚✚	✚	●	●	✚	●	✚	✚✚
80	✚	✚	●	✖	✖	●	●	●	✚✚
55-65	●	●	●	✖	✖	●	●	✖	●
37	●	●	●	●	●	✚✚	✚	✚	✚✚
25	●	●	●	✚✚✚	✚✚✚	✚	●	✚✚✚	✚✚
20	●	●	●	✚✚✚	✚✚✚	✚	✚	✚✚✚	✚✚
15	✚	✚	●	●	●	✚	✚	●	✚✚✚
$\leq$ 10	✚✚✚	✚✚	●	●	●	✚✚	✚✚	✚✚	✚✚✚

Proteins with molecular weights between 40 kDa and 150 kDa seem to be completely absent on SAM-CH_3 and SAM-CF_3 and almost absent on SAM-COOH. On the other surfaces, different patterns of weak bands can be detected in the range between 55–65 kDa and at approximately 80 kDa. Contrary to that, a red band at roughly 150 kDa is visible on all surface modifications but weaker on SAM-CH_3, SAM-CF_3 and SAM-Py. At higher molecular weights, several weak bands are obtained for SAM-Py. In addition to that, staining might be visible at the bottom of the wells (e.g. on unmodified substrates), meaning that high molecular weight proteins did not move into the gel.

In the second step, immunoblotting with a variety of antibodies was applied to identify some of the salivary proteins, separated with SDS-PAGE. As the saliva proteome is assumed to comprise up to 10,000 different proteins [170], only a small fraction of those can be examined (see Figure 13.12 and Table 13.6). But it can be seen there that the composition of the protein pellicle on the SAMs depends on properties of the substrate, as it is expected [326].

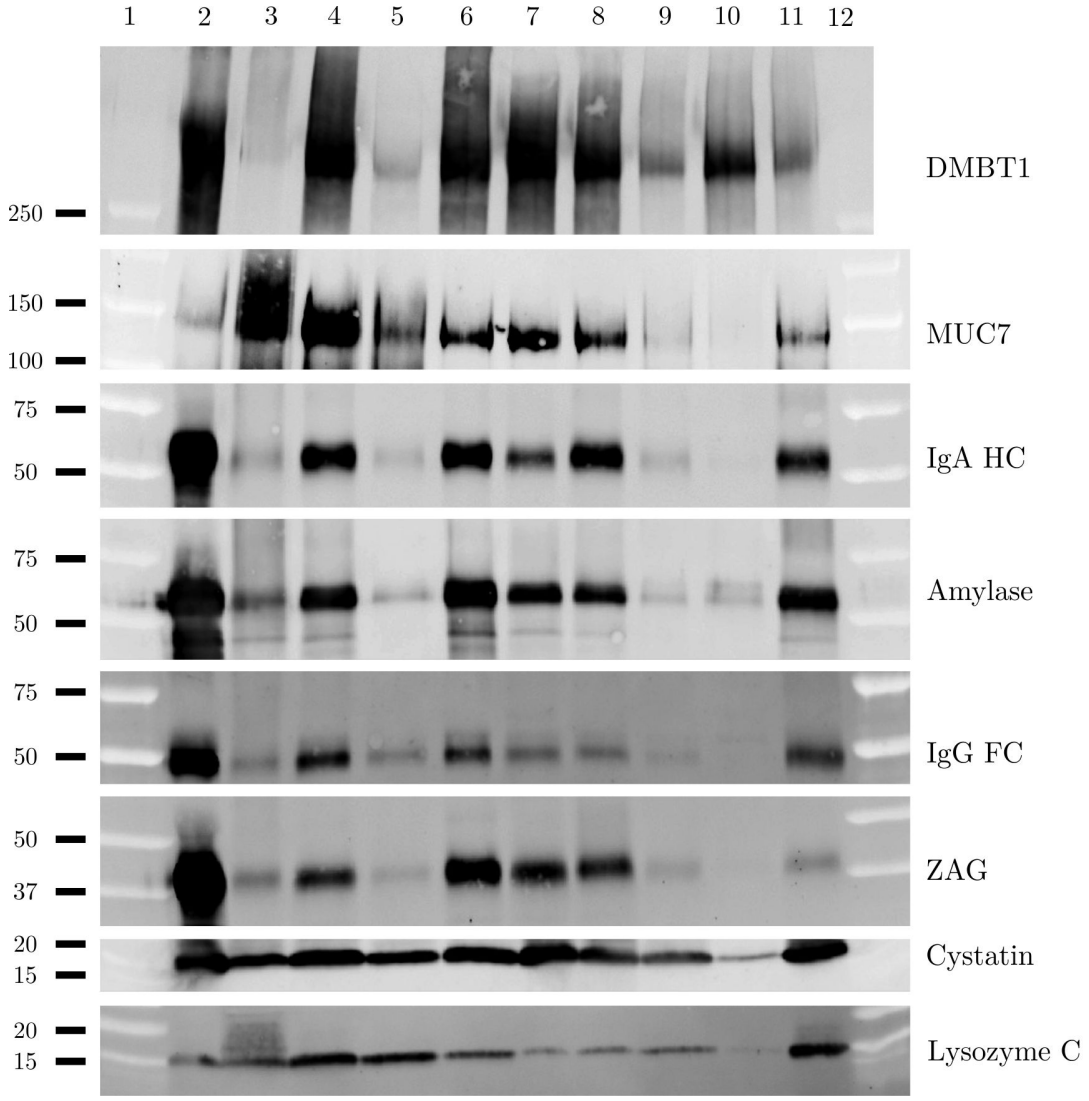

Figure 13.12: Immunostaining of selected salivary proteins adsorbed to SAMs with different functional groups after SDS-PAGE and western blot. The surface modifications are: (3) unmodified beads, (4) oxidized beads, (5) SAM-COOH, (6) SAM-PEG, (7) SAM-NH_2, (8) SAM-Py, (9) SAM-CH_3, (10) SAM-CF_3 and (11) SAM-SO_3H. Whole human saliva (2) as well as a molecular weight standard (1, 12, molecular weight provided in kDa) are included for reference.

No immunoblotting for proteins with a molecular weight $< 15\,\mathrm{kDa}$ was performed. Thus, the strong bands $\leq 10\,\mathrm{kDa}$, appearing on unmodified and oxidized beads as well as on SAM-NH_2, SAM-Py, SAM-COOH and SAM-SO_3H, could not be identified. It can be assumed, however, that this band comprises histatins and potentially also statherin.

Histatins are low molecular weight (roughly 6 kDa), histidine-rich and, hence, very basic proteins [163, 327]. Thus, it is plausible that they can adsorb to negatively charged surfaces, such as SAM-COOH and SAM-SO_3H, via attractive electrostatic interactions. In literature, adsorption to unmodified titanium surfaces has been described [327]. Statherin possesses a very similar molecular weight. It, however, is characterized by its amphipathic nature, i.e. by the presence of both hydrophobic as well as hydrophilic areas on its surface [163, 328]. Due to the resulting surface activity, it is expected to adsorb on a variety of surfaces. Yet, stronger accumulation on more hydrophobic surfaces was observed in other studies [163, 328, 329].

Table 13.6: Summarized analysis of the immunoblotting with antibodies against different salivary proteins adsorbed on SAMs with varying functional groups. The following situations are differentiated here: no band detected (✖), band weakly visible (●), band similar to reference lane with saliva (✚), medium or strong accumulation with respect to saliva reference (✚✚ and ✚✚✚).

Protein	Surface Modifications								
	Unm.	Ox.	-PEG	-CH_3	-CF_3	-NH_2	-Py	-COOH	-SO_3H
DMBT1	✖	✚✚	✚	●	✚	✚✚	✚✚	●	●
MUC7	✚✚	✚✚	✚	✖	✖	✚	✚	●	●
IgA HC	●	✚✚	✚✚	✖	✖	✚	✚✚	✖	✚
Amylase	●	✚✚	✚✚	●	●	✚	✚	●	✚✚
IgG FC	●	✚	✚	✖	✖	●	●	●	✚
ZAG	●	✚	✚✚	✖	✖	✚	✚	✖	●
Cystatin	✚	✚✚	✚✚	●	●	✚✚	✚	✚	✚✚
Lysozyme C	●	✚✚	✚	●	✖	●	●	✚✚	✚✚✚

The pronounced band at approximately 15 kDa on several surfaces (unmodified, oxidized, SAM-NH_2, SAM-Py and SAM-SO_3H) is revealed to be the consequence of the adsorption of two proteins of similar molecular weight, lysozyme C and cystatin. Due to its abundance and low molecular weight (11–16 kDa), cystatin can reach the surface quickly and adsorb rapidly after the initial contact [328, 330]. In addition to that, this protein presents acidic, basic as well as hydrophobic residues on its surface, allowing it to adsorb to any kind of surface [328]. This is confirmed by the results of the immunoblotting in our study. Cystatin is present on all surfaces, even weakly on SAM-CF_3. In addition to that, the presence of lysozyme C, a small basic protein with an IEP of 11.1, was found on some of the surfaces [155]. Strong accumulation is observed on oxidized substrates, SAM-COOH and SAM-SO_3H, which can primarily be

explained with attractive electrostatic interactions between those negatively charged surfaces and the positively charged protein. As lysozyme is a "hard" protein, i.e. does not denature upon adsorption, only small amounts are detected on the other surface modifications [155]. These results agree with data obtained from experiments with isolated lysozyme [28, 219], i.e. it retains is electrostatically-driven adsorption behavior despite the complexity of the biofluid and the presence of other proteins.

In the stained SDS-PAGE gel, several protein bands in the range from 20 to 25 kDa can be seen, most pronounced on SAM-CH_3, SAM-CF_3 and SAM-COOH, and more weakly on SAM-NH_2 and SAM-SO_3H. These proteins have not been identified in the immunoblotting, but they could potentially belong to the group of proline-rich proteins (PRPs). This family of proteins is characterized by the eponymous high content in proline (25-42%) [331] but is otherwise very diverse. They can be acidic, basic or glycosylated and may possess molecular weights in a broad range from 15 kDa to 70 kDa [163, 328, 331]. Some of them were found to adsorb to more hydrophobic surfaces, which was similarly observed in this thesis [329].

A sharp band close to the 37 kDa-marker in the stained SDS-PAGE gel was identified as the Zn-α_2-glycoprotein (ZAG). In immunoblotting, it was not present on SAM-CH_3, SAM-CF_3 and SAM-COOH, very weakly visible on unmodified beads and SAM-SO_3H and more pronounced on oxidized surfaces, SAM-PEG, SAM-NH_2 and SAM-Py. The glycoprotein possesses a molecular weight of 42 kDa, matching the position of the protein band in SDS-PAGE, as well as an IEP of 5.1 [332].

Blotting for fragments of different immunoglobulins helped identify the band at approximately 50 kDa. Here, bands are not or very weakly visible on unmodified substrates, SAM-CH_3, SAM-CF_3 and SAM-COOH, more pronounced on SAM-NH_2, SAM-Py and SAM-SO_3H and very prominent on SAM-PEG and oxidized substrates. In their native conformation, immunoglobulins possess a Y-shape with a total molecular weight of roughly 150 kDa and consist of two identical so-called heavy chains (HC, each $\approx$ 50 kDa) and two identical light chains (LC, $\approx$ 25 kDa), which are associated with disulfide bonds and non-covalent interactions [169, 333]. As these linkages are broken under the reductive conditions applied during the desorption of the proteins, fragments with lower molecular weight are usually separated and identified in SDS-PAGE and immunoblotting. Proteolysis with the enzymes papain and pepsin can also lead to the formation of characteristic fragments, namely of two Fab fragments and one Fc fragment or of the F(ab')$_2$ fragment respectively [333]. In this western blot, two of the five different classes of immunoglobulins have been investigated, immunoglobulin G (IgG)

and immunoglobulin A (IgA), the latter being the most abundant antibody in secretions, such as saliva [334]. Therefore, larger amounts of IgA seem to be seen on the fouling surfaces. The detected fragments of those two antibodies both exhibit molecular weights between 50 and 60 kDa, in accordance with literature data [308, 333, 334].
The adsorption pattern of those immunoglobulins, i.e. no adsorption on the hydrophobic coatings and strong adsorption on the hydrophilic modifications, including SAM-PEG, contradicts the results of many other studies available in literature. Previous research often detected increased adsorption of immunoglobulins on hydrophobic surfaces. Silin el al., for instance, also examined the adsorption of IgG on SAMs with different terminal groups and found that the largest amount of antibody adsorbed on SAM-CH_3 and the least on hydroxyl group or OEG-terminated surfaces [335]. Similar observations have previously been made by Lassen et al. [336]. In separate studies, it was detected that maximized adsorption of immunoglobulins occurred at pH values close to the IEP of the antibodies [337, 338]. For IgG, IEPs between 6 and 7 can be found in literature [303, 337]. For salivary IgA, a slightly lower range between 4.8 and 6.5 could be detected [339]. Therefore, it can be assumed that IgA is more negatively charged under physiological conditions than IgG. Thus, adsorption on surfaces carrying positively charged groups (SAM-NH_2 and SAM-Py) is reasonable due to attractive electrostatic interactions. Yet, IgA also adsorbs on the hydrophilic and negatively charged surfaces.

Immunoblotting for amylase led to bands at approximately 55 kDa on oxidized surfaces, SAM-PEG, SAM-NH_2, SAM-Py and SAM-SO_3H. This protein seems be almost completely absent on unmodified substrates, SAM-CH_3, SAM-CF_3 and SAM-COOH. Amylase, the slightly acidic enzyme α-1,4-glucan-4-glucanohydrolase (EC 3.2.1.1), is the single most abundant protein in saliva [163, 332, 340]. In other studies, amylase was found to adsorb on surfaces of varying hydrophilicity, resulting in a band at 56–59 kDa [328]. They hypothesized that amylase adsorption was mediated via the previously adsorbed cystatins. Due to its small size and amphiphilicity, cystatin adsorbs quickly to almost all surfaces and can then enhance amylase attachment via a variety of electrostatic or hydrophobic interactions [328].

The broad band at a molecular weight of approximately 150 kDa could be assigned to mucins in immunoblotting. They are absent on SAM-CH_3 and SAM-CF_3 and weakly visible on the acidic modifications SAM-COOH and SAM-SO_3H. More pronounced bands can be detected on SAM-PEG, SAM-NH_2 and SAM-Py, whereas the broadest bands are found for unmodified and oxidized substrates. Mucins fulfill a variety of functions in saliva as they prevent desiccation, support lubrication in the oral cavity and are a vital part of the acquired pellicle [161]. The subclass of MUC7 possesses

a molecular weight between 120 and 150 kDa [341], which is in accordance with its position in SDS-PAGE and immunoblotting. Mucins are heavily glycosylated, with carbohydrates accounting for roughly 70% of the total protein mass of MUC7 [341]. They consist of a linear peptide backbone, densely surrounded by oligosaccharide chains [342]. Extensive glycosylation and sialylation render the overall charge of the glycoprotein negative [332]. In literature, no clear dependence of the observed mucin adsorption on surface properties can be derived. Lindh et al. observed stronger adsorption on hydrophobic surfaces [343], whereas Aroonsang et al. identified a stronger band of a 180 kDa glycoprotein, presumably mucin, on the more hydrophilic substrates [328].

At molecular weights above 150 kDa, no band was visible in the stained SDS-PAGE gel (except for SAM-Py), although some staining of the wells themselves may be seen. In contrast, the presence of the high molecular weight glycoprotein DMBT1 (deleted in malignant brain tumors-1 protein) was proven by immunoblotting. Strongly pronounced, blurred bands are observed on oxidized substrates, SAM-PEG, SAM-CF_3, SAM-NH_2 and SAM-Py, weak bands are visible on SAM-CH_3, SAM-COOH and SAM-SO_3H. Encoded by the DMBT1 gene but appearing in saliva, this protein is also named salivary agglutinin [344]. It possesses a molecular weight of 340 kDa, belongs to the family of scavenger receptor cysteine-rich proteins and has been shown to interact with a variety of pathogens and host proteins, such as IgA and lactoferrin [344, 345].

Adsorption Pattern of Serum Proteins

The results of the SDS-PAGE of protein experiments with HABS are depicted in Figure 13.13 and in Table 13.7. At first glance, they are in accordance with the data obtained from the quantitative BCA assay. The protein-repellency of SAM-CH_3, SAM-CF_3 and SAM-COOH, already observed in the BCA assay, is also striking here as no protein bands are visible in the stained gel. On unmodified substrates, a pronounced band at 25 kDa can be seen. Apart from that, very weak and blurred coloring can be observed between 40 kDa and 75 kDa, but no clear bands can be distinguished here. All remaining surface coatings (oxidized, SAM-PEG, SAM-NH_2, SAM-Py and SAM-SO_3H) share the same pattern of protein bands, which vary in intensity among the different modifications. Protein bands can be observed at 25 kDa, 40 kDa, 50 kDa, 65 kDa and 75 kDa. For all of them, staining is more intense on the oxidized substrates than on the other surfaces, which exhibit a rather similar color intensity. At molecular weights > 80 kDa, no clear bands can be seen for neither of the surfaces, although coloring of the whole lane is observed for oxidized substrates.

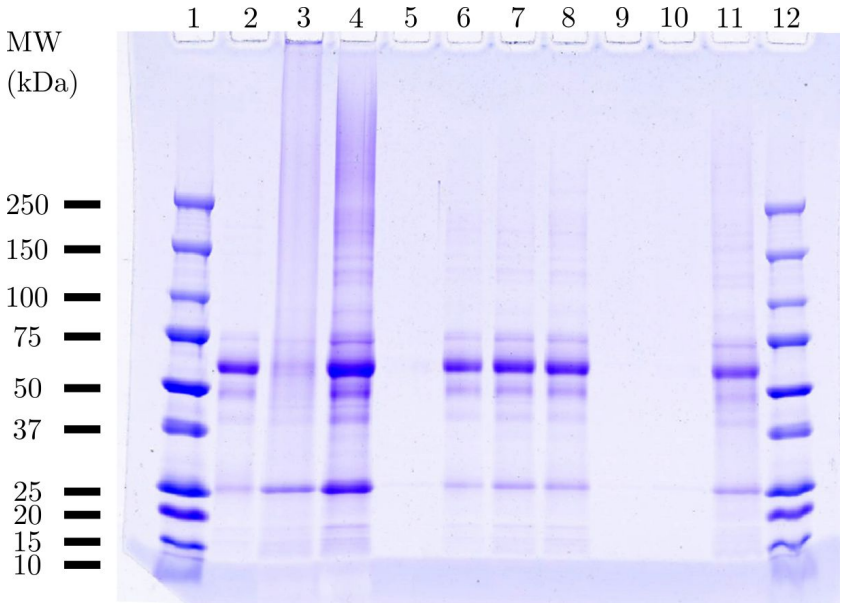

Figure 13.13: Representative stained gel after SDS-PAGE of human serum proteins adsorbed to (3) unmodified beads, (4) oxidized beads, (5) SAM-COOH, (6) SAM-PEG, (7) SAM-NH_2, (8) SAM-Py, (9) SAM-CH_3, (10) SAM-CF_3 and (11) SAM-SO_3H. Human serum (2, dilution 1:100) and a molecular weight standard (1, 12) are included for reference.

Table 13.7: Summarized analysis of the bands obtained on the stained gel after SDS-PAGE of proteins, adsorbed from human serum onto SAMs with different functional groups. The following situations are differentiated here: no band detected (✖), band weakly visible (●), band similar to reference lane with serum (✚), medium or strong accumulation with respect to serum reference (✚✚ and ✚✚✚).

MW	Surface Modifications								
[kDa]	Unm.	Ox.	-PEG	-CH_3	-CF_3	-NH_2	-Py	-COOH	-SO_3H
> 100	✖	✖	✖	✖	✖	✖	✖	✖	✖
75	●	✚✚	✚	✖	✖	✚	✚	✖	✚
65	●	✚✚✚	✚	✖	✖	✚	✚	✖	✚
50	✖	✚✚	✚	✖	✖	✚	✚	✖	✚
40	✖	✚✚	✚	✖	✖	✚	✚	✖	✚
25	✚✚	✚✚✚	✚	✖	✖	✚✚	✚✚	✖	✚✚
≤ 15	✖	●	✖	✖	✖	●	●	✖	✖

The SDS-PAGE gels were used to identify several serum proteins via immunoblotting. The results are shown in Figure 13.14 and summarized in Table 13.8. None of the tested proteins, however, were detected on SAM-CH_3, SAM-CF_3 and SAM-COOH. Similar to the results for the gel electrophoresis, almost no bands can be identified on unmodified silica beads.

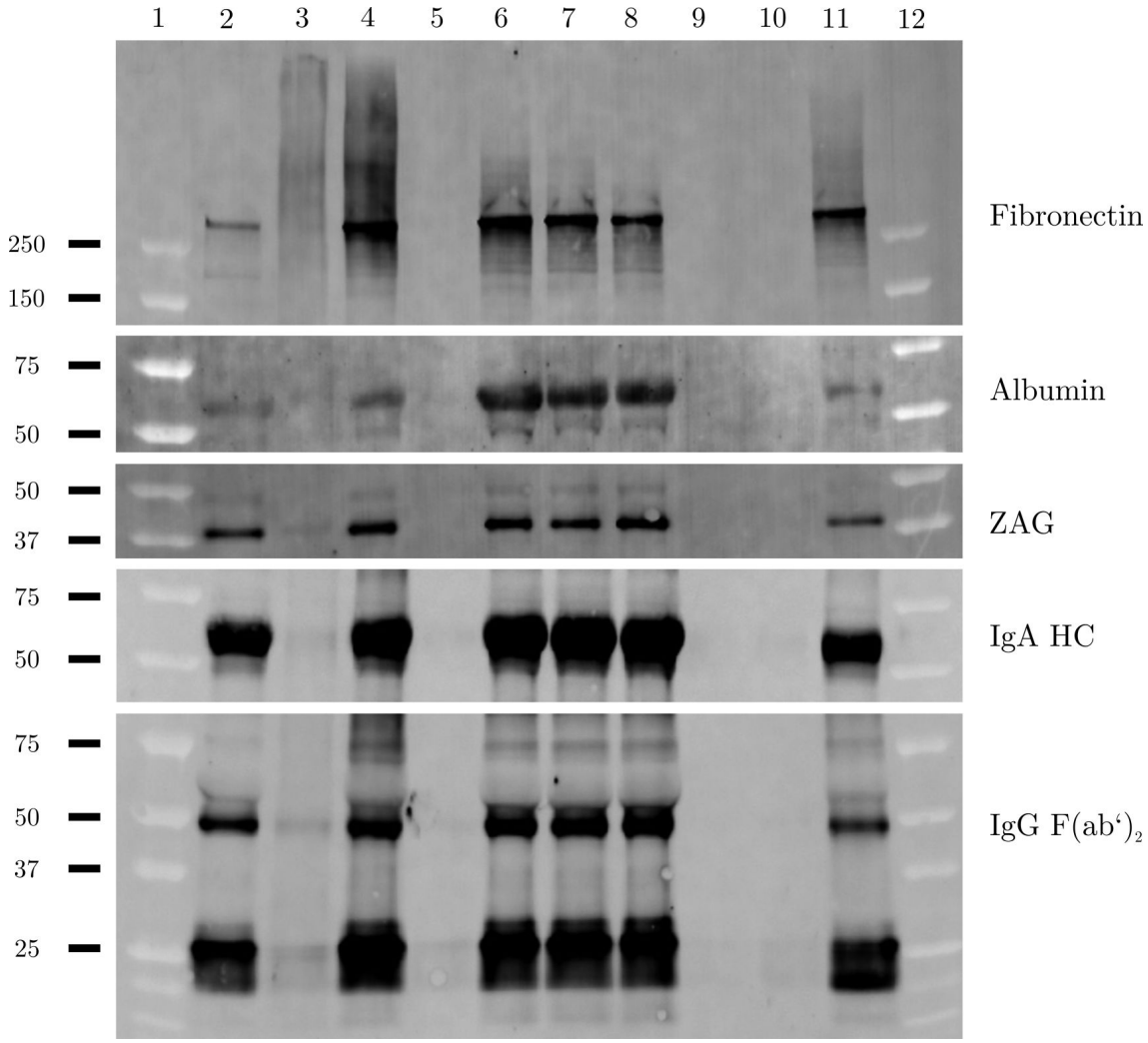

Figure 13.14: Immunostaining of selected serum proteins adsorbed to SAMs with different functional groups after SDS-PAGE and western blot. The surface modifications are: (3) unmodified beads, (4) oxidized beads, (5) SAM-COOH, (6) SAM-PEG, (7) SAM-NH_2, (8) SAM-Py, (9) SAM-CH_3, (10) SAM-CF_3 and (11) SAM-SO_3H. Diluted human serum (2, dilution 1:100) as well as a molecular weight standard (1, 12, MW provided in kDa) are included for reference.

Blotting for fragments of the immunoglobulins IgG and IgA (IgG F(ab')$_2$ and IgA HC respectively) led to very similar results. These proteins strongly adsorb on oxidized substrates, SAM-PEG, SAM-NH_2 and SAM-Py, to a lesser extent also on SAM-SO_3H. As already discussed for the adsorption of immunoglobulins from saliva, the bands occur at the correct molecular masses. For the heavy chain of IgA, a molecular weight of roughly 60 kDa is expected [334]. For IgG, fragments of approximately 50 kDa and 28 kDa were observed under reductive conditions [346]. In contrast to saliva, IgA is only present in minor amounts in serum, whereas IgG constitutes approximately 10–20% of the total protein, being the most abundant immunoglobulin [169, 334]. As also mentioned previously, the adsorption pattern of IgG and IgA is only partially in accordance with other studies available in literature. As for the adsorption from saliva, no

adsorption is visible on the most hydrophobic substrates SAM-CH_3 and SAM-CF_3, whereas strong adsorption occurs on the hydrophilic modifications, such as oxidized substrates and SAM-PEG. This again poses a stark contrast to the results of many other studies, indicating stronger protein adsorption on hydrophobic surfaces [335, 336]. At the same time, maximized adsorption was obtained if the environmental pH was close to the IEP of the protein [337, 338], as discussed earlier. Here, it can be expected that at pH 7.4 IgG is nearly uncharged, while IgA probably already carries a minor negative charge. Thus, enhanced adsorption of nearly uncharged IgG might serve as an explanation for the strong adsorption on hydrophilic surfaces. IgA can adsorb via attractive electrostatic interactions on SAM-Py, but no conclusive interpretation can be made for the adsorption on negatively charged, hydrophilic surfaces.

Table 13.8: Summarized analysis of the immunoblotting with antibodies against different human serum proteins adsorbed on SAMs with varying functional groups. The following situations are differentiated here: no band detected (✖), band weakly visible (●), band similar to reference lane with serum (✚), medium or strong accumulation with respect to serum reference (✚✚ and ✚✚✚).

Protein	Surface Modifications								
	Unm.	Ox.	-PEG	-CH_3	-CF_3	-NH_2	-Py	-COOH	-SO_3H
Fibronectin	✖	✚✚	✚✚	✖	✖	✚✚	✚✚	✖	✚✚
Albumin	✖	●	✚✚	✖	✖	✚✚	✚✚	✖	●
ZAG	●	✚✚	✚✚	✖	✖	✚✚	✚✚	✖	✚
IgA Hc	✖	✚✚	✚✚	✖	✖	✚✚	✚✚	✖	✚
IgG F(ab')$_2$	●	✚✚	✚✚	✖	✖	✚✚	✚✚	✖	✚

The sharp band at roughly 40 kDa, in SDS-PAGE mainly detected on oxidized substrates, but also weakly visible on SAM-PEG, SAM-NH_2, SAM-Py and SAM-SO_3H, seems to stem from the adsorption of ZAG, which has been described previously. No conclusive explanation can be found for the adsorption of this negatively charged glycoprotein on hydrophilic and positively or negatively charged surfaces.

Via immunoblotting the presence of albumin on oxidized substrates, SAM-PEG, SAM-NH_2, SAM-Py and SAM-SO_3H was proven. Thus, these results are in accordance with the pronounced bands at approximately 65 kDa in gel electrophoresis. This soft, medium-sized protein (MW 66.5 kDa, IEP 4.7 [26, 155]) is the most abundant in human serum [168] and can adsorb onto every kind of surface upon denaturation [155]. As discussed in more detail in section 14.4, stronger adsorption is usually obtained for hydrophobic surfaces [304, 320]. Additionally, albumin adsorbs more to positively

charged surfaces via electrostatic interactions as it carries a negative charge under physiological conditions [312]. These general trends cannot be observed for the examined self-assembled monolayers. Here, albumin only adsorbs on the hydrophilic substrates, which cover a wide range of zeta potentials from strongly negative (oxidized substrate) to positive (SAM-Py).

At last, immunoblotting reveals the adsorption of fibronectin on oxidized substrates, SAM-PEG, SAM-NH_2, SAM-Py and SAM-SO_3H, although no distinct bands $> 100\,\mathrm{kDa}$ are visible in the stained PAGE gel. In this glycoprotein, disulfide bonds covalently link two subunits (roughly 250 kDa each), which are, hence, separated under reductive conditions [347]. The complete protein, which occurs in plasma in a concentration of $300\,\mu\mathrm{g\,mL^{-1}}$, possesses an elongated structure and an IEP of 5.6 to 6.1 [347–349]. Therefore, preferential adsorption on positively charged surfaces has been observed in previous studies [12, 350]. Regarding the influence of surface free energy and wettability, larger amounts of fibronectin were quantified on substrates with higher polar components of the SFE by Michiardi et al., whereas more fibronectin was found by Keselowsky et al. on more hydrophobic substrates, although the protein retained higher activity on more hydrophilic surfaces [12, 309, 351]. In this study, fibronectin adsorption partially follows these lines. The glycoprotein adsorbs to the cationic SAM-Py surface but also on the hydrophilic and negatively charged oxidized substrate and SAM-SO_3H, not being present on the hydrophobic monolayers SAM-CH_3 and SAM-CF_3. As fibronectin belongs to the group of extracellular adhesion proteins and is of vital importance for cell adhesion, growth and differentiation (see section 5.2.2), it plays a vital role in cell behavior *in vitro* and *in vivo*, e.g. in wound healing [12, 347, 348]. If the adsorption behavior observed on SAMs occured similarly on PAMAM dendrimers with -NH_2, -CH_3 and -COOH endgroups, a lack of fibronectin on PAMAM-CH_3 and PAMAM-COOH could serve as an explanation for the poor performance of those surfaces in previous *in vitro* cell adhesion studies of our work group [20].

Concluding Remarks

Summarizing and interpreting the numerous results regarding the quantitative and qualitative protein adsorption on the studied SAMs with different terminal groups, some general statements and conclusions can be made.
At first, it is worth mentioning that the study conducted here can help in bridging a gap in the research on the interaction of biomaterial surfaces with biofluids. In the past, a plethora of studies has investigated the adsorption of single proteins and linked their behavior to the physicochemical properties of the respective surface [28, 219, 304, 309, 312]. Less research, however, has been conducted about the interaction of complex biological fluids with surfaces, and it was mainly focused on quantitative analysis only [306, 311, 314, 336]. So far, qualitative protein adsorption has mainly been investigated on actual clinical biomaterials [352, 353], whose poorly controllable surface properties (such as surface roughness, wettability and charge) do not permit the prediction of the effect of single surface properties on protein adsorption. The work with model substrates has been limited to studies with very few model surfaces [308, 328]. Studying qualitative protein adsorption from saliva and serum on eight different model surfaces, covering a broad range of surface hydrophilicities and zeta potentials, thus contributed valuable new information to the subject of biomaterial-biofluid interaction.

The first main result can be obtained by comparing the overall protein adsorption pattern on the various surface modifications, as it was observed in SDS-PAGE and western blotting. For saliva, a complex pattern is obtained, which seems to be surface-specific and thus highly influenced by the different surfaces and their characteristics. A different picture presents itself for the adsorption of serum proteins. Rather uniform lanes are obtained in gel electrophoresis for the protein-adsorbing surface modifications, varying mainly in their intensity. Considering that albumin and IgG are the two most abundant proteins in human serum [168, 169], it can be concluded that protein adsorption here is mainly governed by the abundance of the proteins in solution.

For both biofluids, linking the adsorbed amounts of single proteins to specific surface properties is only possible for very few examples. The most striking one is lysozyme in saliva. Due to its IEP of 11.1 [155], it is positively charged under physiological conditions and, therefore, adsorbs to the surfaces with negatively charged groups (oxidized, SAM-COOH, SAM-SO_3H) based on attractive electrostatic interactions, as mentioned earlier. This behavior was similarly observed for the adsorption of single purified proteins [28, 219].
Many other proteins, however, do not follow simple physicochemical rules in their adsorption behavior. The salivary glycoproteins MUC7 and ZAG, for instance, both carry

a negative charge under physiological conditions due to their extensive glycosylation and sialylation (IEP 3.2 or 5.1 respectively) [332]. If their adsorption behavior was dominated by electrostatic effects, they would adsorb only on surfaces with positively charged groups (SAM-NH_2, SAM-Py). Instead, they are also present on the oxidized silica surface and on SAM-PEG, which are both hydrophilic and negatively charged under physiological conditions. Further proteins from saliva and serum, such as amylase and immunoglobulins, were found to adsorb to a variety of surfaces with different properties as well.

The impossibility to link the adsorption behavior of single components of the biofluids or the total amount of adsorbed proteins to the physicochemical properties of the investigated SAMs may have a variety of reasons. At first, protein-protein interactions among different proteins may occur in solution and affect protein adsorption. For saliva, the presence of so-called salivary micelles has been described [354, 355]. These globular complexes with a size between 100 and 500 nm consist of a variety of different salivary proteins and their composition differs from the protein ratios of whole saliva or uncomplexed proteins [354, 355]. Western blotting by Soares et al. showed that mucins, lactoferrin and secretory IgA are enriched in the complexes, whereas amylase, PRPs or lysozyme were absent or only present in very small amounts [354]. These complexes probably expose a plethora of different functionalities, allowing them to adsorb to a large variety of different surfaces. Proteins, contained in these micelles, can thus be "dragged" to a surface despite unfavorable physicochemical interactions. This way, the concerted adsorption of mucins, immunoglobulins and amylase can possibly be explained.
Protein-protein interactions are probably also important between proteins on the surface. For saliva, the structure of the salivary pellicle has been studied in detail and can be described with a two-layer model [326, 328]. The inner layer is formed quickly after the first contact between the surface and saliva. It is thin, dense, firmly attached to the surface and contains only small amounts of trapped water [326]. In this layer, adsorption is usually ruled by protein-surface interactions and dominated by small, i.e. quickly diffusing and abundant proteins. Therefore, this inner layer contains, for instance, statherins, acidic PRPs, cystatin and amylase [326, 328]. The thicker outer layer is formed in a maturation process over a longer period of time and strongly influenced by protein-protein interactions. It is characterized by a less dense packing of more flexible molecules, comprising mainly mucins and trapped water [326, 328].
In addition to protein-protein interactions in solution and on the surface influencing the adsorption process, the protein layer on the surface may further be altered by protein exchange via the Vroman effect. This process has been reported for the adsorption of

plasma proteins. Here, it was observed that initially adsorbed albumin was replaced by IgG and then by fibronectin [356]. If this process is similar when a surface is in contact with blood serum not plasma, the protein exchange may serve as an explanation why the immunostained bands of albumin are rather weak despite albumin being the most abundant protein in human serum [168].

Although no easy and predictable physicochemical driving forces for protein adsorption from biofluids on differently functionalized surfaces were found, it was, however, observed that the pattern of adsorbed proteins depended on the surface modification, especially for adsorption from human saliva. Some of these proteins are known to affect the adhesion of bacteria or tissue cells. Lysozyme and cystatin, for example, exhibit antibacterial properties [357]. Other proteins, such as DMBT1 and MUC7, are able to bind to pathogenic bacteria, which, however, may enhance bacterial adhesion if they are adsorbed to a surface [344, 357, 358]. Among the serum proteins, the extracellular adhesion protein fibronectin is known to promote cell adhesion [12]. Therefore, those proteins probably have a large influence on the fate of an implant, promoting bacterial colonization or supporting tissue cell attachment and tissue integration.

14 Oligomeric and Polymeric Amine Group-Terminating Modifications

Inspired by the PAMAM dendrimer, a variety of amine-terminated surface functionalizations with different structure, namely short oligomers, linear polymers and dendrimers, was investigated in the scope of this thesis. In this following section, the results for all those modifications with terminal amine groups as well as their precursors will be discussed and compared. Therefore, the respective surface modifications are first summarized in Figure 14.1.

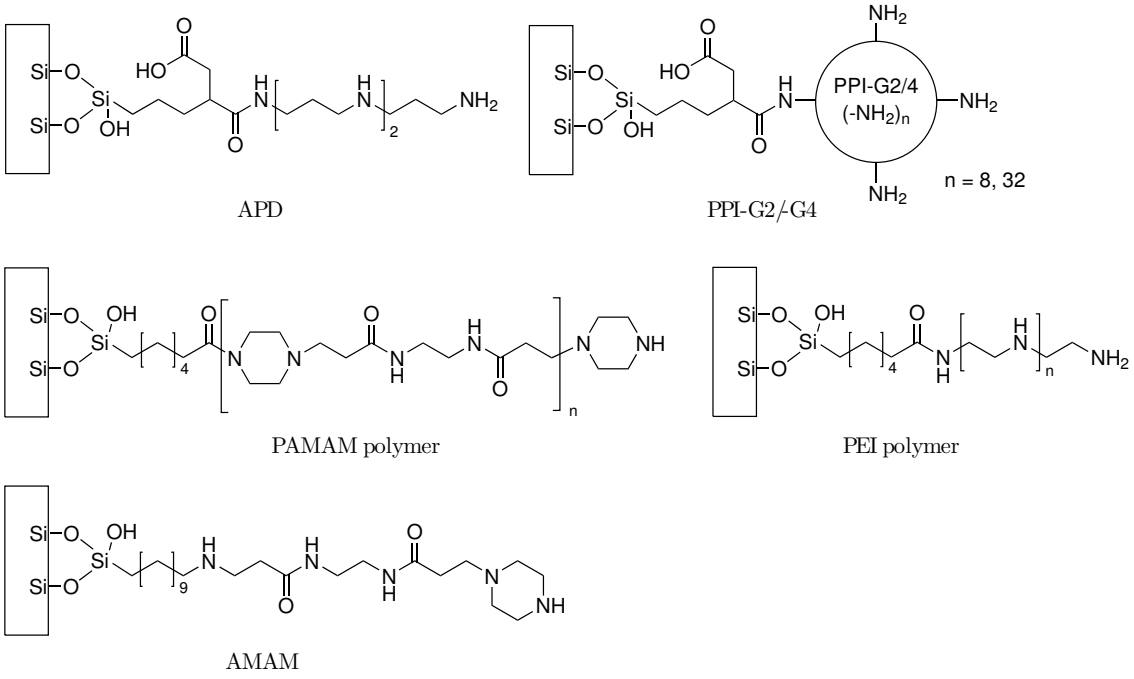

Figure 14.1: Overview of the oligomeric and polymeric surface modifications, containing amine and partially amide motifs, as well as their abbreviated names.

14.1 Analysis of the PAMAM Polymer

Prior to the analysis of the final surface modifications, the characterization of the linear PAMAM polymer is presented briefly. The polymer was synthesized via polyaddition of EBA and piperazine (see chapter 8) and was analyzed via IR spectroscopy, ^{1}H- and ^{13}C-NMR spectroscopy as well as mass spectrometry. This analysis has also been carried out and described in the preceding master's thesis [22].

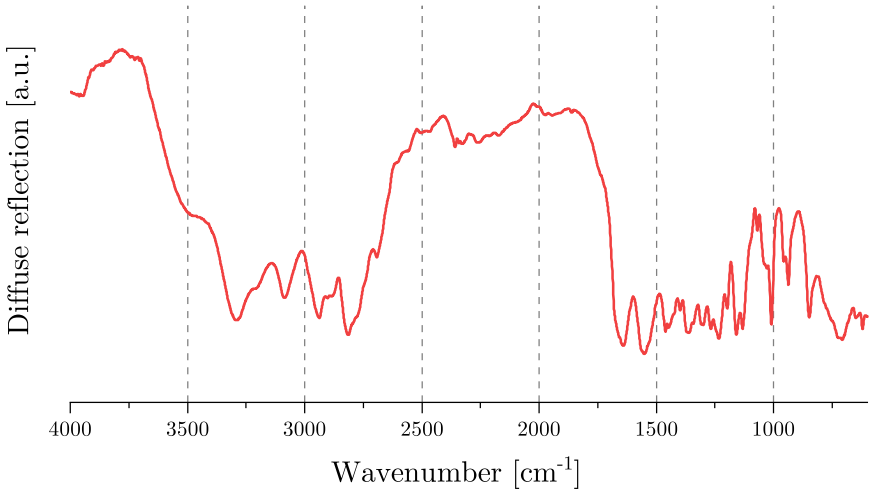

Figure 14.2: IR spectrum of the linear PAMAM polymer, obtained via DRIFT spectroscopy.

Among the chemical functionalities of the polymer chain, namely secondary amide and tertiary amine groups, the former can be identified clearly in IR spectroscopy. The bands at 3294 cm^{-1} and 3087 cm^{-1} can be assigned to the N-H stretching vibration of the amide group, and the corresponding C=O stretching vibration occurs at 1640 cm^{-1} [285]. The amide II band, comprising C-N stretching as well as N-H deformation vibrations, can be identified at 1550 cm^{-1} [285]. The tertiary amine groups, however, cannot be assigned unambiguously. Due to the lack of hydrogen atoms in this functional group, only the C-N stretching vibration may be used for identification, which, however, is rather weak and occurs in the range between 1210 cm^{-1} and 1150 cm^{-1}, i.e. in the fingerprint region [285]. No band can be identified definitely in this range. In contrast to that, the hydrocarbon units (-CH_2-) of the polymer can be observed clearly. The signals at 2937 cm^{-1} and 2815 cm^{-1} can be assigned to the asymmetric and symmetric C-H stretching vibration [285]. The corresponding C-H scissor vibration is positioned at 1460 cm^{-1}. The C-C stretching vibration of the polymer backbone is probably responsible for the doublet at 1159 cm^{-1} and 1132 cm^{-1} [285].
The identification of the polymer end groups via IR spectroscopy was not successful for two reasons. Firstly, their contribution to the IR spectrum in comparison with the functional groups of the polymer backbone is presumably rather small, especially for

long polymer chains. Secondly, the bands of both possible end groups, a secondary amine or an acrylamido group, are expected to overlap with bands of functional groups present in the polymer chain. The stretching and deformation vibration of a secondary amine, for instance, can coincide with the bands of the secondary amide groups [285]. The C-H or C=C stretching vibrations of a terminal vinyl group possibly overlap with the N-H stretching or C=O stretching vibration of the secondary amide group as well [285]. Thus, the identification of the terminal groups had to be achieved via NMR spectroscopy and mass spectrometry.

In order to facilitate the assignment of the signals of the NMR spectra, the different -CH_2- groups of the repeating unit of the polymer were labeled as seen in Figure 14.3. The analysis of the NMR spectra was performed with the SpinWorks 4 software (Kirk Marat, University of Manitoba, Winnipeg, Canada).

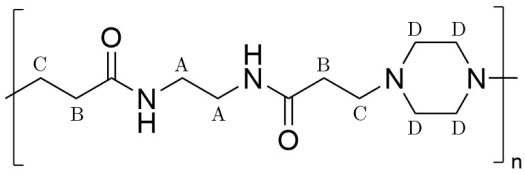

Figure 14.3: Repeating unit of the PAMAM polymer chain with labeled -CH_2- units.

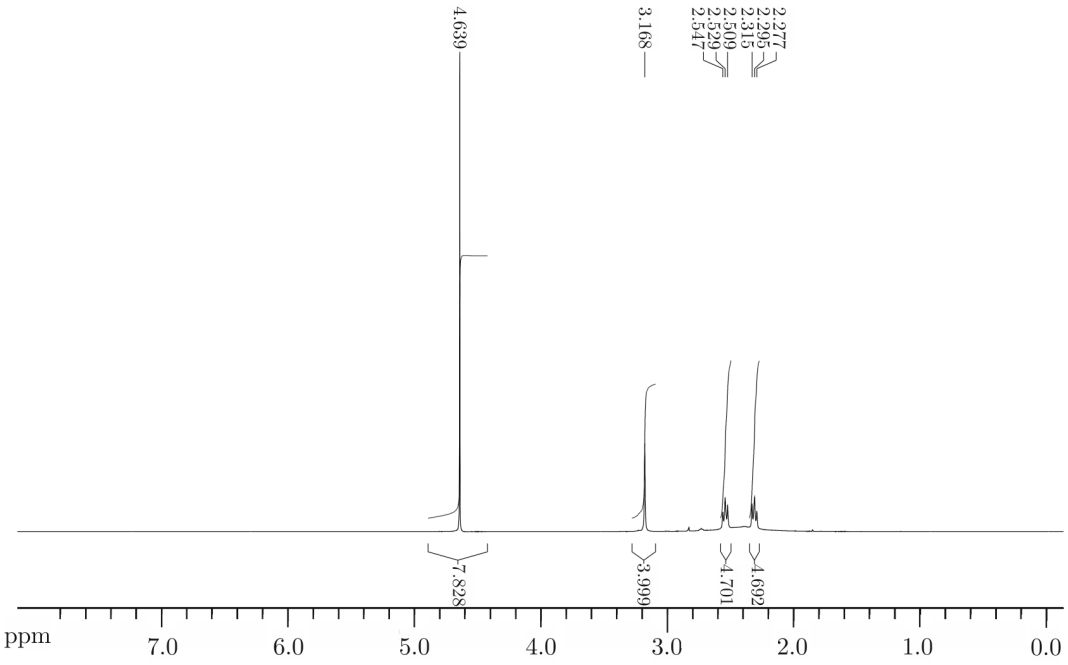

Figure 14.4: ^{1}H-NMR spectrum of the linear PAMAM polymer in D_2O.

In the ^{1}H-NMR spectrum (see Figure 14.4), the triplet at 2.295 ppm (J = 7.6 Hz) is caused by the -CH_2- units next to the carbonyl group (B), the coupling triplet at 2.529 ppm (J = 7.6 Hz) can be assigned to the neighboring hydrocarbon unit (C). The singlet at 3.168 ppm is caused by the ethylene unit between the amide groups (A), whereas the singlet at 4.639 ppm is attributed to the -CH_2- units of the piperazine ring (D). The integrals are approximately consistent with this assignment. It can be reasoned that the polymer possesses terminal piperzine units because no signals are observed above 5 ppm, which would be related to vinyl groups [359].

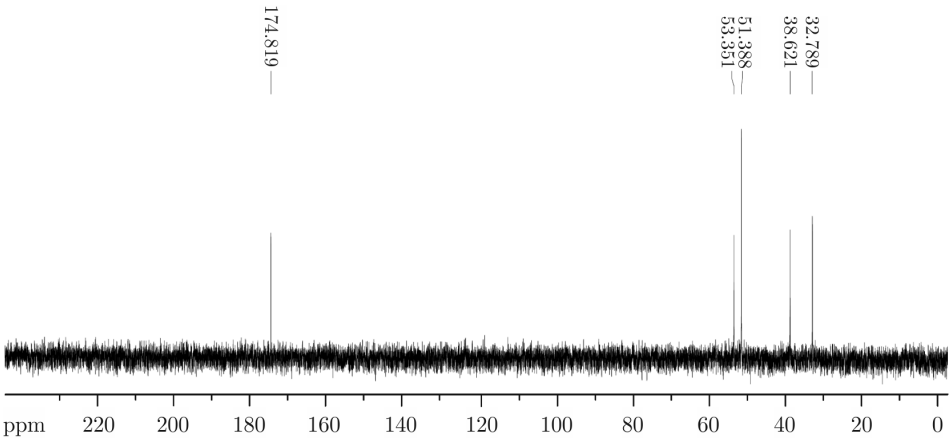

Figure 14.5: ^{13}C-NMR spectrum of the linear PAMAM polymer in D_2O.

The corresponding ^{13}C-NMR spectrum (see Figure 14.5) of the linear PAMAM polymer exhibits five different signals, which can be expected for the five magnetically unequal carbon atoms of the repeating unit. The signals at 33 ppm and 39 ppm can be assigned to the carbon atoms on both sides of the amide group (A and B) [359]. Furthermore, the signals at 51 ppm and 53 ppm belong to the carbon atoms next to the tertiary amine (C and D). At last, the signal at 175 ppm can be assigned to the carbon atom of the amide group [359]. No vinylic carbons are present in the polymer as signals are absent in the range from 120 ppm to 135 ppm [359].
Via HPLC-ESI-MS, the size of the PAMAM polymer could be estimated. After dialysis, the number of monomer units was determined to be at least 10 and reach up to 50, leading to a molecular weight of the polymer between 2500 g mol^{-1} and 12 500 g mol^{-1}. Detailed analysis of the spectra confirmed that the polymer chains are terminated by piperazine units.

14.2 Verification of Successful Surface Coating

Prior to further analysis, the amine-based surface modifications were at first characterized via XPS, sulfo-SDTB assay (for the determination of the amine groups density) and IR spectroscopy. The results have recently been published in Lehnfeld et al. [273].

14.2.1 Determination of the Chemical Composition via XPS

In order to verify the successful immobilization of the amine group-bearing reagents (APD, PPI-G2, PPI-G4, PAMAM polymer, PEI polymer and EBA/piperazine) and to determine the chemical composition of the coatings, XPS spectra were recorded of functionalized wafers. The results, i.e. the composition in at-% as well as important elemental ratios, are summarized in Table 14.1.

Table 14.1: Chemical composition of amine group-bearing surface modifications with oligomeric or polymeric structure in comparison with the intermediate SAMs, determined via XPS.

Surface modification	XPS data [at-%]				Element ratios		
	Si	C	O	N	N/C	N/Si	C/Si
Oxidized	44	17	32	1	0.06	0.02	0.39
TESPSA[a]	22	42	35	0	0.00	0.00	1.91
APD	17	47	29	6	0.13	0.35	2.76
PPI-G2	12	56	23	8	0.14	0.67	4.67
PPI-G4	10	58	20	11	0.19	1.10	5.80
SAM-COOH[a]	41	26	33	0	0.00	0.00	0.63
PAMAM polymer	23	40	27	10	0.25	0.43	1.74
PEI polymer	30	34	31	6	0.18	0.20	1.13
SAM-NH_2	35	34	28	2	0.06	0.06	0.97
AMAM	30	37	29	4	0.11	0.13	1.23

[a] XPS data was taken from Katzur et al. [18].

In the first step, the different surface modifications can be compared to their respective precursor SAMs. In all cases, an increased carbon content but decreased silicon content can be observed, which indicates the formation of a thicker organic layer. Furthermore, a higher nitrogen content is obtained with respect to the intermediate SAMs, which is the consequence of the successful immobilization of amine group-containing reagents. These results are reflected by higher N/C, N/Si and C/Si ratios for the final functionalizations.

Among the coatings formed via immobilization on a TESPSA monolayer, from APD via PPI-G2 to PPI-G4, an increasing nitrogen content, leading to increasing N/Si and N/C ratios, can be found. This is accompanied by a decrease in the silicon content and a rising carbon content, resulting in larger C/Si values. These observations correspond to the idea that a denser, thicker organic layer is formed with increasing molecule size and dendrimer generation. In literature, however, almost no data is available for comparison. Zhang et al. immobilized generation 5 PPI dendrimers with 64 terminal amine groups on a polymeric substrate, but they only obtained a nitrogen content of 6% [360]. Due to the different substrate and grafting technique, though, no comparison can be made. An immobilization procedure identical to the one used in this thesis was applied by Katzur et al. for the modification of surfaces with PAMAM dendrimers of generation 5, which exhibited an elemental composition similar to the modification with PPI-G4 [18].
Comparing both polymers, PAMAM and PEI polymer, among each other, some differences can be observed. For the PAMAM coating, higher carbon and nitrogen contents, accompanied by lower oxygen and silicon percentages, are obtained. Thus, it can be assumed that a denser or thicker organic layer was formed for PAMAM polymer despite the higher molecular weight of the PEI polymer.
In summary, successful surface functionalization can be confirmed for all six modifications via comparison with the respective intermediate SAMs.

14.2.2 Density of Amine Groups

The success of the immobilization reactions was additionally evaluated with the sulfo-SDTB assay via the determination of the density of surface amine groups. To that purpose, the amount of released trityl cations is calculated from spectrophotometric measurements and assumed to be equal to the number of accessible amine groups on the surface. Dividing by the surface area of the beads in the sample, the amine group density is obtained. Here, this expression does not only apply to terminal amino groups but all amines that are accessible to the sulfo-SDTB dye. The obtained results are provided in Figure 14.6.
Having a look at the results of the sulfo-SDTB assay, some very general conclusions can be drawn at first. It can be seen that unspecific interactions between the sulfo-SDTB reagent and a surface without amine groups only lead to a result that is equal to an amine group density of 100 to 200 $\mathrm{nmol\,m^{-2}}$. This is significantly lower than the densities obtained for the intermediate SAM-NH_2 and all amine-modified substrates. The increase in amine group density for the final modifications compared to their precursor SAMs also confirms successful synthesis. This statement applies to all modifications, except for the AMAM structure. Here, the amine groups density remains almost unchanged as already the intermediate SAM-NH_2 exhibits primary amine groups.

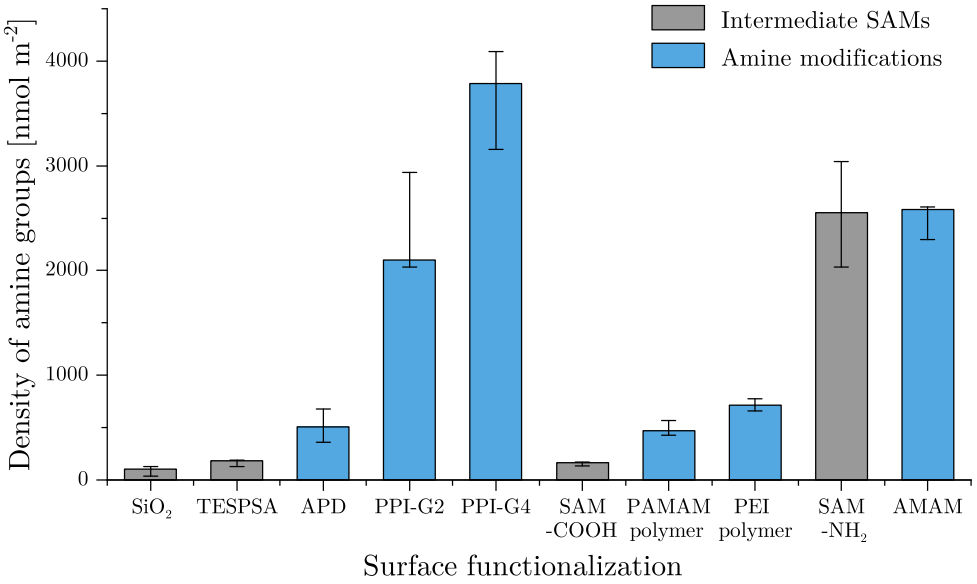

Figure 14.6: Amine group densities, obtained via Sulfo-SDTB assay, for intermediate SAMs and amine-based surface modifications.

At this point, however, two disadvantages of the sulfo-SDTB assay have to be considered. First of all, it can be assumed that the result obtained for the amine group density of the SAM-NH_2 monolayer is too low and does not reflect the actual density of functional groups in the monolayer. The theoretical density of a monolayer, in which one silane molecule occupies an area of approximately 25 $Å^2$, can be calculated as 6.7 $\mu mol\, m^{-2}$ [32]. The number obtained from the colorimetric assay is significantly lower, which may be the consequence of sterical hindrance among the bulky sulfo-SDTB molecules in the initial immobilization step.

The results obtained for the different surface modifications of this thesis have to be dealt with carefully for another reason as well. The sulfo-SDTB assay is frequently used for the quantification of primary amine groups on solid surfaces [361, 362]. The immobilization of the sulfo-SDTB molecule, however, is presumably also possible via formation of an amide bond with secondary amines, and thus secondary amine groups possibly contribute to the formation of trityl cations in the assay. Yet, no clear statement can be made with respect to the relative reactivites. On the one hand, secondary amines are more nucleophilic than primary amines [363], whereas on the other hand, steric hindrance due to bulky residues or rigid ring structures may lead to a reduced trityl cation formation. Therefore, no direct quantitative comparisons should be made between the three groups of surface modifications, with primary and secondary amines (APD, PEI polymer), primary and tertiary amines (PPI-G2, PPI-G4) and only secondary and tertiary amines (PAMAM polymer, AMAM).

Some conclusions can be drawn, though, especially among modifications with primary amines as terminal groups and the basic SAM-NH_2. The amine group density obtained for APD-functionalized surfaces indicates that a disordered surface layer was formed because the density of functional groups is significantly lower than the one for SAM-NH_2. The opposite observation can be made for the PPI dendrimers, whose amine group densities are similar (PPI-G2) or significantly higher (PPI-G4) than those of SAM-NH_2. This leads to the conclusion that the amine groups are rather crowded, especially on the PPI-G4 surface. It is interesting to note that the amine group densities for PPI-G2 and PPI-G4 are both significantly higher than those of surfaces modified with a different dendrimer, the PAMAM dendrimer of generation 5, which possesses even 128 primary amine groups per molecule. In this case, only amine group densities of approximately $1000\,\mathrm{nmol\,m^{-2}}$ were obtained [20]. The higher results for PPI dendrimers might be explained with the shorter branch length of PPI dendrimers, leading to a denser and more crowded structure.

For the PEI polymer surface, again a rather low density of approximately $700\,\mathrm{nmol\,m^{-2}}$ can be observed and can perhaps be explained by the "grafting to" approach that was used for polymer immobilization. This technique is known to yield low-density coverage of surfaces with polymers in the mushroom regime [116, 364]. Regarding the amine group densities of the remaining surface modifications, PAMAM polymer and AMAM, no comparisons can be made with SAM-NH_2 as both coatings do not exhibit any primary amine groups. It can only be concluded that secondary amine moieties can also be detected with the sulfo-SDTB assay. In addition to that, it can be stated that PAMAM polymer was successfully immobilized on the surface. No conclusion can be drawn from the results of the AMAM modification.

14.2.3 Analysis of IR Spectra

The IR spectra of the terminal amine-based modifications were recorded from functionalized silica spheres via diffuse reflectance and are presented in Figure 14.7. They have partially been included in the preceding master's thesis [22] and have recently been published (as part of the supporting information) [273].
As it can be seen, all spectra share a negative band at $3740\,\mathrm{cm^{-1}}$. This is caused by the disappearance of surface silanol groups and their respective stretching vibrations and, hence, confirms successful silanization [285]. The -CH_2- units of the silane molecules and the amine reagents are responsible for the asymmetric and symmetric C-H stretching vibrations, appearing approximately at $2940\,\mathrm{cm^{-1}}$ and $2840\,\mathrm{cm^{-1}}$ [285].

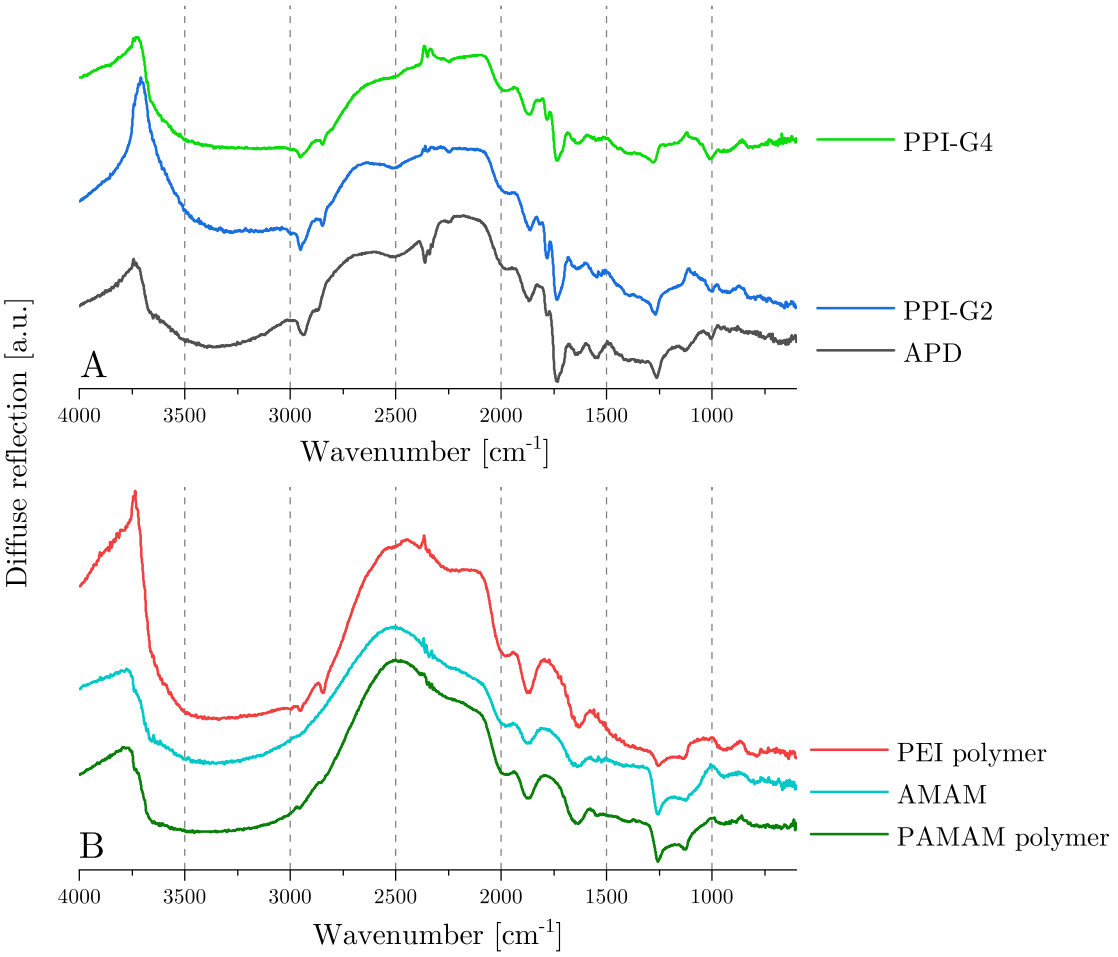

Figure 14.7: DRIFT spectra of silica spheres, coated with the amine-based surface functionalizations (A) APD, PPI-G2 or PPI-G4, or (B) PAMAM polymer, PEI polymer or AMAM.

The band at 1730 cm^{-1} can be assigned to the C=O stretching vibration of the carboxylic group, which is generated upon the ring-opening of the succinic anhydride ring of TESPSA [285]. The band at 1640 cm^{-1} is related to the amide I band, i.e. the C=O stretching vibration of the secondary amide, as well as to the N-H deformation vibration of primary amine groups [285]. Further assignment of vibrational bands in the "fingerprint" region below 1500 cm^{-1} is often ambiguous. Some explanations, however, may be possible. The vibration at 1250 cm^{-1} may be caused by the Si-CH_2-R vibration of the silane, the one at 1130 cm^{-1} can possibly be assigned to C-C skeletal vibrations [285]. These bands may coincide with the C-N stretching vibrations of secondary amide (amide III band) and amine groups [285]. At last, the weak band at 1000 cm^{-1} is possibly related to the silane layer as well, showing Si-O-Si vibrations [285].

14.3 Analysis of Physicochemical Properties

The amine-functionalized surfaces were further analyzed with respect to their key physicochemical characteristics, such as hydrophilicity and surface free energy (see section 14.3.1), dynamic wetting behavior (see section 14.3.2) and their zeta potential (see section 14.3.3). The obtained results have partially been included in the preceding master's thesis [22] and have been published recently [273]. As only modified silicon and silica substrates were characterized, the reader is referred to section 16.1 for the analysis of titanium substrates and their comparison with silicon-based modifications.

14.3.1 Wettability and SFE

The wetting properties of the functionalized silicon wafers were determined with static contact angle measurements via the sessile drop technique.
The hydrophilicity of the surface modifications can be derived from contact angle measurements with water (see Table 14.2). It can be seen there that all surface coatings possess water contact angles which are higher than those of oxidized wafers but lower than those of the intermediate SAMs. All amine-based surface functionalizations can be regarded as hydrophilic because they exhibit water contact angles below 60°. The polymer-based surface coatings are the most hydrophilic ones, showing the lowest contact angles (27° for the PAMAM polymer and 35° for the PEI polymer). Contact angles in the range between 39° and 46° are observed for PPI-G4, PPI-G2 and APD-functionalized surfaces. The modification with APD is more hydrophilic than a SAM in which each silane molecule contains one inner secondary and one surface primary amine group. In that case, Sugimura et al. obtained a contact angle of approximately 60° [365]. The increased hydrophilicity of the APD coating might be the consequence of the larger number on amine groups as well as of the immobilization procedure, which leads to the generation of an amide and a carboxylic acid group. The AMAM modification leads to the least hydrophilic surface, which possesses a water contact angle of 57°.
As for the self-assembled monolayers, the SFE (as well as its components) of the amine-based functionalizations was calculated from the static contact angles with sf-water, formamide and diiodomethane, according to the LW/AB approach. The components of the surface tensions of those testing liquids are summarized in section 13.2.1.
The obtained SFEs, as well as their polar and dispersive components, are depicted in Figure 14.8. As it can be seen there, the final surface modifications possess rather similar SFEs, ranging from 46 to 54.3 $\mathrm{mN\,m^{-1}}$.

Table 14.2: Static contact angles (with water, formamide and diiodomethane) for amine-based surface modifications. Results for contact angles with formamide or diiodomethane have partially been published in the preceding master's thesis [22].

Surface modification	Contact angle [°]		
	Water	Formamide	Diiodomethane
Oxidized	14 (12-16)	10 (6-12)	37 (33-42)
TESPSA	60 (59-62)	-	-
APD	46 (41-53)	34 (33-35)	26 (24-28)
PPI-G2	45 (39-54)	31 (29-32)	32 (29-33)
PPI-G4	39 (31-47)	30 (24-32)	40 (39-42)
SAM-COOH	47 (47-48)	-	-
PAMAM polymer	27 (22-36)	19 (16-23)	37 (27-40)
PEI polymer	35 (33-41)	31 (29-33)	39 (35-40)
SAM-NH_2	66 (64-67)	-	-
AMAM	57 (46-60)	40 (38-40)	45 (43-48)

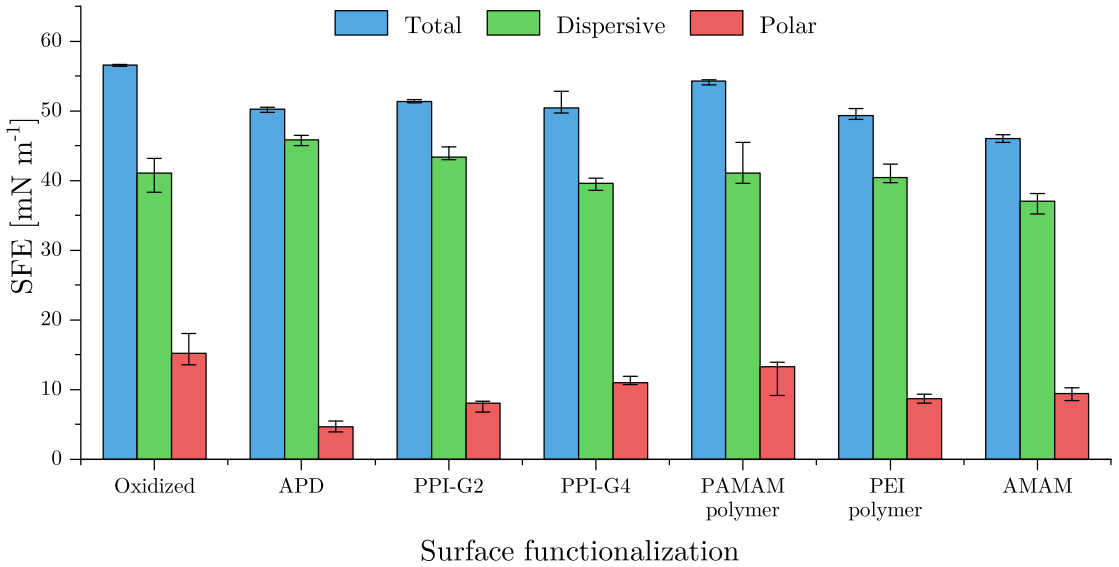

Figure 14.8: Surface free energies (as well as polar and dispersive components) of amine-based surface coatings in comparison with oxidized wafers.

The lowest SFE is obtained for the AMAM surface, which also possesses the lowest dispersive component ($37\,\mathrm{mN\,m^{-1}}$), whereas the highest SFE is determined for the PAMAM polymer-covered surface, along with the highest polar component (54.3 and $13.3\,\mathrm{mN\,m^{-1}}$ respectively). The SFE of the PPI-G4 dendrimer-modified surface is in

good accordance with the results obtained for a surface functionalization with amine-terminated PAMAM dendrimers, as measured by Katzur et al. [18]. This modification exhibited a similar polar component of the SFE (roughly $12\,\mathrm{mN\,m^{-1}}$), but a lower total SFE of roughly $45\,\mathrm{mN\,m^{-1}}$ was obtained because the dispersive component was lower. This difference can possibly be explained by the presence of inner amide groups in the PAMAM dendrimer coating.
Comparing the structurally related modifications APD, PPI-G2 and PPI-G4, which only possess amine groups but no amide groups as functional moieties, no differences can be observed for the total SFE. Having a closer look at the dispersive and polar component, however, two opposing trends can be observed. The former decreases from APD via PPI-G2 to PPI-G4, whereas the latter is increasing. Both tendencies are probably caused by the increasing number of inner and surface amine groups.
Surface functionalizations with inner amine and amide groups seem to possess larger polar contributions in general as the polar components of AMAM and PAMAM polymer-modified surfaces exceed 20% of the total SFE, which is only matched by the polar component of the PPI-G4 coating (22%).

14.3.2 Dynamic Contact Angles

In addition to the hydrophilicity and the surface free energy, the wetting behavior of the amine-based surface modifications was investigated via dynamic contact angle measurements, using the Wilhelmy plate technique. For a complete picture, the tensiometric measurements were performed not only with the final amine-functionalized surfaces but also with oxidized wafers as well as the intermediate SAMs TESPSA, SAM-COOH and SAM-NH_2. Measurements were performed with water as well as with PBS (pH 7.4, ionic strength $150\,\mathrm{mmol\,L^{-1}}$). The obtained force-immersion cycles as well as advancing and receding contact angles are summarized in the appendix (Table VI.1 and Figures VI.4, VI.5 and VI.7). The advancing contact angles, receding contact angles, hysteresis and its changes are depicted in Figures 14.9 to 14.12.

As ten immersion cycles were recorded for each measurement, detailed information about the surface properties can be obtained from the data, especially the contact angle hysteresis. The thermodynamic hysteresis, which is constant over time and thus also over several immersion cycles, can be caused by surface roughness, chemical heterogeneity or the reorientation of functional groups [230]. A transient hysteresis, the kinetic hysteresis, which changes in the course of the measurement, may have its origin in surface deformation or swelling or might be caused by the adsorption of species of the liquid phase [230]. In order to extract as much information as possible, a detailed analysis of the tensiometric data was carried out.

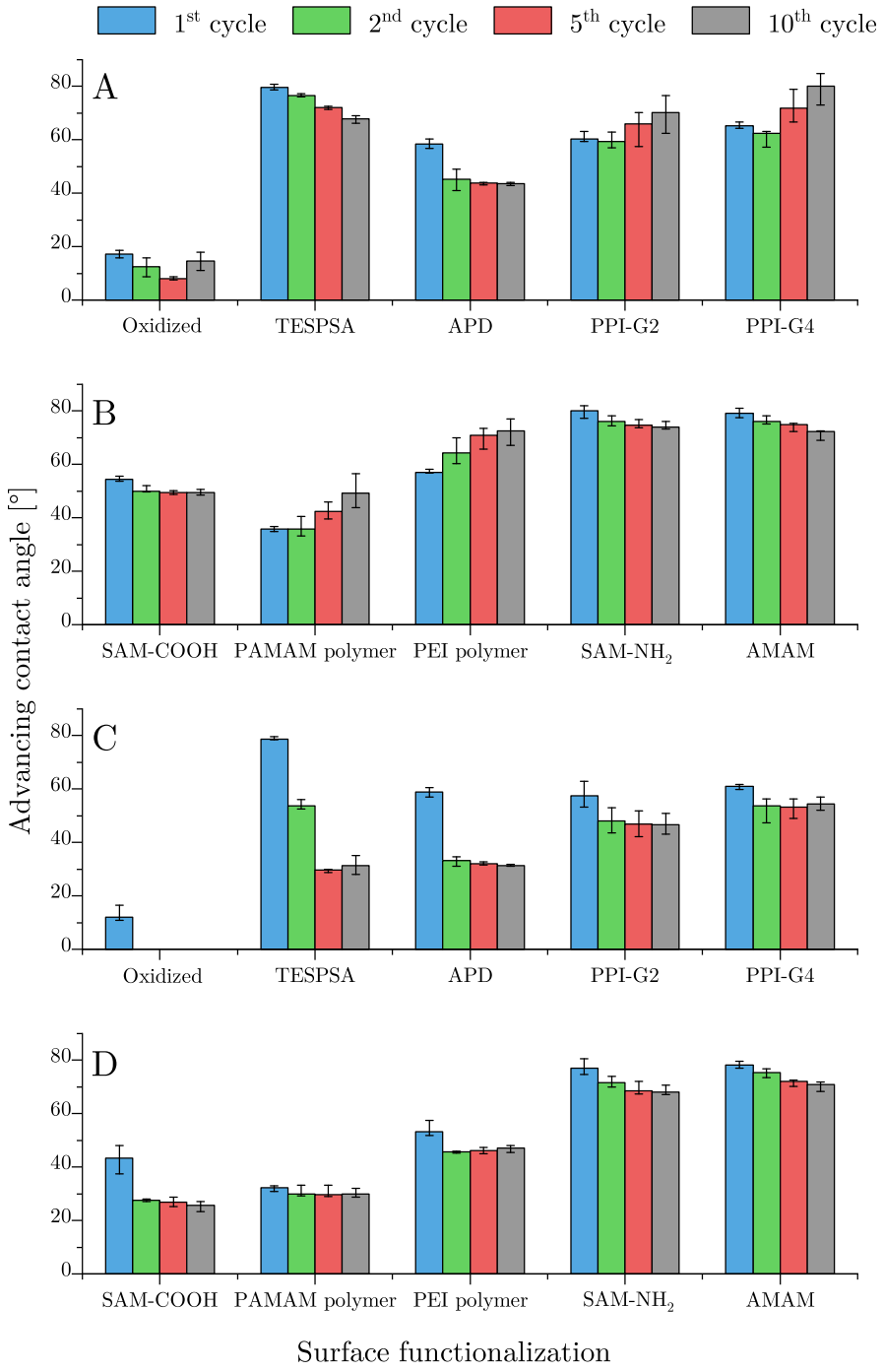

Figure 14.9: Advancing contact angles obtained from dynamic contact angle measurements with water (A and B) or PBS (C and D). In addition to the amine-terminated functionalizations, also the intermediate SAMs are provided. Results for cycles 1, 2, 5 and 10 are given.

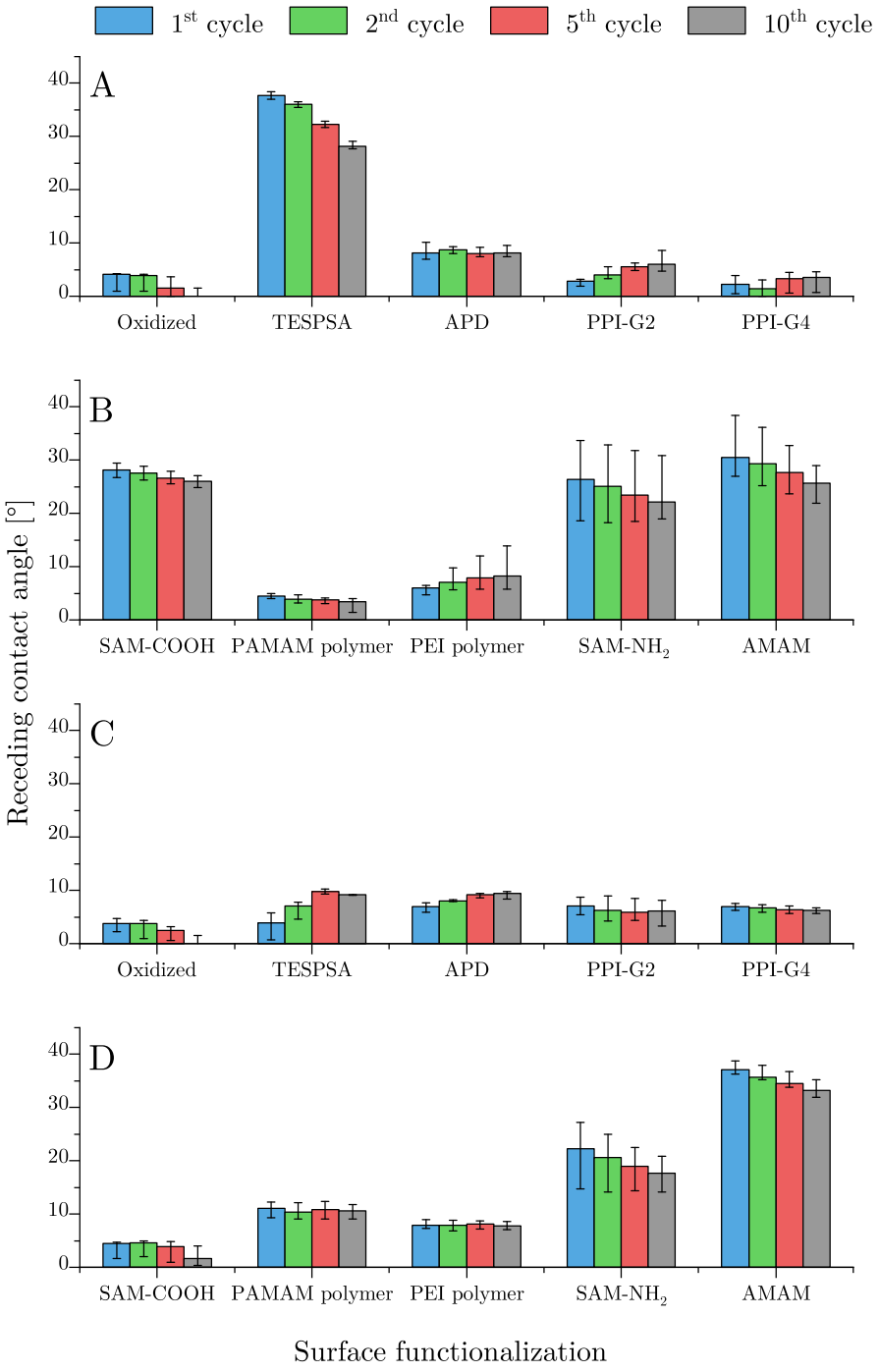

Figure 14.10: Receding contact angles obtained from dynamic contact angle measurements with water (A and B) or PBS (C and D). In addition to the amine-terminated functionalizations, also the intermediate SAMs are provided. Results for cycles 1, 2, 5 and 10 are given.

Having a general look at the advancing contact angles of functionalized substrates, it can be stated that they are in general higher than those of oxidized but unmodified substrates. They, however, cover a wide range from 30° (e.g. APD or PAMAM polymer with PBS) to 80° (such as TESPSA, PPI-G4, SAM-NH_2 or AMAM with sf-water). The high advancing contact angles and hysteresis for PPI-G4 dendrimers are in good accordance with results by Zhang et al. for PPI-G5 dendrimers [360]. The contact angles for two of the self-assembled monolayers, namely SAM-COOH and SAM-NH_2, are in the range reported in literature. For the carboxylic SAM, higher advancing and receding contact angles were reported by Katzur et al. (66° and 38° respectively), whereas more hydrophilic properties were obtained by Shyue et al. (46° and 14°) [18, 272]. Likewise, the wetting behavior observed for the amine SAM is not identical but similar to data obtained by Katzur et al. (57° and 10°) and Shyue et al. (70° and 40° respectively) [18, 272]. No major differences between intermediate SAMs and final amine modifications with respect to the range of contact angles can be observed.

The receding contact angles can be divided into two groups. The first one exhibits very low contact angles ($< 10°$) both in measurements with water and with PBS. This group comprises all amine-based modifications, except AMAM, as well as oxidized wafers. The second group consists of modifications which show higher receding contact angles between 20° and 35° at least in measurements with sf-water (TESPSA, SAM-COOH) or in measurements with sf-water and PBS (SAM-NH_2, AMAM). Thus, higher receding angles are primarily observed for the intermediate SAMs.

Among the measurements in pure water, the dendritic and polymeric modifications (PPI-G2, PPI-G4, PAMAM and PEI polymer) show an increase in their advancing contact angles and their hysteresis with an increasing number of immersion loops. This behavior is not found for the oligomeric modifications (APD and AMAM) or the intermediate SAMs. Katzur et al., however, also observed increasing advancing angles and hysteresis for PAMAM dendrimers of generation 5 [18]. The large hysteresis in the first cycle, i.e. the thermodynamic hysteresis, is presumably caused by the flexibility and reorientation of the surface functional groups of those polymeric modifications, compared to the short-chained analogues. The polymer chains or dendritic branches of those coatings are probably able to reorient themselves. This way, they can expose hydrophilic amine or amide groups to the water interface or hydrophobic -CH_2- units to the air interface. For PPI dendrimers, the flexibility required for this reorientation of branches was proven in molecular dynamics simulations by Scherrenberg et al. [74]. For surface-immobilized polymers with both hydrophilic and hydrophobic groups, a flexible rearrangement of those groups has also been suggested by Kobayashi et al. [366].

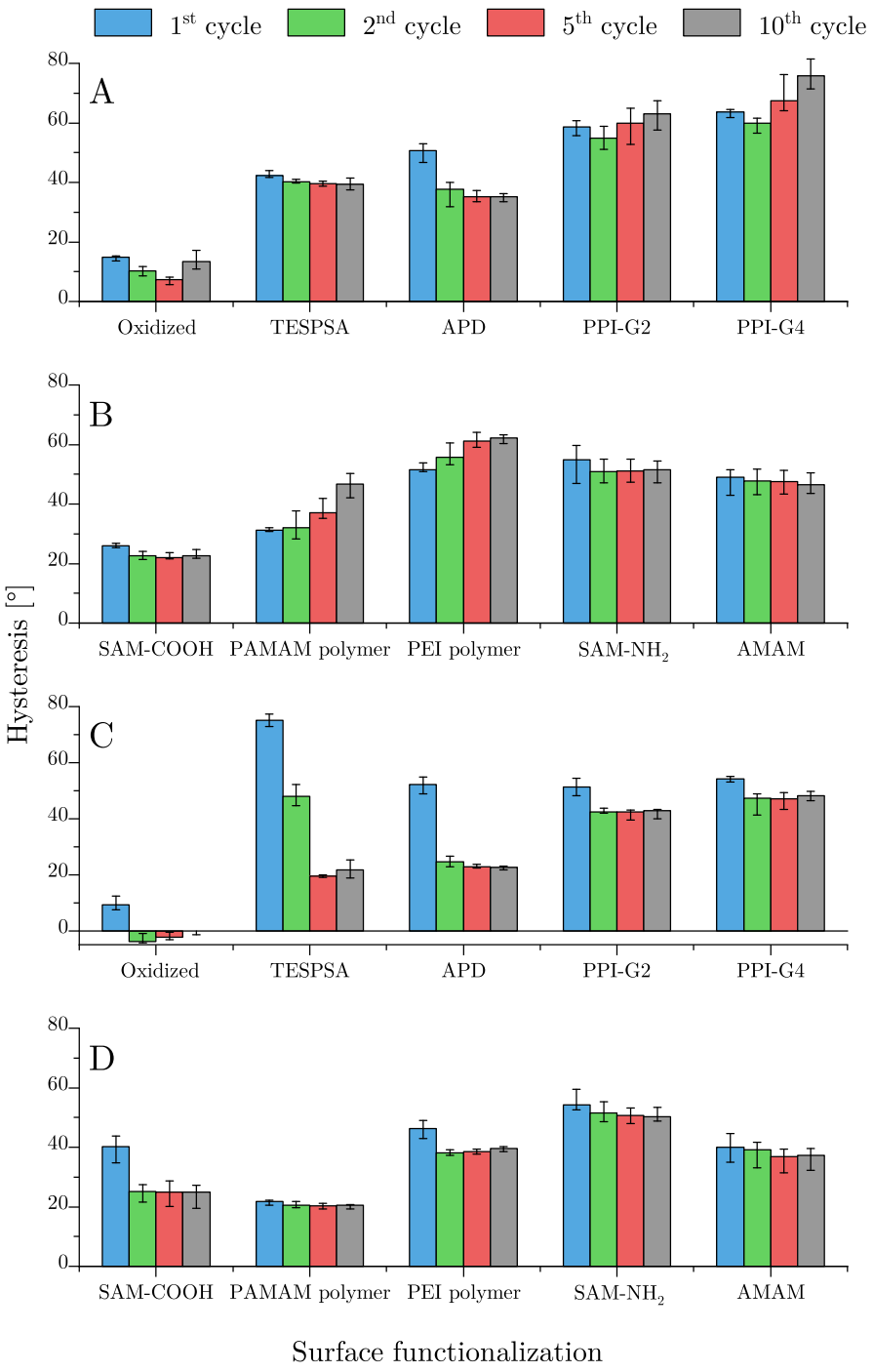

Figure 14.11: Hysteresis of amine-functionalized surfaces, determined as the difference between the advancing and receding contact angles of tensiometric measurements with water (A and B) or PBS (C and D). Results are provided for cycles 1, 2, 5 and 10.

Surface roughness and inhomogeneity, however, cannot be excluded as further reasons for the thermodynamic hysteresis because the surface of substrates modified with PAMAM-G5 dendrimer was found to exhibit roughness on a nanometer scale [19]. The increasing hysteresis with increasing number of immersion loops, i.e. the kinetic hysteresis, which is most prominent for the PAMAM polymer coating, can probably be explained with swelling of the surfaces.

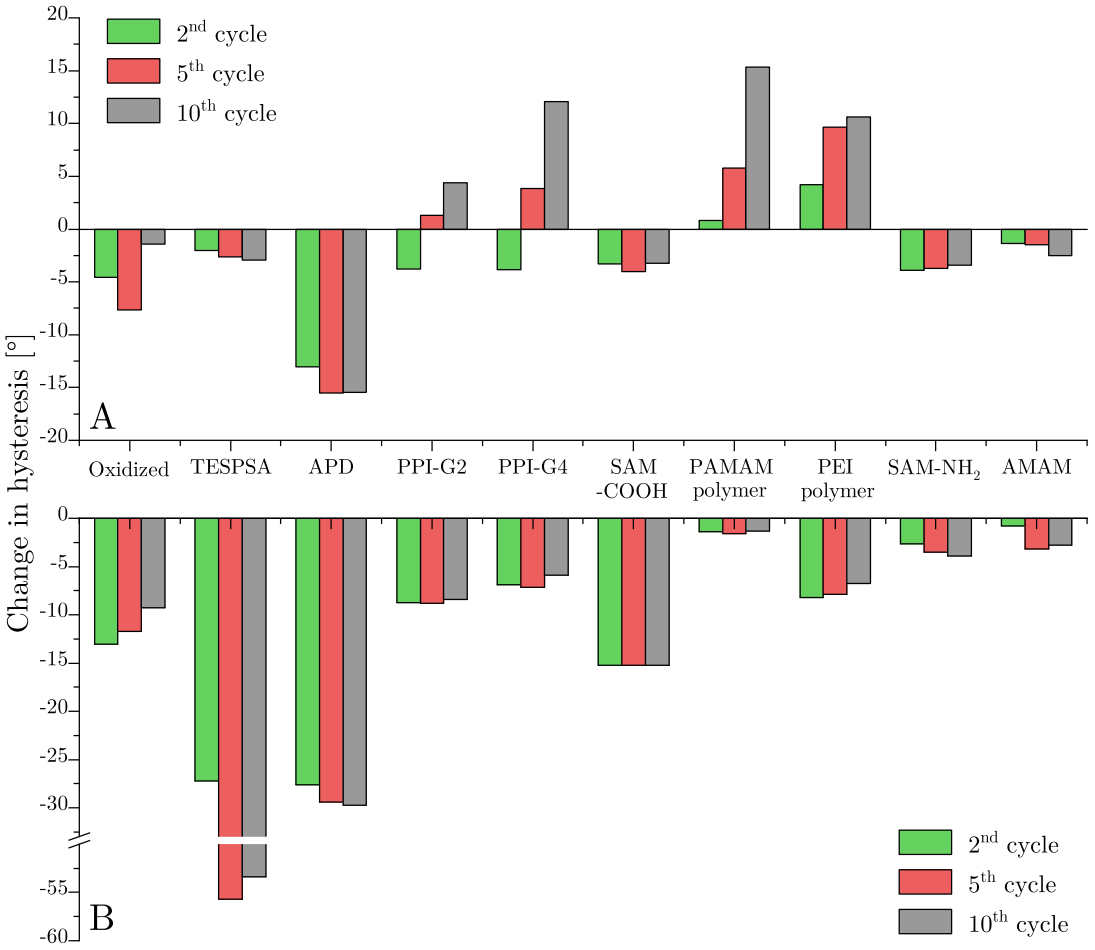

Figure 14.12: Loop-dependent change of the dynamic contact angle hysteresis for the cycles 2, 5 and 10 in comparison to the 1^{st} cycle. Both measurements with sf-water (A) as well as PBS (B) are provided.

A comparison between dynamic contact angle measurements with water and PBS reveals both similarities and differences. On the one hand, almost no difference between the advancing angles of the first immersion cycle in water or PBS is observed for each modification, which – at this point – has not yet come into contact with any measuring liquid. Thus, this contact angle can be regarded as a characteristic feature of the surface modification only. On the other hand, advancing angles and hystereses of measurements in PBS after the first cycle are in general lower than the correspondent values of measurements in water. In addition to that, advancing angles in PBS decrease

with increasing number of immersion loops for all modifications. The stark decrease in the advancing angle of the TESPSA-modified surface might be explained by the hydrolysis of the succinic anhydride under basic conditions, leading to the formation of deprotonated, i.e. negatively charged carboxylic acid groups. Thus, a contact angle similar to that of the SAM-COOH coating is obtained throughout the measurement.

For the modifications with amine groups, the obtained results are surprising at first because a higher contact angle can be expected for those coatings at the higher pH of PBS buffer due to the deprotonation of amine groups. In contrast to the SAMs studied by Holmes-Farley [367], however, the investigated amine modifications of this thesis carry a net charge at pH 5.5 and pH 7.4 (see section 14.3.3), although the zeta potential differs in sign and amplitude. Apart from a higher pH, the presence of inorganic ions, mainly sodium chloride, might serve as an explanation for the reduced advancing angles and decreasing hysteresis of measurements in PBS. In literature, no evidence has been found for the influence of ions on the tensiometric properties of uncharged polymers [368]. Monte Carlo simulations of PPI dendrimers by Welch and Muthukumar, however, revealed that the dendrimers adapt a compact and crowded conformation under high ionic strength conditions [78]. Thus, charge screening and, therefore, a collapse into a dense structure with reduced branch flexibility and swelling might serve as an explanation for the observed reduced contact angles and decreasing hysteresis.

14.3.3 Zeta Potential

In order to characterize the amine-based surface modifications further, their zeta potentials were examined via two different techniques. At first, electrophoresis measurements of functionalized silica spheres were performed. For the coatings with PPI dendrimers or PEI polymer, these were supported by additional streaming current measurements of single-side polished wafers with the respective coating because those coatings led to an aggregation of the silica particles close to the IEP and thus caused large experimental errors. The electrophoretic experiments were carried out over a pH range from pH 3 to pH 9 or 10 respectively, which allowed for the extraction of the isoelectric point and the ζ-potential at physiological pH (pH 7.4) from the complete potential curves. The results are depicted in Figures 14.13 and 14.14 and summarized in Table 14.3.
Looking at the IEPs in Table 14.3 in general, it can be noted that they are all significantly higher than the IEP of oxidized but unfunctionalized substrates. In addition to that, the final amine modifications exhibit higher IEPs than their respective precursor SAMs.

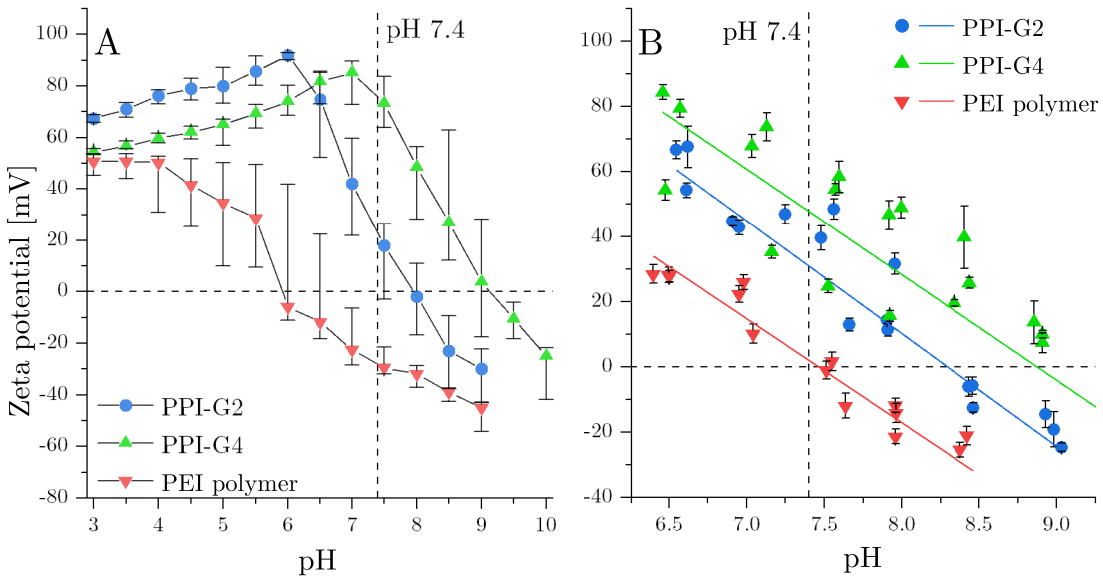

Figure 14.13: Zeta potential of surfaces modified with PPI-G2, PPI-G4 or PEI polymer obtained from (A) electrophoresis measurements or (B) streaming current experiments (mean average ± standard deviation). All zeta potential measurements were performed in 1 mmol L^{-1} KCl solution.

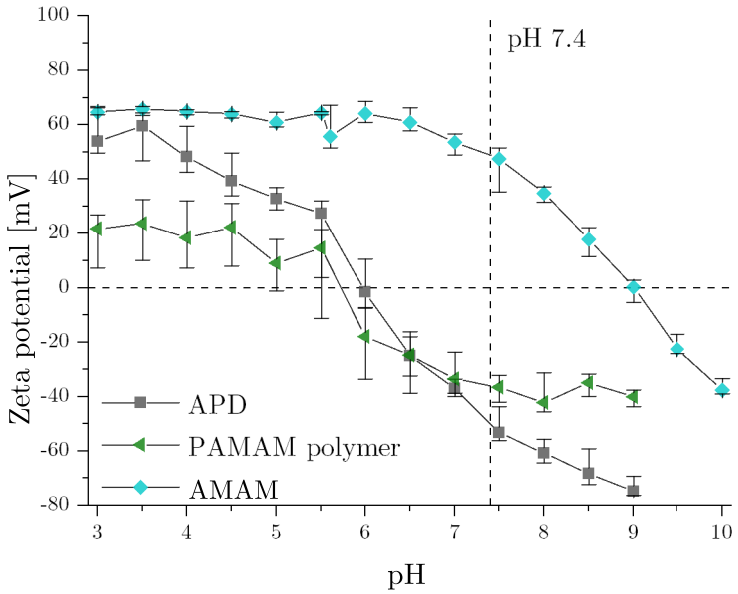

Figure 14.14: Zeta potential of surfaces modified with APD, PAMAM polymer or AMAM obtained from electrophoresis measurements. All zeta potential measurements were performed in 1 mmol L^{-1} KCl solution.

Analyzing the different surface coatings in detail, the results for the APD modification will be discussed at first. This coating possesses an IEP of 6.0 and thus carries a negative surface charge (−50 mV) under physiological conditions. This result is surprising at first glance as the IEP is lower than it has been reported for the SAM-NH_2 monolayer with a terminal primary amine group (IEP 7.1) [13].

Table 14.3: Isoelectric point and zeta potential at pH 7.4 of amine-based surface functionalizations as well as of their precursor SAMs, as determined from electrophoretic and streaming current measurements.

Surface Coating	Zeta potential			
	Electrophoresis		Streaming current	
	IEP	At pH 7.4 [mV]	IEP	At pH 7.4 [mV]
Oxidized[a,b,c]	3.0	−70	2.8	−105
TESPSA[b]			-	−40
APD	6.0	−50		
PPI-G2	7.9	+25	8.3	+31
PPI-G4	9.1	+75	8.9	+48
SAM-COOH[a,b,c]			-	−25
PAMAM polymer	5.7	−35		
PEI polymer	5.9	−30	7.5	+2
SAM-NH_2[a,b]			7.1	−3
AMAM	9.0	+50		

[a] Data has previously been published in Eichler et al. [19].
[b] Data has been taken from the PhD thesis of Verena Katzur [13].
[c] Data has previously been published in Katzur et al. [18].

Also Sugimura et al. obtained a higher IEP between 7.5 and 8.0 for a silane monolayer in which each silane molecule contained one inner secondary and one terminal primary amine group [365]. An IEP above pH 7 should be expected because the APD modification also carries two secondary and one primary amine group per APD molecule. These amine groups are expected to be protonated and positively charged at lower pH values and deprotonated, i.e. uncharged at higher pH values. The IEP in the slightly acidic range as well as the negative zeta potentials at higher pH values are thus probably the consequence of a variety of further influencing factors.
First of all, the influence of the silicon or silica substrate must not be neglected. The surface silanol groups can dissociate in water, generating negative charges [291]:

$$Si - OH \rightleftharpoons SiO^- + H^+ \tag{14.1}$$

Therefore, an IEP between 1.0 and 3.0 is obtained for an oxidized and unmodified silica surface [20, 272, 369]. Some of the silanol groups probably remain unfunctionalized during the silanization reaction and thus contribute negative charges. In addition to that, the immobilization of APD is achieved via a ring-opening reaction of the succinic acid

anhydride of the TESPSA monolayer and the formation of an amide bond. During this reaction, one carboxylic acid group is generated for each surface-bound APD molecule. These COOH groups also contribute charges in almost the complete pH range between pH 3 and pH 9 because the deprotonation of these groups starts below pH 5 [272].
At last, the differing protonation behavior of surface-immobilized amines must be discussed. In contrast to amines in solution, which roughly possess a pK_a value of 10, surface-immobilized amines exhibit a fundamentally different behavior. Here, no steep decrease in the portion of charged amine groups is observed, instead the degree of protonation changes gradually. In addition to that, deprotonation already starts below pH 0 and at pH 1 only half of the amine groups are still protonated [272]. The reasons for that are probably electrostatic repulsion of likewise charges as well as bridging, which prevent the protonation of neighboring amine groups next to charged groups [272].
A phenomenon, which might not be the most relevant for the interpretation of the potential curves of APD but needs to be mentioned and will be relevant for later surface modifications, is the preferential adsorption of anions, especially hydroxide ions, on surfaces because these are generally less well hydrated than cations [272].

In comparison with the APD modification, the surface coatings with PPI-G2 or PPI-G4 exhibit significantly higher IEPs of 7.9 or 9.1 respectively in electrophoretic measurements. These results are in good accordance with the IEPs obtained for PPI dendrimers of generation 2 or 5 immobilized on negatively charged cotton fibers, where IEPs of roughly 7.5 and 8.2 were obtained respectively [370]. As a consequence, they posssess a strongly positive zeta potential at pH 7.4. These values even exceed the IEP of a surface with amine-terminated PAMAM dendrimers and are the consequence of the higher amine group density, which has been shown in the sulfo-SDTB assay (see chapter 14.2.2).
The highly positive zeta potential in the acidic range and the steep decrease starting at approximately pH 6 to 7 can be explained by the unique onion-like protonation behavior of PPI dendrimers, which has been explained previously (see section 3.1.4) [72]. 2/3 of the amine groups remain protonated up to pH 10 (in solution) and are thus responsible for the high zeta potential at lower pH values. The deprotonation of those amine groups then causes the sudden change of the ζ-potential to negative values. Here, the onset of this deprotonation is shifted from pH 10 to pH 6-7, which might again be explained by unfavorable electrostatic interactions between the crowded amine groups, as they were observed for an amine SAM by Shyue et al. [72, 272].
A unique property, which was not found for any other surface modification apart from the PPI dendrimer coatings, is the increase in the zeta potential with increasing pH

in the range between pH 3 to pH 6. First of all, one might assume that a change in the dendrimer conformation might lead to an increased number of exposed protonated amine groups. Theoretical calculations of the radial density distribution profiles of PPI dendrimers, however, refuted that assumption. Jain et al. showed that the radial densities remain unchanged between pH 4 and pH 7.4, a difference only occurs upon increase of the pH to pH 10 [76]. Thus, no satisfactory explanation can be found.

The PAMAM and PEI polymer, which were immobilized on SAM-COOH, exhibit IEPs of 5.7 and 5.9 respectively, which go hand in hand with negative zeta potentials under physiological conditions. Despite this being a drastic increase in the IEP, compared to the intermediate SAM-COOH, the IEPs are still slightly in the acidic range, as observed for APD. Here, the grafting-to approach, which was used for the attachment of the polymers, might serve as an explanation. This immobilization procedure probably leads to a low-density surface coverage with polymers in the mushroom regime [116, 364]. As the coupling of further polymer chains becomes increasingly impeded with surface coverage due to kinetic hindrance, it can be assumed that only a small fraction of the surface carboxylic acid groups was converted to amide groups [116]. Thus, the remaining carboxylic acid groups (as well as probably some silanol groups) contribute negative charges to the overall zeta potential of the surface, as alreadey explained for the APD-modified surface.

In contrast to the polymers, the oligomeric AMAM modification exhibits a very high IEP of 9.0 and a strongly positive zeta potential (+ 50 mV) at pH 7.4. This can be regarded as the additive result of the underlying amine monolayer (with an IEP of 7.1) as well as of the AMAM modification with a terminal piperazine molecule, which possesses a pK_a value of 9.71 in solution [18, 371].

The results of the electrophoretic measurements of PPI-G2 or PPI-G4 surfaces have mainly been confirmed by the data obtained from streaming current measurements. Larger differences are observed for the PEI polymer, which might be explained by variations in the batch-dependent grafting density of the linear polymer.

14.4 Investigation of Protein Adsorption

In addition to the investigation of the physicochemical properties of the amine-based surface modifications, a quantitative analysis of the protein adsorption was performed with the BCA assay. These results have recently been published [273]. Both single protein solutions (HSA and lysozyme) of various concentrations as well as the physiological fluids human saliva and FBS were studied. The latter were characterized prior to the adsorption experiments (see section 13.3).

14.4.1 Overview

The results for the concentration-dependent adsorption of HSA and lysozyme on the surfaces with different amine modifications are depicted in the appendix in Figure VI.8. Here, vast differences in the total amount can be observed between the different surface functionalizations and often also between the adsorption of the two different proteins on the same surface coating. With the exception of the PEI coating, an increase in the amount of adsorbed protein with protein concentration can be identified, in many cases resembling a saturation curve. For the PEI modification, generally low protein adsorption with comparably large experimental errors is observed. Seemingly, however, overshooting occurs, leading to a maximum in adsorption at a protein concentration in solution of $10\,\mathrm{mg\,mL^{-1}}$.

In order to provide a clear overview, the results for the adsorption from single protein solutions with a protein content of $10\,\mathrm{mg\,mL^{-1}}$ as well as the data for the adsorption from saliva and FBS are summarized in Figure 14.15. Here, also the results of protein adsorption on oxidized but unmodified SiO_2 substrates as well as on the SAM-COOH and SAM-NH_2 coating are included for reference. Please note that no measurements were performed for TESPSA-modified substrates. Results equivalent to high protein adsorption were expected in that case as covalent linkage of proteins via reaction between the succinic acid anhydride and amine groups of the proteins would have occurred.

As seen in Figure 14.15, differences in the amounts of adsorbed proteins are not only observed for HSA and lysozyme but also for saliva and FBS. Nevertheless, some general trends can be observed. In most cases (with exception of the APD modification and SAM-COOH), more HSA than lysozyme is found to adsorb to the substrates. This general trend can probably be attributed to the susceptibility of HSA as a "soft" protein to denaturate upon adsorption as well as to electrostatic interactions [26, 155].

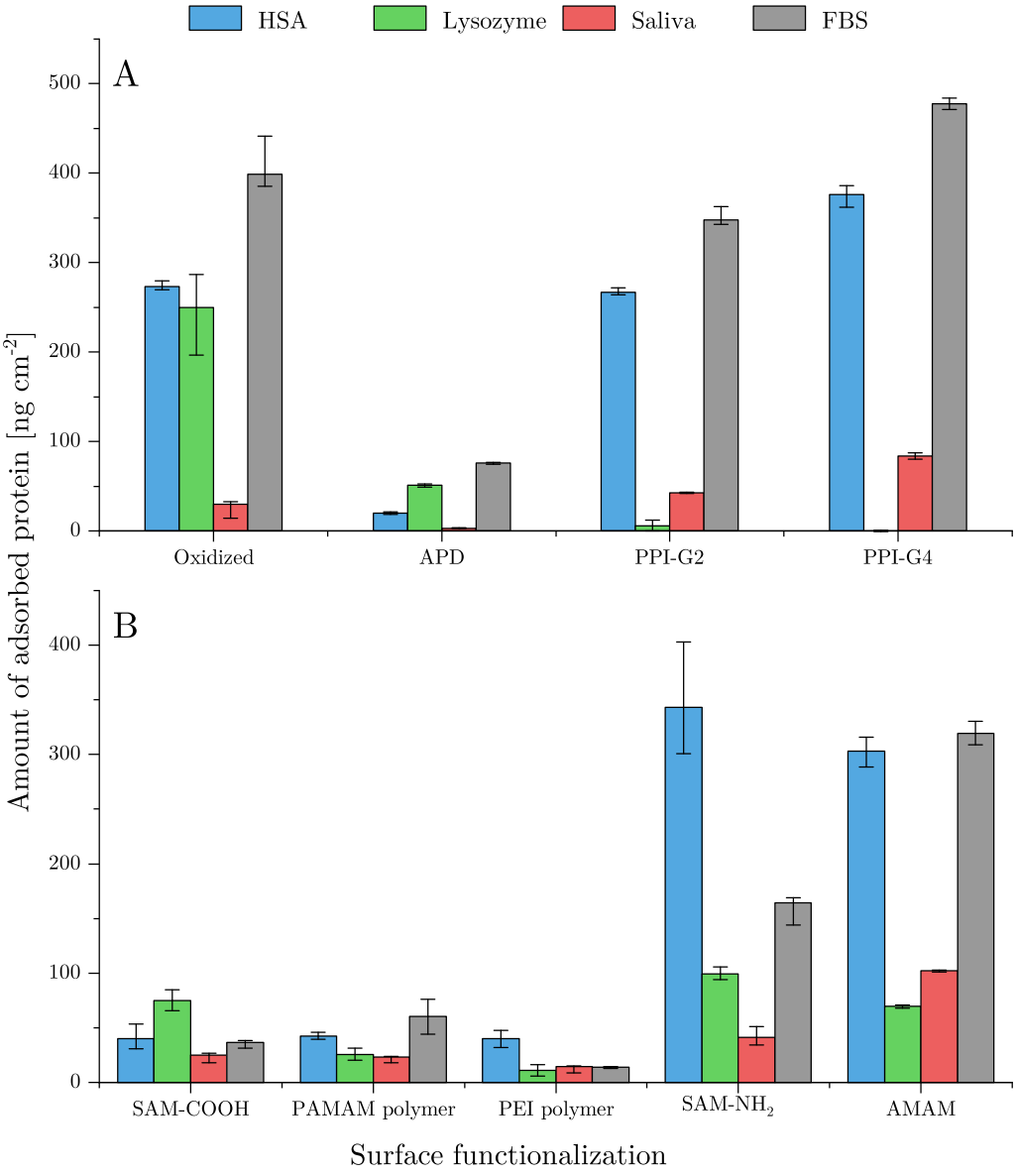

Figure 14.15: Amount of adsorbed protein from HSA or lysozyme solutions (concentration 10 mg mL^{-1} in PBS buffer), undiluted human saliva or FBS on silica beads with amine-based modifications or the respective intermediate SAMs. Results are displayed for (A) oxidized beads and substrates modified with APD, PPI-G2 or PPI-G4, or (B) surfaces with PAMAM polymer, PEI polymer, AMAM as well as the intermediate monolayers SAM-COOH and SAM-NH$_2$. For each protein solution, the results of the different surface modifications have been compared via Mann-Whitney-U test. For improved clarity, the results are not shown in the figure as p-values ≥ 0.05 have only been obtained for few pairs, which are listed in the following. HSA: oxidized – PPI-G2, oxidized – SAM-NH$_2$, APD – SAM-COOH, PPI-G4 – SAM-NH$_2$, SAM-COOH – PAMAM polymer, SAM-COOH – PEI polymer, PAMAM polymer – PEI polymer, SAM-NH$_2$ – AMAM. Lysozyme: PPI-G2 – PPI-G4, PPI-G2 – PEI polymer, PPI-G4 – PEI polymer, SAM-COOH – AMAM. Saliva: oxidized – SAM-COOH, oxidized – PAMAM polymer, PPI-G2 – SAM-NH$_2$, SAM-COOH – PAMAM polymer. FBS: APD – PAMAM polymer, PPI-G2 – SAM-NH$_2$.

Comparing the amount of adsorbed protein from HSA solutions and FBS for the same surface modification, they usually have the same order of magnitude, but more protein adsorbs from FBS. This result can be expected because albumin represents the most abundant protein of serum, whose total protein content, however, exceeds the protein content of the HSA solution selected for the figure [165]. Likewise, the lower protein adsorption from saliva (compared to FBS) can be explained with the 40-fold protein content of FBS [159, 165].

Switching the focus from the differences among the proteins to the differences among the surface modifications, roughly two different groups of surface coatings can be differentiated. In the first group, enhanced protein adsorption for at least two of the four tested solutions, compared to the SiO_2 reference, can be observed for coatings with PPI dendrimer, the SAM-NH_2 surface and the AMAM modification. In contrast to that, protein adsorption is strongly reduced on APD, SAM-COOH, PAMAM polymer and PEI polymer surfaces. Here, the best overall performance is observed for the PEI polymer modification as the amount of adsorbed protein from FBS is only 3.5% of the amounts of protein on the SiO_2 reference.

14.4.2 Dependence of Protein Adsorption on Surface Properties

In the final part of this chapter, an attempt will be made to correlate the results from the protein adsorption experiments with the data obtained from physicochemical analysis of the amine-based modifications. Parts of that detailed discussion have previously been described in the preceding master's thesis (for the adsorption of HSA only) [22] and have been published recently [273]. In addition to that, similar analysis has been performed for the adsorption of salivary and serum proteins on SAMs with varying end groups (see section 13.3).
As only the total amount of adsorbed protein was studied here, only data for amounts of adsorbed protein will be used for comparison, although surface properties also influence a variety of other characteristics of the formed protein layer, such as layer density, protein folding and hydration [372]. In addition to that, it has to be kept in mind that the results in literature for the amounts of adsorbed proteins have been determined on a variety of substrates, using different proteins and analytical techniques. The obtained data will thus only be employed in qualitative comparisons as it is not advisable to compare the exact numbers quantitatively.

Structure, Grafting Density and Flexibility of the Surface Modifications

First of all, it will be investigated if and how the structural properties of the immobilized modifications influence protein adsorption. The amine-based modifications studied in this thesis can be divided into three structural categories: short-chained oligomers (APD, AMAM), dendrimers (PPI-G2, PPI-G4) and linear polymers (PAMAM polymer, PEI polymer). Regarding the first two groups, no overall trend is observable. It can be stated, however, that both unbranched polymers exhibit very good protein-repelling properties. Their satisfactory performance in all protein adsorption experiments may be the consequence of their low grafting density, which leads to a surface layer of flexible polymers in the mushroom regime [116, 364]. The flexibility of the polymer chains is not only a consequence of the "grafting to" approach chosen for immobilization, but it can also be estimated from the results of the dynamic contact angle measurements (see section 14.3.2).

In literature, controversial results are obtained for the influence of polymer flexibility on protein deposition. Almost no or no influence of chain flexibility on the adsorption of HSA was observed by Berglin et al. and Vyner et al., whereas the latter noticed a strong dependence of fibronectin or IgG adsorption on the chain mobility [192, 373]. Theoretical calculations by Carignano and Szleifer led to the result that the best protein-repellent properties were observed for flexible polymers, whereas Singh et al. found no peptide adsorption in the brush regime in contrast to the more flexible mushroom regime [191, 374].
In summary, the effect of the flexibility of the surface modification on protein adsorption is not clear and may be exceeded by the influence of other surface properties.

Influence of Amine Group Density and Type

In this thesis, the density of amine groups has been estimated with the sulfo-SDTB assay. The results for the amine-based modifications are summarized in section 14.2.2. This assay does not allow the detection of tertiary amine groups and no statement can be made whether primary and secondary amine groups possess equal reactivity in this assay. Nevertheless, plotting the amount of adsorbed protein against the obtained amine group density (comprising primary and secondary amine groups) (see Figure 14.16), an almost linear relation is obtained for HSA and FBS. The amount of adsorbed salivary proteins increases with increasing amine group density as well. With exception of the AMAM coating, an opposite behavior can be assumed for lysozyme, i.e. reduced protein adsorption with higher amine group densities.

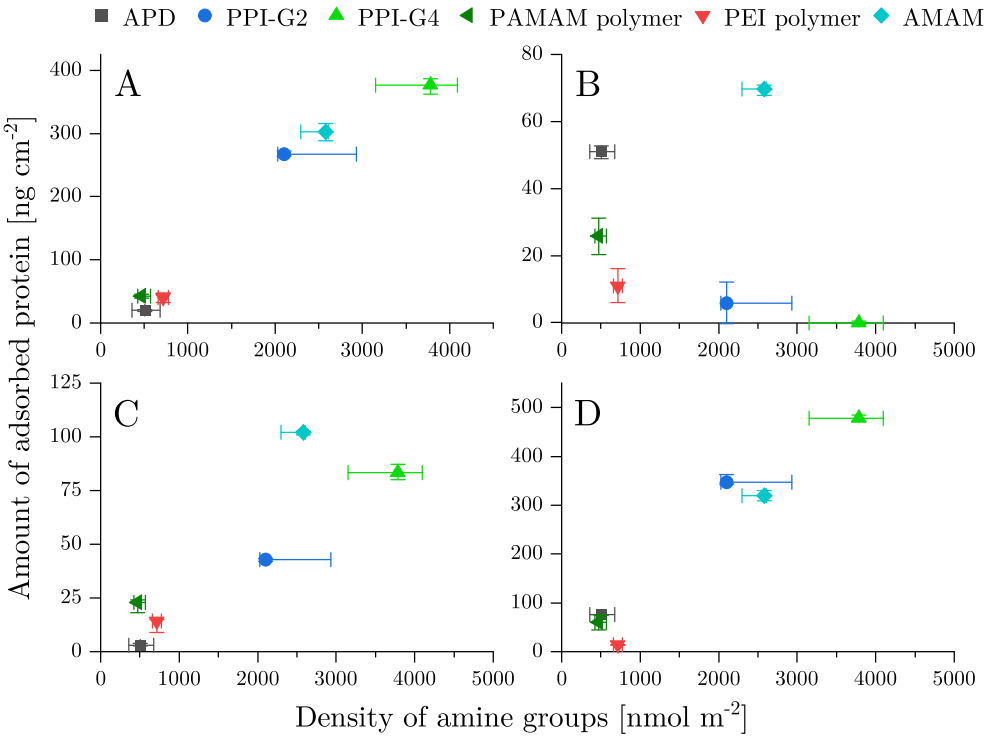

Figure 14.16: Dependence of the protein adsorption from solutions of (A) HSA or (B) lysozyme (concentration 10 mg mL^{-1}) as well as (C) saliva and (D) FBS on the amine group density of the amine-based surface coatings, as determined via the sulfo-SDTB assay.

The influence of certain functional groups on protein adsorption has only been studied sparsely. One exception was published by Gessner et al., who examined the influence of different amino groups (primary to quaternary) on the adsorption of human serum proteins [179]. They noticed that preferentially proteins with an IEP < 5.5 adsorbed on surfaces with basic amine groups [179]. As HSA and many salivary proteins are part of this group, the strong adsorption from HSA solutions, FBS and saliva matches these observations.

Effect of Surface Wettability and SFE

Regarding the influence of surface wettability or SFE on protein adsorption, no correlation is observed at all. Thus, only the results for the protein adsorption in dependence on the cosine of the water contact angle are depicted here (see Figure 14.17). Further figures, including the total SFE, its polar and dispersive component, are provided in the appendix (see Figures VI.10 to VI.12).

In literature, however, a clear relation between surface wettability and protein adsorption can be observed in many cases. Fundamental research on this topic was performed by Xu and Siedlecki as well as Sethuraman et al. [193, 303]. In both cases, they studied the adhesion forces of different model proteins on a variety of surfaces with differing

hydrophilicities via AFM and discovered a stepwise dependence of the adhesion force on the surface wettability [193, 303]. In general, strong adhesion was observed for hydrophobic surfaces (contact angle $\Theta > 60$–$65°$), whereas adhesion was weak for hydrophilic surfaces ($\Theta < 60°$) [193, 303].

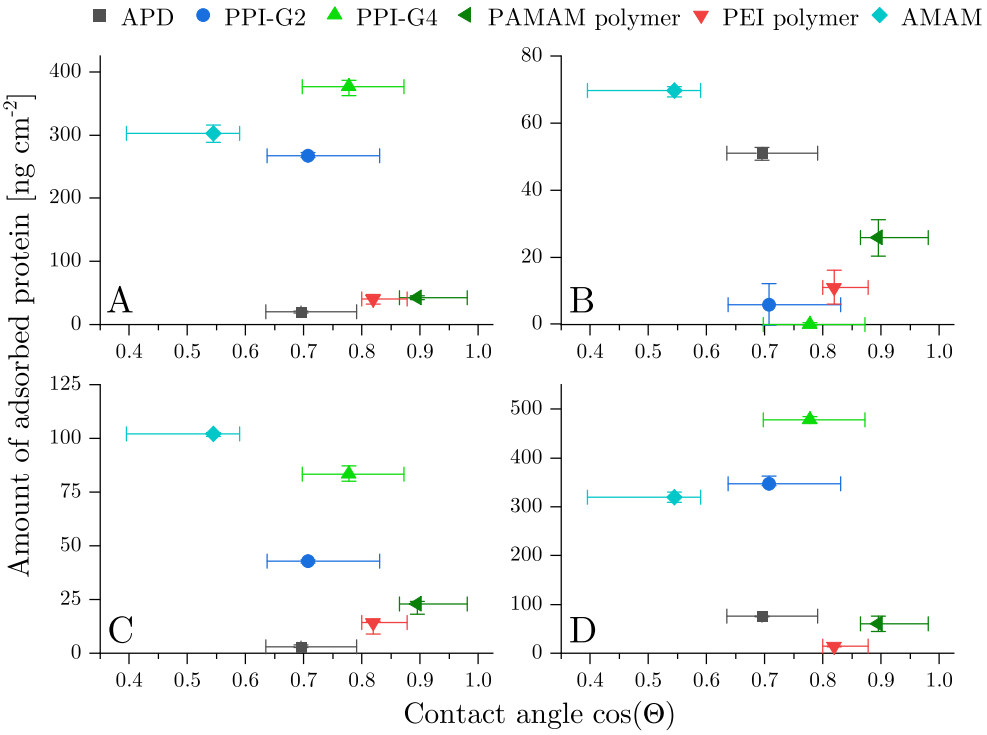

Figure 14.17: Dependence of the protein adsorption from solutions of (A) HSA or (B) lysozyme (concentration 10 mg mL^{-1}) as well as (C) saliva and (D) FBS on the hydrophilicity of the amine-based coatings, as determined via the static contact angle Θ.

As a consequence of these results, lower protein adsorption on hydrophilic surfaces was measured for many model proteins in comparison to adsorption on hydrophobic surfaces. Sigal et al. measured a decrease in the adsorbed protein mass with increasing hydrophilicity of the self-assembled monolayer for several single proteins, but they had quantified surface wettability via measurement of the water contact angle under cyclooctane [304]. They also observed size dependency, i.e. small proteins, such as lysozyme, only adsorbed on the least hydrophilic surfaces and exhibited a stark step-wise pattern, whereas larger proteins were found to also adsorb on more wettable surfaces but to a lower extent [304]. Reduced protein adsorption of the model proteins used in this thesis (HSA and lysozyme) on hydrophilic substrates was confirmed by many studies [4, 320]. Some studies, however, could not find a relation between the contact angle and the adsorption of single proteins [305] or detected an opposite behavior, i.e. higher protein amounts on hydrophilic surfaces [321]. Wertz and Santore explained the latter observation with the higher spreading rate of proteins on more hydrophobic surfaces, leading to a lower maximum coverage of the surface [321].

Mixed results were also obtained for protein adsorption experiments with complex physiological fluids. Here, Lindh et al. as well as Vassilakos et al. observed increased protein adsorption from saliva on hydrophobic surfaces, whereas no correlation between surface wettability and protein adsorption from FBS could be determined by Staehlke et al. [20, 306, 307].

A similar situation presents itself with respect to the relation between protein adsorption and the SFE. In contrast to the results of this thesis, a correlation between those two quantities was discovered at least in some studies, although significantly less data is available than for surface wettability. Research was focused on single-protein solutions. Furthermore, even for the same model protein, in many cases albumin, contradictory results were obtained. As an example, Michiardi et al. found a linear increase of HSA adsorption with the increasing polar component of the substrate's SFE [309]. Similarly, de Bartolo et al. were able to show that an increase in the Lewis base parameter γ^- was related to an increased adsorption of human albumin, fibrinogen or IgG [310]. The opposite behavior was observed by Miyata et al. for globulin and fibrinogen, i.e. decreasing protein adsorption with an increase of the SFE and its polar component [153]. No relation, however, was found for the adsorption of HSA in this study [153].

In this thesis, however, none of these correlations of the surface wettability and SFE (or components thereof) with the amount of adsorbed protein can be observed. This may partially be caused by the fact that the amine-based surface modifications exhibit similar hydrophilicities and their SFEs are in a similar range. In addition to that, the effects of surface hydrophilicity and free energy can possibly be dominated by other surface properties, such as the zeta potential (see below).

Influence of the Zeta Potential on Protein Adsorption

In contrast to the previous section, a strong correlation between the zeta potential of the amine modifications and the adsorption of HSA, salivary proteins and serum proteins is visible. With exception of the AMAM coating, a decrease in the amount of adsorbed lysozyme with increasing zeta potential can be observed. Please note that the potentials used in Figure 14.18 reflect the zeta potentials of the surface coatings at the respective pH of the different protein solutions.

In general, the results presented here strongly resemble the dependence of protein adsorption on amine group density (see Figure 14.16). This observation can easily be explained by the characteristics of the different proteins. At the respective pH values, albumin as well as the majority of salivary proteins carry a negative net charge, whereas

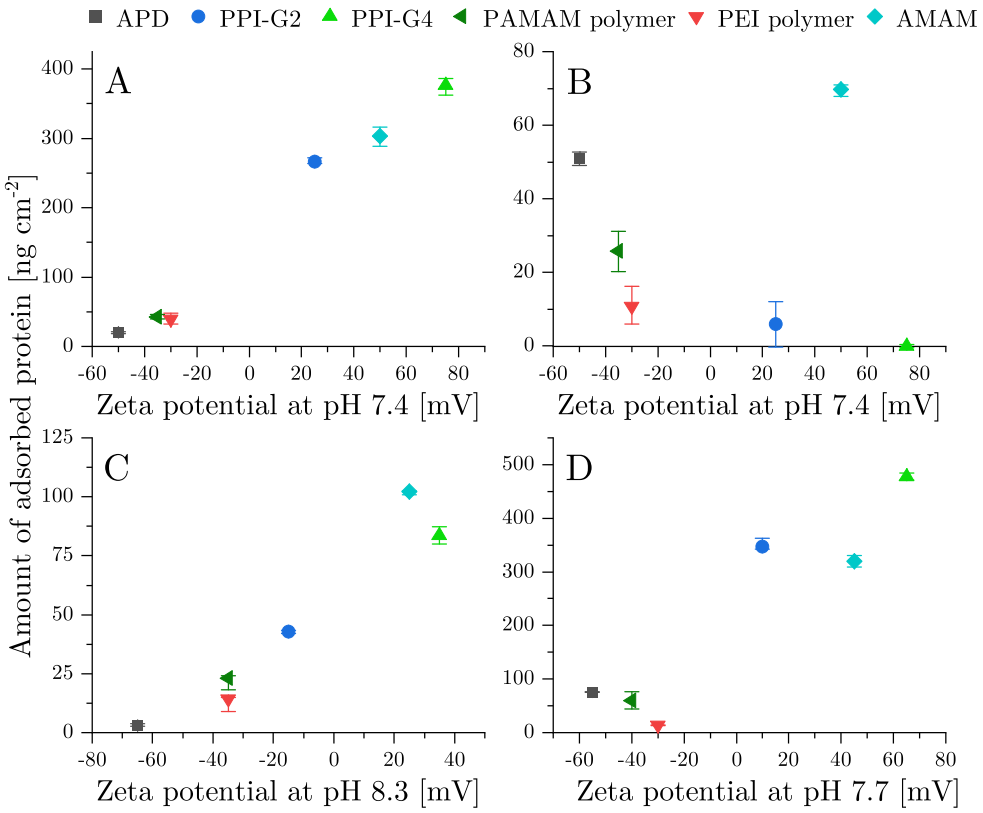

Figure 14.18: Dependence of the protein adsorption from solutions of (A) HSA or (B) lysozyme (concentration 10 mg mL^{-1}) as well as (C) saliva and (D) FBS on the zeta potential of the surface coatings at the pH of the respective protein solution.

lysozyme is positively charged at pH 7.4 [26, 155, 162]. An increase of albumin adsorption with increasing zeta potential was similarly observed by Patil et al. on cerium oxide nanoparticles as well as by Staehlke et al. on substrates functionalized with PAMAM dendrimers with differing end groups [20, 312]. The opposite trend for lysozyme, i.e. lower protein adsorption at higher zeta potentials similar to the results of this thesis, was described by Rezwan et al. or Guo et al. [28, 219]. Less literature supporting the observations of this thesis, however, is available for the physiological fluids. No studies have been published for saliva, whereas contradictory results were obtained for FBS. Staehlke et al. did not find a dependence of the adsorption of serum proteins on the zeta potential of the PAMAM modification [20]. In contrast, El-Ghannam et al. measured slightly lower amounts of serum proteins on more negatively charged surfaces [314].

Summarizing the Results

In a nutshell, protein adsorption on amine-functionalized surfaces seems to be correlated with the zeta potential due to the dominating effect of electrostatic interactions. Comparing the surface coatings to the requirements for protein-repellent surfaces, described in section 4.3.1, it can be stated that the Whitesides rules are partially obeyed [195]. All coatings exhibit polar groups with hydrogen bond-accepting moieties, but they also possess H-bond donors as well as net charges. The dendrimer and polymer-based functionalizations can be assumed to be flexible and swellable as well, which probably contributes to protein-repellency [190].
The best resistance towards protein adsorption is exhibited by the polymer coatings (PAMAM polymer and PEI polymer). These modifications do not perform as well as established protein-repellent coatings, such as PEG [178, 199], but they show strongly reduced protein adsorption. The amount of adsorbed HSA (approximately $40\,\mathrm{ng\,cm^{-2}}$), for example, is significantly lower than the amount found for a HSA monolayer (250–$600\,\mathrm{ng\,cm^{-2}}$, depending on protein orientation) [304].
Due to their physicochemical properties and/or their performance in protein adsorption experiments, some of the surface modifications were selected for cell experiments (see chapter 16).

15 Osmolyte-Based Functionalizations

This third chapter will describe and discuss the data obtained for the osmolyte-based surface modifications, which are summarized in Figure 15.1.

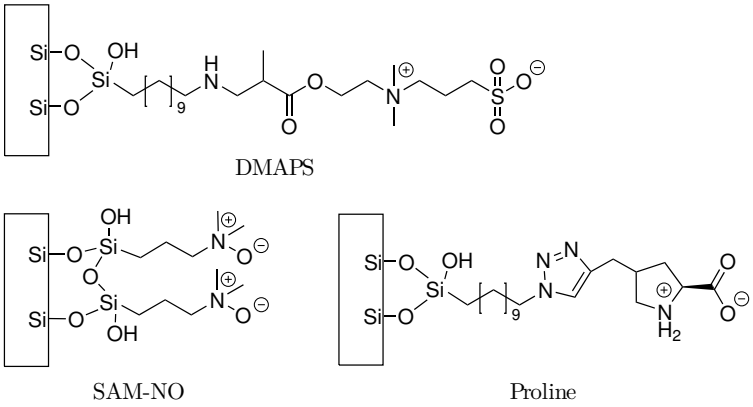

Figure 15.1: Overview of the osmolyte-based surface functionalizations as well as their abbreviated names.

As the synthesis of a proline monolayer was only performed on silica beads, only results for the sulfo-SDTB assay and for some protein adsorption experiments (with saliva and FBS) were obtained. No reaction was performed on silicon wafers or silica spheres. Therefore, no data is available for XPS, IR spectroscopy, contact angle or zeta potential measurements. Instead, the following section will deal in detail with the development of a synthesis route for the proline functionalization. After that, the results of the characterization of sulfobetaine or amine oxide-modified surfaces will be summarized analogously to chapter 14.

15.1 Proline Immobilization – Considerations and Challenges

The following section is dedicated to a more detailed description of the synthesis of a surface modification carrying proline groups. Here, the planning of the reaction procedure, the obstacles observed throughout synthesis as well as recommendations for further investigation will be given.
First of all, it has to be stated that the aim was the synthesis of a proline surface modification in which both the amino as well as the carboxylic acid group remained unsubstituted in order to maintain the zwitterionic osmolyte character of proline. Thus, immobilization had to be achieved by coupling with a functional group attached to the carbon atom 3 or 4.
In literature, a variety of reactions has been described for the modification of SAMs [40, 43]. Firstly, coupling can be achieved via formation of an amide or ester group. To that purpose, an acylchloride, acid anhydride or (activated) carboxylic acid is required in combination with an amine or hydroxyl group respectively [40, 43]. A urethane or urea can be formed via an addition reaction between a hydroxyl or amine group and an isocyanate group [40, 43]. The reaction of a primary amine with an aldehyde group leads to the formation of a Schiff base [40, 43]. β-hydroxy secondary amines or ethers can be generated via the reaction of an epoxide with a primary amine or hydroxy group [43]. Inspired by nature, proteins can be immobilized via formation of a disulfide bond between two thiol groups [43].

Most of those reactions, however, suffer from one major disadvantage. Amine groups, such as the amine group of proline, are very nucleophilic and thus rather reactive [375]. In order to avoid the unwanted coupling of proline via its amine group, the introduction of an appropriate protecting group is necessary.
To that purpose, a broad variety of protecting groups is available [376], but in order to be considered for this thesis, two requirements had to be fulfilled. First of all, the removal of the protecting group after immobilization of proline was supposed to be accomplishable with the laboratory equipment available. Secondly, the deprotection must not need reaction conditions which destroy the underlying self-assembled monolayer, e.g. basic conditions [41, 46]. The best choice seemed to be the Boc protecting group, which can be cleaved under acidic conditions, such as trifluoroacetic acid in DCM, or HCl in organic solvents [376]. This group and its deprotection procedure, however, was expected to be incompatible with an amide, ester or urethane group as all these groups can undergo hydrolysis under acidic conditions [377, 378].

In addition to the reactivity of the amine group of proline, two further obstacles were observed. Firstly, certain functional groups, such as the hydroxy group, are easily available and broadly applied in thiol SAMs but significantly less accessible for silane SAMs [33, 38]. Furthermore, proline derivates are commercially available only with a small number of additional functional groups on the desired carbon atoms.

The attempt to immobilize proline via one of the reactions mentioned above was, hence, discarded. Instead, the surface functionalization was carried out with a "click chemistry" approach via a Huisgen 1,3-dipolar cycloaddition between an azide and an alkyne function. This approach was advantageous with respect to a variety of aspects. First of all, an azide-terminated SAM can be easily obtained from a bromine-substituted monolayer (see section 9.3.5). Secondly, the alkyne-substituted proline is commercially available. At last, such click reactions have been applied successfully in a broad range of surface reactions in the last years [34, 51].
The initial results obtained from sulfo-SDTB measurements (see section 15.2.2), however, did not yield the expected results as the measured amino group density was rather low. This way, though, no information was obtained about the question which reaction step had failed. Possible problems might have been (a) an incomplete formation of the SAM-N_3 monolayer, (b) a non-quantitative click reaction, (c) an incomplete deprotection reaction or (d) the (partial) destruction of the SAM in one of the aforementioned steps.

Thus, a more detailed analysis of each reaction step is necessary, which in turn requires the synthesis of the modification on different substrate geometries and the application of various analysis techniques.
At first, the presence of bromine in the SAM-Br as well as its disappearance in the subsequent substitution step to SAM-N_3 can easily be monitored via XPS on functionalized wafers (see section 13.1.1). In addition to that, the successful substitution reaction can also be confirmed by the appearance of the characteristic absorption band of azides in IR spectroscopy at approximately $2100\,\mathrm{cm}^{-1}$ [285]. Quantitative immobilization of N-Boc-protected proline via "click" chemistry should result in the complete disapperance of the aforementioned azide band in the IR spectrum. At last, successful deprotection of the amine groups without the loss of organic modification can be checked with the sulfo-SDTB assay, in which the secondary amine groups of the unprotected proline can be detected. The results of each reaction step can be supported by other techniques, such as contact angle and zeta potential measurements. This way, each reaction step can be monitored and the synthesis of a proline-functionalized surface can be proven.

15.2 Verification of Successful Surface Coating

15.2.1 Determination of the Chemical Composition via XPS

In order to evaluate if the surface modifications were successful, the results of XPS measurements of the final modifications (DMAPS and SAM-NO) will be analyzed and compared to the respective intermediate SAMs (SAM-NH_2 and SAM-NMe_2). The obtained data, i.e. the composition in at-% as well as the resulting elemental ratios, are summarized in Table 15.1.

Table 15.1: Elemental composition of osmolyte-based surface coatings and their precursor SAMs, as determined via XPS.

Surface coating	XPS data [at-%]					Element ratios		
	Si	C	O	N	S	N/C	N/Si	C/Si
SAM-NH_2	35	34	28	2		0.06	0.06	0.97
DMAPS	16	51	28	3	3	0.06	0.19	3.19
SAM-NMe_2	40	20	37	3		0.15	0.08	0.50
SAM-NO	42	18	38	2		0.11	0.05	0.43

Comparing the results for the sulfobetaine (DMAPS) modification with the SAM-NH_2 monolayer, a significant decrease in the measured silicon content is noticeable. This change is accompanied by a strong increase in the carbon content, which leads to a roughly threefold C/Si ratio. This is the consequence of the immobilization of the sulfobetaine molecule, almost doubling the layer thickness. Successful immobilization is further indicated by the increased nitrogen content (and N/Si ratio) and the appearance of a sulfur peak. The results for the nitrogen and sulfur content agree very well with the data obtained by Yeh et al. for their sulfobetaine monolayer [379].

With regard to the amine oxide modification, different observations can be made. In this case, very little changes are observed in general because no further reagents are immobilized on the surface. The slight decrease in carbon content indicates that the self-assembled monolayer may suffer minor loss during the oxidation reaction. Indeed, even stronger surface degradation was observed by Dobrzanska et al. [154]. In this work, however, the SAM-NO exhibits sufficient stability and the slightly increased oxygen content suggests successful oxidation.

15.2.2 Analysis of Surface Amine Groups

The Sulfo-SDTB Assay

As already mentioned in secion 14.2.2, the sulfo-SDTB assay can be used for the detection of primary (and secondary) amine groups. Thus, it was only performed with beads with DMAPS or proline modification as well as their precursor SAMs. For the SAM-NMe_2 surface and the consecutive SAM-NO modification, a qualitative analysis was carried out with chloranil (see below). The results for the SAM-NH_2, DMAPS, SAM-N_3 and proline coating are summarized in Figure 15.2.

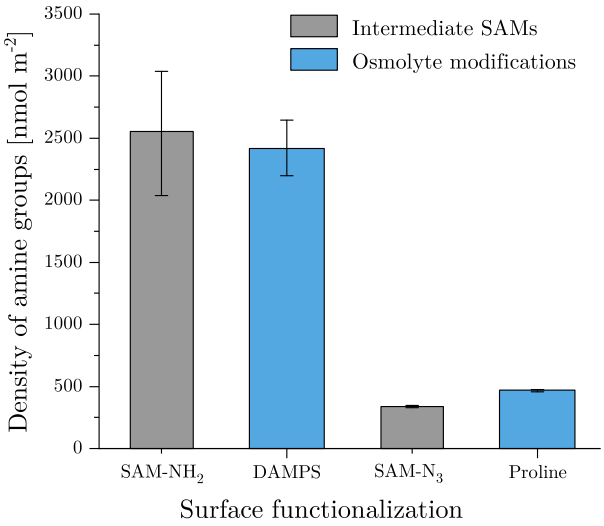

Figure 15.2: Amine group densities, obtained via sulfo-SDTB assay, for the intermediate SAMs, SAM-NH_2 and SAM-N_3, and their subsequent osmolyte-based modifications, DMAPS and proline.

Having a look at the DMAPS modification at first, one can observe a very small, not significant reduction of amine group density upon immobilization of the sulfobetaine. This, however, is logical as the primary amine groups of the SAM-NH_2 are converted into secondary amine groups, which can still be detected with the sulfo-SDTB assay, but are probably less accessible due to the sulfobetaine on the surface.

A different situation can be observed for the proline modification. In this case, the absorbance measured for the intermediate SAM-N_3 monolayer leads to an amine group density of more than 300 $\mathrm{nmol\,m^{-2}}$, which is significantly higher than the results for the unspecific interaction of the sulfo-SDTB dye with surface modifications without amine groups (see 14.2.2). This observation leads to the conclusion that possibly some of the azide groups have accidentally been reduced to primary amine groups, although this assumption has not been investigated further. After immobilization and deprotection of the proline, only a slight increase in detected amine groups can be observed.

This result, however, does not allow any statement about the success of the coupling and/or deprotection reaction. A detailed discussion of the obstacles during synthesis and analysis of a proline monolayer has already been provided in the previous section.

The Chloranil Test

The chloranil test was only used for the intermediate SAM-NMe_2 and the subsequent amine oxide monolayer in order to determine if the oxidation reaction of the tertiary amine groups was successful. Here, a color development within 30 min was observed for the intermediate amine-terminated SAM-NMe_2, although the color intensity depended on the specific surface area of the silica particles. Only a gray color was observed on the surface of silica beads, a dark blue color was obtained on smaller silica particles with higher surface area. In contrast, no color development was visible on SAM-NO modified substrates, indicating the successful conversion of the terminal tertiary amine groups.

15.2.3 Analysis of IR Spectra

IR spectra of silica particles with the osmolyte-based functionalizations DMAPS and SAM-NO, as well as the intermediate SAM-NMe_2, were recorded and are shown in Figure 15.3. The DRIFT spectrum of the precursor monolayer of DMAPS (SAM-NH_2) has already been included in section 13.1.2.
The results from XPS measurements as well as sulfo-SDTB assay and chloranil test have unambiguously proven successful modification of the substrates with the respective modification. Only little information, however, can be obtained from the corresponding infrared spectra. This is expected for the SAM-NMe_2 and the consecutive SAM-NO coating because the functional groups present here, namely a tertiary amine group or an amine oxide, do not possess strong and characteristic vibrational bands. A different situation, however, should be observed for the sulfobetaine coating, including a secondary amine, an ester, a quaternary ammonium group as well as a sulfonic acid moiety per molecule.
Successful silanization can still be proven for the SAM-NMe_2 and the SAM-NO modification as the negative band of the silanol groups is observed at 3740 cm^{-1} [285]. This negative band is absent in the IR spectrum of the sulfobetaine coating, but very weak signals at 2940 and 2850 cm^{-1}, belonging to the asymmetric and symmetric C-H stretching vibrations of the -CH_2- units, suggest the immobilization of silane molecules [285]. In all three IR spectra, two signals can be detected between 2000 cm^{-1} and 1750 cm^{-1}, which cannot be assigned to any functional group of the modifications.

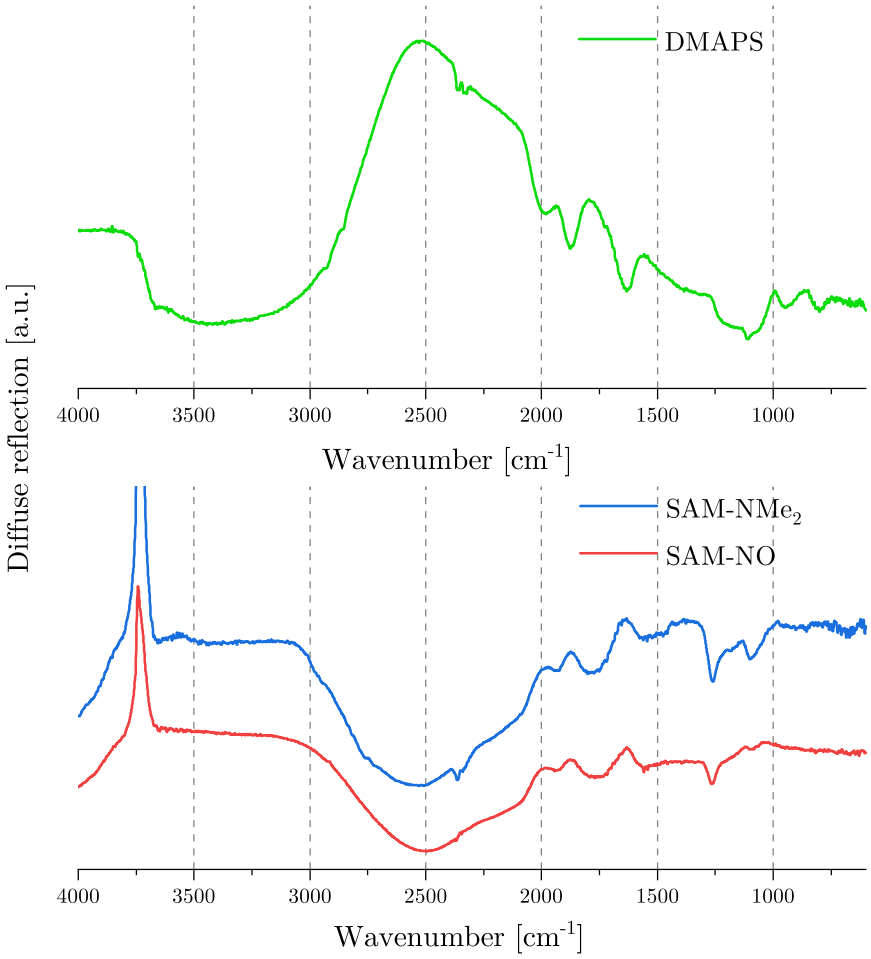

Figure 15.3: DRIFT spectra of silica particles, coated with the osmolyte-based surface functionalizations DMAPS and SAM-NO as well as the precursor monolayer SAM-NMe_2.

For the sulfobetaine coating, three other vibrational bands can be identified. The band at 1630 cm^{-1} is maybe caused by the C=O stretching vibration of the ester group, although this vibration is usually expected to appear at higher wavenumbers (1750–1725 cm^{-1}) [285]. The signal at 1110 cm^{-1}, with a pronounced shoulder at 1200 cm^{-1}, can be the result of several overlapping vibrations. The C-N stretching vibration of the amine group, the asymmetric and symmetric vibration of the sulfonic acid group, the C-O-C stretching vibration of the ester group and the Si-CH_2-R vibration of the silane backbone are all expected in that wavenumber range and may contribute to the signals [285]. With respect to the SAM-NMe_2 and the SAM-NO modification, only two or respectively one further vibrational band can be identified and assigned. The signals at 1260 cm^{-1} (both) and 1100 cm^{-1} (only SAM-NMe_2) are possibly caused by C-N stretching vibrations and vibrations of the silane part of the modification (Si-CH_2-R) [285]. It has to be noted that the characteristic N-O stretching vibration of the amine oxide group at 970 to 950 cm^{-1} cannot be detected in the IR spectrum, although the chloranil test proved successful conversion of the tertiary amine groups [285].

15.3 Investigation of Physicochemical Properties

15.3.1 Wettability and SFE

The static contact angle measurements with water revealed that both osmolyte-based modifications, i.e. the sulfobetaine-terminated DMAPS and SAM-NO, as well as the SAM-NMe_2 precursor are rather hydrophilic and possess water contact angles below 35° (see Table 15.2). The hydrophilic character of the sulfobetaine coating is in accordance with literature, where even lower water contact angles < 20° were obtained for coatings with sulfobetaine polymers or SAMs [366, 379].
In contrast to that, higher contact angles have been reported in literature for monolayers with terminal tertiary amine groups. Dobrzanska et al. observed contact angles between 34° and 38°, whereas Huang and Chang measured water contact angles of 51.4° [154, 380]. These differences can perhaps be explained by the protonation of the amine groups. Depending on the pH of the measuring liquid, the terminal amine groups can either be protonated and charged, leading to a lower contact angle, or deprotonated and uncharged, causing a higher contact angle. Such a pH dependency of the static contact angle was shown by Holmes-Farley et al. for various surface modifications containing secondary or tertiary amine groups [367].
The conversion of the terminal amine groups of SAM-NMe_2 into amine oxide groups (SAM-NO) in this thesis is associated with an increase of the contact angle by approximately 5°. Dobrzanska et al., however, observed an opposite behavior as the oxidation reaction was accompanied by a reduction of the contact angle (to 25–30°) [154]. Yet, the resulting contact angles of SAM-NO are rather similar and the final surface functionalizations display hydrophilic properties. In combination with the data from the XPS measurements as well as the chloranil test, it can be concluded that the surface functionalization with amine oxide groups could be performed successfully.

Table 15.2: Contact angles (with water, formamide and diiodomethane) for osmolyte-functionalized surfaces, as obtained from static contact angle measurements.

Surface modification	Contact angle [°]		
	Water	Formamide	Diiodomethane
SAM-NH_2	66 (64-67)	44 (44-44)	39 (36-42)
DMAPS	34 (33-37)	14 (13-15)	43 (39-46)
SAM-NMe_2	28 (26-33)	31 (30-32)	31 (29-32)
SAM-NO	33 (31-41)	27 (26-29)	31 (28-35)

From the static contact angles, measured with water, formamide and diiodomethane, the SFEs of the osmolyte-based modifications were calculated, using the surface tension components summarized in Table 13.3. The resulting SFEs, as well as their dispersive and polar components, are summarized in Figure 15.4.

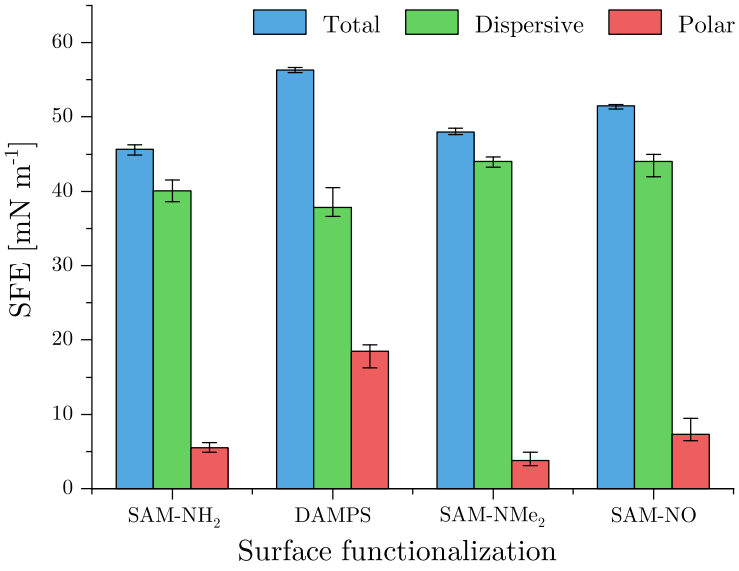

Figure 15.4: SFEs (as well as their polar and dispersive components) of modifications with osmolyte motifs and of intermediate SAMs, calculated via the LW/AB approach.

All surface modifications exhibit similar total SFEs in the range between 45.7 and 56.3 $\mathrm{mN\,m^{-1}}$. If the final modifications are compared with their respective precursor SAM, several similarities can be observed. Both for the pair SAM-NH_2/DMAPS as well as SAM-NMe_2/SAM-NO, very similar dispersive components of the SFE are determined. In both systems, an increase in the polar components accompanies the introduction of the osmolyte motif, leading to an increase in the total SFE, which can be explained by the introduction of very polar or zwitterionic groups.

In order to compare the obtained results with literature data, primarily polymeric coatings, exhibiting sulfobetaine motifs or tertiary amine groups, are available. Kobayashi et al. determined the SFE of a sulfobetaine polymer via the approach of van Oss, Chaudhury and Good, leading to a total SFE of 49 $\mathrm{mN\,m^{-1}}$ and a polar component of 18.8 $\mathrm{mN\,m^{-1}}$ [366]. Here, the polar contribution matches almost exactly the results for DMAPS (18.5 $\mathrm{mN\,m^{-1}}$). The total SFE of their polymeric modification, however, is lower due to a smaller dispersive component [366]. Their group also calculated the SFE of a polymer exhibiting tertiary amine groups, in this case via the approach of Owens and Wendt, which yields higher polar components in general [366]. Thus, these results have to be compared carefully. The calculated total SFE of 50.8 $\mathrm{mN\,m^{-1}}$ matches very

well with the results of this thesis (48.0 mN m^{-1}), whereas a drastically higher polar component was obtained from the Owens-Wendt calculation (17.4 mN m^{-1}), compared to the LW/AB approach of this thesis (3.8 mN m^{-1}) [366]. No data, however, could be found for surface modifications carrying amine oxide motifs as these coatings have rarely be synthesized at all so far.

15.3.2 Dynamic Wetting Behavior

Further insight into the osmolyte-based surface modifications (and their precursor SAMs) was obtained via dynamic contact angle measurements with water and PBS. The results are summarized in the Figures 15.5 to 15.8 as well as in Table VI.2 in the appendix. The force-immersion cycles are provided in the appendix in Figure VI.6, too.

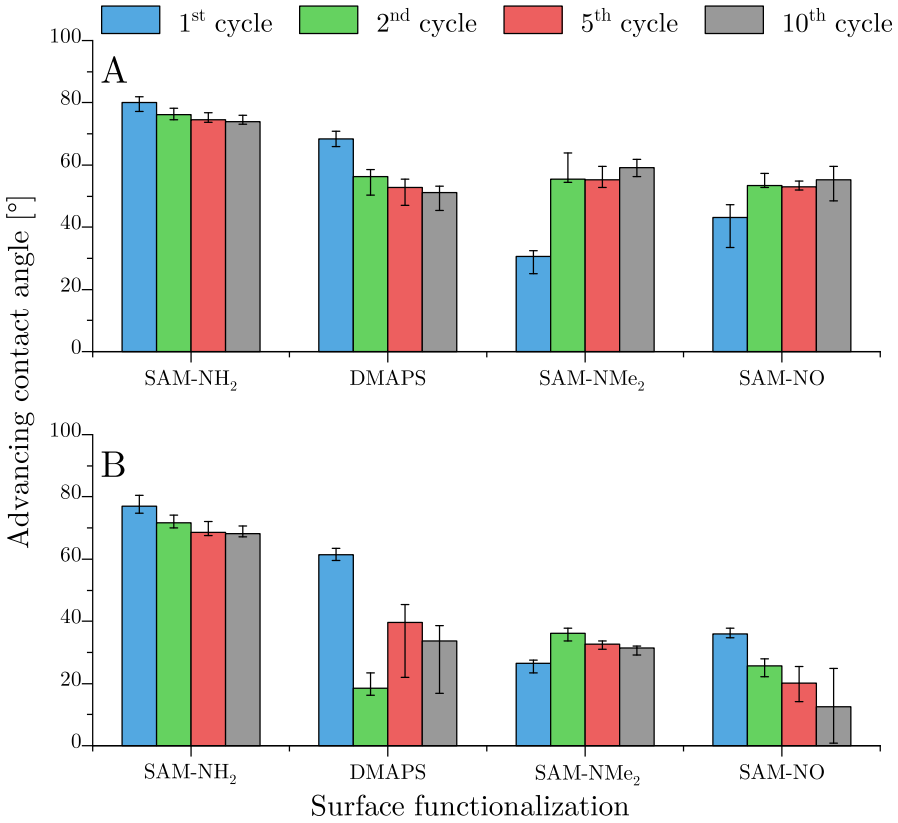

Figure 15.5: Advancing contact angles, calculated from dynamic contact angle measurements with (A) water or (B) PBS. Results for the cycles 1, 2, 5 and 10 of osmolyte-derived modifications as well as their precursor SAMs are presented.

Here, some general observations can be made at first. The advancing angles cover a wide range from 12° for SAM-NO in PBS to almost 80° for SAM-NH_2 in sf-water. Likewise, receding angles between 5° (for SAM-NO or DMAPS) and roughly 25° for SAM-NH_2 were measured. As for the measurements of amine modifications, the advancing angles of the first immersion loop of each modification are rather similar for measurements with water and PBS. This again suggests that this measured angle is a characteristic

property of the surface modification prior to any contact with liquid. Comparable to the results for amine-based coatings, lower advancing angles and lower hysteresis are observed for measurements with PBS with respect to measurements with water.

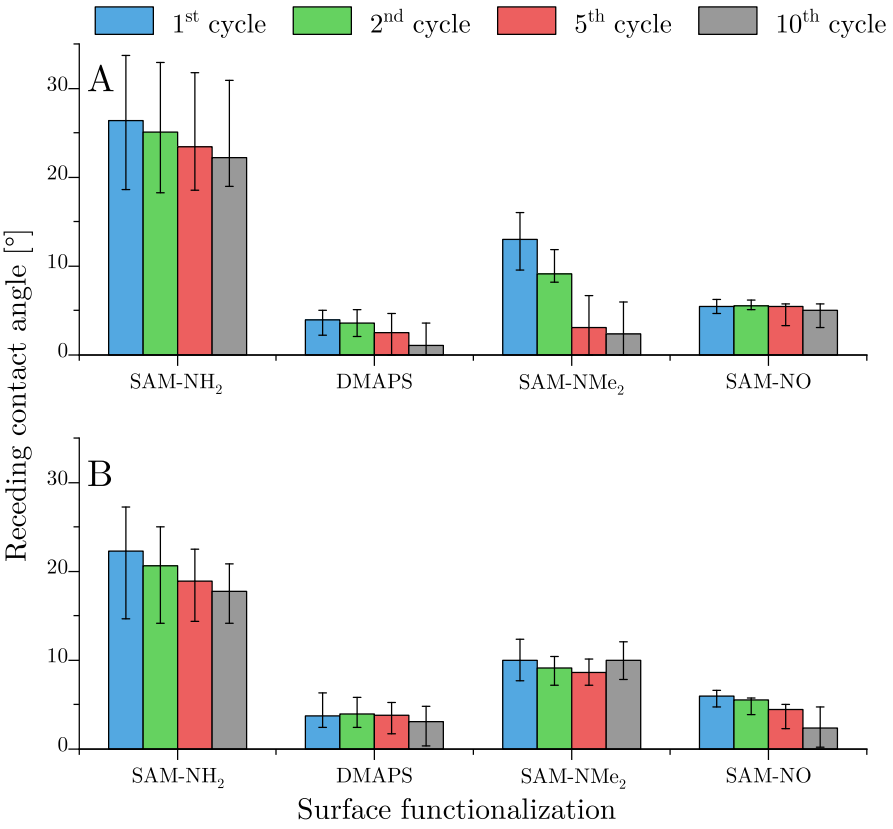

Figure 15.6: Receding contact angles, obtained from dynamic contact angle measurements with (A) water or (B) PBS. Results for the cycles 1, 2, 5 and 10 of osmolyte-derived modifications and their precursor SAMs are provided.

Having a closer look at the tensiometric measurements in water, an opposite behavior is observed for the system SAM-NH_2/DMAPS and SAM-NMe_2/SAM-NO. Whereas the former exhibits decreasing advancing angles and hysteresis with increasing number of immersion cycles, the opposite behavior, i.e. increasing hydrophobicity, is observed for the latter. The same correlation can be observed for the hysteresis. Furthermore, SAM-NH_2 and DMAPS differ in their advancing contact angles, which DMAPS being significantly more hydrophilic, wheras no difference can be observed between SAM-NMe_2 and SAM-NO after the first immersion cycle. These results are in accordance with the data obtained from static contact angle measurements and SFE calculation.

Dynamic contact angle measurements in PBS lead to less coherent results. For SAM-NH_2 and SAM-NO surfaces, a decrease in the advancing angle and the hysteresis is observed with increasing number of immersion cycles. For DMAPS or SAM-NMe_2-functionalized surfaces, however, no clear trend is obtained. Especially the results for

the DMAPS-modified samples must be handled with care as these measurements exhibit a partial non-linear (non-equilibrium) behavior in the immersion part of the measurement cycles. These cycles resemble measurements of Kleingartner et al. with switchable polymer multilayers at higher measurement speeds and have similarly be described by Rupp et al. for dynamic contact angle measurements with protein solutions [239, 381]. The obtained values for advancing and receding contact angles as well as contact angle hysteresis thus have to be interpreted carefully.

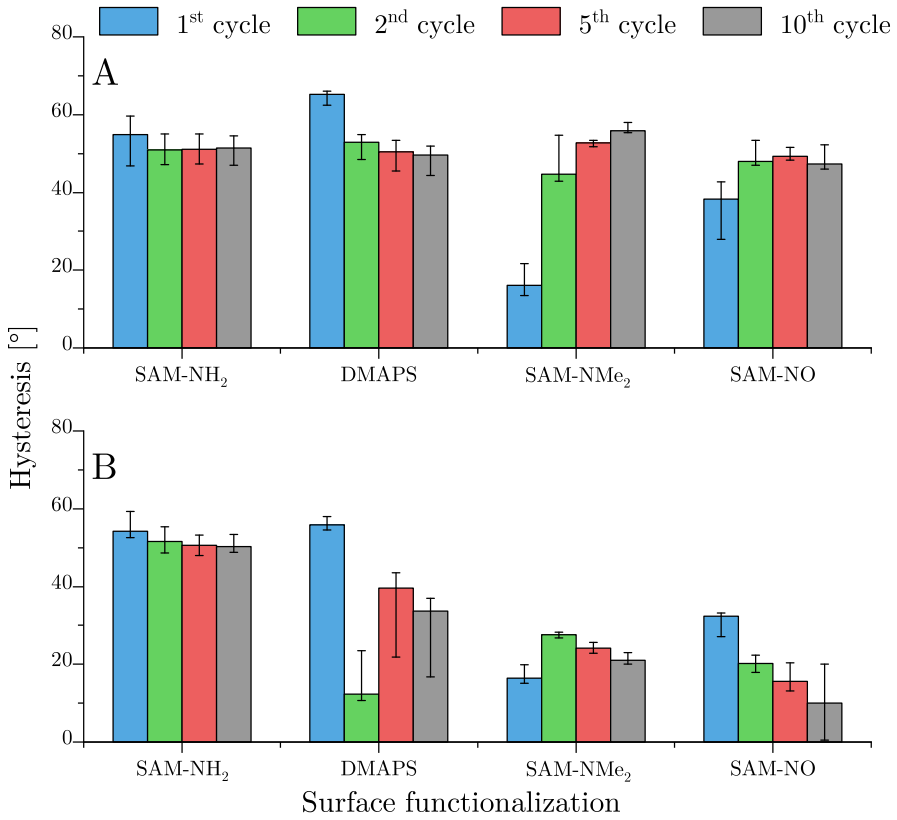

Figure 15.7: Contact angle hysteresis of osmolyte-derived coatings as well as their precursor SAMs from dynamic contact angle measurements with (A) water or (B) PBS.

For the comparison of the DMAPS modification with literature, only data of polymer coatings with sulfobetaine groups is available. Kobayashi et al. determined an advancing contact angle of 24° and a receding angle of $< 3°$, Wu et al. even observed complete wetting (advancing and receding angle $\approx 0°$) [366, 382]. Thus, these polymer coatings exhibited more hydrophilic properties and reduced contact angle hysteresis. This may be the consequence of the larger number of zwitterionic groups in the polymer in comparsion with the SAM, which additionally still contains the hydrophobic -$(CH_2)_{11}$- chain of the initial SAM-NH_2.

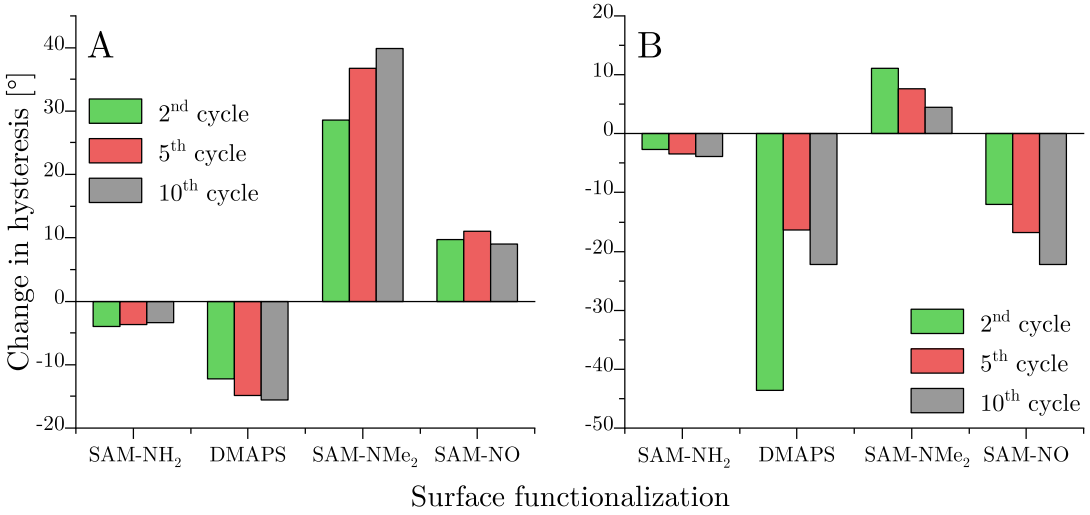

Figure 15.8: Loop-dependent change of the contact angle hysteresis of osmolyte-based modifications and their precursor SAMs with respect to the first cycle for measurements with (A) water or (B) PBS.

For the other two modifications, SAM-NMe_2 and SAM-NO, only very little data is available in literature because such an amine oxide modification has rarely been synthesized before. Striking, however, is the large and strongly increasing hysteresis of the SAM-NMe_2 coating in combination with a very small hysteresis in the first cycle of the tensiometric measurement with water. This result indicates that the thermodynamic hysteresis is small due to limited flexibility of the short-chained modification. The large jump in hysteresis from the first to the second immersion loop, i.e. the kinetic hysteresis, can then be caused by a strong swelling of the surface coating. In comparison, a polymeric coating with terminal tertiary amine groups examined by Kobayashi et al. showed more hydrophobic properties (advancing angle 78° and receding angle 27°). This modification, however, also possessed a hydrophobic methyl side group in each repeating unit of the hydrocarbon backbone of the polymer [366].

15.3.3 Zeta Potential

The surface modifications with osmolyte motifs were analyzed with respect to their electrokinetic properties via zeta potential measurements. As already described for the amine modifications, electrophoresis experiments were performed with functionalized particles. As the results for the DMAPS coating were not satisfactory, the data was supplemented by additional streaming current measurements of this coating on silicon wafers. Electrophoresis experiments were again performed in the pH range between pH 3 and pH 9, allowing the presentation of the complete potential curve but also the extraction of the IEPs and the ζ-potential under physiological conditions. The results are depicted in Figures 15.9 and 15.10 as well as in Table 15.3.

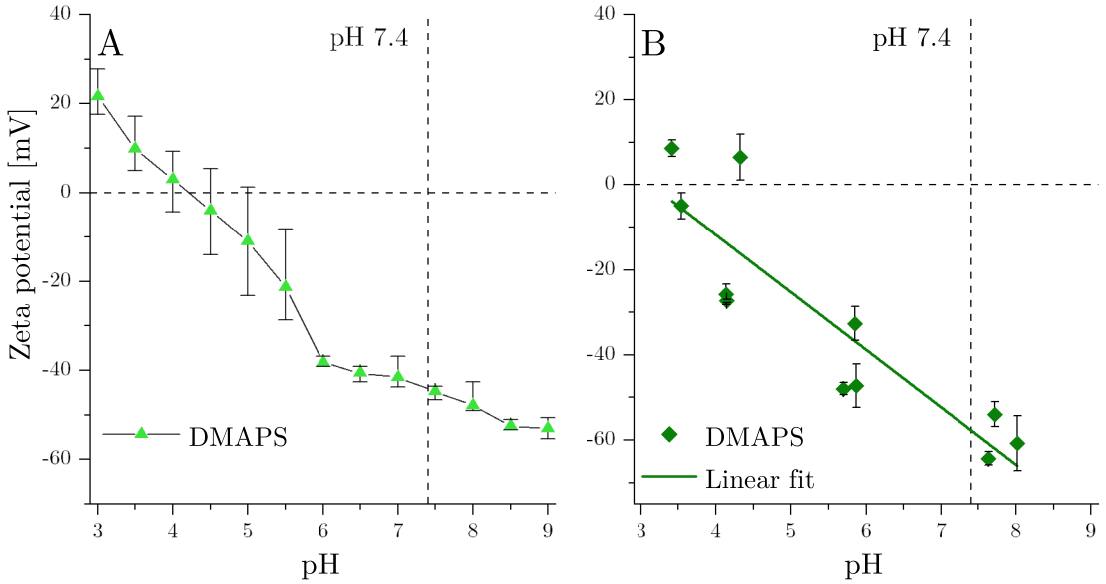

Figure 15.9: Zeta potential of a sulfobetaine-modified surface (DMAPS), obtained from (A) electrophoresis measurements or (B) streaming current experiments (mean average ± standard deviation). All zeta potential measurements were performed in 1 mmol L^{-1} KCl solution.

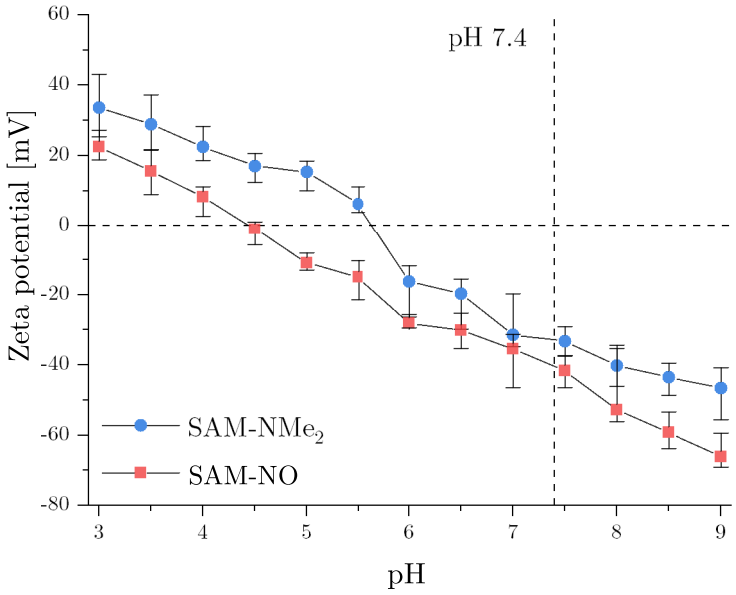

Figure 15.10: Zeta potential of surfaces modified with SAM-NMe_2 or SAM-NO obtained from electrophoresis measurements. All zeta potential measurements were performed in 1 mmol L^{-1} KCl solution.

The DMAPS modification was synthesized by immobilization of a sulfobetaine moiety via aza-Michael addition of the acrylate-substituted molecule to the primary amine group of the SAM-NH_2. In contrast to this precursor SAM, the sulfobetaine modification exhibits a significantly lower IEP of 4.2 in electrophoretic experiments or 3.1 in streaming current measurements, respectively. As a consequence, the zeta potential at

pH 7.4 is strongly negative. This represents a strong decrease of the IEP by approximately 3 pH units, compared to the IEP of SAM-NH_2 of 7.1 (see section 13.2.2 and [13]). In the study of thiol-based self-assembled monolayers with terminal sulfobetaine groups by Shen and Lin, a rather similar negative zeta potential of −35 to −55 mV was measured at pH 7.4 [383]. This data, however, can only be compared with great care. The aza-Michael reaction of the amine SAM with the acrylate-substituted sulfobetaine reagent is expected to lead to the formation of an inner secondary amine group. As the sulfobetaine moiety itself introduces equal positive and negative charges, no major change in the IEP compared to the SAM-NH_2 should be expected. So far, no explanation can be found for this unpredicted decrease in zeta potential. The results from streaming current experiments also have to be considered very carefully. Due to unusually prolonged storage times of more than two months, degradation of the surface modifications cannot be excluded.

Table 15.3: Isoelectric point and zeta potential at pH 7.4 of osmolyte-based modifications and their respective precursor SAMs, as determined from electrophoretic and streaming current measurements.

Surface Coating	Zeta potential			
	Electrophoresis		Streaming current	
	IEP	At pH 7.4 [mV]	IEP	At pH 7.4 [mV]
SAM-NH_2 [a,b]			7.1	−3
DMAPS	4.2	−45	3.1	−58
SAM-NMe_2	5.6	−35		
SAM-NO	4.5	−40		

[a] Data is derived from zeta potential curves presented by Verena Katzur in her PhD thesis [13].
[b] The data has previously been published in Eichler et al. [19].

In contrast to that, the results of the electrophoretic measurements of SAM-NMe_2 and SAM-NO are in good accordance with literature data, if available. The self-assembled monolayer with terminal tertiary amine groups exhibits an IEP of 5.6 and a negative zeta potential of −35 mV at pH 7.4. These results are lower than those for the SAM-NH_2 monolayer with an IEP of 7.1 but similar to those of the APD coating (with an IEP of 6.0) [13]. The slightly reduced zeta potential might be explained with the shorter hydrocarbon spacer of SAM-NMe_2 (only three -CH_2- units), compared to the hydrocarbon chain of the SAM-NH_2 monolayer, which contains 11 -CH_2- groups. Thus, the remaining dissociated surface silanol groups, which carry and contribute negative charges, are less shielded (see also chapter 14.3.3).

Conversion of the terminal tertiary amine groups into amine oxide groups leads to a reduction of the zeta potential, which can be seen by a shift of the IEP (from 5.6 to 4.5) and a lower zeta potential under physiological conditions. The reduction by more than one pH unit compared to the intermediate SAM confirms successful oxidation of the terminal tertiary amine groups. These results for SAM-NO fall in line with the zeta potential curves of other surface modifications with non-ionizable surface groups, which usually exhibit an IEP of approximately 4. Examples hereof are SAM-CH_3 (IEP 3.8) and SAM-PEG (IEP 3.2) (see section 13.2.2 and [13]). The reasons for such negative zeta potentials at higher pH values are probably the contribution of the dissociating silanol groups of the substrate as well as the preferential adsorption of less well hydrated anions, especially hydroxide ions, on the surface [272, 291]. Here, the amine oxide modification is treated as a non-ionizable group as well, although it can be protonated with a corresponding pK_a value between 4.5 and 5 in solution [134]. As observed by Shyue et al. and discussed in detail in chapter 14.3.3 for the APD modification, these constants, however, can be strongly altered for functional groups in the crowded environment of a SAM [272]. Thus, it is assumed that the pK_a value of the protonated amine oxide is reduced by several units, as determined for the pK_a of protonated primary amine groups, and only unprotonated amine oxide groups, acting as non-ionizable groups in the selected pH range, are present [272].

15.4 Analysis of Protein Adsorption

In addition to the detailed characterization of the physicochemical properties, the adsorption of proteins from HSA and lysozyme solutions as well as from saliva and FBS on the osmolyte-functionalized surfaces was studied via BCA assay. To that purpose, the protein content of the physiological fluids was determined via the BCA assay as well (see chapter 13.3).

As previously described for the amine-modified substrates, adsorption experiments were performed with a series of HSA or lysozyme solutions, with their concentrations ranging between $1\,\mathrm{mg\,mL^{-1}}$ and $50\,\mathrm{mg\,mL^{-1}}$. The data obtained from these measurements is summarized in Figure VI.9 in the appendix. It has to be stated here that these measurements were only performed for the DMAPS and the SAM-NO coating as well as their precursor SAMs. So far, no data is available for the adsorption of HSA or lysozyme on proline-modified surfaces. Two general observations can be made for the concentration-dependent adsorption of HSA and lysozyme. Similar to the amine coatings, the amount of adsorbed protein increases with increasing protein concentration in solution. For the DMAPS and the SAM-NMe_2 coating, saturation occurs. For the adsorption of HSA on the SAM-NO surface, negative values were obtained for amounts of adsorbed proteins with low HSA concentrations in solution. In this case, the unspecific interaction of the BCA reagent with the functionalized surface without attached protein leads to higher absorbance values in the assay than the samples with small amounts of attached protein. These results will be treated as zero protein adsorption.

The results for the protein adsorption from HSA or lysozyme solutions with a concentration of $10\,\mathrm{mg\,mL^{-1}}$ as well as from saliva or FBS are summarized in Figure 15.11. Here, data for the attachment of proteins on oxidized but unmodificed silica substrates is added for reference.
Some general trends, already observed for the protein adsorption on amine surfaces, can also be confirmed for osmolyte-based modifications. With the exception of the SAM-NO surface, more HSA than lysozyme is adsorbed onto surfaces because it is a "soft" protein prone to denaturation [155]. If determined, the amount of adsorbed protein from the HSA solution and FBS is of the same order of magnitude as well. At last, larger amounts are adsorbed from FBS than from saliva in all cases, which is related to the significantly higher protein content in FBS [159, 165].

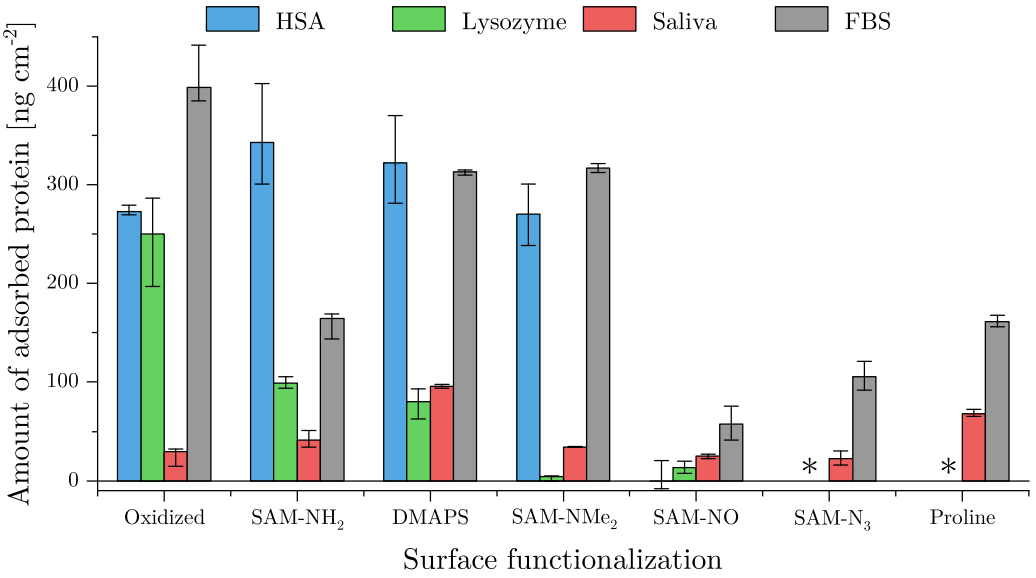

Figure 15.11: Amount of adsorbed protein from HSA or lysozyme solutions (concentration $10\,\mathrm{mg\,mL^{-1}}$ in PBS buffer), undiluted human saliva or FBS on silica beads with osmolyte-based modifications or their precursors. Adsorption of HSA or lysozyme on SAM-N_3 and the proline-functionalized surface has not been determined yet (∗). For improved clarity, the results of the Mann-Whitney-U test are not included in the figure as all pairwise comparisons among each protein solution showed significance except for the following: HSA: oxidized – SAM-NH_2, oxidized – SAM-NMe_2, SAM-NH_2 – DMAPS, DMAPS – SAM-NMe_2; saliva: oxidized – SAM-NO, oxidized – SAM-N_3, SAM-NH_2 – SAM-NMe_2, SAM-NO – SAM-N_3; FBS: SAM-NH_2 – proline, DMAPS – SAM-NMe_2.

In the following, the various osmolyte-based surface modifications will be evaluated in detail. As these coatings do not share a common functional group (as the amine-based functionalizations) and only two of the three modifications could be analyzed completely, a different approach will be chosen for the detailed analysis of the protein adsorption. Instead of linking the results from BCA assays to the measured physicochemical properties, as performed for the amine-based coatings, a separate discussion of each modification is presented in the following.

The coating carrying sulfobetaine moieties, the DMAPS modification, performs poorly in all protein adsorption experiments. Compared to the precursor monolayer SAM-NH_2, only slightly improved results are obtained for adsorption from the single protein solutions. Increased protein adsorption, however, is observed for experiments with physiological fluids. In many other studies, sulfo- and carboxybetaines with quaternary ammonium groups have presented themselves as suitable candidates for protein-repellent applications because of their properties. They are strongly hydrated, exhibit only low to moderate self-association and weak interaction with proteins [132]. Accordingly, the results obtained in this thesis are in stark contrast to the performance of

zwitterionic modifications in literature, where excellent protein-repellency and non-fouling properties have been reported for polymers and SAM coatings exhibiting, for example, sulfobetaine groups [150, 201, 202, 360, 379]. At this point, no satisfactory explanation can be provided in order to explain the results for the sulfobetaine monolayer in this thesis. The XPS data proves the immobilization of the sulfobetaine due to the appearance of the sulfur peak. It can, however, be assumed that this reaction was not quantitative and the remaining amine groups are responsible for the strong protein adsorption. Contradictory to this hypothesis, the increased hydrophilicity and drastically reduced zeta potential indicate that only a small portion of the amine groups might not have reacted with the methacrylate group. Further detailed investigation has to be performed with the objective of explaining the modification reaction as well as the protein adsorption on the resulting surface.

The monolayer with tertiary amine groups (SAM-NMe_2) gives mixed results. Whereas low adsorption of lysozyme and medium amounts of salivary proteins are determined, HSA and serum proteins strongly adsorb on that surface modification. Strong adsorption of albumin on this monolayer was also reported by Huang and Chang, who measured 148.7 $ng\,cm^{-2}$ via quartz microbalance after exposure to a 1 $mg\,mL^{-1}$ BSA solution [380]. Compared to SAM-NH_2, bearing primary amine groups, lower HSA and lysozyme adsorption can be observed, whereas more proteins from FBS adsorb to SAM-NMe_2 than to SAM-NH_2. These differences in protein adsorption have similarly been observed by Gessner et al. for human serum [179]. Their quantification of the protein amounts adsorbed on nanoparticles carrying different amine groups (primary to quaternary) also revealed that the total amount of adsorbed proteins on the coating with tertiary amine groups was approximately twice as much as on the surface with primary amine groups. At the same time, they observed a higher affinity of albumin for primary amine groups compared to tertiary amine groups, applying two-dimensional electrophoresis [179].
The surface properties are completely altered upon conversion of the tertiary amine groups into amine oxide functionalities. The resulting SAM-NO, resembling the natural osmolyte TMAO, exhibits very good protein-repellency towards all tested solutions. In comparison with the precursor SAM-NMe_2, a strong reduction in the amount of attached HSA and serum proteins can be noted. In fact, no adsorbed HSA can be detected. The excellent performance of this modification can probably be explained with the very strong hydration of TMAO (as explained in section 3.3.3). The resulting, strongly hydrated surface thus exhibits protein-repellency according to the water barrier model because the displacement of hydrogen-bonded water molecules by a protein is enthalpically unfavorable and leads to a repulsive solvation force [188, 192, 193].

The analysis of the interaction of the proline-modified surface and its azide-terminated precursor SAM is limited to the experiments with physiological fluids. Here, however, no protein-repellency can be observed. Whereas rather low protein adsorption is observed for the intermediate SAM-N_3 ($22.7\,\mathrm{ng\,cm^{-2}}$ and $105.8\,\mathrm{ng\,cm^{-2}}$ for salivary or serum proteins respectively), increased adsorption is observed for the final modification step. The comparably high amounts of attached proteins, especially from saliva ($68.1\,\mathrm{ng\,cm^{-2}}$), lead to the conclusion that the modification procedure was not successful. This assumption has also been suggested by the results from the amine-group detecting sulfo-SDTB assay (see 15.2.2), where the measured amine group density of the proline-based modification was rather low and only marginally increased compared to the precursor SAM-N_3. One possible explanation for the increased protein adsorption could be a successful immobilization of the protected amino acid but a failed deprotection reaction. Thus, the remaining *tert*-butyl group of the Boc protecting group could enhance protein attachment as it renders the surface hydrophobic [181].

Combining the results for all osmolyte-based surface modifications, it can be stated concludingly that they fulfill the requirements for protein-repellent surfaces summarized in the Whitesides rules almost completely [195]. Sulfobetaine and amine oxide groups as well as the proline molecule are polar and provide H-bond acceptors. In contrast to the amine modifications, they also do not exhibit net charges. Furthermore, the sulfobetaine and the amine oxide moiety do not possess hydrogen-bond donors. The fact that these requirements are met almost completely in combination with the promising results for betaine-functionalized surfaces by other researchers encourages further efforts, e.g. more detailed investigation of the sulfobetaine monolayer and of the synthesis of the proline modification.

16 Results from Cell Experiments

In order to gain a better understanding if the surface modifications developed and analyzed in this thesis are promising with respect to later application as coatings for titanium implants, cell experiments were performed on selected functionalizations, representing the three different structural motifs (oligomer, dendrimer and linear polymer). Thus, experiments were carried out on APD, PPI-G4 and PEI polymer-modified titanium wafer substrates by Dr. Susanne Stählke at the Department of Cell Biology at the Rostock University Medical Center. Prior to that, successful coating was monitored via XPS, and key physicochemical features (wettability, surface free energy and zeta potential) were determined. Thus, these properties will be presented first, before discussing and analyzing the results from cell experiments.

16.1 Evaluation of Physicochemical Properties

16.1.1 Verification of Successful Surface Modification via XPS

In the following, the results of the XPS analysis of oxidized titanium wafers and titanium substrates with APD, PPI-G4 and PEI polymer will be compared to the respective coatings on silicon wafers. To that purpose, the elements of the substrate (either silicon or silicon and titanium respectively) will be summarized as "Sub" for substrate in Table 16.1.

Table 16.1: Elemental composition of oxidized or APD, PPI-G4 or PEI polymer-modified titanium wafers in comparison with silicon wafer substrates.

Surface coating	Substrate	XPS data [at-%]				Element ratios		
		Sub	C	O	N	N/C	N/sub	C/sub
Oxidized	Si	44	17	32	1	0.06	0.02	0.39
	Ti	24	20	55	0	0.0	0.0	0.83
APD	Si	17	47	29	6	0.13	0.35	2.76
	Ti	10	46	39	4	0.09	0.40	4.60
PPI-G4[a]	Si	10	58	20	11	0.19	1.10	5.80
	Ti	5	57	25	14	0.25	2.80	11.40
PEI polymer[a]	Si	30	34	31	6	0.18	0.20	1.13
	Ti	17	29	49	5	0.17	0.29	1.71

[a] Data for functionalizations on titanium substrates has previously been published in the supporting information of Gruening et al. [384].

Only a brief comparison will be presented in the following (for a more detailed analysis of the amine-coatings see section 14.2.1).
Similar to the results for silicon substrates presented there, successful functionalization of the titanium substrates is confirmed by a decrease in the content of substrate elements and oxygen, accompanied by an increase in the carbon and nitrogen content. Comparing the elemental composition of oxidized silicon and titanium wafers among each other, it can be noticed that titanium wafers exhibit a lower content of titanium and silicon but a significantly higher percentage of oxygen than oxidized silicon wafers. This discrepancy can possibly be explained by differences in the thickness of the oxide layer formed via oxidation. Whereas for titanium a thickness of 8 nm was reported, the oxide layer of silicon was found to be only 1.0–1.5 nm, resulting in a lower content of oxygen [26, 39].

For the surface modifications, however, the data for functionalized titanium surfaces is in good agreement with the ones obtained from silicon wafers because similar nitrogen contents and N/C ratios (among the same functionalization) are observed. Due to the lower percentages of substrate elements, however, higher N/substrate and C/substrate ratios were measured on titanium substrates. In general, it can be said that the surface functionalizations were also successful on titanium substrates, leading to very similar surface coatings.

16.1.2 Characterization of Wettability and SFE

In addition to confirming successful surface modification via XPS, the resulting coatings were characterized via static contact angle measurements with sf-water, formamide and diiodomethane. The obtained angles are summarized in Table 16.2. As for the determination of the elemental composition, the results for functionalizations on silicon wafers are also included for comparison.

As seen there, the contact angles on titanium wafers are all lower than the respective angles on silicon wafers. On titanium substrates, angles formed by droplets of formamide or diiodomethane are all $< 20°$, whereas up to 40° are obtained for silicon substrates. Surface modifications on Ti wafers exhibit higher hydrophilicities than on Si wafers as water contact angles between 20° (PEI polymer) and 32° (PPI-G4) were measured. This overall observation can be explained with differences in surface roughness between the silicon and the titanium wafers. For the latter, a nanoscale roughness was calculated from AFM data ($R_a = 2.44$ nm) [216]. In contrast to that, the surface of pure silicon wafers was found to be smooth in AFM measurements ($R_a = 0.08$ nm) [19].

Table 16.2: Static contact angles (with water, formamide and diiodomethane) on titanium wafers without functionalization (oxidized) or with APD, PPI-G4 or PEI polymer coating. Contact angles of the same modifications on silicon wafers are added for comparison.

Surface modification	Substrate	Contact angle [°]		
		Water	Formamide	Diiodomethane
Oxidized	Si	14 (12-16)	10 (6-12)	37 (33-42)
	Ti	18 (17-20)	9 (7-10)	14 (13-15)
APD	Si	46 (41-53)	34 (33-35)	26 (24-28)
	Ti	23 (22-24)	13 (12-15)	17 (13-19)
PPI-G4	Si	39 (31-47)	30 (24-32)	40 (39-42)
	Ti	32 (25-37)	18 (10-22)	17 (13-21)
PEI polymer	Si	35 (33-41)	31 (29-33)	39 (35-40)
	Ti	20 (17-26)	7 (5-8)	9 (9-11)

On rough surfaces, only apparent contact angles an be obtained in general [385]. For homogeneous surfaces and sufficiently large drops (compared to the roughness scale), the relationship between the apparent contact angle Θ_a and ideal contact angle Θ_i can be described by the Wenzel equation [233, 385]:

$$cos\Theta_a = r \cdot cos\Theta_i \tag{16.1}$$

Here, these two quantities are related via the roughness ratio r, which is defined as the ratio between the actual surface area and the apparent surface area. Thus, only values of ≥ 1 can be observed for r [385, 386]. As a consequence of this equation, the contact angle on a rough hydrophobic surface ($\Theta_i > 90°$) is expected to increase even further, whereas the opposite, i.e. decreasing contact angles, is observed for surfaces with ideal contact angles $< 90°$ [387]. Different regimes for the effect of surface roughness on contact angles were found by Busscher et al. for polymer surfaces with a roughness $R_a > 1\,\mu m$, measuring contact angles with various liquids including water, formamide and diiodomethane. They observed increasing apparent contact angles if the respective ideal contact angle was $> 86°$ [388]. No change was noticeable in the range between 60° and 86°, whereas decreasing contact angles were determined for ideal angles $< 60°$ [388]. Similar observations could be made for the changes in measured contact angles with all three probing liquids on titanium substrates in comparison with the results on silicon substrates. Shifts in water contact angles, not only of the final amine modifications but also of the intermediate SAMs, are summarized in Figure 16.1.

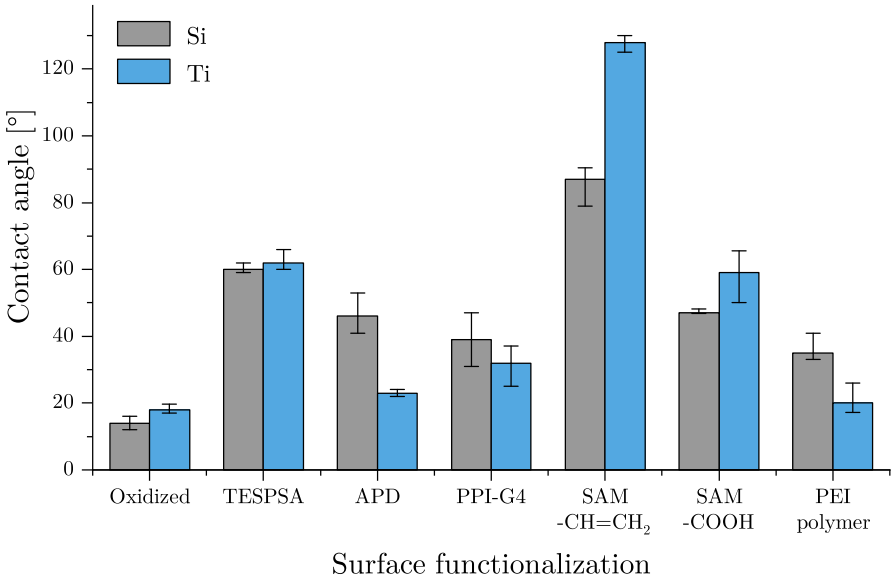

Figure 16.1: Comparison of static water contact angles on silicon or titanium-based substrates without coating (oxidized), with intermediate SAMs (TESPSA, SAM-CH=CH_2, SAM-COOH) or with amine-based functionalizations.

Some of the trends, described by Busscher et al. for polymer surfaces, can be observed here. A strong increase of the contact angle is not only observed for the hydrophobic SAM-CH=CH_2 monolayer but also, yet less pronounced, for the moderately hydrophilic SAM-COOH. In contrast to that, no significant difference in the contact angle is observed between silicon or titanium substrates with TESPSA coating. In both cases, a static contact angle of approximately 60° is obtained. As mentioned previously, for the hydrophilic amine-terminated coatings, a lower contact angle is observed on the rough titanium substrates. The higher contact angle of the oxidized titanium wafer, however, can be the consequence of the shorter oxidation time, not the result of the surface roughness.

As described in section 6.3.3, the surface free energy of a surface can be obtained from measured contact angles via Young's equation. This, however, implies the measurement of the actual ideal contact angle [231]. As the contact angle measurement on rough surfaces only yields apparent contact angles, only an apparent surface free energy can be calculated. This number does not necessarily reflect the actual thermodynamic quantity of the SFE. The SFE calculation was performed as described in section 13.2.1, the results are summarized in Figure 16.2.

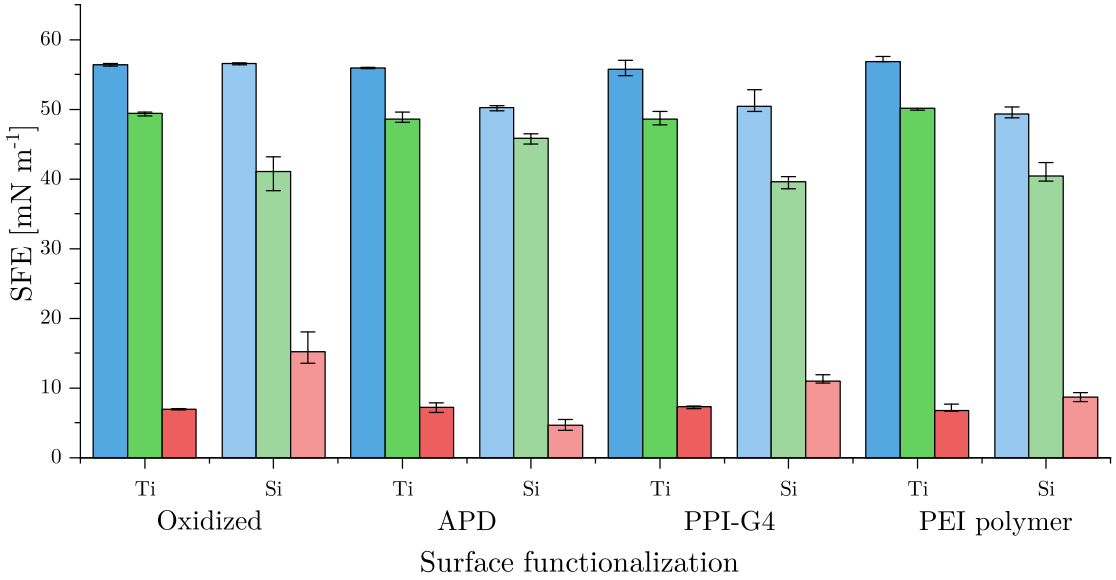

Figure 16.2: Surface free energies as well as their polar and dispersive components of oxidized or functionalized titanium wafers in comparison with the respective functionalization on silicon substrates (as described in chapter 14).

The apparent SFEs calculated for the functionalized titanium surfaces do not differ significantly among each other. For all modifications a total SFE of 55–57 $\mathrm{mN\,m^{-1}}$ is obtained, which is composed of a dispersive component of 48–50 $\mathrm{mN\,m^{-1}}$ and a polar component of 6.5–7.5 $\mathrm{mN\,m^{-1}}$. For the three modifications, APD, PPI-G4 and PEI polymer, the apparent SFEs are slightly higher than the results for the smooth silicon wafers. This increase can be explained by the lower contact angles measured on the rougher titanium substrates. In summary, rather similar results are observed for the three surface modifications as they are hydrophilic coatings with moderately high surface free energies.

16.1.3 Zeta Potential of Functionalized Titanium Surfaces

In contrast to the wettability behavior, the electrokinetic properties differ strongly among the selected amine modifications. For all surfaces, streaming current measurements were performed at the Department of Cell Biology at the Rostock University Medical Center, either by Dr. Susanne Stählke (oxidized, APD) or by Martina Grüning (PPI-G4, PEI polymer). The results for PPI-G4 or PEI polymer-functionalized substrates have recently been published [384]. The measured data is shown in Figure 16.3, the IEPs and zeta potentials at pH 7.4 obtained from linear regression are summarized in Table 16.3. Here, the respective electrokinetic properties of functionalized silicon substrates are again included for comparison.

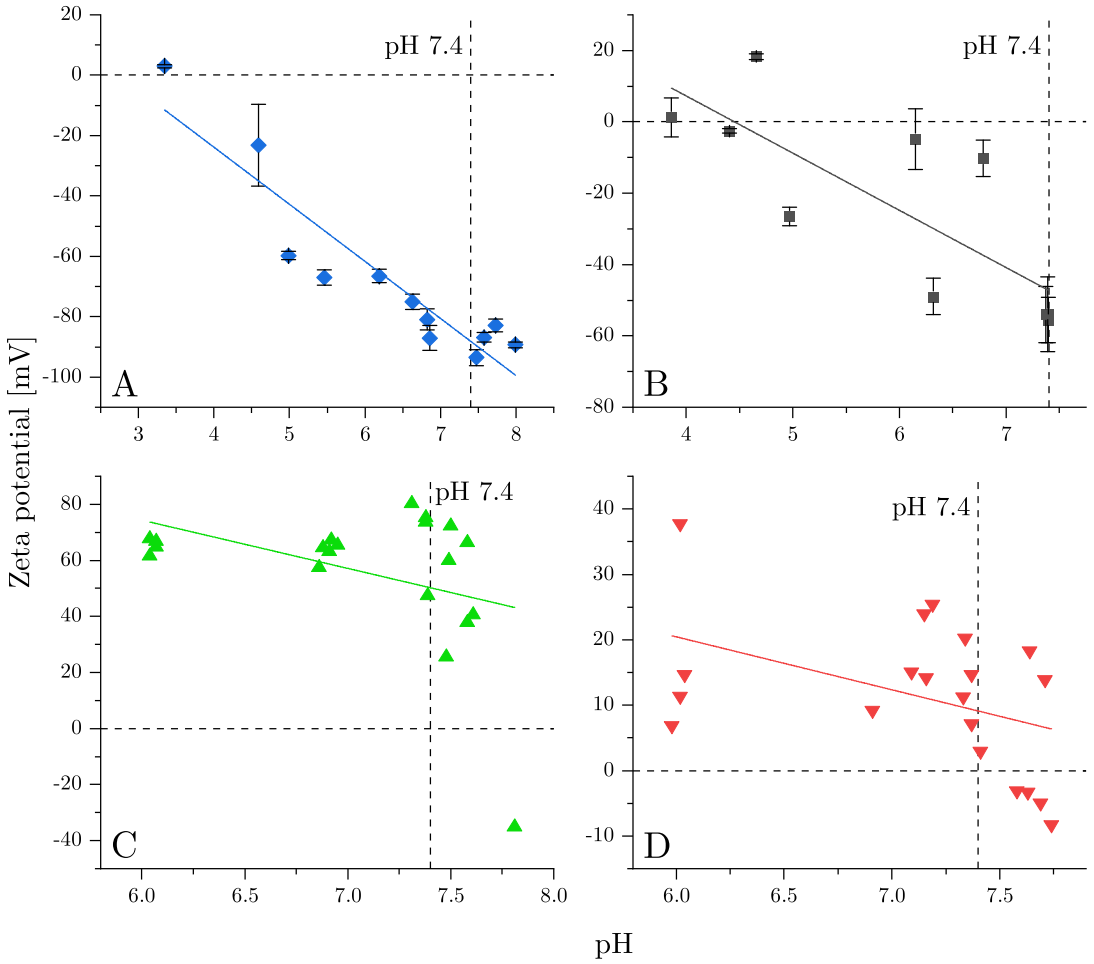

Figure 16.3: Zeta potential of (A) oxidized Ti wafers as well as titanium substrates modified with (B) APD, (C) PPI-G4 or (D) PEI polymer obtained from streaming current experiments (mean average ± standard deviation, linear fit shown). All zeta potential measurements were performed in 1 mmol L^{-1} KCl solution.

No difference can be observed between the electrokinetic behavior of oxidized titanium wafers and silicon wafers, which was determined by Staehlke et al. [20]. Almost identical isoelectric points and strongly negative zeta potentials at pH 7.4 are obtained for both substrates. The IEP of oxidized titanium measured in this thesis, however, is lower than the IEP obtained by Roessler et al. who determined an IEP of 4.5 for a sputtered titanium layer after formation of an oxide layer in air [389].

The APD-functionalized surface exhibits a higher IEP of 4.5 and a less negative zeta potential of −47 mV under phyiological conditions. No comparison, however, is possible with the respective coating on silicon wafers because no streaming current measurements were performed for that modification. For particulate silica substrates, a similar zeta potential at pH 7.4 but a significantly higher IEP (at pH 6.0) was obtained from electrophoretic measurements (see 14.3.3).

Table 16.3: Isoelectric point and zeta potential at pH 7.4, determined from streaming current measurements of oxidized or functionalized titanium wafers. Elektrokinetic data for silicon substrates, obtained via streaming current or electrophoretic measurements, is included for comparison.

Surface Coating	Zeta potential			
	Ti substrate		Si substrate	
	IEP	At pH 7.4 [mV]	IEP	At pH 7.4 [mV]
Oxidized[a]	2.7	−88	2.7	−90
APD[b]	4.5	−47	6.0	−50
PPI-G4[c,d]	10.3	+50	8.9	+48
PEI polymer [c,d]	8.5	+9	7.5	+2

[a] Data of streaming current measurements of oxidized silicon wafers are taken from Staehlke et al. [20].

[b] Zeta potential data on silicon substrates was obtained via electrophoretic measurements.

[c] Streaming current measurements of PPI-G4 and PEI polymer on titanium wafers have been performed by Martina Grüning and have been published in Gruening et al. [384].

[d] Zeta potential on silicon substrates was obtained via streaming current measurements, performed by Martina Grüning.

Rather similar observations can be made for the remaining surface modifications, PPI-G4 and PEI polymer. In both cases, the zeta potentials at pH 7.4 of functionalized titanium substrates resemble the results of coated silicon wafers. For PPI-G4, a strongly positive zeta potential of approximately 50 mV is obtained, whereas the immobilization of the PEI polymer leads to a surface with a slightly positive charge. In both cases, however, the isoelectric points are not in good agreement with the results of coated silicon substrates. Especially in the case of the PPI coating, this deviation may be the result of the extrapolation. The linear fit was obtained from zeta potentials in a range between pH 6 and pH 8, where predominantly still very high zeta potentials were measured. Thus, the error of the isoelectric point obtained from linear regression might be rather large.

16.2 Analysis of Cell Biological Experiments

The surface functionalizations, characterized in the previous section, served as the basis for cell biological investigations with osteoblast-like MG-63 cells. Their spreading, morphology, actin cytoskeleton organization as well as cell cycle were analyzed by Dr. Susanne Stählke at the Department of Cell Biology at the Rostock University Medical Center. The results for the behavior of the cells on those three surface coatings will always be presented in comparison with the data obtained for oxidized but otherwise unmodified titanium substrates.

16.2.1 Cell Spreading

The spreading of the MG-63 cells, i.e. the respective cell area after 1 h and 24 h of cultivation, was obtained from SEM images. The results are summarized in Figure 16.4.

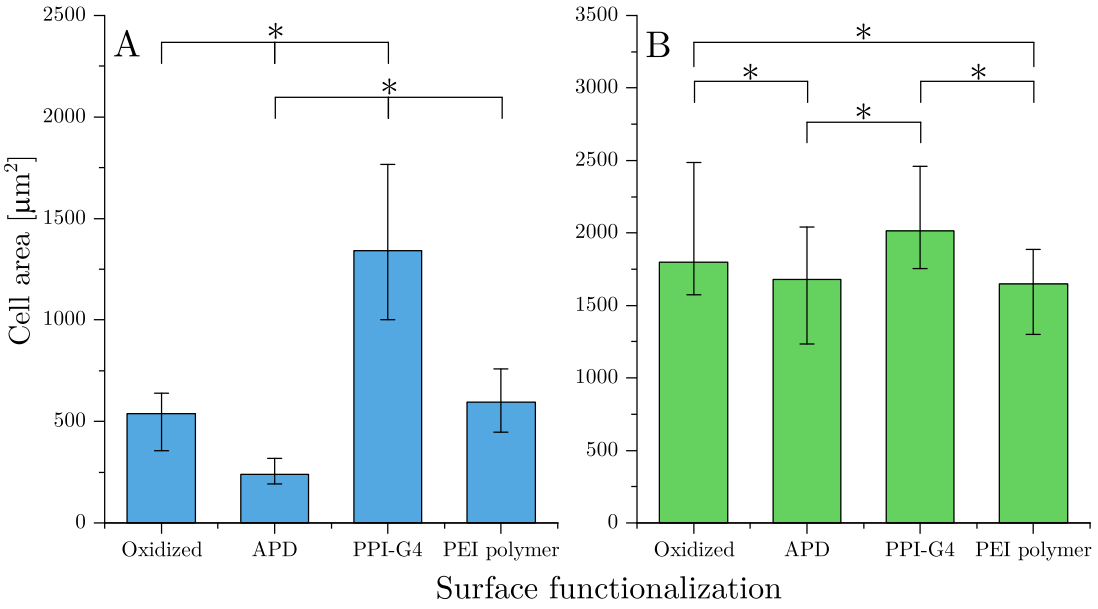

Figure 16.4: Spreading of osteoblastic MG-63 cells on differently functionalized titanium substrates. Cell areas are obtained from SEM images after cultivation for (A) 1 h or (B) 24 h. (Statistics: Mann-Whitney-U-Test, $^*p < 0.05$).

After 1 h (Figure 16.4A), strongly differing cell areas are obtained on the three surface coatings. On PEI polymer-coated substrates, the MG-63 cells behave similarly to those on bare titanium wafers and possess a surface area of approximately 500 µm². On APD-functionalized surfaces, a strongly reduced cell area is observed (approximately 250 µm²). Oppositely, the area of MG-63 cells is strongly increased (roughly 3-fold) on PPI-G4 in comparison with oxidized titanium substrates. Similarly to these results, a strong enhancement of cell growth after 1 h of cultivation was observed on surfaces with PAMAM dendrimer of generation 5, which also possesses a large number of surface amine groups [20].

After 24 h, the differences in cell area among the different surface modifications have disappeared almost completely, with cell areas ranging from 1650 µm^2 to 2000 µm^2 (see Figure 16.4B). Still, however, a slightly reduced cell area is obtained on APD-functionalized surfaces, whereas the largest growth is observed on PPI-G4-covered substrates. This data partially disagrees with the results from Gruening et al. [384]. Here, similar cell areas were observed for PEI-functionalized substrates after 24 h ($\approx$ 1620 µm^2) [384]. In contrast to that, however, MG-63 cells strongly decreased in size on PPI G4, resulting in a cell area of $\approx$ 550 µm^2 after 24 h in their study [384].

16.2.2 Cell Morphology

From the SEM images of the MG-63 cells on the various substrates after 1 h and 24 h of cultivation, further information can be gathered about the development of the cell morphology (see Figures 16.5 and 16.6, additional figures provided in the appendix).

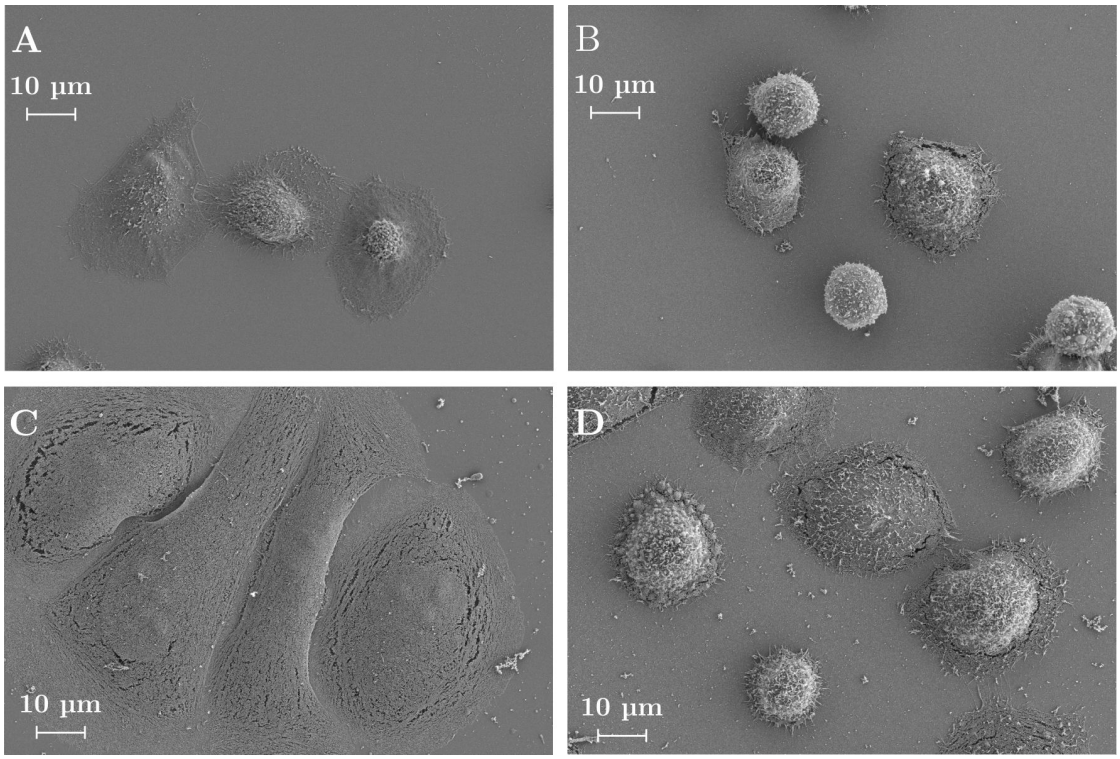

Figure 16.5: Analysis of the morphology of MG-63 cells after 1 h of incubation on (A) oxidized titanium substrates, (B) APD, (C) PPI-G4 or (D) PEI polymer coating from SEM images (bars = 10 µm).

As for the cell spreading, similar results are obtained for unmodified and PEI polymer-coated substrates after 1 h. In both cases, most cells exhibit a rounded shape, but the flattening of the cell periphery indicates cell spreading. In contrast to that, the cell morphology of the MG-63 cells is strongly impaired on APD-functionalized substrates. The cell shape is strongly rounded and circular, and the cells possess only a small

contact area with the surface. A completely different picture presents itself on PPI-G4. Here, the cells have adapted a flat and elongated morphology with numerous filopodia, increasing their contact area with the underlying substrate.

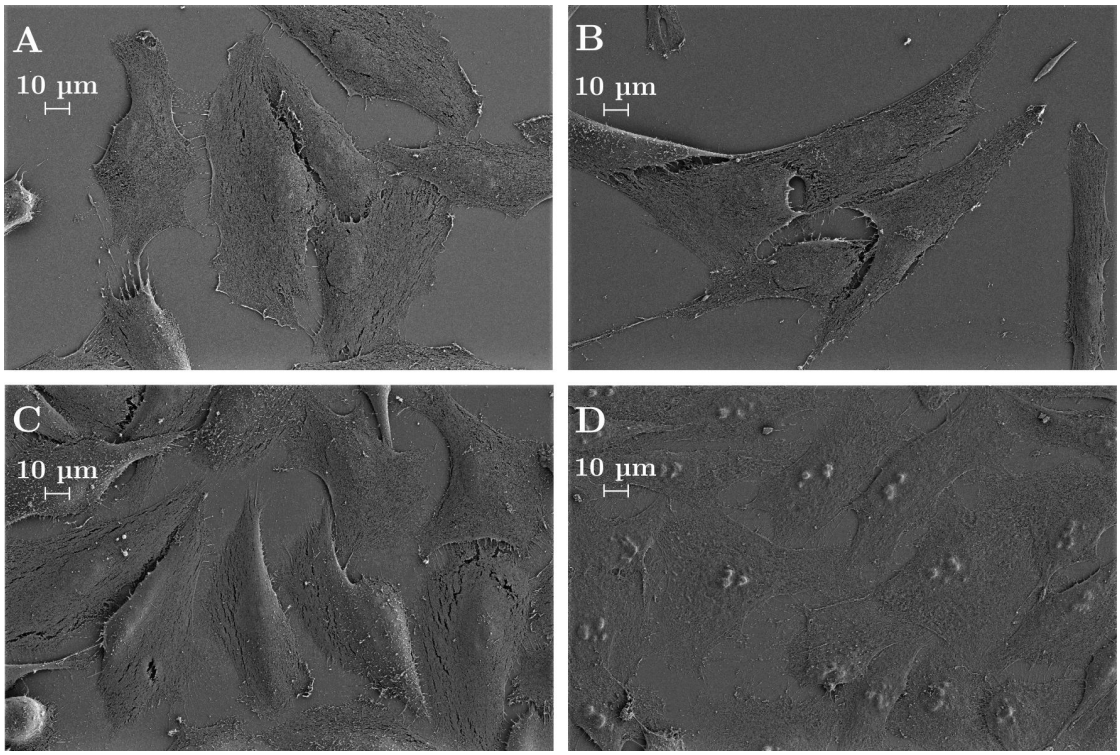

Figure 16.6: Analysis of the morphology of MG-63 cells after 24 h of incubation on (A) oxidized titanium substrates, (B) APD, (C) PPI-G4 or (D) PEI polymer coating from SEM images (bars = 10 µm).

Longer cultivation times lead to an assimilation of cell morphologies, as previously described for the cell areas. On oxidized titanium substrates, MG-63 cells exhibit their typical morphology. Thus, flat and polygonal cells can be observed [390]. The cells on PEI substrates possess a similar shape. They seemed to have flattened even more than those on bare titanium wafers as they can barely be distinguished in contrast against the substrate. The small convex structures, which can be observed, are probably the nucleoli, components of the nucleus, as these structures were identified in a very similar cell morphology on substrates with plasma-polymerized allylamine [391]. Similarly, Gruening et al. described elongated MG-63 cells with low circularity on unmodified or PEI polymer-coated Ti surfaces after 24 h [384]. On APD, the osteoblastic cells also possess an elongated shape. They, however, seem to be less flattened on the surface and exhibit less filopodia. Contrary to that, large, flattened and elongated cells with numerous filopodia are obtained on PPI-G4-functionalized substrates. As mentioned previously, these observations are in contrast to the results of Gruening et al. on PPI-G4-modified substrates [384]. Here, a retraction of the cells was observed, resulting in small and circular cells [384].

16.2.3 The Actin Cytoskeleton

The results obtained for cell area and morphology, derived from SEM images, can be supported by images of the actin cytoskeleton via confocal laser scanning microscopy. Exemplary CLSM images are summarized in Figure 16.7 and Figure 16.8, additional images are provided in the appendix (Figure VI.17 to VI.20).

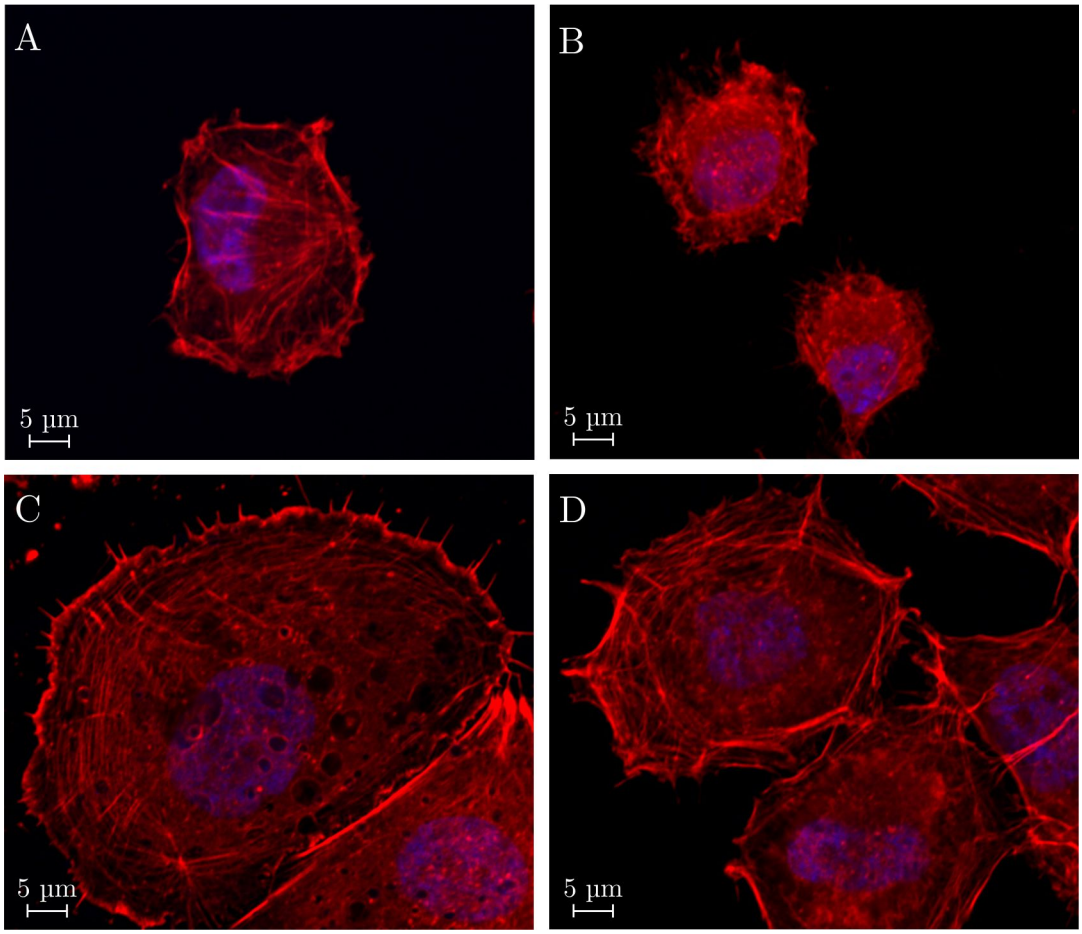

Figure 16.7: Actin cytoskeleton of MG-63 cells after 1 h of cultivation on (A) oxidized titanium substrates, (B) APD, (C) PPI-G4 or (D) PEI polymer coating, obtained via CLSM (red: actin, blue: nucleus, bars = 5 µm).

After 1 h of cultivation on oxidized titanium substrates or PEI polymer-coated surfaces, the cells have formed actin filaments in the cortical area and fine fibers in the cell body. On APD-functionalized substrates, only a diffuse distribution of actin can be found. In contrast to that, MG-63 cells on PPI-G4 have not only developed actin microfilaments in the cortical area and the filopodia but also thin fibers throughout the cell body.

After 24 h, the differences in cytoskeleton organization among the cells on different surface coatings are strongly reduced. The osteoblasts on the reference titanium substrate exhibit a strongly developed actin cytoskeleton with actin filaments in the cortical area and stress fibers spanning through the cell.

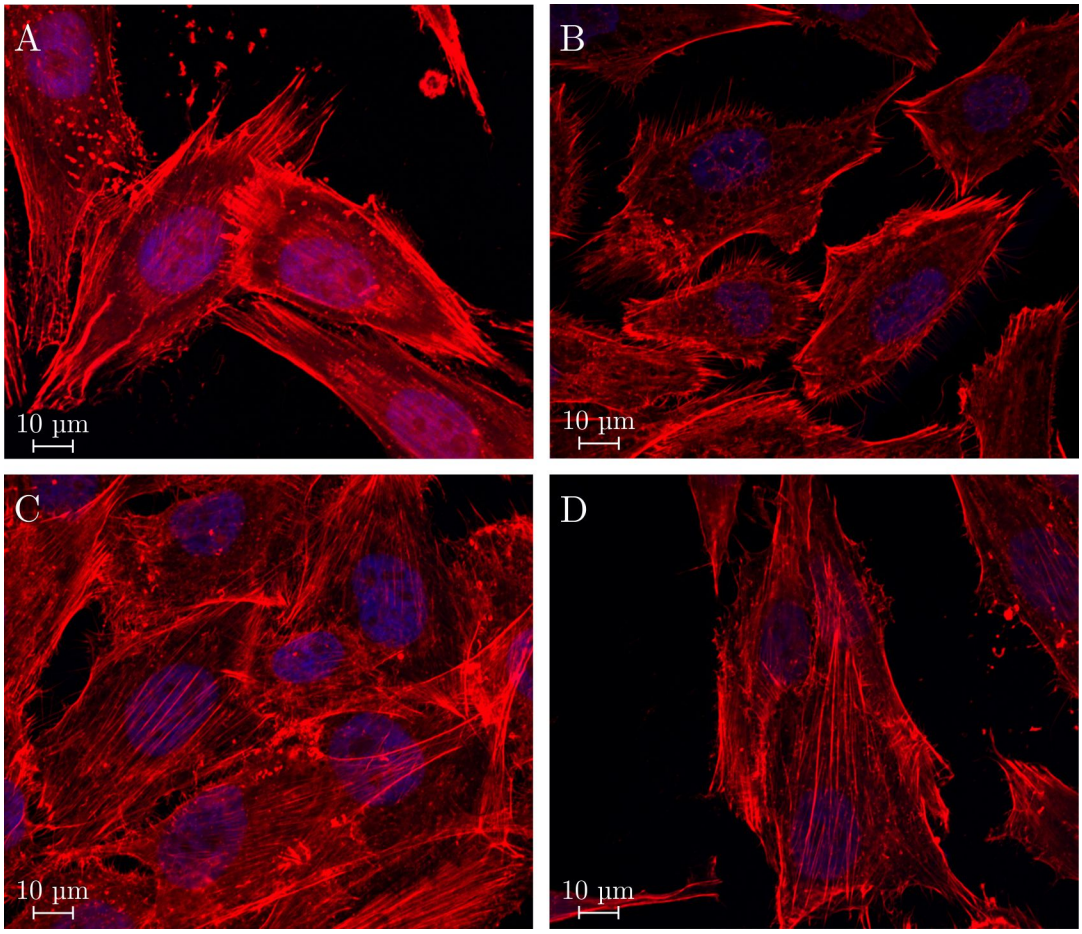

Figure 16.8: Actin cytoskeleton of MG-63 cells after 24 h of cultivation on (A) oxidized titanium substrates, (B) APD, (C) PPI-G4 or (D) PEI polymer coating, obtained via CLSM (red: actin, blue: nucleus, bars = 10 µm).

An almost identical situation is observed for the cells on PEI polymer-coated substrates. On APD-functionalized surfaces, the cells organize actin filaments in the cortical area, but only less strongly developed stress fibers are visible in the cell body. In MG-63 osteoblasts on PPI-G4 surfaces, actin is strongly present in the cortical area and organized in stress fibers spanning the entire cell body.

16.2.4 Cell Cycle, Proliferation and Apoptosis

From the measurements by flow cytometry after cultivation for 24 h, cell cycle analysis of the MG-63 cells on the different surface coatings was performed. The portion of proliferative cells was calculated as the sum of cells in S phase or G2/M-phase, the percentage of apoptotic cells was obtained from cytometric data as well. The results are summarized in Figures 16.9 and 16.10.

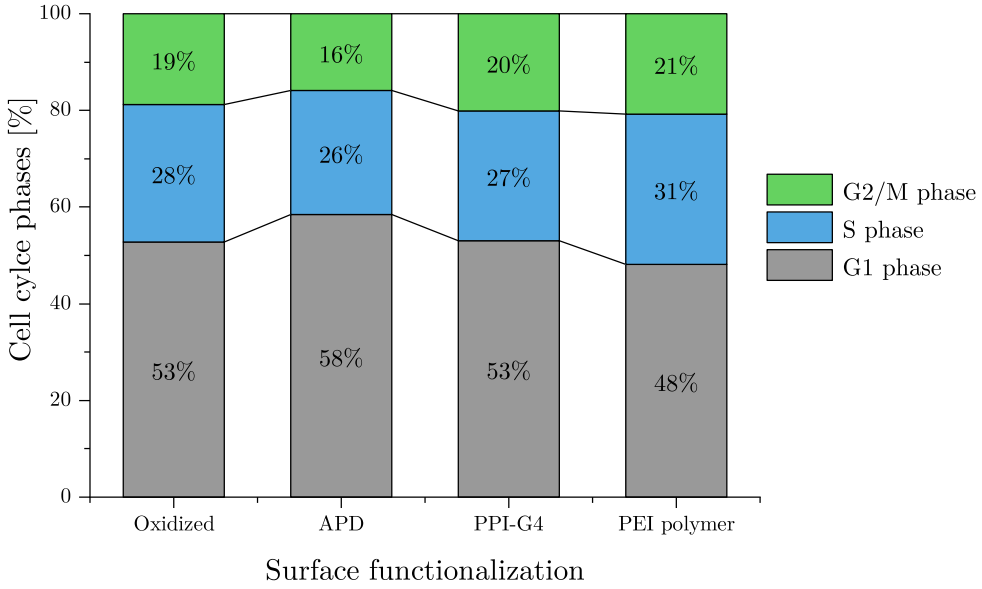

Figure 16.9: Cell cylce phases of osteoblast-like MG-63 cells on differently functionalized titanium substrates.

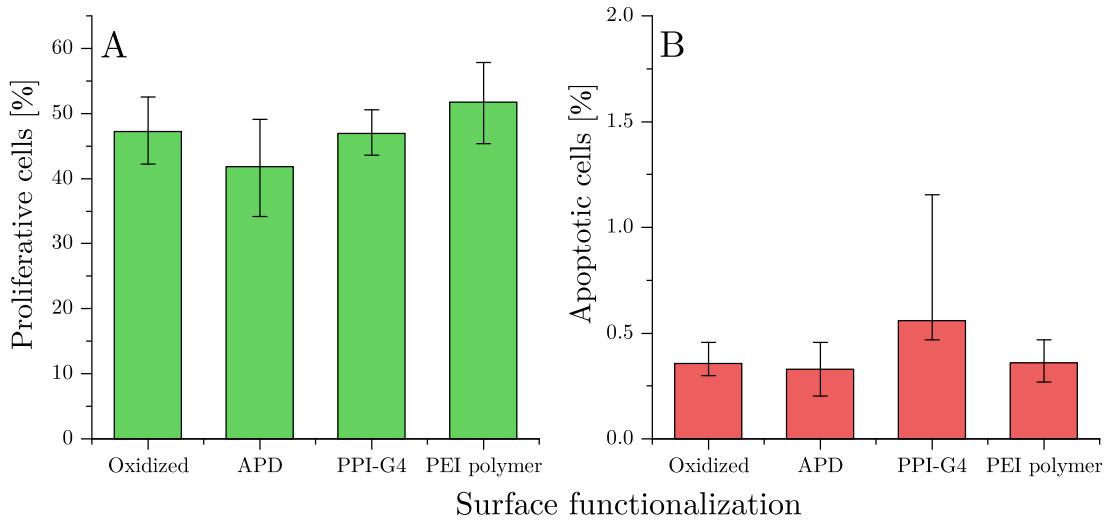

Figure 16.10: Percentage of (A) proliferative and (B) apoptotic MG-63 cells on differently functionalized titanium substrates, as obtained from cytometric measurements (Statistics: Mann-Whitney-U-Test not significant with $^*p < 0.05$).

As it can be seen there, no big differences can be observed among cells on different surface coatings. It can, however, be noted that the portion of non-proliferative cells in G1 phase is slightly larger for cells on APD-covered substrates in comparison to osteoblasts on titanium, whereas a slightly increased fraction of proliferative cells can be observed for the PEI polymer coating.

The percentage of apoptotic cells is below 1% for all surface modifications, although a slight increase in apoptosis can be observed for cells on PPI-G4-modified substrates.

In summary, large differences in cell behavior can be observed among the different surface coatings after 1 h of cultivation. Osteoblast cells on PPI-G4-covered surfaces are characterized by strong spreading, large surface areas and a typical cell morphology. In contrast to that, the APD modification seems to hinder cell attachment and spreading, leading to impaired cell morphologies and small cell areas. Cells on PEI-functionalized surfaces do not differ significantly from those on the reference titanium substrate.
After 24 h, the differences have decreased significantly or disappeared completely. On all surfaces, elongated cells with similar cell areas and strongly developed actin cytoskeletons can be observed. In accordance with that, only minor differences are obtained for the percentage of proliferative or apoptotic cells from cell cycle analysis.

16.2.5 Dependence of Cell Behavior on Surface Properties

The observed differences in cell behavior on the three modified substrates are the consequence of differences in surface properties of those coatings. Thus, their influence on cell adhesion and morphology is discussed and compared to previously conducted research in the following.

Influence of Surface Topography and Rigidity

Osteoblasts are sensitive to surface roughness and are able to detect topographical features in the nanometer regime (> 10 nm) [11]. No data, however, is available about the topographical properties of the examined surface modifications themselves. Yet, the size of PPI dendrimers up to generation 8 in solution was examined by Gupta and Biswas, who obtained radii of gyration below 3 nm from molecular dynamics simulation studies [77]. Surface immobilized PAMAM dendrimers of generation 5 have been studied via AFM by Eichler et al. [19]. Here, roughness parameters smaller than 2 nm were observed. Therefore, it can be assumed that the surface coatings examined in this thesis do not exhibit a roughness perceptible to the cells, and thus surface topography may not influence cell behavior. Further analysis of the coatings, e.g. via AFM, is nevertheless recommendable.
Surface rigidity and flexibility are known to affect cell behavior as well, as cells, for instance, adhere better on stiffer substrates [212]. In this context, however, gels with varying macroscopic properties (e.g. modulus of elasticity) have been examined [212]. Regarding the different modifications studied in this thesis, the results of the dynamic contact angle measurements suggest a higher flexibility of surface-immobilized PPI-G4 and PEI polymer than APD on a molecular level. It is unclear, however, if these differences can be sensed by the osteoblasts directly or indirectly (via the reduced protein adsorption on PEI polymer coatings) and if they influence cell behavior.

Effect of Surface Wettability and Surface Free Energy

Many studies have examined the influence of surface hydrophilicity on cell behavior. In general, cells were found to adhere better to hydrophilic than to hydrophobic surfaces [12, 213]. The best results were obtained with moderately hydrophilic surfaces [212]. Faucheux et al., for instance, observed the strongest attachment and best spreading of fibroblasts on self-assembled monolayers with terminal -COOH or -NH_2 groups, exhibiting water contact angles between 48° and 62° [220]. Maximized adhesion of human mesenchymal stem cells was observed on self-assembled monolayers with water contact angles of 40° to 70° [392]. A surface coating of plasma-polymerized allylamine with a contact angle of 57° was the only one able to support the adhesion of osteoblasts in such a way that the cells could overcome topographical restrictions [393].

The surface coatings studied in this thesis all show a more hydrophilic behavior below the 40° threshold on the titanium substrates. It, however, is worth mentioning that the PPI dendrimer coating, which leads to the best initial cell response, exhibits a contact angle of 32°, approximately 10° higher than those of the other surface coatings (23° and 20° respectively). Thus, the more hydrophilic behavior of the APD or PEI polymer coating might contribute to an impeded cell adhesion.

Almost identical apparent surface free energies were obtained for the three surface coatings with polar components of approximately $7\,\mathrm{mN\,m^{-1}}$ and total surface free energies of roughly $55\,\mathrm{mN\,m^{-1}}$, which are comparably high with respect to the SFEs of polymeric surfaces (usually 5 to $50\,\mathrm{mN\,m^{-1}}$) [29]. In previous research, improved cell behavior was usually observed on surfaces with higher surface free energies, in many cases following a sigmoidal behavior. Van der Valk et al., for example, investigated the spreading of mouse lung fibroblasts on different polymer surfaces [394]. They observed a stark increase in cell spreading on surfaces with a SFE of at least $40\,\mathrm{mN\,m^{-1}}$ [394]. Similarly, Lim et al. found that cell attachment and proliferation of human fetal osteoblastic cells strongly correlated with surface free energy and were strongly enhanced on surfaces with high SFEs ($> 40\,\mathrm{mN\,m^{-1}}$) [395]. Therefore, the SFEs of APD, PPI-G4 and PEI polymer-functionalized surfaces are also in the cell-adhesive range and can be expected to promote osteoblast adhesion and spreading. The differences observed in cell behavior are thus caused by other surface characteristics overruling the positive effect of the high surface free energy.

Influence of the Surface Functional Groups

In contrast to the previous surface characteristics, such as contact angle and SFE, which are rather similar among the studied surface modifications, the coatings differ drastically with respect to the density of functional groups. The density of primary and secondary amine groups has only been determined on functionalized silica beads with the sulfo-SDTB assay (see section 14.2.2). Functionalization of surfaces with the PPI-G4 dendrimer led to a significantly higher density of amine groups ($\approx 3800\,\mathrm{nmol\,m^{-2}}$) than modifications with APD or PEI polymer ($\approx 500\,\mathrm{nmol\,m^{-2}}$ and $\approx 700\,\mathrm{nmol\,m^{-2}}$ respectively).

A positive effect of surface amine groups on cell behavior has also been observed in a variety of other studies. Faucheux et al., for example, found that human fibroblasts spread and grew best on self-assembled monolayers with terminal -COOH or -NH_2 groups in comparison with SAMs carrying -CH_3, PEG or -OH groups [220]. Additionally, the best initial cell adhesion (after 2 h) was observed on the amine-functionalized surfaces [220]. In a study by Lee et al., K100 erythroleukemia cells were found to adhere most strongly to an amine SAM in comparison with functionalizations with epoxide, carboxylic acid or methyl groups [56]. Modification of surfaces with a plasma polymer containing amino groups was shown to positively affect every stage of cell-surface interactions, i.e. enhancing adhesion, spreading, proliferation and gene expression of MG-63 cells [221]. Especially cell adhesion was increased, compared to uncoated titanium, tissue culture plastic, and even collagen I-coated petri dishes [221]. In this context, the superior performance of PPI-G4-functionalized surfaces can be explained with the high density of amine groups presented by the surface coating.

Effect of Surface Charge

The advantageous properties of surfaces functionalized with amine groups have in many cases been related to a positive zeta potential, which is known to positively influence cell behavior [12, 212]. Plasma-polymerized allylamine, for example, led to very good results in cell experiments with osteoblast-like MG-63 cells because it supported focal adhesion formation and cytoskeleton development [31], enhanced viability [396] and promoted gene expression [221]. This functionalization even was the only one able to override the guiding effect of surface microgrooves [393]. In those various studies, the zeta potential of this plasma polymer was found to be moderately positive (+8.6 mV [396], +9 mV [221] or +8.6 mV [393]).
The positive effect of these surface coatings with moderately positive charges is probably based on the interaction with pericellular hyaluronan, facilitating cell adhesion [31].

This high molecular weight glycosaminoglycan is highly negatively charged and has been shown to mediate the early stages of cell-surface interactions [31, 218, 397]. The pericellular coat of MG-63 cells, containing hyaluronic acids, renders the cell surface negatively charged. An overall zeta potential of −15.6 mV was obtained for suspended cells [398], which allows attractive electrostatic interactions with positively charged surface groups.

Contradictory results, however, have been obtained with relation to the ideal magnitude of those positive surface charges. In this thesis, enhanced initial adhesion and spreading is observed on the PPI-G4 surface with a strongly positive zeta potential at pH 7.4 of +50 mV. The modification with PEI polymer, bearing a slightly positive charge (+9 mV), behaves very similar to the reference titanium surface, whereas reduced cell adhesion and initial spreading is obtained for the APD modification (−47 mV). In some studies, similar results were observed. Guo et al. investigated the adhesion of fibroblasts on surfaces with different wettabilities and zeta potentials [219]. They obtained the highest cell adhesion on one of the substrates with an IEP > 9 [219].

Differing or even opposing results were obtained by a large number of other researchers, who found that surfaces with highly positive charges often negatively affect cell behavior. Guo et al., for instance, observed higher initial adhesion of fibroblast cells to polyelectrolyte multilayers with an IEP > 9 but decreased cell proliferation after the first day in comparison with negatively charged surfaces [399]. A surface with poly(diallyldimethylammonium chloride) (polyDADMAC), exhibiting a positive zeta potential of +50 mV, supported the initial spreading of osteoblastic MG-63 cells (after 1 h), but after prolonged cultivation times (3 h, 12 h and 24 h), the cells significantly retracted from the surface, leading to a reduced cell area [400]. Interestingly, the adverse effects of strongly positively charged surfaces were confirmed in another study by Gruening et al. [384]. Here, both the polyDADMAC as well as a PPI-G4 modification, identical to the one in this thesis, negatively affected osteoblast behavior in multiple ways. They observed an impaired rounded cell morphology, cell retraction and reduced cell areas [384]. In addition to that, both cell viability and proliferation were reduced in comparison with the titanium reference substrate [384].

Role of Adsorbed Proteins in Cell Behavior

As already briefly discussed in section 5.2.1, the topographical and chemical properties of the surface do not only influence the reaction of cells directly, but to a large extent, they govern cell behavior via a mediating layer of adsorbed proteins [11, 12, 220]. In this context, the effect of surface precoating with proteins on the outcome

and interpretation of the cell experiments has to be discussed. It was, for instance, observed by Staehlke et al. that serum precoating of substrates with PAMAM dendrimers with varying endgroups reduced the differences in cell spreading among the modifications [20]. In contrast to that, almost no effect of protein precoating was visible for mouse fibroblasts and MG-63 cells on various self-assembled monolayers [15].

As the substrates of this thesis were precoated with FBS, the effect of protein adsorption on the results of the cell biological investigations has to be considered. The attachment of serum proteins may serve as a further explanation for the excellent performance of the PPI-G4 surface in initial adhesion and spreading tests. As stated previously, especially the preferential adhesion of fibronectin and vitronectin in an active conformation is very beneficial for osteoblast attachment [12]. It was observed by Kikuchi et al. that the adsorption of both proteins increased with increasing polyamine content of a polystyrene-*graft*-polyamine copolymer [401]. Shelton et al. discovered that fibronectin preferentially adsorbed on positively charged surfaces [350]. Thus, as both proteins can also be found in bovine serum [402], it is possible that these adhesive proteins are accumulated on the PPI-G4 surface and promote initial cell adhesion. This assumption can neither be confirmed nor confuted with the results of the BCA assay on the amine-functionalized surfaces because only the total amount of adsorbed proteins was quantified that way (see section 14.4). On the one hand, it can be seen there that large amounts of albumin adhere to the surface with PPI-G4 coating. Pretreatment of surfaces with denatured BSA has been shown to significantly reduce the adhesion of K100 erythroleukemia cells [56]. On the other hand, past studies have proven that fibronectin and vitronectin are preferentially adsorbed, even in the presence of an excess of albumin [403]. The precoating of the functionalized wafers, performed in the experiments of this thesis, thus probably has an effect on the cell behavior and can possibly explain the differences to the results obtained by Gruening et al. [384], who did not pretreat the specimens with protein solution.

Influence of the Intrinsic Toxicity of the Immobilized Molecules

As mentioned previously, the molecules used for the surface modifications have been suspected and confirmed to exhibit cytotoxic properties in solution. Thus, it is necessary to evaluate if and how this toxicity is experienced by cells if the molecules are covalently immobilized on a surface.

At first, the APD molecule strongly resembles the naturally occurring polyamine spermine [404], for which interesting results have been obtained in *in vitro* toxicity experiments. In combination with ruminant serum, cytostatic and cytotoxic effects were observed for spermine [405, 406]. These results can be explained by the presence

of an enzyme in the sera, the copper-containing bovine serum amine oxidase (E.C. 1.3.2.6). The oxidation of the polyamine here leads to the formation of aldehydes and hydrogen peroxide, negatively affecting cell behavior [405, 406]. In this thesis, wafer substrates were exposed to FBS, prior to the cell adhesion experiments. Thus, it is possible that the APD surface coating was altered due to enzymatic oxidation, leading to unfavorable cell-surface interactions. Therefore, the poor performance of the APD coating regarding cell spreading and morphology after 1 h may not only be an effect of the overall negative zeta potential but also of the change of surface functionalities.

The toxicity of PPI dendrimers on cells [407] and in *in vivo* applications [80] has already partially been described previously in section 3.1.4. The experiments in this thesis, however, indicate different results. After 1 h of cultivation, a strongly increased cell spreading is observed. After 24 h, strongly spread MG-63 cells, exhibiting a well-developed actin cytoskeleton, are obtained. As mentioned previously, these results present a stark contrast to the data observed by Gruening et al. [384]. In their experiments, cells on PPI-G4-modified surfaces showed an impaired morphology as well as reduced viability [384]. From their results, it can be hypothesized that highly positive surface charges interact so strongly with the cell membrane that the membrane integrity is compromised. This is also suggested by the observation that positively charged dendrimers were able to disrupt model membranes, forming dendrimer-filled lipid vesicles and leaving holes in the membranes [408]. Interestingly, however, no such membrane-disruptive properties were observed for the same PAMAM dendrimer with surface amine groups after surface immobilization, i.e. this coating did not show adverse effects on cell behavior even after 24 h [20]. Therefore, it can be stated that the effect of surface-immobilized dendrimers with positively charged functional groups on cells is not fully understood and requires further research.

A situation similar to the one of PPI dendrimers is observed for the PEI polymer. Cytotoxic effects of PEI polymers in solution have been described previously [100], although lower cytotoxicity was observed for linear PEI polymers [105] (see also section 3.2.2). The experiments on cell behavior on PEI polymer-modified substrates in this thesis do not suggest cytotoxic effects of the surface coating. Cell spreading and cytoskeleton development after 1 h and 24 h are very similar to the data obtained on the unmodified titanium substrates. No significant changes in the cell cycle or enhanced apoptosis rates are observed. In literature, however, ambiguous results can be found for the effect of surface-immobilized PEI polymer on cell behavior. No cytotoxicity on fibroblasts was observed by Hernandez-Montelongo et al. for up to 7 days [409], whereas in a study by Brunot et al., a PEI surface layer reduced fibroblast and osteoblast adhesion and

proliferation [410]. The opposite influence of PEI polymer was found by Liu et al. because, in that case, PEI polymer coating drastically increased cell adhesion, proliferation, viability and function [411]. Similarly, Gruening et al. observed an improved mobilization of the secondary messenger Ca^{2+} in MG-63 cells on PEI polymer surfaces, i.e. the cells exhibited improved cell function [384, 396]. Comparison and analysis of these strongly differing studies, however, are very difficult as crucial information about the PEI polymer (size, branching) and the resulting surface (such as zeta potential) are often lacking. Thus, more systematic research is necessary in order to fully understand the effect of surface-immobilized PEI polymer on cell behavior.

Part V

Conclusion and Outlook

Biomaterials are indispensable in the medical field for the support or replacement of the function of various tissues or organs. The performance of these materials, especially of implants, is determined by the "race for the surface", a competition between bacteria and tissue cells for surface attachment. This event is largely influenced by the presence and composition of the initially adsorbed protein layer. Up to the present, however, the complex process of protein adsorption in a biological system is not yet fully understood, neither has the guiding effect of proteins on bacteria and cell attachment been completely revealed. Thus, further research is essential in order to improve the performance of biomaterials, particularly implants, in patients in the future.

Therefore, this thesis was aimed at supporting the development of surface coatings suitable for implant materials. In this context, the thesis was directed towards two different goals. At first, the relation between the physicochemical characteristics of surface coatings on the one hand and the interaction of those surfaces with proteins or cells on the other hand was examined in order to expand the knowledge of how biological systems react to surface properties. The second aim, more directed towards practical application, was to develop surface coatings which withstand unspecific protein adsorption and – ideally simultaneously – support adhesion and proliferation of tissue cells. The in-depth analysis of the surface modifications here always comprised three major aspects. At first, the successful synthesis of the desired coatings was confirmed on the different substrate geometries via appropriate methods, such as XPS, IR spectroscopy and sulfo-SDTB assay. In the second part, a detailed physicochemical characterization was carried out, analyzing static and dynamic wetting behavior as well as electrokinetic properties of the surfaces. At last, the interaction of these modifications with proteins or cells was investigated and interpreted.

In this thesis, three different groups of surfaces modifications have been studied, whose results will be summarized separately in the following.
In the first part, self-assembled monolayers with seven different functional moieties were studied in detail and compared to oxidized substrates (as well as intermediate SAMs). Data from physicochemical analysis showed that the coatings possessed strongly differing surface properties. As expected, very low hydrophilicities and SFEs were obtained for the SAMs with hydrocarbon and perfluorocarbon chains, whereas a very hydrophilic behavior was observed for the oxidized substrate. The zeta potentials, calculated from streaming current measurements, ranged from strongly negative (for the modification with sulfonic acid groups) to positive (for the coating with pyridinium groups) under physiological conditions. The differences in the surface modifications and their characteristics were demonstrated to strongly affect quantitative protein adsorption from

human saliva and human serum. Yet, the amounts of adsorbed protein could not be linked to single surface properties. With respect to the qualitative protein adsorption, investigated via SDS-PAGE and western blotting, differences could be observed between the results with saliva and with serum. The adsorption of serum proteins seemed to be mainly controlled by the abundance of the proteins in solution, whereas strongly differing surface-specific protein patterns were observed for salivary proteins. Only for a very small number of proteins, their adsorption behavior could be linked to the physicochemical properties of the surface, as seen for lysozyme, which adsorbed to negatively charged surfaces via attractive electrostatic interactions. For the majority of proteins, however, such relations could not be found, presumably because of complicated protein-protein interactions in those complex biofluids and on the surface.

The second chapter consisted of the detailed study of six different modifications with terminal amine groups but varying inner functional groups and differing structure, being short-chained oligomers, dendrimers or linear polymers. These functionalizations were found to possess similar, moderate hydrophilicities and surface free energies, but they differed with respect to their amine group density, flexibility and electrokinetic properties. It has to be pointed out that these coatings covered a wide range of zeta potentials under physiological conditions despite carrying basic amine groups. On these surfaces, quantitative protein adsorption was tested with single protein solutions as well as physiological fluids. Here, the coatings bearing linear polymers, especially the PEI polymer, exhibited protein-repellent properties. Combining physicochemical data with the results for protein adsorption, no correlation could be observed between adsorbed protein amounts and wetting properties. Protein adsorption, however, strongly depended on the amine group density and the surface zeta potential and was clearly ruled by electrostatic interactions.

Inspired by the protein-stabilizing effects of osmolytes in nature, it was attempted to synthesize novel surface coatings based on osmolyte motifs, namely sulfobetaine groups, TMAO and proline. Here, the first two modifications could be synthesized and analyzed thoroughly, whereas only very preliminary results are available for the proline-based coating. The sulfobetaine and amine oxide functionalization shared similar physicochemical characteristics, such as their hydrophilicity and their negative zeta potential under physiological conditions. In quantitative protein adsorption experiments with single proteins and physiological fluids, however, these coatings performed completely differently. Large amounts of protein were measured on the sulfobetaine coating, contradicting the protein-repellency reported for similar coatings in literature. In contrast to that, the amine oxide coating resisted protein adsorption.

Three amine-based modifications with differing structure, namely a short-chained oligomer (APD), a dendrimer (PPI-G4) and a linear polymer (PEI polymer), were tested even further in cell biological investigations. To that purpose, the functionalizations were immobilized on titanium-sputtered wafers. Despite the nanoroughness of these specimens, the coated surfaces exhibited properties similar to those obtained for flat silicon substrates. The modifications were hydrophilic, but they differed strongly in their zeta potential. On those surfaces, the behavior of osteoblastic MG-63 cells, i.e. the cell area, morphology, actin cytoskeleton organization and cell cycle, was investigated for up to 24 h. After short cultivation times (1 h), large differences could be observed among the modifications. On the oligomeric surface (APD), the cells displayed a reduced cell area and impaired morphology in comparison with unmodified titanium substrates. The PEI coating did not affect the cell behavior after 1 h, whereas drastically increased spreading was observed on the dendrimer coating (PPI-G4). These differences in cell behavior, however, strongly decreased with prolonged cultivation times (up to 24 h) and can be explained with the initial interaction between the substrate surface and the cells. The negative zeta potential of the oligomer coating APD disfavors cell attachment, whereas the strongly positive charge of the PPI dendrimer modification acts as a cell-adhesive. The PEI polymer coating, which exhibited a slightly positive zeta potential, did not improve cell behavior significantly but simultaneously showed a protein-repellent behavior. Thus, this material might be promising for *in vivo* applications.

The amplitude of data and results, obtained and analyzed in the course of this thesis, has shed light on novel surface functionalizations, their physicochemical properties and their interaction with proteins and cells. Nevertheless, in all parts of this research project, further investigations are recommendable. Regarding synthesis, the procedure for the functionalization of surfaces with proline moieties can be improved and refined, as already discussed earlier. In addition to that, the promising results for the amine oxide monolayer may be an incentive for the development of novel surface modifications bearing other osmolyte motifs.
The analysis of the resulting coatings can be broadened as well. Further information about the structure, topography and stiffness can, for instance, be gained from AFM measurements. Data about the stability of the modifications, especially under *in vivo* conditions, may be obtained from QCM measurements and complement the results.
With respect to the protein adsorption experiments, the quantification with the BCA assay performed on SAMs via two different procedures raised several questions. Further studies are recommendable in order to investigate how protein adsorption on the SAMs depends on temperature and if complete protein desorption can be achieved with the

applied procedure. On amine and osmolyte-based coatings, protein quantification can be supplemented by additional qualitative analysis via SDS-PAGE and immunoblotting, as it was performed with the group of self-assembled monolayers with different functional groups. This way, further insight can hopefully be gained into the relation between the composition of the layer of adsorbed proteins and the observed cell behavior. Additional information, for example about the kinetics and the reversibility of the adsorption process, can be obtained from QCM measurements as well. More sophisticated techniques, such as isothermal titration calorimetry (ITC), can provide an insight into the thermodynamics of protein adsorption.

Directing research more towards the application of surface coatings in the oral cavity, e.g. on dental implants, the interaction with living organisms must be studied more thoroughly. In order to determine which species would win the "race for the surface", cell attachment must be examined in more detail and must be complemented by bacterial adhesion studies. Comparative and competitive studies of the adhesion of bacteria and tissue cells are particularly recommendable on the monolayer surfaces with different functional groups, which have been shown to accumulate proteins, which are known to impact those processes *in vivo*, in order to determine how these proteins affect adhesion on the biomaterial surface. Cell experiments can be expanded by prolonging the observation time and monitoring the metabolic activity of the cells on the surface. This way, more information can, for instance, be gathered about the long-term behavior of osteoblastic cells on the PPI-G4 dendrimer coating, since the good cell spreading and proliferation obtained in this thesis contradicts results of other researchers observing cytotoxic effects of PPI-G4.

In summary, combining further physicochemical analysis, more detailed protein adsorption studies and expanded cell adhesion experiments with bacterial attachment studies will help continue the work of this thesis.

Part VI

Appendix

Protein Adsorption on SAMs

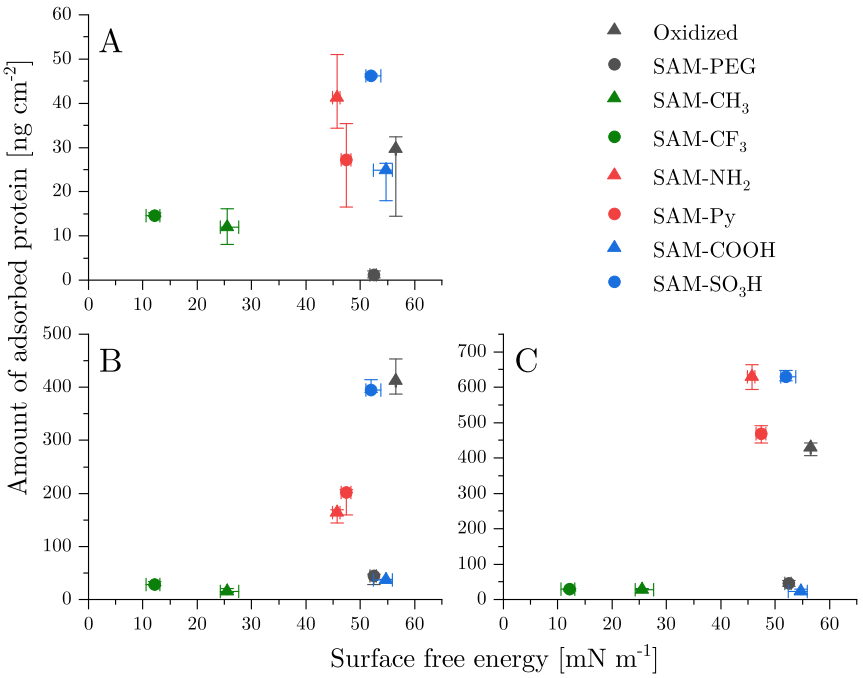

Figure VI.1: Dependence of the protein adsorption from (A) saliva or (B) FBS as well as (C) HABS on the surface free energy of the self-assembled monolayers. Protein adsorption was determined on the surfaces via BCA assay.

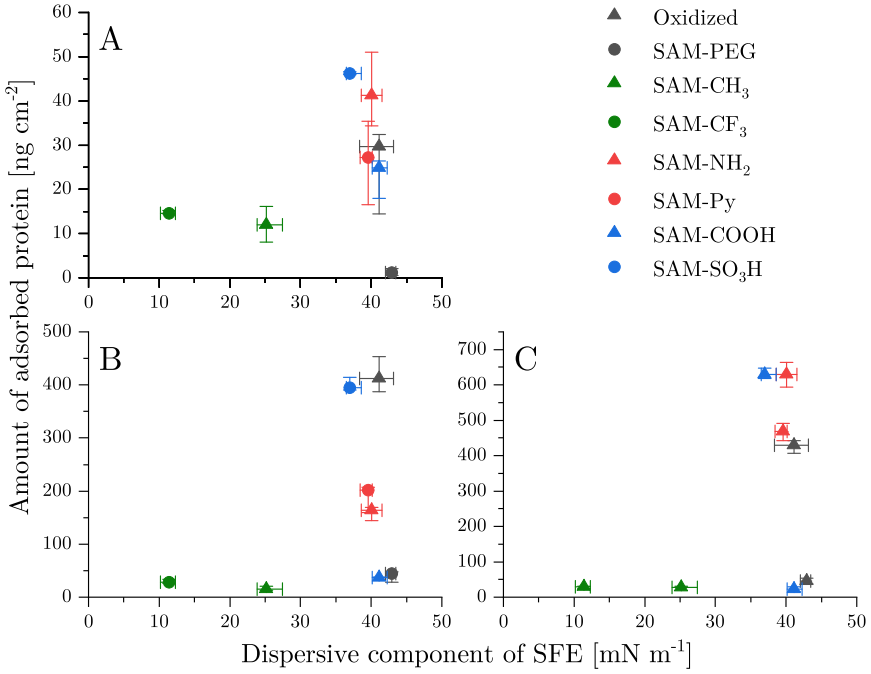

Figure VI.2: Dependence of the protein adsorption from (A) saliva or (B) FBS as well as (C) HABS on the dispersive component of the SFE of the self-assembled monolayers. Protein adsorption was determined on the surfaces via BCA assay.

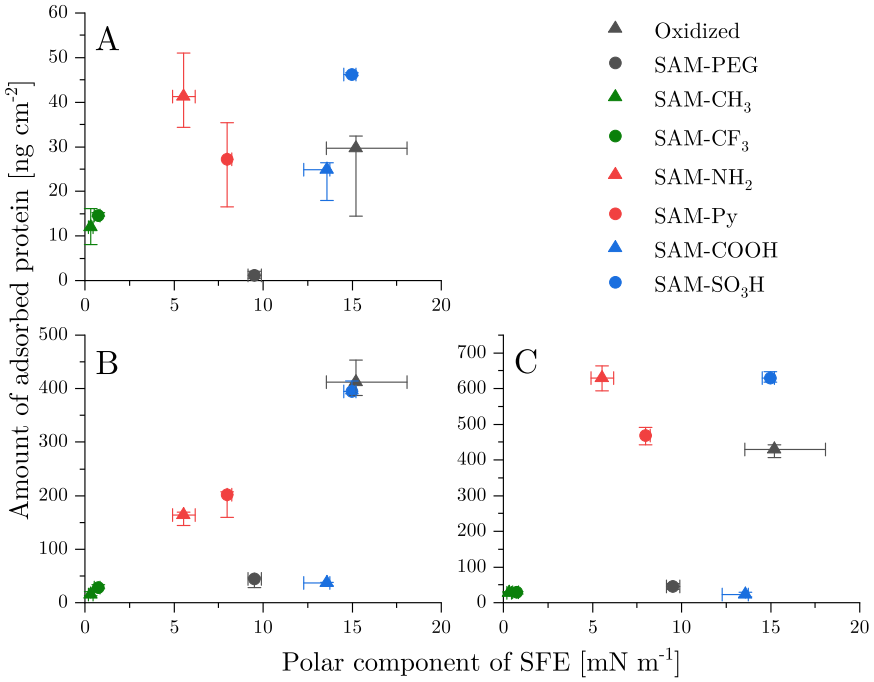

Figure VI.3: Dependence of the protein adsorption from (A) saliva or (B) FBS as well as (C) HABS on the polar component of the SFE of the self-assembled monolayers. Protein adsorption was determined on the surfaces via BCA assay.

Tensiometric Measurements

Table VI.1: Survey of the dynamic contact angles obtained from tensiometric measurements with sf-water and PBS buffer of amine-based functionalizations and their precursor SAMs. Advancing and receding angles are provided for the cycles 1, 2, 5 and 10.

		Advancing contact angle [°]				Receding contact angle [°]			
		1st cycle	2nd cycle	5th cycle	10th cycle	1st cycle	2nd cycle	5th cycle	10th cycle
Oxidized	Water	17 (16-19)	12 (9-16)	8 (8-9)	14 (11-18)	4 (1-4)	4 (1-4)	2 (0-4)	0 (0-2)
	PBS	12 (11-17)	0 (0-0)	0 (0-0)	0 (0-0)	4 (2-5)	4 (1-4)	2 (1-3)	0 (0-2)
TESPSA	Water	80 (79-81)	77 (76-77)	72 (71-72)	68 (66-69)	38 (37-38)	36 (35-37)	32 (32-33)	28 (28-29)
	PBS	79 (78-80)	54 (53-56)	30 (29-30)	31 (28-35)	4 (1-6)	7 (5-8)	10 (9-10)	9 (9-9)
APD	Water	58 (57-60)	45 (41-49)	44 (43-44)	44 (43-44)	8 (7-10)	9 (8-9)	8 (7-9)	8 (7-10)
	PBS	59 (57-61)	33 (31-35)	32 (32-33)	31 (31-32)	7 (6-8)	8 (8-8)	9 (9-9)	9 (8-10)
PPI-G2	Water	60 (59-63)	59 (57-63)	66 (57-70)	70 (62-77)	3 (2-3)	4 (3-6)	6 (5-6)	6 (5-9)
	PBS	58 (53-63)	48 (44-53)	47 (42-52)	47 (43-51)	7 (5-9)	6 (4-9)	6 (4-8)	6 (3-8)
PPI-G4	Water	65 (64-67)	62 (57-63)	72 (67-79)	80 (73-85)	2 (0-4)	1 (0-3)	3 (1-5)	4 (1-5)
	PBS	61 (60-62)	54 (47-56)	53 (49-56)	54 (52-57)	7 (6-8)	7 (6-7)	6 (6-7)	6 (6-7)
SAM-COOH	Water	54 (54-56)	50 (50-52)	49 (49-50)	49 (49-51)	28 (27-29)	28 (26-29)	27 (26-28)	26 (25-27)
	PBS	43 (37-48)	28 (27-28)	27 (25-29)	26 (23-27)	4 (2-5)	5 (2-5)	4 (1-5)	2 (0-4)
PAMAM polymer	Water	36 (35-37)	36 (33-41)	42 (40-46)	49 (44-56)	4 (4-5)	4 (3-5)	4 (3-4)	3 (1-4)
	PBS	32 (31-33)	30 (29-33)	30 (29-33)	30 (29-32)	11 (9-12)	10 (9-12)	11 (9-12)	11 (9-12)
PEI polymer	Water	57 (57-58)	64 (60-70)	71 (66-74)	73 (67-77)	6 (5-6)	7 (6-10)	8 (6-12)	8 (6-14)
	PBS	53 (52-58)	46 (45-46)	46 (45-47)	47 (46-48)	8 (7-9)	8 (7-9)	8 (7-9)	8 (7-9)
SAM-NH_2	Water	80 (77-82)	76 (75-78)	75 (74-77)	74 (73-76)	26 (19-34)	25 (18-33)	23 (19-32)	22 (19-31)
	PBS	77 (75-81)	72 (70-74)	68 (67-72)	68 (67-71)	22 (15-27)	21 (14-25)	19 (14-22)	18 (14-21)
AMAM	Water	79 (78-81)	76 (75-78)	75 (72-75)	72 (69-73)	30 (27-38)	29 (25-36)	28 (24-33)	26 (22-29)
	PBS	78 (77-80)	75 (73-77)	72 (70-72)	71 (68-72)	37 (36-39)	36 (35-38)	35 (34-37)	33 (32-35)

Table VI.2: Survey of the dynamic contact angles obtained from tensiometric measurements with sf-water and PBS buffer of osmolyte-based coatings and their precursor SAMs. Advancing and receding angles are provided for the cycles 1, 2, 5 and 10.

		Advancing contact angle [°]				Receding contact angle [°]			
		1st cycle	2nd cycle	5th cycle	10th cycle	1st cycle	2nd cycle	5th cycle	10th cycle
$SAM\text{-}NH_2$	Water	80 (77-82)	76 (75-78)	75 (74-77)	74 (73-76)	26 (19-34)	25 (18-33)	23 (19-32)	22 (19-31)
	PBS	77 (75-81)	72 (70-74)	68 (67-72)	68 (67-71)	22 (15-27)	21 (14-25)	19 (14-22)	18 (14-21)
DMAPS	Water	68 (66-71)	56 (50-59)	53 (47-56)	51 (45-53)	4 (2-5)	4 (2-5)	2 (0-5)	1 (0-4)
	PBS	61 (60-64)	18 (16-23)	40 (22-45)	34 (17-39)	4 (2-6)	4 (2-6)	4 (2-5)	3 (0-5)
$SAM\text{-}NMe_2$	Water	31 (25-32)	55 (54-64)	55 (53-60)	59 (56-62)	13 (10-16)	9 (8-12)	3 (0-7)	2 (0-6)
	PBS	27 (23-27)	36 (34-38)	33 (31-34)	31 (29-32)	10 (8-12)	9 (7-10)	9 (7-10)	10 (8-12)
SAM-NO	Water	43 (33-47)	53 (53-57)	53 (52-55)	55 (48-59)	5 (5-6)	6 (5-6)	5 (3-6)	5 (3-6)
	PBS	36 (35-38)	26 (22-28)	20 (14-25)	12 (1-25)	6 (5-7)	6 (4-6)	4 (2-5)	2 (0-5)

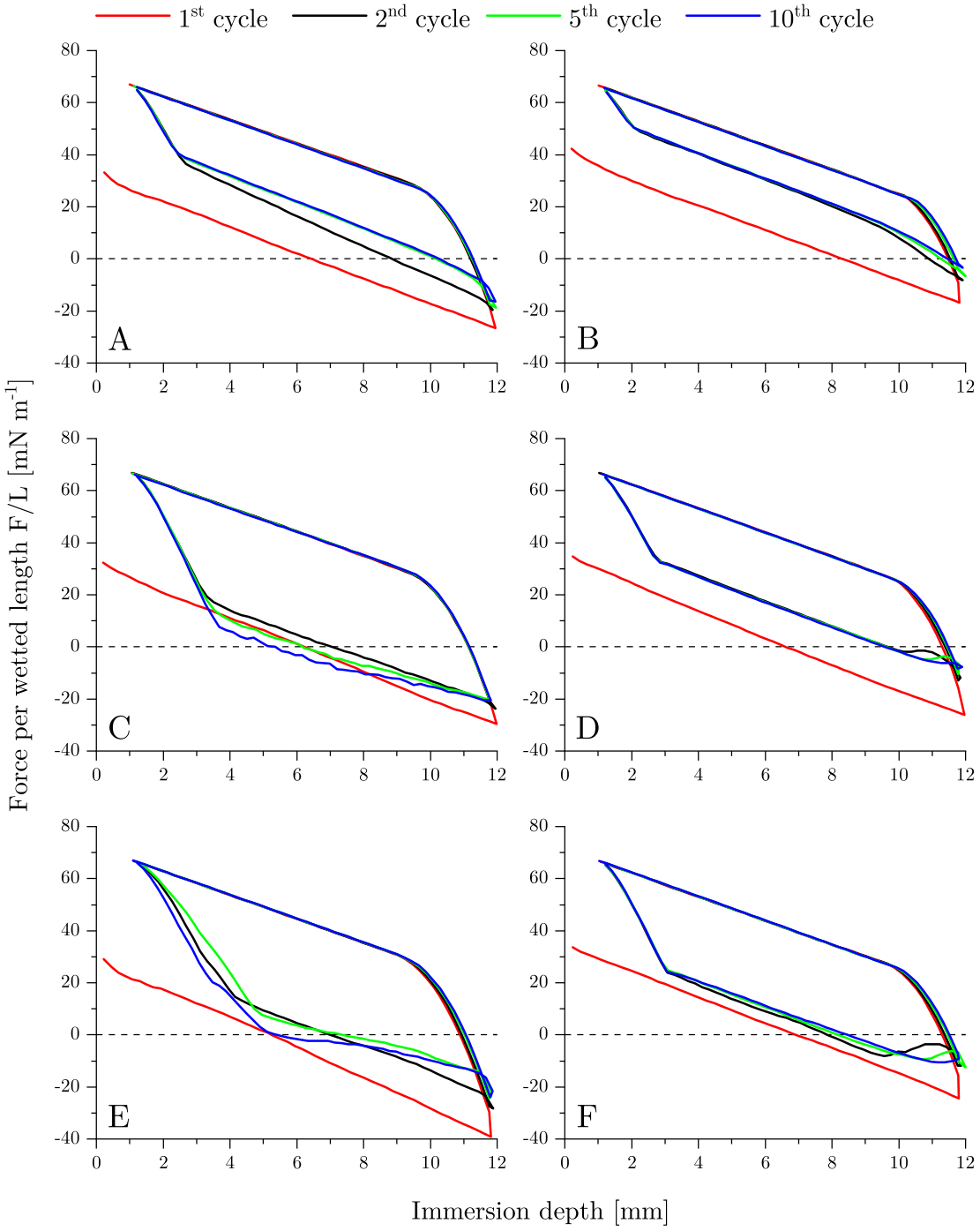

Figure VI.4: Force-immersion cycles of dynamic contact angle measurements of functionalized silicon wafers with water (left) or PBS (right). Force-distance loops of the 1st, 2nd, 5th and 10th cycle are depicted for (A) APD – sf-water, (B) APD – PBS, (C) PPI-G2 – sf-water, (D) PPI-G2 – PBS, (E) PPI-G4 – sf-water and (F) PPI-G4 – PBS.

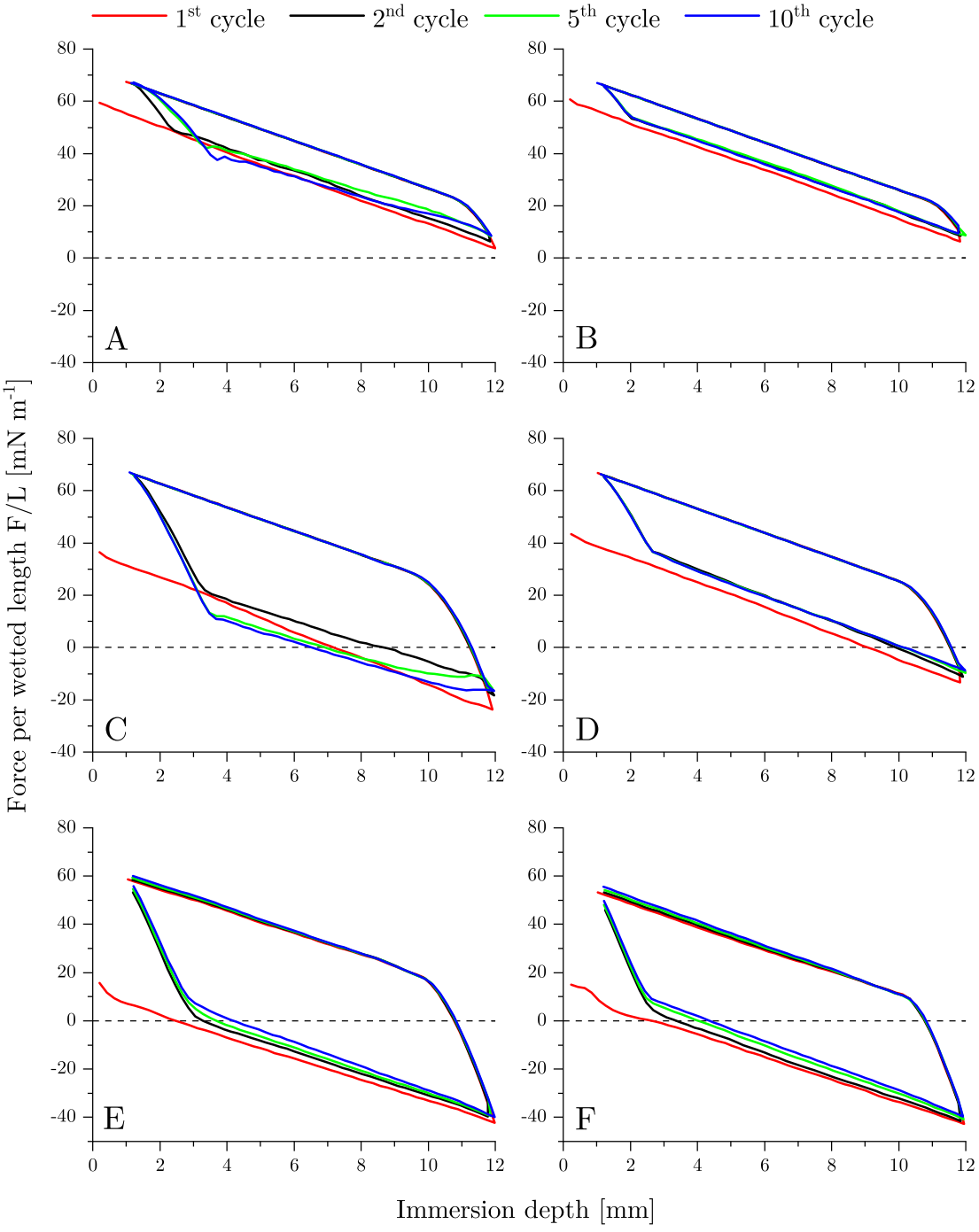

Figure VI.5: Force-immersion cycles of dynamic contact angle measurements of functionalized silicon wafers with water (left) or PBS (right). Force-distance loops of the 1st, 2nd, 5th and 10th cycle are depicted for (A) PAMAM polymer – sf-water, (B) PAMAM polymer – PBS, (C) PEI polymer – sf-water, (D) PEI polymer – PBS, (E) AMAM – sf-water and (F) AMAM – PBS. Note the different y-axis in diagrams (E) and (F).

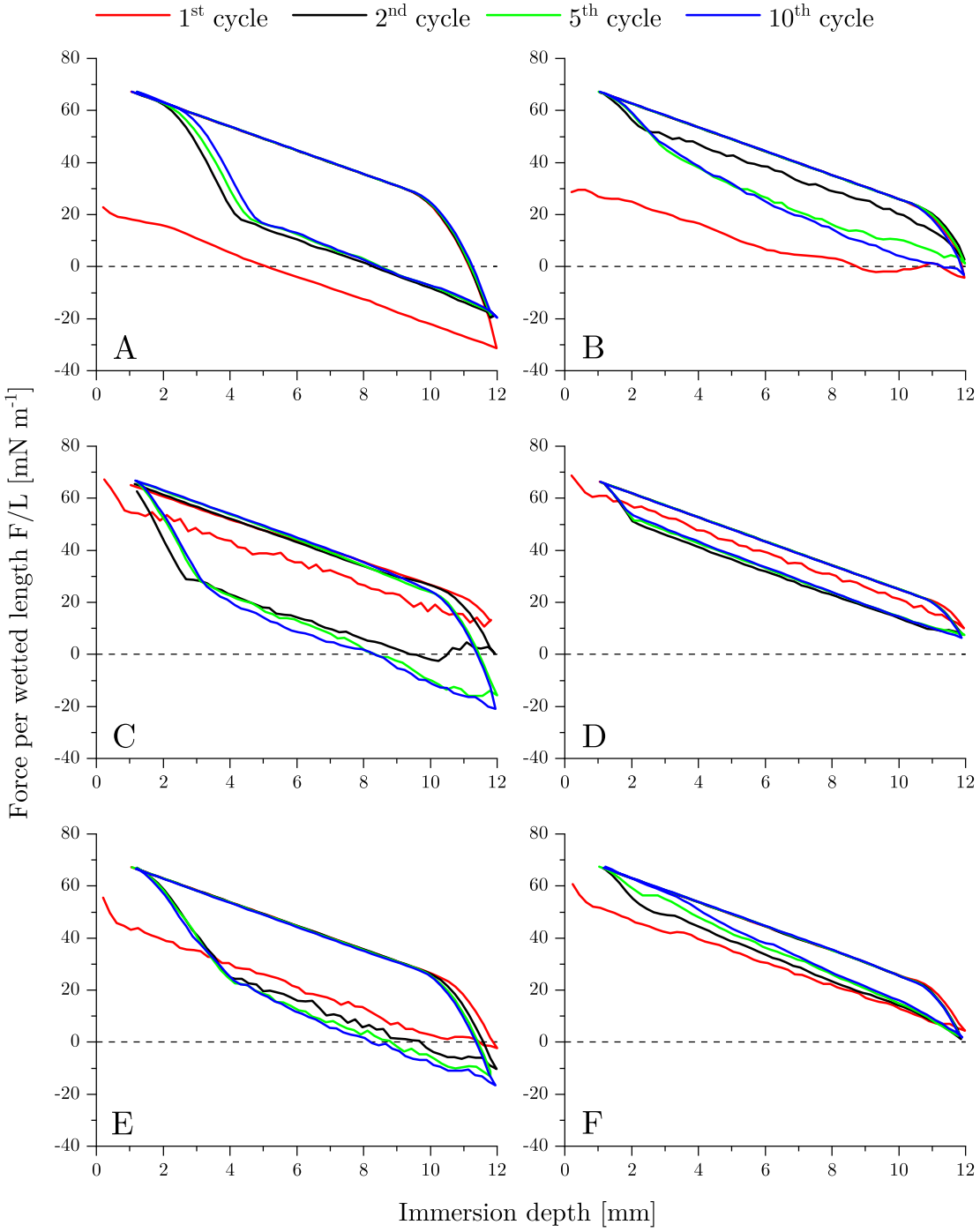

Figure VI.6: Force-immersion cycles of dynamic contact angle measurements of functionalized silicon wafers with water (left) or PBS (right). Force-distance loops of the 1st, 2nd, 5th and 10th cycle are depicted for (A) DMAPS – sf-water, (B) DMAPS – PBS, (C) SAM-NMe_2 – sf-water, (D) SAM-NMe_2 – PBS, (E) SAM-NO – sf-water and (F) SAM-NO – PBS.

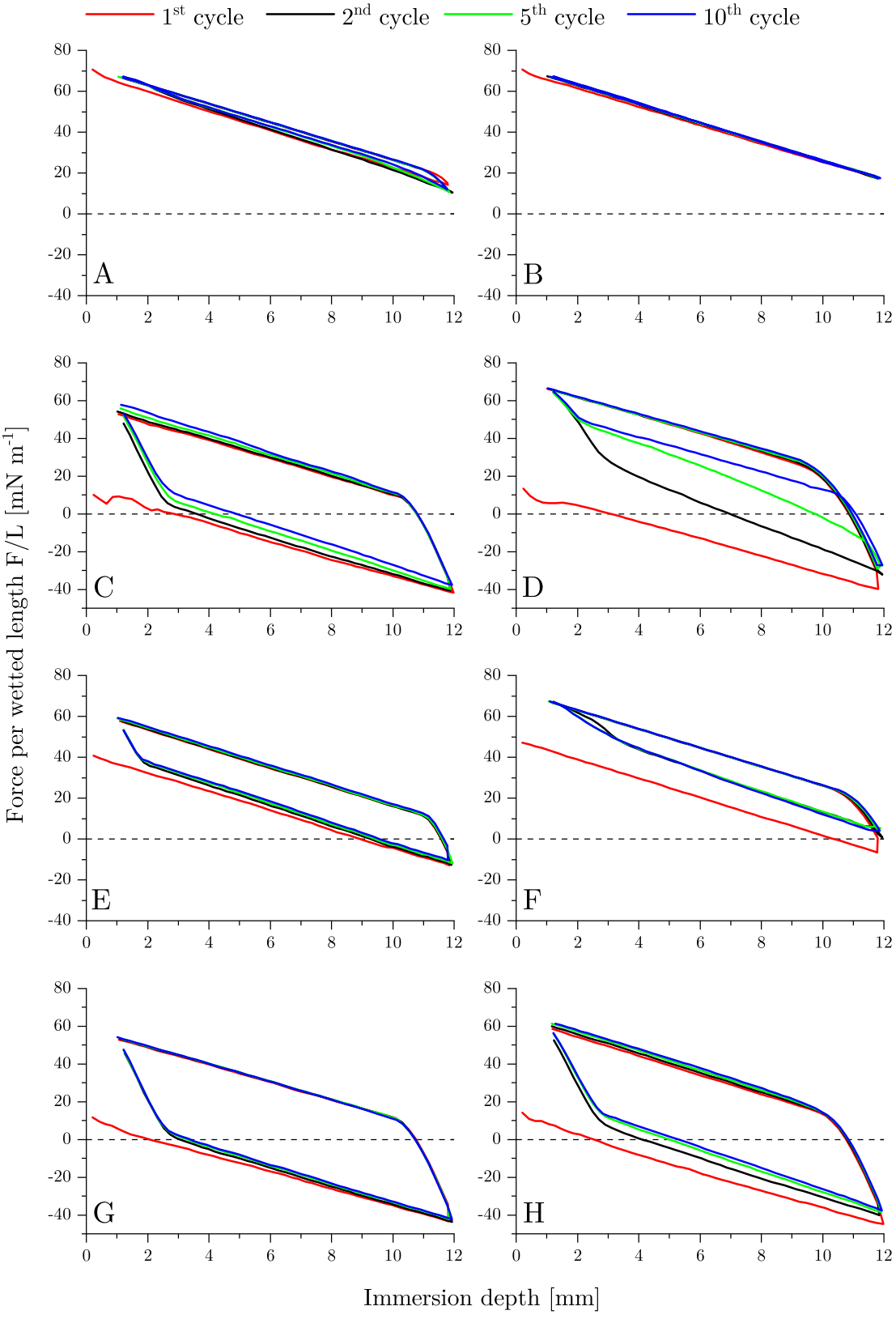

Figure VI.7: Force-immersion cycles of dynamic contact angle measurements of functionalized silicon wafers with water (left) or PBS (right). Force-distance loops of the 1st, 2nd, 5th and 10th cycle are depicted for (A) oxidized wafer – sf-water, (B) oxidized wafer – PBS, (C) TESPSA – sf-water, (D) TESPSA – PBS, (E) SAM-COOH – sf-water, (F) SAM-COOH – PBS, (G) SAM-NH_2 – sf-water and (H) SAM-NH_2 – PBS. Note the different y-axis in diagrams (C), (D), (G) and (H).

Protein Adsorption on Amine and Osmolyte Coatings

Protein Adsorption of HSA and Lysozyme

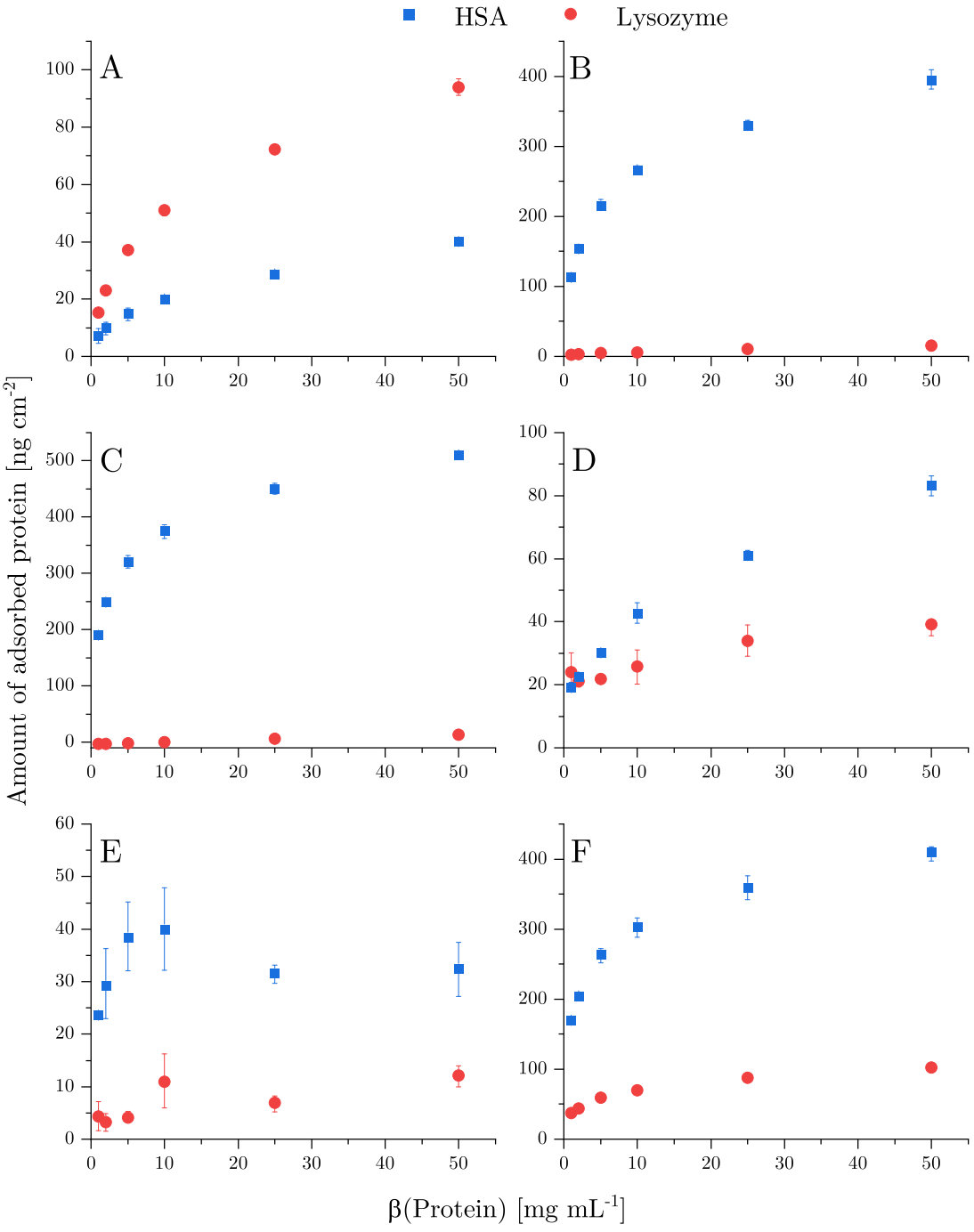

Figure VI.8: Amount of adsorbed protein (HSA or lysozyme) in dependence of the concentration of the protein solution on surfaces with (A) APD, (B) PPI-G2, (C) PPI-G4, (D) PAMAM polymer, (E) PEI polymer or (F) AMAM. Please note the differing y-axes.

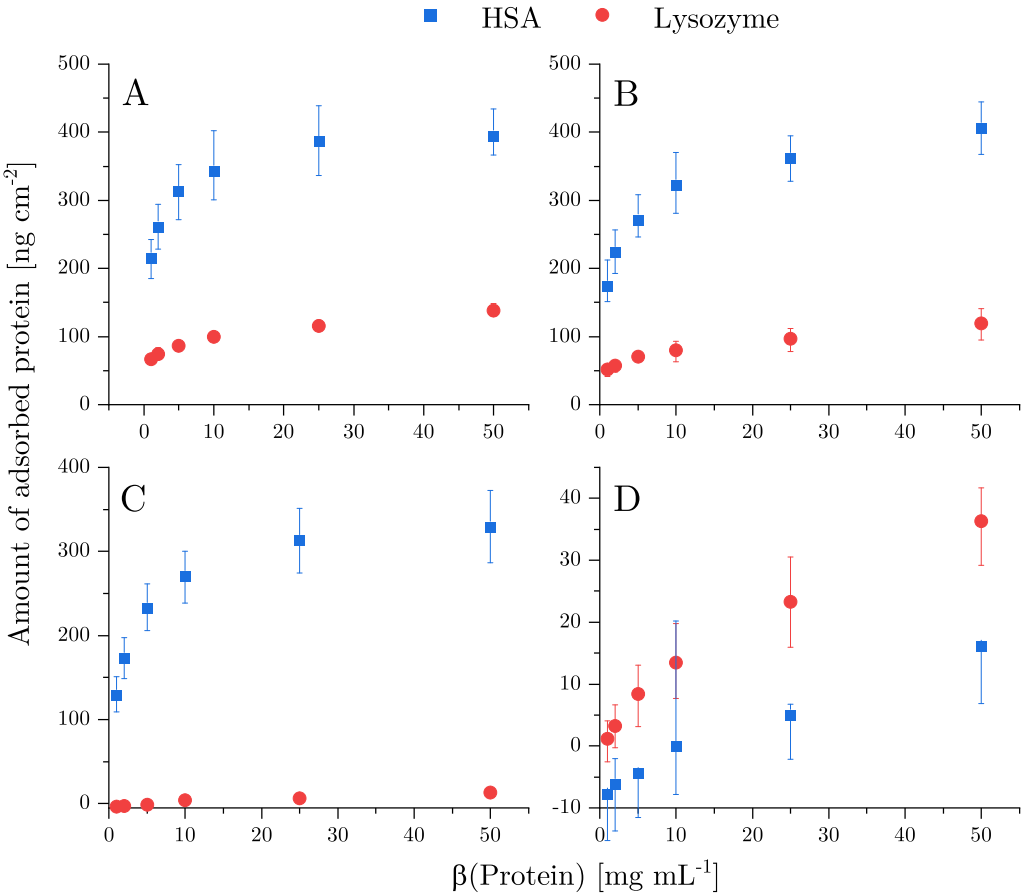

Figure VI.9: Amount of adsorbed protein (HSA or lysozyme) in dependence of the concentration of the protein solution on surfaces with (A) SAM-NH_2, (B) DMAPS, (C) SAM-NMe_2 and (D) SAM-NO. Please note the differing y-axes.

Dependence of Protein Adsorption on SFE

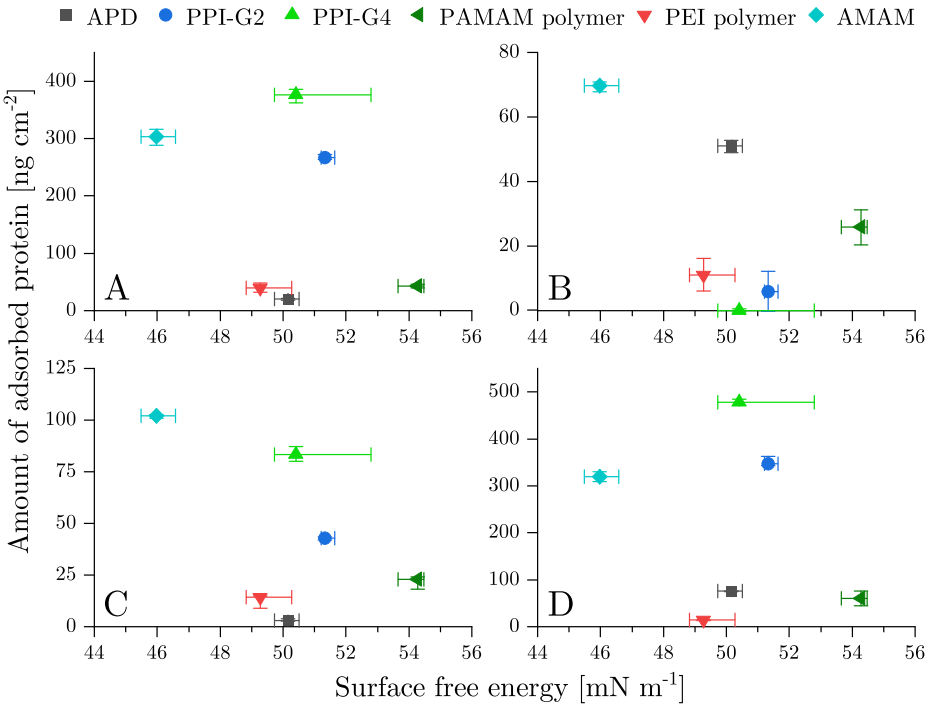

Figure VI.10: Dependence of the protein adsorption from solutions of (A) HSA or (B) lysozyme as well as (C) saliva and (D) FBS on the total SFE of the surface modifications.

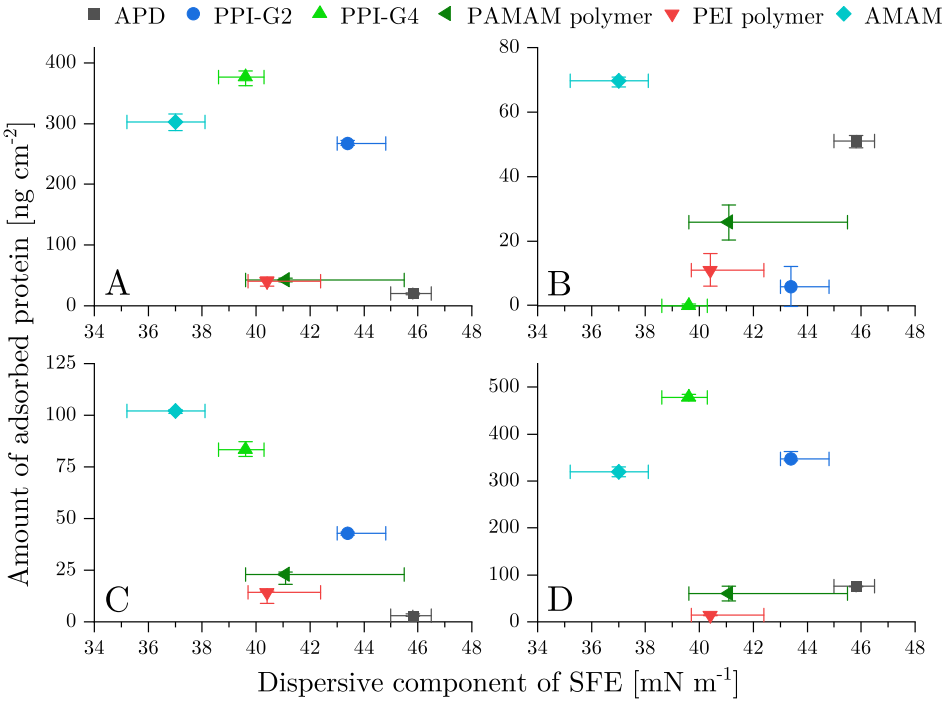

Figure VI.11: Dependence of the protein adsorption from solutions of (A) HSA or (B) lysozyme as well as (C) saliva and (D) FBS on the dispersive component of the SFE of amine-based modifications.

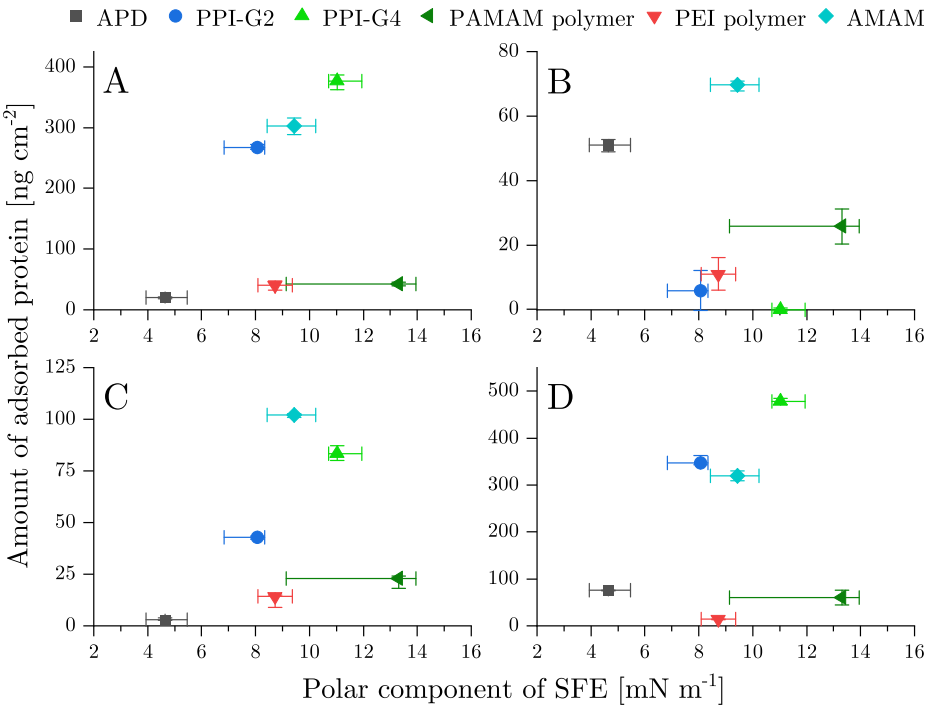

Figure VI.12: Dependence of the protein adsorption from solutions of (A) HSA or (B) lysozyme as well as (C) saliva and (D) FBS on the polar component of the SFE of amine-based coatings.

Cell Experiments

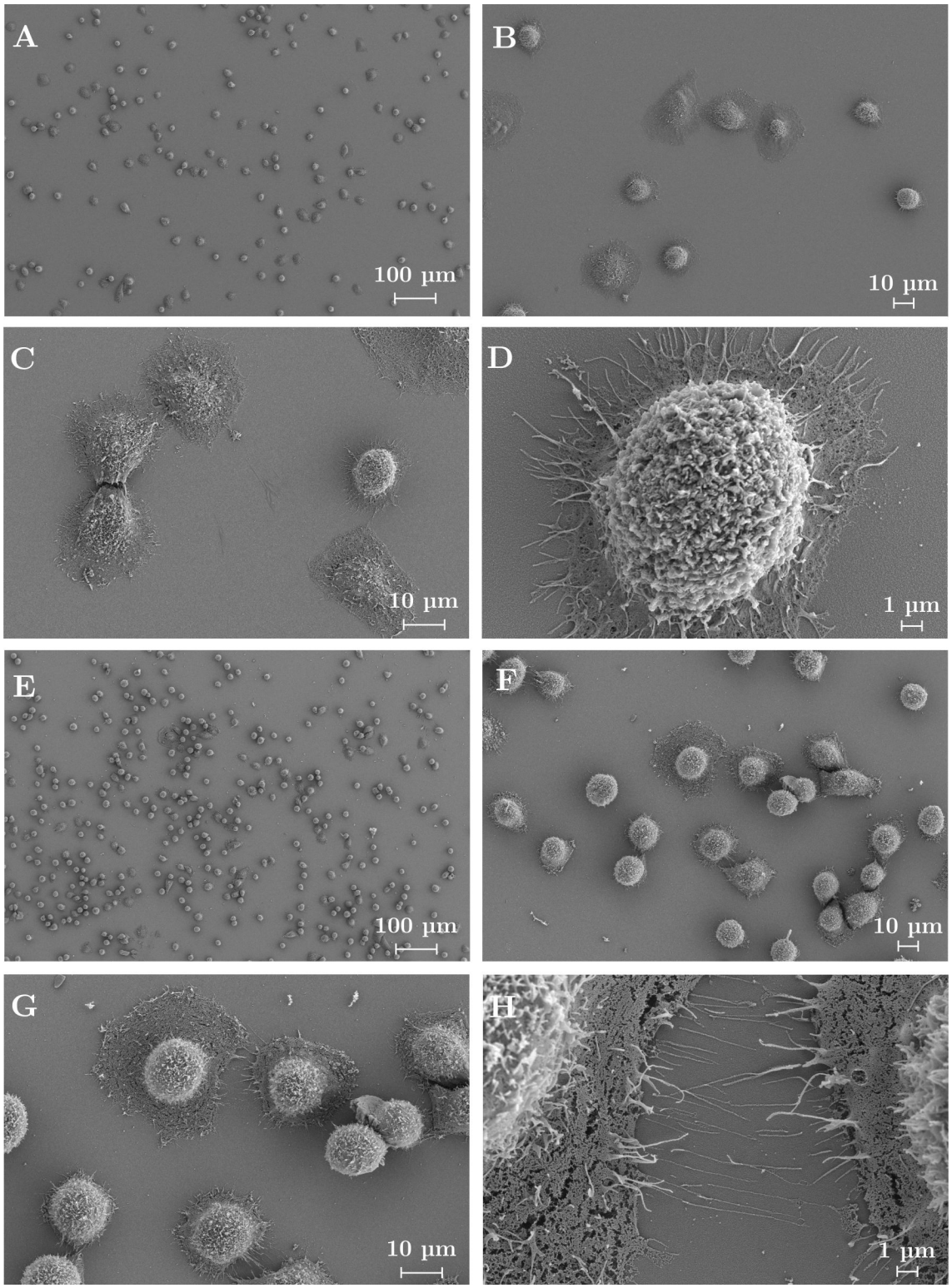

Figure VI.13: Analysis of the morphology of MG-63 cells after 1 h of cultivation on oxidized titanium substrates (A–D) or APD-modified surfaces (E–H), obtained from SEM images.

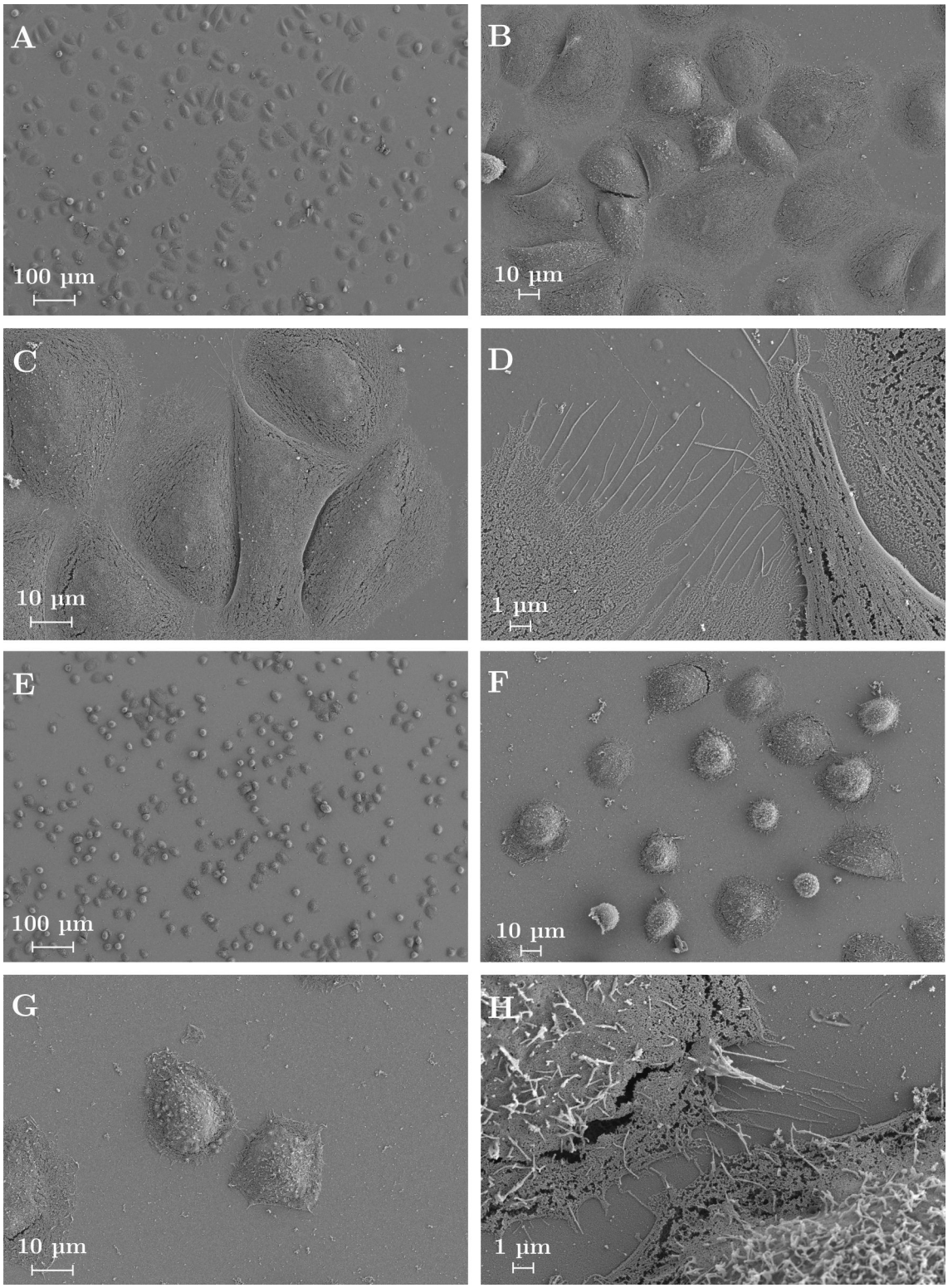

Figure VI.14: Analysis of the morphology of MG-63 cells after 1 h of cultivation on PPI-G4-modified substrates (A–D) or PEI polymer-coated wafers (E–H), obtained from SEM images.

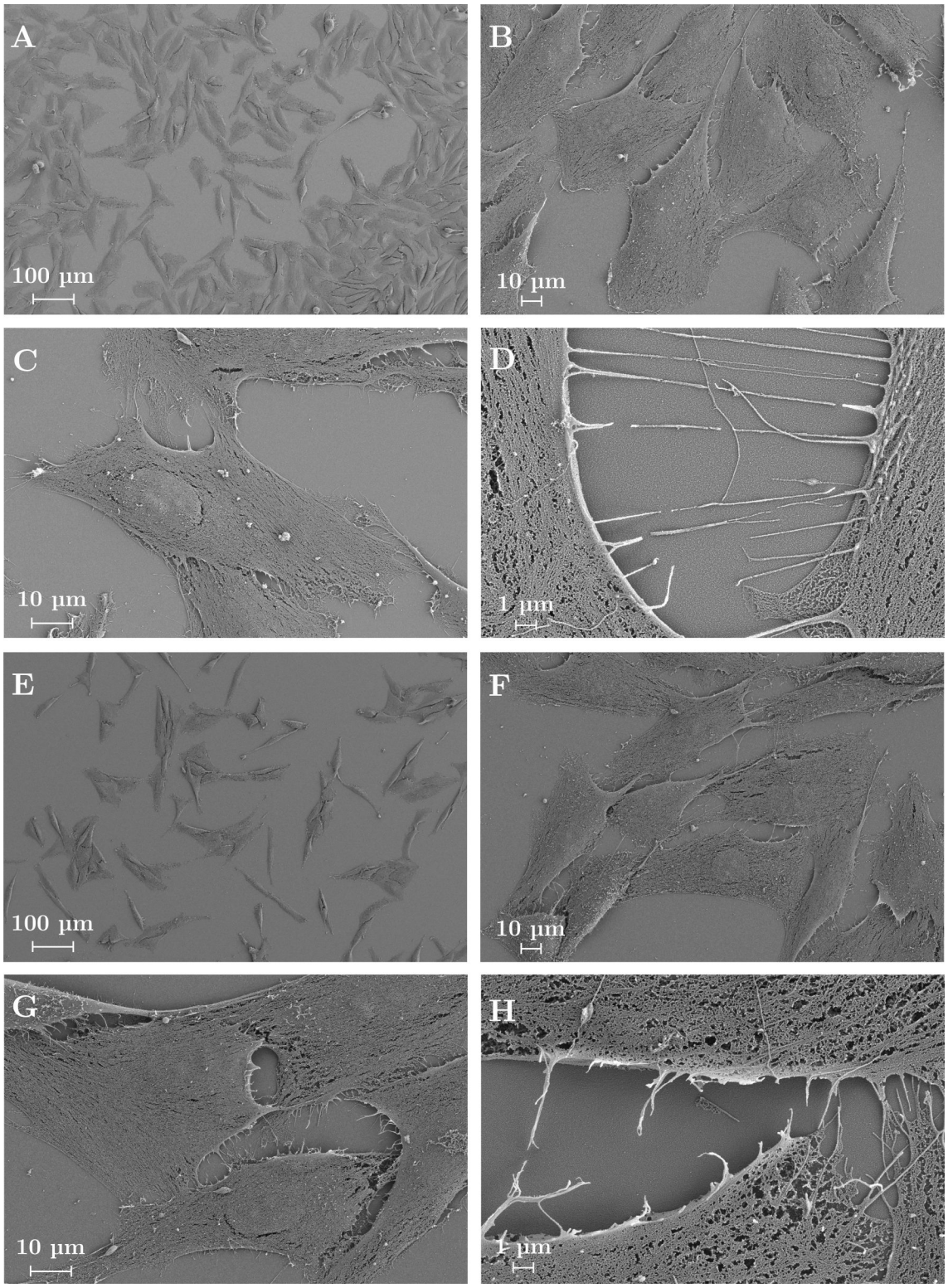

Figure VI.15: Analysis of the morphology of MG-63 cells after 24 h of cultivation on oxidized titanium substrates (A–D) or APD-modified surfaces (E–H), obtained from SEM images.

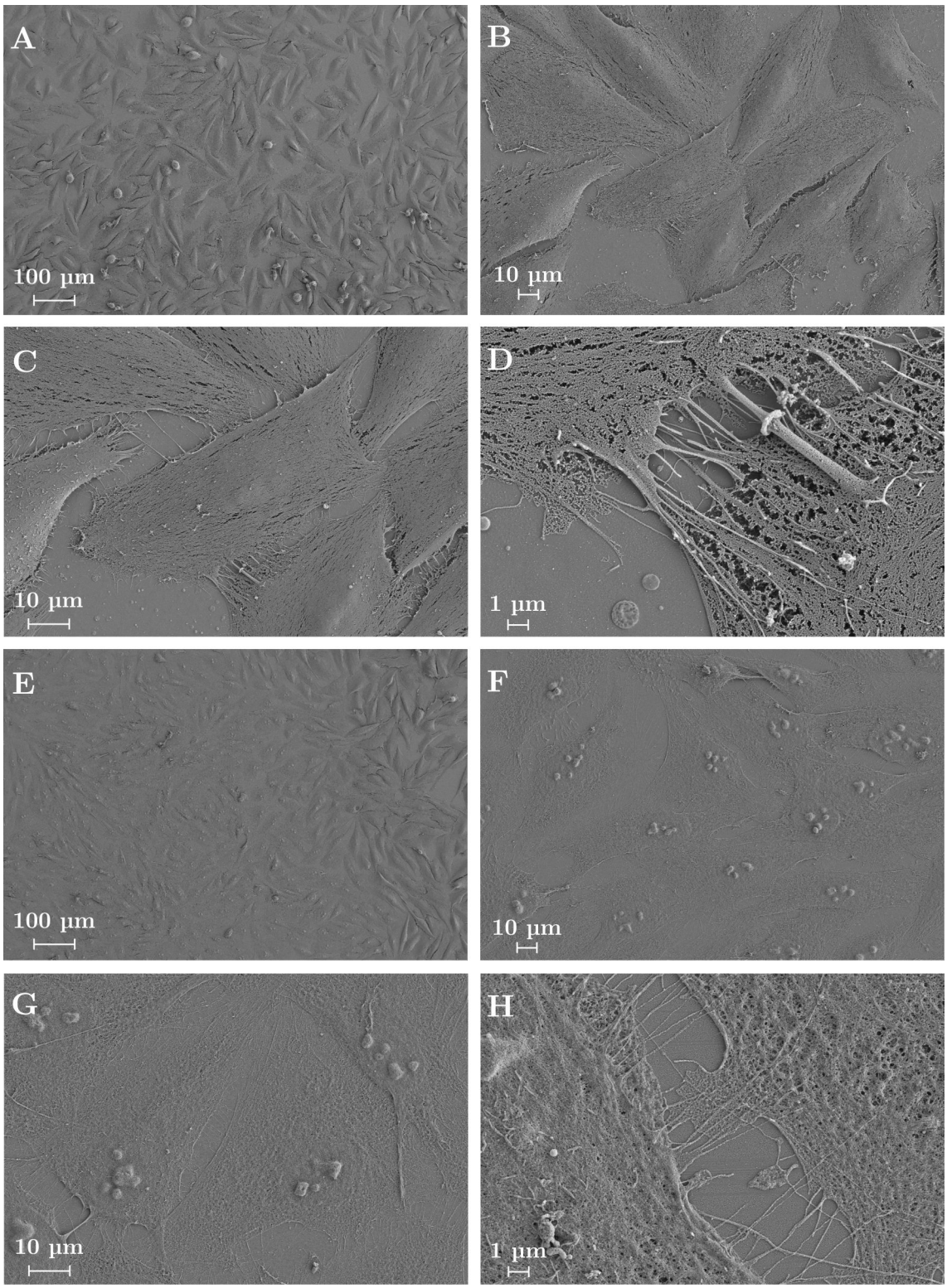

Figure VI.16: Analysis of the morphology of MG-63 cells after 24 h of cultivation on PPI-G4-modified substrates (A–D) or PEI polymer-coated wafers (E–H), obtained from SEM images.

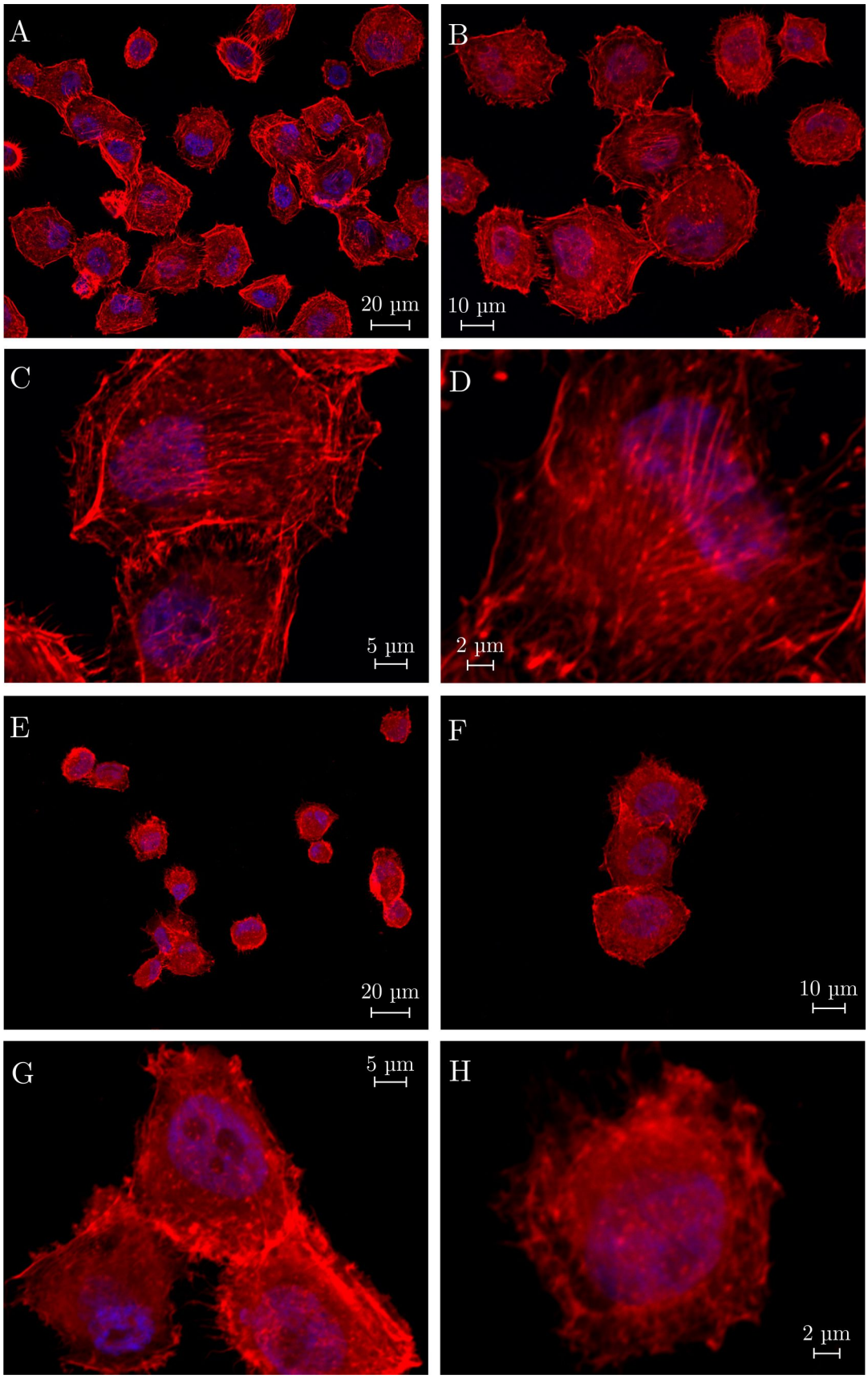

Figure VI.17: Actin cytoskeleton of MG-63 cells after 1 h of cultivation on oxidized titanium substrates (A–D) or APD-modified surfaces (E–H) (red: actin, blue: nucleus).

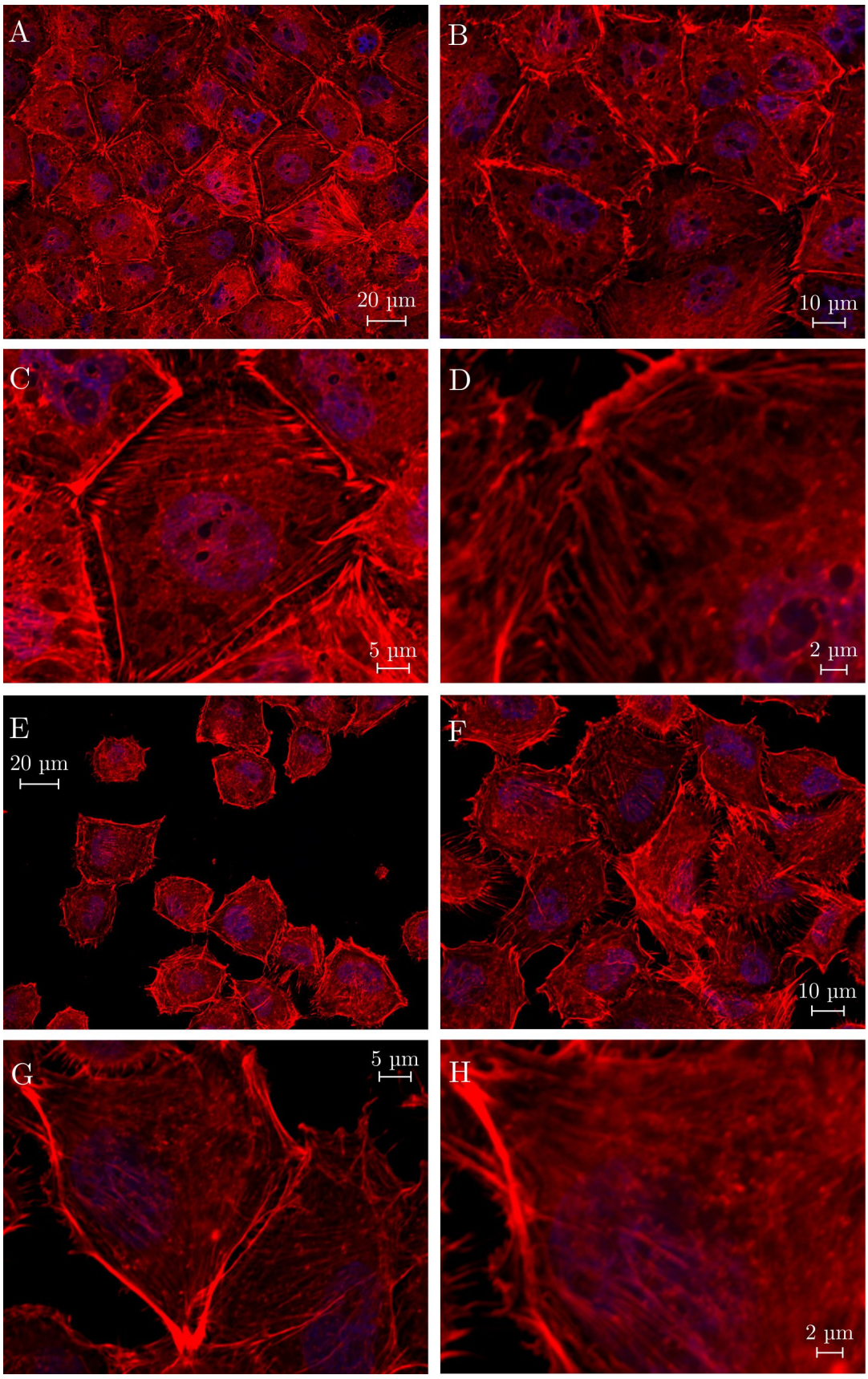

Figure VI.18: Actin cytoskeleton of MG-63 cells after 1 h of cultivation on PPI-G4-modified substrates (A–D) or PEI polymer-coated wafers (E–H) (red: actin, blue: nucleus).

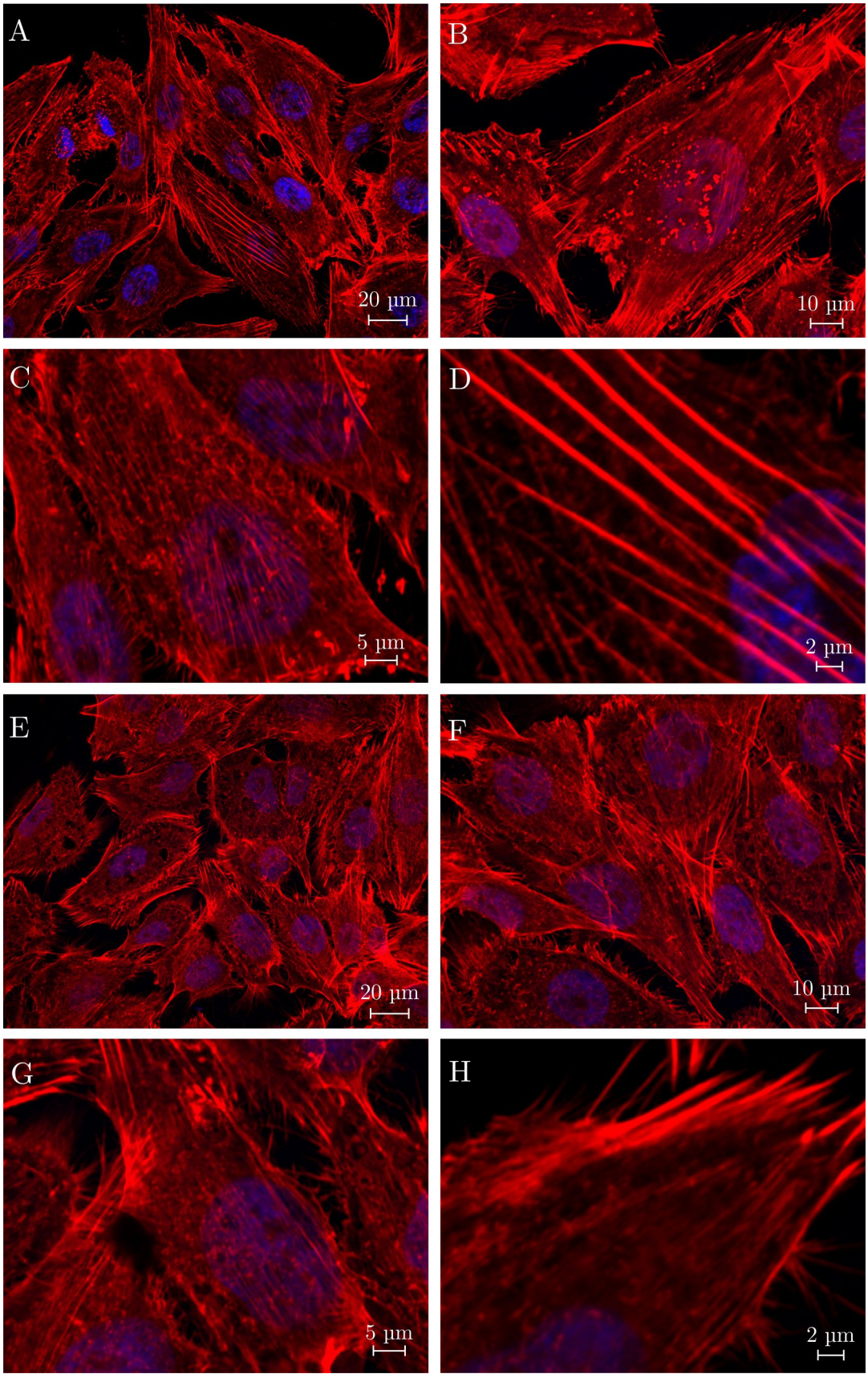

Figure VI.19: Actin cytoskeleton of MG-63 cells after 24 h of cultivation on oxidized titanium substrates (A–D) or APD-modified surfaces (E–H) (red: actin, blue: nucleus).

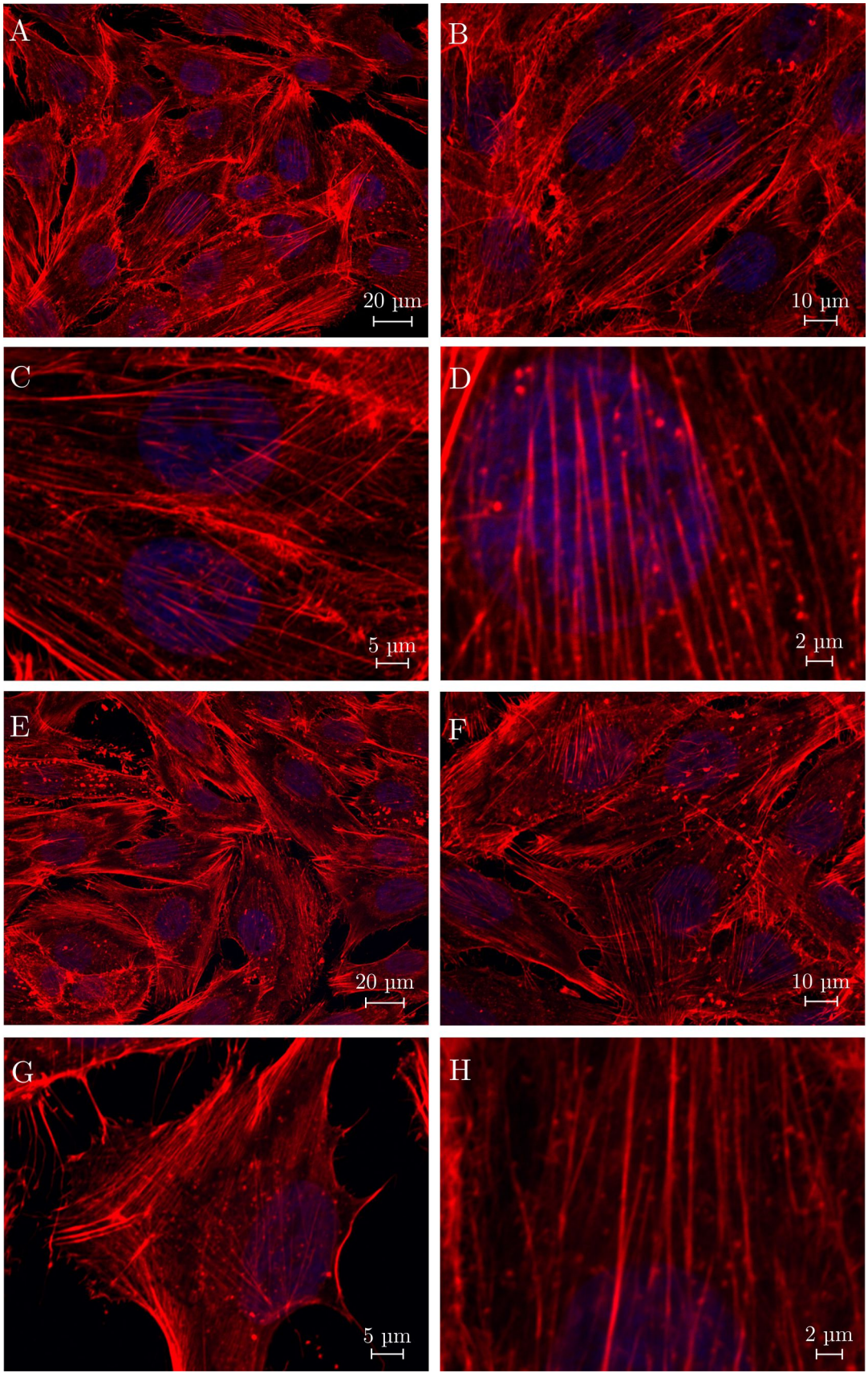

Figure VI.20: Actin cytoskeleton of MG-63 cells after 24 h of cultivation on PPI-G4-modified substrates (A–D) or PEI polymer-coated wafers (E–H) (red: actin, blue: nucleus).

List of Abbreviations

The abbreviated terms are listed in alphabetical order, sorted according to the abbreviation, not the complete name. Abbreviations are only included if mentioned more than once.

AFM	atomic force microscopy
AMAM	amido amine (short chain analogue to PAMAM polymer)
APD	N,N'-bis(3-aminopropyl)-1,3-propanediamine
BCA	bicinchoninic acid
Boc	*tert*-butyloxycarbonyl (protecting group)
BSA	bovine serum albumin
CBB	Coomassie Brilliant Blue
CCD	charge-coupled device
chloranil	tetrachloro-1,4-benzoquinone
CLSM	confocal laser scanning microscopy
DAPI	4',6-diamidino-2-phenylindole
DCM	dichloromethane
DLVO	Derjaguin-Landau-Verwey-Overbeek
DMAPS	self-assembled monolayer with terminal sulfobetaine groups
DMBT1	deleted in malignant brain tumors 1 (glycoprotein)
DMSO	dimethyl sulfoxide
DRIFT	diffuse reflectance infrared Fourier transform
EBA	N,N'-ethylenebisacrylamide
ECM	extracellular matrix
EDC	N-(3-dimethylaminopropyl)-N'-ethylcarbodiimide hydrochloride
EDL	electric double layer
ESI	electrospray ionization
FBS	fetal bovine serum
G	generation (of a dendrimer)

HABS	human AB serum
HPLC	high performance liquid chromatography
HRP	horseradish peroxidase
HSA	human serum albumin
IEP	isoelectric point
IgA	immunoglobulin A
IgG	immunoglobulin G
IHL	inner Helmholtz layer
IHP	inner Helmholtz plane
IR	infrared
LW/AB	Lifshitz-van der Waals/acid-base
mCPBA	*meta*-chloroperbenzoic acid (also 3-chloroperbenzoic acid)
MES	2-(N-morpholino)ethanesulfonic acid
MS	mass spectrometry
MW	molecular weight
NHS	N-hydroxysuccinimide
NMR	nuclear magnetic resonance
OEG	oligo(ethylene glycol)
OHL	outer Helmholtz layer
OHP	outer Helmholtz plane
oxone	monopersulfate compound ($2\ KHSO_5 \cdot KHSO_4 \cdot K_2SO_4$)
PAA	poly(amido amine) polymer (class of linear polymers)
PAGE	polyacrylamide gel electrophoresis
PAMAM	poly(amido amine) (polymer examined in this thesis, dendrimer)
PAS	periodic acid-Schiff (stain)
PBS	phosphate-buffered saline
PEG	poly(ethylene glycol)
PEI	poly(ethylene imine)
polyDADMAC	poly(diallyldimethylammonium chloride)
PPI	poly(propylene imine)
PRP	proline-rich protein

SAM	self-assembled monolayer
SAM-Br	self-assembled monolayer with terminal bromine groups
SAM-CF_3	self-assembled monolayer with perfluorocarbon chains
SAM-CH_3	self-assembled monolayer with hydrocarbon chains
SAM-$CH{=}CH_2$	self-assembled monolayer with terminal alkene moieties
SAM-COOH	self-assembled monolayer with terminal carboxylic acid groups
SAM-N_3	self-assembled monolayer with terminal azide groups
SAM-NH_2	self-assembled monolayer with terminal primary amine groups
SAM-NMe_2	self-assembled monolayer with terminal tertiary amine groups
SAM-NO	self-assembled monolayer with terminal amine oxide groups
SAM-PEG	self-assembled monolayer with five ethylene glycol units
SAM-Py	self-assembled monolayer with terminal pyridinium groups
SAM-$SCOCH_3$	self-assembled monolayer with terminal thioester groups
SAM-SO_3H	self-assembled monolayer with terminal sulfonic acid groups
SDS	sodium dodecyl sulfate
SEM	scanning electron microscopy
SFE	surface free energy
sulfo-SDTB	sulfo-succinimidyl-4-O-(4,4'-dimethoxytrityl)-butyrate
TBS	Tris-buffered saline
TBS-T	Tris-buffered saline with Tween 20
TESPSA	self-assembled monolayer with succinic acid anhydride groups
TFA	trifluoroacetic acid
THF	tetrahydrofuran
TMAO	trimethylamine N-oxide
Tris	tris(hydroxymethyl)aminomethane
TRITC	tetramethylrhodamine isothiocyanate
Triton X-100	4-(1,1,3,3-tetramethylbutyl)phenyl-poly(ethylene glycol)
XPS	X-ray photoelectron spectroscopy
ZAG	Zn-α_2-glycoprotein

List of Figures

I.1 Examples of the application of various biomaterials in the human body [1–3]. 2
I.2 Overview of the structural motifs of the self-assembled monolayers with varying terminal functional groups, oligomeric or polymeric (amido)-amine-based modifications (bearing inner secondary or tertiary amines as well as partially amide groups in combination with terminal primary or secondary amine groups) and the osmolyte modifications (based on taurine, TMAO and proline). 4

2.1 Schematic illustration of the synthesis of trichlorosilanes, as described in literature [40–42]. 13
2.2 Scheme of the formation of a monolayer of silane molecules via self-assembly on a hydroxylated silicon surface, as suggested by Finklea et al. and Silberzan et al. [44, 45]. The silane molecules form a two-dimensional network and are immobilized on the surface via few Si-O-Si linkages [45]. 14

3.1 Schematic depiction of a dendrimer of generation 4 with a three-branched core. 18
3.2 Comparison of the dendrimer synthesis via (A) divergent or (B) convergent approach [62]. The terminal functional groups are depicted in blue, reactive sites in red. The core moiety is colored in green. 19
3.3 Scheme of the synthesis of a PPI dendrimer of generation 1 (PPI-G1) via Michael addition of acrylonitrile, followed by catalyzed hydrogenation [61]. Repeating these reaction steps leads to the formation of a PPI dendrimer of generation 4 (PPI-G4) [62]. 20
3.4 Dendrimer conformation in solution according to (A) the "dense shell" model by De Gennes or (B) with backfolding of dendrimer branches. . 22
3.5 Synthesis of linear PAA polymers from bisacrylamides and (A) primary amines or (B) secondary diamines [88]. 26
3.6 Synthesis of (A) a branched PEI polymer via ring-opening polymerization of aziridine and of (B) a linear PEI polymer via polymerization of 2-oxazolines and subsequent hydrolysis [100]. 29
3.7 Schematic depiction of the three regimes of surface-immobilzed polyers: (A) pancake regime, (B) mushroom regime and (C) brush regime [120]. 32

3.8 Survey of typical examples of the three main osmolyte categories: (A) polyols and carbohydrates, (B) amino acids and their derivatives and (C) methylammonium compounds, according to Yancey et al. [14]. . . 34
3.9 Thermodynamic cycle of the denaturation of a protein from its native conformation (N) into a denatured state (D) and its transfer from pure water (indicated by index W) to an osmolyte solution (indicated by index O). Transfer Gibbs energies are given as ΔG_{trans}, Gibbs free energies of the denaturation process are abbreviated as ΔG_{den}. The scheme was adopted from Bolen and Baskakov [126]. 35

5.1 Scheme of the cell-cell and cell-surface interactions of a cell attached to a biomaterial substrate, according to [213]. ECM: Extracellular matrix, Pax: Paxillin, Vinc: Vincullin. 51

6.1 Scheme of the color-forming reaction during the sulfo-SDTB assay for amino group detection [226, 227]. 55
6.2 Scheme of the color-forming reaction in the chloranil assay via reaction of a tertiary amine with chloranil [228]. 56
6.3 Static contact angle of a drop of liquid on an ideal surface in thermodynamic equilibrium, as described by Young's equation [230, 231]. . . 56
6.4 Graphic illustration of the Wilhelmy plate method [233] (W: width of the plate, t: thickness of the plate, d: immersion depth, Θ: contact angle). 58
6.5 Schematic representation of the EDL and the corresponding potential $\phi(d)$ at a negatively charged surface, according to the Gouy-Chapman-Stern-Grahame model [243, 245]. IHP: inner Helmholtz plane; OHP: outer Helmholtz plane. 61
6.6 Illustration of the formation of the colored Cu^{+}-BCA complex [252] . 66
6.7 Schematic of a SDS-PAGE with a molecular weight standard (red) for the separation of proteins according to their molecular weight [254, 256]. 67
6.8 Scheme of the transfer of proteins onto a membrane via electroblotting (western blot) [256, 259]. 69
6.9 Schematic of the chemiluminescence reaction and its detection in the indirect western blot (HRP: horseradish peroxidase) [256, 262]. 69
6.10 Schematic of a confocal laser scanning microscope [263, 264]. 70

8.1 Synthesis of the linear PAMAM polymer from EBA and piperazine. . 78

9.1 Glass devices for the silanization of single-side polished wafers at elevated temperatures. 80

9.2 Reaction scheme of the formation of an alkane monolayer via silanization of a hydroxylated surface with octyltrichlorosilane. 83
9.3 Reaction scheme of the immobilization of a trichlorosilane carrying a perfluorinated alkane chain on a hydroxylated surface. 83
9.4 Schematic representation of the formation of a carboxylic acid-terminated SAM, via immobilization of an alkene-terminated SAM, followed by conversion of the olefine groups into carboxylic acid groups via oxidation with $KMnO_4$. 84
9.5 Schematic illustration of the synthesis of a pyridinium SAM, via immobilization of a bromine-terminated SAM, followed by substitution of the terminal bromine atom with pyridine. 85
9.6 Schematic illustration of the synthesis of an amine-terminated SAM (SAM-NH_2), via substitution of the terminal bromine atom with an azide group, followed by the reduction with $LiAlH_4$. 86
9.7 Scheme of the synthesis of a self-assembled monolayer with terminal sulfonic acid groups via formation of a thioester (SAM-$SCOCH_3$), followed by oxidation with oxone [272]. 87
9.8 Schematic depiction of the immobilization of N-(triethoxysilylpropyl)-O-polyethylene oxide urethane for the formation of SAM-PEG. 87
9.9 Reaction scheme of the immobilization of the silane 3-(triethoxy)propyl succinic acid anhydride on hydroxylated surfaces, leading to a SAM with terminal succinic acid anhydride groups (TESPSA). 88
9.10 Schematic illustration of the synthesis of a self-assembled monolayer with tertiary amine moieties. 89
9.11 Schematic illustration of the immobilization of (A) APD and (B) PPI-G2 or PPI-G4 on TESPSA substrates via formation of an amide bond. 90
9.12 Scheme of the immobilization of the (A) PAMAM or (B) PEI polymer on SAM-COOH via formation of an active ester with EDC/NHS. . . . 92
9.13 Schematic representation of the formation on an amido amine (AMAM) structure via aza-Michael coupling of EBA and piperazine. 93
9.14 Schematic representation of the immobilization of the acrylate-substituted sulfobetaine on SAM-NH_2-functionalized substrates via aza-Michael reaction. 94
9.15 Schematic representation of the conversion of SAM-NMe_2 into an amine oxide monolayer via oxidation with mCPBA. 95
9.16 Scheme for the immobilization of N-Boc-protected proline via click reaction with an azide-terminated SAM, followed by deprotection with trifluoroacetic acid (TFA). 96

13.1 Overview of the examined SAMs with different functional groups as well as their abbreviated name. 115
13.2 IR spectra of self-assembled monolayers with (A) non-ionizable and (B) ionizable functional groups, recorded via DRIFT spectroscopy. The IR spectra have partially been published by Verena Katzur in her PhD thesis [13]. 118
13.3 Water contact angles of self-assembled monolayers and intermediate SAMs as a measure of the modifications' wettability. 119
13.4 SFE as well as its polar and dispersive component of self-assembled monolayers with varying functional end groups, calculated according to the LW/AB approach. 122
13.5 Zeta potential of wafer substrates functionalized with a perfluoroalkane SAM (SAM-CF_3) or with pyridinium groups (SAM-Py). 123
13.6 Amount of adsorbed protein from whole human saliva on SAMs with different end groups. Protein quantification was performed with the BCA assay, either on the substrate surface or after protein desorption. Results have partially been published previously [13, 17, 19, 21]. For improved clarity, the results of the Mann-Whitney-U test are not included in the figure but will be summarized here. Comparing the results of the BCA assay on the surface, all pairwise comparisons among adsorbed proteins showed significance except for the following: oxidized – SAM-CF_3/SAM-Py/SAM-COOH, SAM-CH_3 – SAM-CF_3, SAM-NH_2 – SAM-SO_3H and SAM-Py – SAM-COOH. For the protein amounts determined from the eluate, $^*p < 0.05$ was only obtained for: oxidized – SAM-CH_3/SAM-NH_2/SAM-SO_3H, SAM-CH_3 – SAM-NH_2/SAM-Py/SAM-COOH/SAM-SO_3H, SAM-CF_3 – SAM-NH_2/SAM-SO_3H, SAM-Py – SAM-SO_3H and SAM-COOH – SAM-SO_3H. 127

13.7 Amount of adsorbed protein from HABS or FBS on SAMs with different end groups. Protein quantification was performed with the BCA assay, either on the substrate surface or after protein desorption. Results for (A) FBS (only on surface) and (B) HABS are displayed. Data for FBS has partially been published previously [13, 16, 17, 21]. For improved clarity, the results of the Mann-Whitney-U test are not included in the figure as most pairwise comparisons of different surface modifications for the same protein solution showed significance for the protein amounts on the surface. Exceptions for FBS are: oxidized – SAM-SO_3H and SAM-NH_2 – SAM-Py. For HABS (on surface), p-values ≥ 0.05 were obtained for oxidized – SAM-Py, SAM-CH_3 – SAM-CF_3, SAM-CH_3 – SAM-COOH, SAM-CF_3 – SAM-COOH and SAM-NH_2 – SAM-SO_3H. In contrast to that, for the protein amounts determined in the eluates $^*p < 0.05$ was obtained for: oxidized – SAM-CH_3/SAM-CF_3/SAM-NH_2/SAM-COOH, SAM-PEG – SAM-CH_3/SAM-COOH, SAM-CH_3 – SAM-NH_2/SAM-Py/SAM-SO_3H, SAM-CF_3 – SAM-NH_2, SAM-NH_2 – SAM-COOH, SAM-Py – SAM-COOH and SAM-COOH – SAM-SO_2H. 128

13.8 Dependence of the protein adsorption from (A) saliva or (B) FBS as well as (C) HABS on the hydrophilicity of the self-assembled monolayers, as determined via the static contact angle Θ. Protein adsorption was determined on the surfaces via BCA assay. 131

13.9 Dependence of the protein adsorption from (A) saliva or (B) FBS as well as (C) HABS on the zeta potential of the self-assembled monolayers at the pH of the respective protein solution. Protein adsorption was determined on the surfaces via BCA assay. 132

13.10 Surface topography of silica beads, as obtained from SEM images. . . 136

13.11 Representative stained gel after SDS-PAGE of the proteins adsorbed to (3) unmodified beads, (4) oxidized beads, (5) SAM-COOH, (6) SAM-PEG, (7) SAM-NH_2, (8) SAM-Py, (9) SAM-CH_3, (10) SAM-CF_3 and (11) SAM-SO_3H. Whole saliva (2) as well as a molecular weight standard (1, 12) are included for reference. Strongly glycosylated proteins appear in red, proteins with little or no glycosylation are stained blue. 137

13.12 Immunostaining of selected salivary proteins adsorbed to SAMs with different functional groups after SDS-PAGE and western blot. The surface modifications are: (3) unmodified beads, (4) oxidized beads, (5) SAM-COOH, (6) SAM-PEG, (7) SAM-NH_2, (8) SAM-Py, (9) SAM-CH_3, (10) SAM-CF_3 and (11) SAM-SO_3H. Whole human saliva (2) as well as a molecular weight standard (1, 12, molecular weight provided in kDa) are included for reference. 139
13.13 Representative stained gel after SDS-PAGE of human serum proteins adsorbed to (3) unmodified beads, (4) oxidized beads, (5) SAM-COOH, (6) SAM-PEG, (7) SAM-NH_2, (8) SAM-Py, (9) SAM-CH_3, (10) SAM-CF_3 and (11) SAM-SO_3H. Human serum (2, dilution 1:100) and a molecular weight standard (1, 12) are included for reference. 144
13.14 Immunostaining of selected serum proteins adsorbed to SAMs with different functional groups after SDS-PAGE and western blot. The surface modifications are: (3) unmodified beads, (4) oxidized beads, (5) SAM-COOH, (6) SAM-PEG, (7) SAM-NH_2, (8) SAM-Py, (9) SAM-CH_3, (10) SAM-CF_3 and (11) SAM-SO_3H. Diluted human serum (2, dilution 1:100) as well as a molecular weight standard (1, 12, MW provided in kDa) are included for reference. 145

14.1 Overview of the oligomeric and polymeric surface modifications, containing amine and partially amide motifs, as well as their abbreviated names. 151
14.2 IR spectrum of the linear PAMAM polymer, obtained via DRIFT spectroscopy. 152
14.3 Repeating unit of the PAMAM polymer chain with labeled -CH_2- units. 153
14.4 ^{1}H-NMR spectrum of the linear PAMAM polymer in D_2O. 153
14.5 ^{13}C-NMR spectrum of the linear PAMAM polymer in D_2O. 154
14.6 Amine group densities, obtained via Sulfo-SDTB assay, for intermediate SAMs and amine-based surface modifications. 157
14.7 DRIFT spectra of silica spheres, coated with the amine-based surface functionalizations (A) APD, PPI-G2 or PPI-G4, or (B) PAMAM polymer, PEI polymer or AMAM. 159
14.8 Surface free energies (as well as polar and dispersive components) of amine-based surface coatings in comparison with oxidized wafers. . . . 161
14.9 Advancing contact angles obtained from dynamic contact angle measurements with water (A and B) or PBS (C and D). In addition to the amine-terminated functionalizations, also the intermediate SAMs are provided. Results for cycles 1, 2, 5 and 10 are given. 163

14.10 Receding contact angles obtained from dynamic contact angle measurements with water (A and B) or PBS (C and D). In addition to the amine-terminated functionalizations, also the intermediate SAMs are provided. Results for cycles 1, 2, 5 and 10 are given. 164
14.11 Hysteresis of amine-functionalized surfaces, determined as the difference between the advancing and receding contact angles of tensiometric measurements with water (A and B) or PBS (C and D). Results are provided for cycles 1, 2, 5 and 10. 166
14.12 Loop-dependent change of the dynamic contact angle hysteresis for the cycles 2, 5 and 10 in comparison to the 1^{st} cycle. Both measurements with sf-water (A) as well as PBS (B) are provided. 167
14.13 Zeta potential of surfaces modified with PPI-G2, PPI-G4 or PEI polymer obtained from (A) electrophoresis measurements or (B) streaming current experiments (mean average ± standard deviation). All zeta potential measurements were performed in $1\,\mathrm{mmol\,L^{-1}}$ KCl solution. . 169
14.14 Zeta potential of surfaces modified with APD, PAMAM polymer or AMAM obtained from electrophoresis measurements. All zeta potential measurements were performed in $1\,\mathrm{mmol\,L^{-1}}$ KCl solution. 169
14.15 Amount of adsorbed protein from HSA or lysozyme solutions (concentration $10\,\mathrm{mg\,mL^{-1}}$ in PBS buffer), undiluted human saliva or FBS on silica beads with amine-based modifications or the respective intermediate SAMs. Results are displayed for (A) oxidized beads and substrates modified with APD, PPI-G2 or PPI-G4, or (B) surfaces with PAMAM polymer, PEI polymer, AMAM as well as the intermediate monolayers SAM-COOH and SAM-NH_2. For each protein solution, the results of the different surface modifications have been compared via Mann-Whitney-U test. For improved clarity, the results are not shown in the figure as p-values ≥ 0.05 have only been obtained for few pairs, which are listed in the following. HSA: oxidized – PPI-G2, oxidized – SAM-NH_2, APD – SAM-COOH, PPI-G4 – SAM-NH_2, SAM-COOH – PAMAM polymer, SAM-COOH – PEI polymer, PAMAM polymer – PEI polymer, SAM-NH_2 – AMAM. Lysozyme: PPI-G2 – PPI-G4, PPI-G2 – PEI polymer, PPI-G4 – PEI polymer, SAM-COOH – AMAM. Saliva: oxidized – SAM-COOH, oxidized – PAMAM polymer, PPI-G2 – SAM-NH_2, SAM-COOH – PAMAM polymer. FBS: APD – PAMAM polymer, PPI-G2 – SAM-NH_2. 174

14.16 Dependence of the protein adsorption from solutions of (A) HSA or (B) lysozyme (concentration 10 mg mL^{-1}) as well as (C) saliva and (D) FBS on the amine group density of the amine-based surface coatings, as determined via the sulfo-SDTB assay. 177
14.17 Dependence of the protein adsorption from solutions of (A) HSA or (B) lysozyme (concentration 10 mg mL^{-1}) as well as (C) saliva and (D) FBS on the hydrophilicity of the amine-based coatings, as determined via the static contact angle Θ. 178
14.18 Dependence of the protein adsorption from solutions of (A) HSA or (B) lysozyme (concentration 10 mg mL^{-1}) as well as (C) saliva and (D) FBS on the zeta potential of the surface coatings at the pH of the respective protein solution. 180

15.1 Overview of the osmolyte-based surface functionalizations as well as their abbreviated names. 182
15.2 Amine group densities, obtained via sulfo-SDTB assay, for the intermediate SAMs, SAM-NH_2 and SAM-N_3, and their subsequent osmolyte-based modifications, DMAPS and proline. 186
15.3 DRIFT spectra of silica particles, coated with the osmolyte-based surface functionalizations DMAPS and SAM-NO as well as the precursor monolayer SAM-NMe_2. 188
15.4 SFEs (as well as their polar and dispersive components) of modifications with osmolyte motifs and of intermediate SAMs, calculated via the LW/AB approach. 190
15.5 Advancing contact angles, calculated from dynamic contact angle measurements with (A) water or (B) PBS. Results for the cycles 1, 2, 5 and 10 of osmolyte-derived modifications as well as their precursor SAMs are presented. 191
15.6 Receding contact angles, obtained from dynamic contact angle measurements with (A) water or (B) PBS. Results for the cycles 1, 2, 5 and 10 of osmolyte-derived modifications and their precursor SAMs are provided. 192
15.7 Contact angle hysteresis of osmolyte-derived coatings as well as their precursor SAMs from dynamic contact angle measurements with (A) water or (B) PBS. 193
15.8 Loop-dependent change of the contact angle hysteresis of osmolyte-based modifications and their precursor SAMs with respect to the first cycle for measurements with (A) water or (B) PBS. 194

15.9 Zeta potential of a sulfobetaine-modified surface (DMAPS), obtained from (A) electrophoresis measurements or (B) streaming current experiments (mean average ± standard deviation). All zeta potential measurements were performed in 1 mmol L^{-1} KCl solution. 195
15.10 Zeta potential of surfaces modified with SAM-NMe_2 or SAM-NO obtained from electrophoresis measurements. All zeta potential measurements were performed in 1 mmol L^{-1} KCl solution. 195
15.11 Amount of adsorbed protein from HSA or lysozyme solutions (concentration 10 mg mL^{-1} in PBS buffer), undiluted human saliva or FBS on silica beads with osmolyte-based modifications or their precursors. Adsorption of HSA or lysozyme on SAM-N_3 and the proline-functionalized surface has not been determined yet (∗). For improved clarity, the results of the Mann-Whitney-U test are not included in the figure as all pairwise comparisons among each protein solution showed significance except for the following: HSA: oxidized – SAM-NH_2, oxidized – SAM-NMe_2, SAM-NH_2 – DMAPS, DMAPS – SAM-NMe_2; saliva: oxidized – SAM-NO, oxidized – SAM-N_3, SAM-NH_2 – SAM-NMe_2, SAM-NO – SAM-N_3; FBS: SAM-NH_2 – proline, DMAPS – SAM-NMe_2. 199

16.1 Comparison of static water contact angles on silicon or titanium-based substrates without coating (oxidized), with intermediate SAMs (TESP-SA, SAM-CH=CH_2, SAM-COOH) or with amine-based functionalizations. 205
16.2 Surface free energies as well as their polar and dispersive components of oxidized or functionalized titanium wafers in comparison with the respective functionalization on silicon substrates (as described in chapter 14). 206
16.3 Zeta potential of (A) oxidized Ti wafers as well as titanium substrates modified with (B) APD, (C) PPI-G4 or (D) PEI polymer obtained from streaming current experiments (mean average ± standard deviation, linear fit shown). All zeta potential measurements were performed in 1 mmol L^{-1} KCl solution. 207
16.4 Spreading of osteoblastic MG-63 cells on differently functionalized titanium substrates. Cell areas are obtained from SEM images after cultivation for (A) 1 h or (B) 24 h. (Statistics: Mann-Whitney-U-Test, $^{*}p < 0.05$). 209
16.5 Analysis of the morphology of MG-63 cells after 1 h of incubation on (A) oxidized titanium substrates, (B) APD, (C) PPI-G4 or (D) PEI polymer coating from SEM images (bars = 10 µm). 210

16.6 Analysis of the morphology of MG-63 cells after 24 h of incubation on (A) oxidized titanium substrates, (B) APD, (C) PPI-G4 or (D) PEI polymer coating from SEM images (bars = 10 µm). 211
16.7 Actin cytoskeleton of MG-63 cells after 1 h of cultivation on (A) oxidized titanium substrates, (B) APD, (C) PPI-G4 or (D) PEI polymer coating, obtained via CLSM (red: actin, blue: nucleus, bars = 5 µm). . 212
16.8 Actin cytoskeleton of MG-63 cells after 24 h of cultivation on (A) oxidized titanium substrates, (B) APD, (C) PPI-G4 or (D) PEI polymer coating, obtained via CLSM (red: actin, blue: nucleus, bars = 10 µm). 213
16.9 Cell cylce phases of osteoblast-like MG-63 cells on differently functionalized titanium substrates. 214
16.10 Percentage of (A) proliferative and (B) apoptotic MG-63 cells on differently functionalized titanium substrates, as obtained from cytometric measurements (Statistics: Mann-Whitney-U-Test not significant with $^{*}p < 0.05$). 214
VI.1 Dependence of the protein adsorption from (A) saliva or (B) FBS as well as (C) HABS on the surface free energy of the self-assembled monolayers. Protein adsorption was determined on the surfaces via BCA assay. 230
VI.2 Dependence of the protein adsorption from (A) saliva or (B) FBS as well as (C) HABS on the dispersive component of the SFE of the self-assembled monolayers. Protein adsorption was determined on the surfaces via BCA assay. 230
VI.3 Dependence of the protein adsorption from (A) saliva or (B) FBS as well as (C) HABS on the polar component of the SFE of the self-assembled monolayers. Protein adsorption was determined on the surfaces via BCA assay. 231
VI.4 Force-immersion cycles of dynamic contact angle measurements of functionalized silicon wafers with water (left) or PBS (right). Force-distance loops of the 1^{st}, 2^{nd}, 5^{th} and 10^{th} cycle are depicted for (A) APD – sf-water, (B) APD – PBS, (C) PPI-G2 – sf-water, (D) PPI-G2 – PBS, (E) PPI-G4 – sf-water and (F) PPI-G4 – PBS. 234
VI.5 Force-immersion cycles of dynamic contact angle measurements of functionalized silicon wafers with water (left) or PBS (right). Force-distance loops of the 1^{st}, 2^{nd}, 5^{th} and 10^{th} cycle are depicted for (A) PAMAM polymer – sf-water, (B) PAMAM polymer – PBS, (C) PEI polymer – sf-water, (D) PEI polymer – PBS, (E) AMAM – sf-water and (F) AMAM – PBS. Note the different y-axis in diagrams (E) and (F). . . 235

VI.6 Force-immersion cycles of dynamic contact angle measurements of functionalized silicon wafers with water (left) or PBS (right). Force-distance loops of the 1st, 2nd, 5th and 10th cycle are depicted for (A) DMAPS – sf-water, (B) DMAPS – PBS, (C) SAM-NMe_2 – sf-water, (D) SAM-NMe_2 – PBS, (E) SAM-NO – sf-water and (F) SAM-NO – PBS. . . . 236
VI.7 Force-immersion cycles of dynamic contact angle measurements of functionalized silicon wafers with water (left) or PBS (right). Force-distance loops of the 1st, 2nd, 5th and 10th cycle are depicted for (A) oxidized wafer – sf-water, (B) oxidized wafer – PBS, (C) TESPSA – sf-water, (D) TESPSA – PBS, (E) SAM-COOH – sf-water, (F) SAM-COOH – PBS, (G) SAM-NH_2 – sf-water and (H) SAM-NH_2 – PBS. Note the different y-axis in diagrams (C), (D), (G) and (H). 237
VI.8 Amount of adsorbed protein (HSA or lysozyme) in dependence of the concentration of the protein solution on surfaces with (A) APD, (B) PPI-G2, (C) PPI-G4, (D) PAMAM polymer, (E) PEI polymer or (F) AMAM. Please note the differing y-axes. 238
VI.9 Amount of adsorbed protein (HSA or lysozyme) in dependence of the concentration of the protein solution on surfaces with (A) SAM-NH_2, (B) DMAPS, (C) SAM-NMe_2 and (D) SAM-NO. Please note the differing y-axes. 239
VI.10 Dependence of the protein adsorption from solutions of (A) HSA or (B) lysozyme as well as (C) saliva and (D) FBS on the total SFE of the surface modifications. 240
VI.11 Dependence of the protein adsorption from solutions of (A) HSA or (B) lysozyme as well as (C) saliva and (D) FBS on the dispersive component of the SFE of amine-based modifications. 240
VI.12 Dependence of the protein adsorption from solutions of (A) HSA or (B) lysozyme as well as (C) saliva and (D) FBS on the polar component of the SFE of amine-based coatings. 241
VI.13 Analysis of the morphology of MG-63 cells after 1 h of cultivation on oxidized titanium substrates (A–D) or APD-modified surfaces (E–H), obtained from SEM images. 242
VI.14 Analysis of the morphology of MG-63 cells after 1 h of cultivation on PPI-G4-modified substrates (A–D) or PEI polymer-coated wafers (E–H), obtained from SEM images. 243
VI.15 Analysis of the morphology of MG-63 cells after 24 h of cultivation on oxidized titanium substrates (A–D) or APD-modified surfaces (E–H), obtained from SEM images. 244

VI.16 Analysis of the morphology of MG-63 cells after 24 h of cultivation on PPI-G4-modified substrates (A–D) or PEI polymer-coated wafers (E–H), obtained from SEM images. 245
VI.17 Actin cytoskeleton of MG-63 cells after 1 h of cultivation on oxidized titanium substrates (A–D) or APD-modified surfaces (E–H) (red: actin, blue: nucleus). 246
VI.18 Actin cytoskeleton of MG-63 cells after 1 h of cultivation on PPI-G4-modified substrates (A–D) or PEI polymer-coated wafers (E–H) (red: actin, blue: nucleus). 247
VI.19 Actin cytoskeleton of MG-63 cells after 24 h of cultivation on oxidized titanium substrates (A–D) or APD-modified surfaces (E–H) (red: actin, blue: nucleus). 248
VI.20 Actin cytoskeleton of MG-63 cells after 24 h of cultivation on PPI-G4-modified substrates (A–D) or PEI polymer-coated wafers (E–H) (red: actin, blue: nucleus). 249

List of Tables

1.1 Summary of the major classes of biomaterials, examples and applications [2]. 9

3.1 Examples of residues tolerable in PAA synthesis [88]. The blue circle depicts the nitrogen atom(s), the moieties are linked to. 26

4.1 Overview of the parameters influencing protein adsorption. 42
4.2 Scheme for the prediction of protein adsorption depending on substrate and protein properties, as proposed by Norde [181]. Blue color indicates protein adsorption under the given conditions. 44

6.1 Summary of the main electrokinetic effects used for the determination of the zeta potential, distinguished according to the mobility of sample surface and the applied driving force [249]. 62

9.1 Summary of the reagent concentrations for the immobilization of APD, PPI-G2 and PPI-G4 on TESPSA-functionalized substrates. 91

11.1 Survey of the primary antibodies used in immunostaining of salivary or serum proteins after separation via SDS-PAGE. 106
11.2 Survey of the fluorescently labeled secondary antibodies used in immunostaining of salivary or serum proteins after separation via SDS-PAGE. 106

IV.1 Overview of the use of different substrate geometries for the various analysis techniques. 112
IV.2 Survey of the investigated surface modifications and applied analytical techniques, presented in this PhD thesis. 113

13.1 Chemical composition of self-assembled monolayers with different terminal functional groups, determined via XPS. 116
13.2 Static contact angles (with water, formamide and diiodomethane) of self-assembled monolayers with different end groups and their precursor SAMs. Similar water conact angles have previously been published [13, 15–18, 20, 21]. 120
13.3 Surface tensions γ as well as their components γ^{LW}, γ^{+} and γ^{-} of water, formamide and diiodomethane for the SFE calculation, summarized by Kwok [290]. 121

13.4 Isoelectric point and zeta potential at pH 7.4 and pH 8.3, obtained from streaming current measurements of wafers with functionalized self-assembled monolayers. 124
13.5 Summarized analysis of the bands obtained on the stained gel after SDS-PAGE of proteins, adsorbed from human saliva onto SAMs with different functional groups. The following situations are differentiated here: no band detected (✖), band weakly visible (🔵), band similar to reference lane with saliva (✚), medium or strong accumulation with respect to whole saliva as reference (✚ ✚ and ✚ ✚ ✚). 138
13.6 Summarized analysis of the immunoblotting with antibodies against different salivary proteins adsorbed on SAMs with varying functional groups. The following situations are differentiated here: no band detected (✖), band weakly visible (🔵), band similar to reference lane with saliva (✚), medium or strong accumulation with respect to saliva reference (✚ ✚ and ✚ ✚ ✚). 140
13.7 Summarized analysis of the bands obtained on the stained gel after SDS-PAGE of proteins, adsorbed from human serum onto SAMs with different functional groups. The following situations are differentiated here: no band detected (✖), band weakly visible (🔵), band similar to reference lane with serum (✚), medium or strong accumulation with respect to serum reference (✚ ✚ and ✚ ✚ ✚). 144
13.8 Summarized analysis of the immunoblotting with antibodies against different human serum proteins adsorbed on SAMs with varying functional groups. The following situations are differentiated here: no band detected (✖), band weakly visible (🔵), band similar to reference lane with serum (✚), medium or strong accumulation with respect to serum reference (✚ ✚ and ✚ ✚ ✚). 146

14.1 Chemical composition of amine group-bearing surface modifications with oligomeric or polymeric structure in comparison with the intermediate SAMs, determined via XPS. 155
14.2 Static contact angles (with water, formamide and diiodomethane) for amine-based surface modifications. Results for contact angles with formamide or diiodomethane have partially been published in the preceding master's thesis [22]. 161
14.3 Isoelectric point and zeta potential at pH 7.4 of amine-based surface functionalizations as well as of their precursor SAMs, as determined from electrophoretic and streaming current measurements. 170

15.1 Elemental composition of osmolyte-based surface coatings and their precursor SAMs, as determined via XPS. 185
15.2 Contact angles (with water, formamide and diiodomethane) for osmolyte-functionalized surfaces, as obtained from static contact angle measurements. 189
15.3 Isoelectric point and zeta potential at pH 7.4 of osmolyte-based modifications and their respective precursor SAMs, as determined from electrophoretic and streaming current measurements. 196

16.1 Elemental composition of oxidized or APD, PPI-G4 or PEI polymer-modified titanium wafers in comparison with silicon wafer substrates. . 202
16.2 Static contact angles (with water, formamide and diiodomethane) on titanium wafers without functionalization (oxidized) or with APD, PPI-G4 or PEI polymer coating. Contact angles of the same modifications on silicon wafers are added for comparison. 204
16.3 Isoelectric point and zeta potential at pH 7.4, determined from streaming current measurements of oxidized or functionalized titanium wafers. Elektrokinetic data for silicon substrates, obtained via streaming current or electrophoretic measurements, is included for comparison. 208
VI.1 Survey of the dynamic contact angles obtained from tensiometric measurements with sf-water and PBS buffer of amine-based functionalizations and their precursor SAMs. Advancing and receding angles are provided for the cycles 1, 2, 5 and 10. 232
VI.2 Survey of the dynamic contact angles obtained from tensiometric measurements with sf-water and PBS buffer of osmolyte-based coatings and their precursor SAMs. Advancing and receding angles are provided for the cycles 1, 2, 5 and 10. 233

Bibliography

[1] H. J. Busscher, H. C. van der Mei, G. Subbiahdoss, et al., "Biomaterial-associated infection: Locating the finish line in the race for the surface", *Sci. Transl. Med.* **2012**, *4*, 153rv10.

[2] J. Park, R. S. Lakes, *Biomaterials: An Introduction*, 3rd ed., Springer, New York, NY, **2007**, pp. 1–16.

[3] D. F. Williams, "On the mechanisms of biocompatibility", *Biomaterials* **2008**, *29*, 2941–2953.

[4] X. Deng, M. Korogiannaki, B. Rastegari, et al., ""Click" chemistry-tethered hyaluronic acid-based contact lens coatings improve lens wettability and lower protein adsorption", *ACS Appl. Mater. Interfaces* **2016**, *8*, 22064–22073.

[5] A. Civantos, E. Martínez-Campos, V. Ramos, et al., "Titanium coatings and surface modifications: Toward clinically useful bioactive implants", *ACS Biomater. Sci. Eng.* **2017**, *3*, 1245–1261.

[6] H. Li, J. Li, J. Jiang, et al., "An osteogenesis/angiogenesis-stimulation artificial ligament for anterior cruciate ligament reconstruction", *Acta Biomater.* **2017**, *54*, 399–410.

[7] J. M. Courtney, N. M. K. Lamba, S. Sundaram, et al., "Biomaterials for blood-contacting applications", *Biomaterials* **1994**, *15*, 737–744.

[8] J. D. Bryers, "Medical biofilms", *Biotechnol. Bioeng.* **2008**, *100*, 1–18.

[9] A. G. Gristina, "Biomaterial-centered infection: Microbial adhesion versus tissue integration", *Science* **1987**, *237*, 1588–1595.

[10] Q. Yang, C. Kaul, M. Ulbricht, "Anti-nonspecific protein adsorption properties of biomimetic glycocalyx-like glycopolymer layers: Effects of glycopolymer chain density and protein size", *Langmuir* **2010**, *26*, 5746–5752.

[11] M. Jäger, C. Zilkens, K. Zanger, et al., "Significance of nano- and microtopography for cell-surface interactions in orthopaedic implants", *J. Biomed. Biotechnol.* **2007**, *2007*, 69036.

[12] C. J. Wilson, R. E. Clegg, D. I. Leavesley, et al., "Mediation of biomaterial-cell interactions by adsorbed proteins: A review", *Tissue Eng.* **2005**, *11*, 1–18.

[13] V. Katzur, "Charged dendrimers as antimicrobial coatings for biomaterials", PhD thesis, University of Regensburg, Regensburg, **2015**.

[14] P. H. Yancey, "Organic osmolytes as compatible, metabolic and counteracting cytoprotectants in high osmolarity and other stresses", *J. Exp. Biol.* **2005**, *208*, 2819–2830.

[15] H. Schweikl, R. Müller, C. Englert, et al., "Proliferation of osteoblasts and fibroblasts on model surfaces of varying roughness and surface chemistry", *J. Mater. Sci. Mater. Med.* **2007**, *18*, 1895–1905.

[16] R. Müller, S. Ruhl, K.-A. Hiller, et al., "Adhesion of eucaryotic cells and Staphylococcus aureus to silicon model surfaces", *J. Biomed. Mater. Res. A* **2008**, *84*, 817–827.

[17] R. Müller, G. Gröger, K.-A. Hiller, et al., "Fluorescence-based bacterial overlay method for simultaneous in situ quantification of surface-attached bacteria", *Appl. Environ. Microbiol.* **2007**, *73*, 2653–2660.

[18] V. Katzur, M. Eichler, E. Deigele, et al., "Surface-immobilized PAMAM-dendrimers modified with cationic or anionic terminal functions: Physicochemical surface properties and conformational changes after application of liquid interface stress", *J. Colloid Interface Sci.* **2012**, *366*, 179–190.

[19] M. Eichler, V. Katzur, L. Scheideler, et al., "The impact of dendrimer-grafted modifications to model silicon surfaces on protein adsorption and bacterial adhesion", *Biomaterials* **2011**, *32*, 9168–9179.

[20] S. Staehlke, J. Lehnfeld, A. Schneider, et al., "Terminal chemical functions of polyamidoamine dendrimer surfaces and its impact on bone cell growth", *Mater. Sci. Eng. C* **2019**, *101*, 190–203.

[21] R. Müller, K.-A. Hiller, G. Schmalz, et al., "Chemiluminescence-based detection and comparison of protein amounts adsorbed on differently modified silica surfaces", *Anal. Biochem.* **2006**, *359*, 194–202.

[22] J. Lehnfeld, "Development of novel surface functionalizations for biomaterials: Synthesis, analysis of physicochemical properties and their influence on protein adsorption", Master's thesis, University of Regensburg, Regensburg, **2016**.

[23] D. Klee, H. Höcker, "Polymers for biomedical applications: Improvement of the interface compatibility" in *Biomedical Applications/Polymer Blends*, Advances in Polymer Science 149, Springer, Berlin, **1999**, pp. 1–57.

[24] F. Poncin-Epaillard, T. Vrlinic, D. Debarnot, et al., "Surface treatment of polymeric materials controlling the adhesion of biomolecules", *J. Funct. Biomater.* **2012**, *3*, 528–543.

[25] R. Müller, J. Abke, E. Schnell, et al., "Influence of surface pretreatment of titanium- and cobalt-based biomaterials on covalent immobilization of fibrillar collagen", *Biomaterials* **2006**, *27*, 4059–4068.

[26] F. Y. Oliva, L. B. Avalle, O. R. Cámara, et al., "Adsorption of human serum albumin (HSA) onto colloidal TiO_2 particles, Part I", *J. Colloid Interface Sci.* **2003**, *261*, 299–311.

[27] S. Tosatti, S. M. De Paul, A. Askendal, et al., "Peptide functionalized poly(L-lysine)-g-poly(ethylene glycol) on titanium: Resistance to protein adsorption in full heparinized human blood plasma", *Biomaterials* **2003**, *24*, 4949–4958.

[28] K. Rezwan, L. P. Meier, L. J. Gauckler, "Lysozyme and bovine serum albumin adsorption on uncoated silica and AlOOH-coated silica particles: The influence of positively and negatively charged oxide surface coatings", *Biomaterials* **2005**, *26*, 4351–4357.

[29] M. M. Gentleman, E. Gentleman, "The role of surface free energy in osteoblast-biomaterial interactions", *Int. Mater. Rev.* **2014**, *59*, 417–429.

[30] J. G. B. Nebe, F. Luethen, R. Lange, et al., "Interface interactions of osteoblasts with structured titanium and the correlation between physicochemical characteristics and cell biological parameters", *Macromol. Biosci.* **2007**, *7*, 567–578.

[31] B. Finke, F. Luethen, K. Schroeder, et al., "The effect of positively charged plasma polymerization on initial osteoblastic focal adhesion on titanium surfaces", *Biomaterials* **2007**, *28*, 4521–4534.

[32] S. Onclin, B. J. Ravoo, D. N. Reinhoudt, "Engineering silicon oxide surfaces using self-assembled monolayers", *Angew. Chem. Int. Ed.* **2005**, *44*, 6282–6304.

[33] A. Ulman, "Formation and structure of self-assembled monolayers", *Chem. Rev.* **1996**, *96*, 1533–1554.

[34] C. Nicosia, J. Huskens, "Reactive self-assembled monolayers: From surface functionalization to gradient formation", *Mater. Horiz.* **2014**, *1*, 32–45.

[35] W. C. Bigelow, D. L. Pickett, W. A. Zisman, "Oleophobic monolayers. I. Films adsorbed from solution in non-polar liquids", *J. Colloid Sci.* **1946**, *1*, 513–538.

[36] J. Sagiv, "Organized monolayers by adsorption. 1. Formation and structure of oleophobic mixed monolayers on solid surfaces", *J. Am. Chem. Soc.* **1980**, *102*, 92–98.

[37] S. Casalini, C. A. Bortolotti, F. Leonardi, et al., "Self-assembled monolayers in organic electronics", *Chem. Soc. Rev.* **2017**, *46*, 40–71.

[38] C. Haensch, S. Hoeppener, U. S. Schubert, "Chemical modification of self-assembled silane based monolayers by surface reactions", *Chem. Soc. Rev.* **2010**, *39*, 2323–2334.

[39] D. K. Aswal, S. Lenfant, D. Guerin, et al., "Self assembled monolayers on silicon for molecular electronics", *Anal. Chim. Acta* **2006**, *568*, 84–108.

[40] N. Herzer, S. Hoeppener, U. S. Schubert, "Fabrication of patterned silane based self-assembled monolayers by photolithography and surface reactions on silicon-oxide substrates", *Chem. Commun.* **2010**, *46*, 5634–5652.

[41] S. R. Wasserman, Y.-T. Tao, G. M. Whitesides, "Structure and reactivity of alkylsiloxane monolayers formed by reaction of alkyltrichlorosilanes on silicon substrates", *Langmuir* **1989**, *5*, 1074–1087.

[42] L. Netzer, R. Iscovici, J. Sagiv, "Adsorbed monolayers versus Langmuir-Blodgett monolayers - Why and how? I: From monolayer to multilayer, by adsorption", *Thin Solid Films* **1983**, *99*, 235–241.

[43] T. P. Sullivan, W. T. S. Huck, "Reactions on monolayers: Organic synthesis in two dimensions", *Eur. J. Org. Chem.* **2003**, *2003*, 17–29.

[44] H. O. Finklea, L. R. Robinson, A. Blackburn, et al., "Formation of an organized monolayer by solution adsorption of octadecyltrichlorosilane on gold: Electrochemical properties and structural characterization", *Langmuir* **1986**, *2*, 239–244.

[45] P. Silberzan, L. Léger, D. Ausserré, et al., "Silanation of silica surfaces. A new method of constructing pure or mixed monolayers", *Langmuir* **1991**, *7*, 1647–1651.

[46] N. S. Bhairamadgi, S. P. Pujari, F. G. Trovela, et al., "Hydrolytic and thermal stability of organic monolayers on various inorganic substrates", *Langmuir* **2014**, *30*, 5829–5839.

[47] A. Chandekar, S. K. Sengupta, J. E. Whitten, "Thermal stability of thiol and silane monolayers: A comparative study", *Appl. Surf. Sci.* **2010**, *256*, 2742–2749.

[48] R. Helmy, A. Y. Fadeev, "Self-assembled monolayers supported on TiO_2 comparison of $C_{18}H_{37}SiX_3$ (X = H, Cl, OCH_3), $C_{18}H_{37}Si(CH_3)_2Cl$, and $C_{18}H_{37}PO(OH)_2$", *Langmuir* **2002**, *18*, 8924–8928.

[49] A. Wang, H. Tang, T. Cao, et al., "In vitro stability study of organosilane self-assemble monolayers and multilayers", *J. Colloid Interface Sci.* **2005**, *291*, 438–447.

[50] D. G. Kurth, T. Bein, “Surface reactions on thin layers of silane coupling agents”, *Langmuir* **1993**, *9*, 2965–2973.

[51] T. Lummerstorfer, H. Hoffmann, “Click chemistry on surfaces: 1,3-Dipolar cycloaddition reactions of azide-terminated monolayers on silica”, *J. Phys. Chem. B* **2004**, *108*, 3963–3966.

[52] N. Balachander, C. N. Sukenik, “Monolayer transformation by nucleophilic substitution: Applications to the creation of new monolayer assemblies”, *Langmuir* **1990**, *6*, 1621–1627.

[53] G. Tesoro, Y. Wu, “Silane coupling agents: The role of the organofunctional group”, *J. Adhes. Sci. Technol.* **1991**, *5*, 771–784.

[54] A. W. Bosman, H. M. Janssen, E. W. Meijer, “About dendrimers: Structure, physical properties, and applications”, *Chem. Rev.* **1999**, *99*, 1665–1688.

[55] S. M. Grayson, J. M. J. Fréchet, “Convergent dendrons and dendrimers: From synthesis to applications”, *Chem. Rev.* **2001**, *101*, 3819–3867.

[56] C. C. Lee, J. A. MacKay, J. M. J. Fréchet, et al., “Designing dendrimers for biological applications”, *Nat. Biotechnol.* **2005**, *23*, 1517–1526.

[57] E. Buhleier, W. Wehner, F. Vögtle, “"Cascade"- and "nonskid-chain-like" syntheses of molecular cavity topologies”, *Synthesis* **1978**, *2*, 155–158.

[58] D. A. Tomalia, H. Baker, J. Dewald, et al., “A new class of polymers: Starburst-dendritic macromolecules”, *Polym. J.* **1985**, *17*, 117–132.

[59] C. J. Hawker, J. M. J. Fréchet, “Preparation of polymers with controlled molecular architecture. A new convergent approach to dendritic macromolecules”, *J. Am. Chem. Soc.* **1990**, *112*, 7638–7647.

[60] C. Wörner, R. Mülhaupt, “Polynitrile- and polyamine-functional poly(trimethylene imine) dendrimers”, *Angew. Chem. Int. Ed.* **1993**, *32*, 1306–1308.

[61] E. M. M. de Brabander-van den Berg, E. W. Meijer, “Poly(propylene imine) dendrimers: Large-scale synthesis by hetereogeneously catalyzed hydrogenations”, *Angew. Chem. Int. Ed.* **1993**, *32*, 1308–1311.

[62] U. Boas, J. B. Christensen, P. M. H. Heegaard, “Dendrimers: Design, synthesis and chemical properties”, *J. Mater. Chem.* **2006**, *16*, 3785–3798.

[63] J.-P. Majoral, A.-M. Caminade, “Dendrimers containing heteroatoms (Si, P, B, Ge, or Bi)”, *Chem. Rev.* **1999**, *99*, 845–880.

[64] A. Imberty, Y. M. Chabre, R. Roy, “Glycomimetics and glycodendrimers as high affinity microbial anti-adhesins”, *Chem. Eur. J.* **2008**, *14*, 7490–7499.

[65] W. B. Turnbull, J. F. Stoddart, "Design and synthesis of glycodendrimers", *Rev. Mol. Biotechnol.* **2002**, *90*, 231–255.

[66] F. Vögtle, S. Gestermann, R. Hesse, et al., "Functional dendrimers", *Prog. Polym. Sci.* **2000**, *25*, 987–1041.

[67] G. R. Newkome, E. He, C. N. Moorefield, "Suprasupermolecules with novel properties: Metallodendrimers", *Chem. Rev.* **1999**, *99*, 1689–1746.

[68] J. P. Tam, "Synthetic peptide vaccine design: Synthesis and properties of a high-density multiple antigenic peptide system", *Proc. Natl. Acad. Sci. USA* **1988**, *85*, 5409–5413.

[69] M. T. Reetz, G. Lohmer, R. Schwickardi, "Synthesis and catalytic activity of dendritic diphosphane metal complexes", *Angew. Chem. Int. Ed.* **1997**, *36*, 1526–1529.

[70] M. J. Cloninger, "Biological applications of dendrimers", *Curr. Opin. Chem. Biol.* **2002**, *6*, 742–748.

[71] G. J. M. Koper, M. H. P. van Genderen, C. Elissen-Román, et al., "Protonation mechanism of poly(propylene imine) dendrimers and some associated oligo amines", *J. Am. Chem. Soc.* **1997**, *119*, 6512–6521.

[72] R. C. van Duijvenbode, M. Borkovec, G. J. Koper, "Acid-base properties of poly(propylene imine) dendrimers", *Polymer* **1998**, *39*, 2657–2664.

[73] R. L. Lescanec, M. Muthukumar, "Configurational characteristics and scaling behavior of starburst molecules: A computational study", *Macromolecules* **1990**, *23*, 2280–2288.

[74] R. Scherrenberg, B. Coussens, P. van Vliet, et al., "The molecular characteristics of poly(propyleneimine) dendrimers as studied with small-angle neutron scattering, viscosimetry, and molecular dynamics", *Macromolecules* **1998**, *31*, 456–461.

[75] M. Chai, Y. Niu, W. J. Youngs, et al., "Structure and conformation of DAB dendrimers in solution via multidimensional NMR techniques", *J. Am. Chem. Soc.* **2001**, *123*, 4670–4678.

[76] V. Jain, V. Maingi, P. K. Maiti, et al., "Molecular dynamics simulations of PPI dendrimer-drug complexes", *Soft Matter* **2013**, *9*, 6482–6496.

[77] S. Gupta, P. Biswas, "Effect of pH on size and internal structure of poly(propylene imine) dendrimers: A molecular dynamics simulation study", *J. Phys. Chem. B* **2018**, *122*, 9250–9263.

[78] P. Welch, M. Muthukumar, "Tuning the density profile of dendritic polyelectrolytes", *Macromolecules* **1998**, *31*, 5892–5897.

[79] J. F. G. A. Jansen, E. M. M. de Brabander-van den Berg, E. W. Meijer, "Encapsulation of guest molecules into a dendritic box", *Science* **1994**, *266*, 1226–1229.

[80] B. Ziemba, A. Janaszewska, K. Ciepluch, et al., "In vivo toxicity of poly(propyleneimine) dendrimers", *J. Biomed. Mater. Res. A* **2011**, *99 A*, 261–268.

[81] A. Felczak, N. Wrońska, A. Janaszewska, et al., "Antimicrobial activity of poly(propylene imine) dendrimers", *New J. Chem.* **2012**, *36*, 2215–2222.

[82] C. Z. Chen, N. C. Beck-Tan, P. Dhurjati, et al., "Quaternary ammonium functionalized poly(propylene imine) dendrimers as effective antimicrobials: Structure-activity studies", *Biomacromolecules* **2000**, *1*, 473–480.

[83] H. Kobayashi, S.-K. Jo, S. Kawamoto, et al., "Polyamine dendrimer-based MRI contrast agents for functional kidney imaging to diagnose acute renal failure", *J. Magn. Reson. Imaging* **2004**, *20*, 512–518.

[84] M. Skwarczynski, M. Zaman, C. N. Urbani, et al., "Polyacrylate dendrimer nanoparticles: A self-adjuvanting vaccine delivery system", *Angew. Chem. Int. Ed.* **2010**, *49*, 5742–5745.

[85] N. Soni, K. Jain, U. Gupta, et al., "Controlled delivery of gemcitabine hydrochloride using mannosylated poly(propyleneimine) dendrimers", *J. Nanoparticle Res.* **2015**, *17*, 458.

[86] H. Liu, Y. Wang, M. Wang, et al., "Fluorinated poly(propylenimine) dendrimers as gene vectors", *Biomaterials* **2014**, *35*, 5407–5413.

[87] K. Yamamoto, T. Imaoka, M. Tanabe, et al., "New horizon of nanoparticle and cluster catalysis with dendrimers", *Chem. Rev.* **2020**, *120*, 1397–1437.

[88] P. Ferruti, "Poly(amidoamine)s: Past, present, and perspectives", *J. Polym. Sci. A Polym. Chem.* **2013**, *51*, 2319–2353.

[89] E. Mohammadifar, A. N. Kharat, M. Adeli, "Polyamidoamine and polyglycerol; Their linear, dendritic and linear-dendritic architectures as anticancer drug delivery systems", *J. Mater. Chem. B* **2015**, *3*, 3896–3921.

[90] E. Ranucci, A. Manfredi, "Polyamidoamines: Versatile bioactive polymers with potential for biotechnological applications", *Chem. Africa* **2019**, *2*, 167–193.

[91] M. Arioli, A. Manfredi, J. Alongi, et al., "Highlight on the mechanism of linear polyamidoamine degradation in water", *Polymers* **2020**, *12*, 1376.

[92] A. A. Almulathanon, E. Ranucci, P. Ferruti, et al., "Comparison of gene transfection and cytotoxicity mechanisms of linear poly(amidoamine) and branched poly(ethyleneimine) polyplexes", *Pharm. Res.* **2018**, *35*, 86.

[93] E. M. Coma-Cros, A. Biosca, J. Marques, et al., "Polyamidoamine nanoparticles for the oral administration of antimalarial drugs", *Pharmaceutics* **2018**, *10*, 225.

[94] F. Girardi, L. Bergamonti, C. Isca, et al., "Chemical–physical characterization of ancient paper with functionalized polyamidoamines (PAAs)", *Cellulose* **2017**, *24*, 1057–1068.

[95] A. Manfredi, F. Carosio, P. Ferruti, et al., "Linear polyamidoamines as novel biocompatible phosphorus-free surface-confined intumescent flame retardants for cotton fabrics", *Polym. Degrad. Stab.* **2018**, *151*, 52–64.

[96] L. Mascheroni, V. Francia, B. Rossotti, et al., "Light-triggered trafficking to the cell nucleus of a cationic polyamidoamine functionalized with ruthenium complexes", *ACS Appl. Mater. Interfaces* **2020**, *12*, 34576–34587.

[97] N. Mauro, F. Chiellini, C. Bartoli, et al., "RGD-mimic polyamidoamine–montmorillonite composites with tunable stiffness as scaffolds for bone tissue-engineering applications", *J. Tissue Eng. Regen. Med.* **2017**, *11*, 2164–2175.

[98] V. Magnaghi, V. Conte, P. Procacci, et al., "Biological performance of a novel biodegradable polyamidoamine hydrogel as guide for peripheral nerve regeneration", *J. Biomed. Mater. Res. A* **2011**, *98 A*, 19–30.

[99] R. K. Dey, A. R. Ray, "Synthesis, characterization, and blood compatibility of polyamidoamines copolymers", *Biomaterials* **2003**, *24*, 2985–2993.

[100] M. Jäger, S. Schubert, S. Ochrimenko, et al., "Branched and linear poly(ethylene imine)-based conjugates: synthetic modification, characterization, and application", *Chem. Soc. Rev.* **2012**, *41*, 4755–4767.

[101] R. Tanaka, I. Ueoka, Y. Takaki, et al., "High molecular weight linear poly(ethylenimine) and poly(N-methylethylenimine)", *Macromolecules* **1983**, *16*, 849–853.

[102] R. G. Smits, G. J. Koper, M. Mandel, "The influence of nearest- and next-nearest-neighbor interactions on the potentiometric titration of linear poly(ethylenimine)", *J. Phys. Chem.* **1993**, *97*, 5745–5751.

[103] J. D. Ziebarth, Y. Wang, "Understanding the protonation behavior of linear polyethylenimine in solutions through Monte Carlo simulations", *Biomacromolecules* **2010**, *11*, 29–38.

[104] K. A. Gibney, I. Sovadinova, A. I. Lopez, et al., "Poly(ethylene imine)s as antimicrobial agents with selective activity", *Macromol. Biosci.* **2012**, *12*, 1279–1289.

[105] V. Kafil, Y. Omidi, "Cytotoxic impacts of linear and branched polyethylenimine nanostructures in A431 cells", *BioImpacts* **2011**, *1*, 23–30.

[106] S. J. Fox, M. H. U. T. Fazil, C. Dhand, et al., "Insight into membrane selectivity of linear and branched polyethylenimines and their potential as biocides for advanced wound dressings", *Acta Biomater.* **2016**, *37*, 155–164.

[107] M. Erol, H. Du, S. Sukhishvili, "Control of specific attachment of proteins by adsorption of polymer layers", *Langmuir* **2006**, *22*, 11329–11336.

[108] R. Mészáros, L. Thompson, M. Bos, et al., "Adsorption and electrokinetic properties of polyethylenimine on silica surfaces", *Langmuir* **2002**, *18*, 6164–6169.

[109] J. Deng, Z. Liu, Z. Du, et al., "Fabrication of PEI-grafted porous polymer foam for CO_2 capture", *J. Appl. Polym. Sci.* **2019**, *136*, 47844.

[110] D. Yang, P. Fu, F. Zhang, et al., "High efficiency inverted polymer solar cells with room-temperature titanium oxide/polyethylenimine films as electron transport layers", *J. Mater. Chem. A* **2014**, *2*, 17281–17285.

[111] Z. Liu, S. Han, C. Xu, et al., "In situ crosslinked PVA-PEI polymer binder for long-cycle silicon anodes in Li-ion batteries", *RSC Adv.* **2016**, *6*, 68371–68378.

[112] J. Sun, F. Zeng, H. Jian, et al., "Grafting zwitterionic polymer chains onto PEI as a convenient strategy to enhance gene delivery performance", *Polym. Chem.* **2013**, *4*, 5810–5818.

[113] T. Gleede, L. Reisman, E. Rieger, et al., "Aziridines and azetidines: Building blocks for polyamines by anionic and cationic ring-opening polymerization", *Polym. Chem.* **2019**, *10*, 3257–3283.

[114] S. H. Pang, R. P. Lively, C. W. Jones, "Oxidatively-stable linear poly(propylenimine)-containing adsorbents for CO_2 capture from ultradilute streams", *ChemSusChem* **2018**, *11*, 2628–2637.

[115] M. L. Sarazen, C. W. Jones, "Insights into azetidine polymerization for the preparation of poly(propylenimine)-based CO_2 adsorbents", *Macromolecules* **2017**, *50*, 9135–9143.

[116] O. Prucker, J. Rühe, "Synthesis of poly(styrene) monolayers attached to high surface area silica gels through self-assembled monolayers of azo initiators", *Macromolecules* **1998**, *31*, 592–601.

[117] N. Hadjesfandiari, M. P. Bajgai, K. Yu, et al., "Polymer brushes" in *Encyclopedia of Polymer Science and Technology*, (Ed.: H. F. Mark), John Wiley & Sons, Hoboken, NJ, **2013**.

[118] W. J. Brittain, S. Minko, "A structural definition of polymer brushes", *J. Polym. Sci. A Polym. Chem.* **2007**, *45*, 3505–3512.

[119] E. Ruckenstein, Z. F. Li, "Surface modification and functionalization through the self-assembled monolayer and graft polymerization", *Adv. Colloid Interface Sci.* **2005**, *113*, 43–63.

[120] D. Kleshchanok, R. Tuinier, P. R. Lang, "Direct measurements of polymer-induced forces", *J. Phys. Condens. Matter* **2008**, *20*, 73101.

[121] D. Marsh, R. Bartucci, L. Sportelli, "Lipid membranes with grafted polymers: Physicochemical aspects", *Biochim. Biophys. Acta Biomembr.* **2003**, *1615*, 33–59.

[122] M. V. Athawale, J. S. Dordick, S. Garde, "Osmolyte trimethylamine-N-oxide does not affect the strength of hydrophobic interactions: Origin of osmolyte compatibility", *Biophys. J.* **2005**, *89*, 858–866.

[123] M. B. Burg, J. D. Ferraris, "Intracellular organic osmolytes: Function and regulation", *J. Biol. Chem.* **2008**, *283*, 7309–7313.

[124] A. Rani, P. Venkatesu, "Changing relations between proteins and osmolytes: A choice of nature", *Phys. Chem. Chem. Phys.* **2018**, *20*, 20315–20333.

[125] S. Sharma, N. Pathak, K. Chattopadhyay, "Osmolyte induced stabilization of protein molecules: A brief review", *J. Proteins Proteom.* **2012**, *3*, 129–139.

[126] D. W. Bolen, I. V. Baskakov, "The osmophobic effect: Natural selection of a thermodynamic force in protein folding", *J. Mol. Biol.* **2001**, *310*, 955–963.

[127] R. S. Rajan, K. Tsumoto, M. Tokunaga, et al., "Chemical and pharmacological chaperones: Application for recombinant protein production and protein folding diseases", *Curr. Med. Chem.* **2011**, *18*, 1–15.

[128] J. S. Ballantyne, J. W. Robinson, "Freshwater elasmobranchs: A review of their physiology and biochemistry", *J. Comp. Physiol. B* **2010**, *180*, 475–493.

[129] M. Lever, S. Slow, "The clinical significance of betaine, an osmolyte with a key role in methyl group metabolism", *Clin. Biochem.* **2010**, *43*, 732–744.

[130] Q. Shao, S. Jiang, "Molecular understanding and design of zwitterionic materials", *Adv. Mater.* **2015**, *27*, 15–26.

[131] R. G. Laughlin, "Fundamentals of the zwitterionic hydrophilic group", *Langmuir* **1991**, *7*, 842–847.

[132] Q. Shao, S. Jiang, "Influence of charged groups on the properties of zwitterionic moieties: A molecular simulation study", *J. Phys. Chem. B* **2014**, *118*, 7630–7637.

[133] Q. Shao, Y. He, A. D. White, et al., "Difference in hydration between carboxybetaine and sulfobetaine", *J. Phys. Chem. B* **2010**, *114*, 16625–16631.

[134] G. Caron, G. Ermondi, D. Boschi, et al., "Structure-property relationships in the basicity and lipophilicity of arylalkylamine oxides", *Helv. Chim. Acta* **1999**, *82*, 1630–1639.

[135] V. Kocherbitov, V. Veryazov, O. Söderman, "Hydration of trimethylamine-N-oxide and of dimethyldodecylamine-N-oxide: An ab initio study", *J. Mol. Struct. THEOCHEM* **2007**, *808*, 111–118.

[136] L. Szabados, A. Savouré, "Proline: A multifunctional amino acid", *Trends Plant Sci.* **2010**, *15*, 89–97.

[137] R. C. Weast, M. J. Astle, (Eds.), *CRC Handbook of Chemistry and Physics*, 63rd ed., CRC Press, Boca Raton, FL, **1982**, pp. D–169.

[138] O. D. Monera, T. J. Sereda, N. E. Zhou, et al., "Relationship of sidechain hydrophobicity and α-helical propensity on the stability of the single-stranded amphipathic α-helix", *J. Pept. Sci.* **1995**, *1*, 319–329.

[139] B. Schobert, H. Tschesche, "Unusual solution properties of proline and its interaction with proteins", *Biochim. Biophys. Acta* **1978**, *541*, 270–277.

[140] T. Hasan, K. Kumari, S. C. Devi, et al., "Osmolytes in vaccine production, flocculation and storage: A critical review", *Hum. Vaccines Immunother.* **2019**, *15*, 514–525.

[141] J. E. Glasgow, S. L. Capehart, M. B. Francis, et al., "Osmolyte-mediated encapsulation of proteins inside MS2 viral capsids", *ACS Nano* **2012**, *6*, 8658–8664.

[142] M. Kanapathipillai, G. Lentzen, M. Sierks, et al., "Ectoine and hydroxyectoine inhibit aggregation and neurotoxicity of Alzheimer's β-amyloid", *FEBS Lett.* **2005**, *579*, 4775–4780.

[143] H. Yoshida, T. Yoshizawa, F. Shibasaki, et al., "Chemical chaperones reduce aggregate formation and cell death caused by the truncated Machado-Joseph disease gene product with an expanded polyglutamine stretch", *Neurobiol. Dis.* **2002**, *10*, 88–99.

[144] C. R. Brown, L. Q. Hong-Brown, J. Biwersi, et al., "Chemical chaperones correct the mutant phenotype of the ΔF508 cystic fibrosis transmembrane conductance regulator protein", *Cell Stress Chaperones* **1996**, *1*, 117–125.

[145] M. Howard, H. Fischer, J. Roux, et al., "Mammalian osmolytes and S-nitrosoglutathione promote ΔF508 cystic fibrosis transmembrane conductance regulator (CFTR) protein maturation and function", *J. Biol. Chem.* **2003**, *278*, 35159–35167.

[146] F. Evers, R. Steitz, M. Tolan, et al., "Reduced protein adsorption by osmolytes", *Langmuir* **2011**, *27*, 6995–7001.

[147] J. R. Wendorf, C. J. Radke, H. W. Blanch, "Reduced protein adsorption at solid interfaces by sugar excipients", *Biotechnol. Bioeng.* **2004**, *87*, 565–573.

[148] G. Anand, S. N. Jamadagni, S. Garde, et al., "Self-assembly of TMAO at hydrophobic interfaces and its effect on protein adsorption: Insights from experiments and simulations", *Langmuir* **2010**, *26*, 9695–9702.

[149] Y. Chang, S. Chen, Z. Zhang, et al., "Highly protein-resistant coatings from well-defined diblock copolymers containing sulfobetaines", *Langmuir* **2006**, *22*, 2222–2226.

[150] W. K. Cho, B. Kong, I. S. Choi, "Highly efficient non-biofouling coating of zwitterionic polymers: Poly((3-(methacryloylamino)propyl)-dimethyl(3-sulfopropyl)-ammonium hydroxide)", *Langmuir* **2007**, *23*, 5678–5682.

[151] S. Colak, G. N. Tew, "Amphiphilic polybetaines: The effect of side-chain hydrophobicity on protein adsorption", *Biomacromolecules* **2012**, *13*, 1233–1239.

[152] J. Sun, F. Zeng, H. Jian, et al., "Conjugation with betaine: A facile and effective approach to significant improvement of gene delivery properties of PEI", *Biomacromolecules* **2013**, *14*, 728–736.

[153] T. Miyata, N. Ootsuki, K. Nakamae, et al., "Protein adsorption on a copolymer having pendant monosaccharide groups. Relationship between surface free energy and protein adsorption", *Macromol. Chem. Phys.* **1994**, *195*, 3597–3607.

[154] D. A. Dobrzanska, A. L. Cooper, C. G. Dowson, et al., "Oxidation of tertiary amine-derivatized surfaces to control protein adhesion", *Langmuir* **2013**, *29*, 2961–2970.

[155] W. Norde, J. Lyklema, "Why proteins prefer interfaces", *J. Biomater. Sci. Polym. Ed.* **1991**, *2*, 183–202.

[156] K.-C. Chou, Y.-D. Cai, "Predicting protein quaternary structure by pseudo amino acid composition", *Proteins* **2003**, *53*, 282–289.

[157] F. Wold, "In vivo chemical modification of proteins (post-translational modification)", *Annu. Rev. Biochem.* **1981**, *50*, 783–814.

[158] C. Czeslik, "Factors ruling protein adsorption", *Z. Phys. Chem.* **2004**, *218*, 771–801.

[159] R. G. Schipper, E. Silletti, M. H. Vingerhoeds, "Saliva as research material: Biochemical, physicochemical and practical aspects", *Arch. Oral Biol.* **2007**, *52*, 1114–1135.

[160] F. Lagerlöf, J. Ekstrand, "The effect of flow rate on the ionized calcium concentration of human parotid saliva", *Caries Res.* **1982**, *16*, 123–128.

[161] M. W. J. Dodds, D. A. Johnson, C.-K. Yeh, "Health benefits of saliva: A review", *J. Dent.* **2005**, *33*, 223–233.

[162] P. Denny, F. K. Hagen, M. Hardt, et al., "The proteomes of human parotid and submandibular/sublingual gland salivas collected as the ductal secretions", *J. Proteome Res.* **2008**, *7*, 1994–2006.

[163] G. H. Carpenter, "The secretion, components, and properties of saliva", *Annu. Rev. Food Sci. Technol.* **2013**, *4*, 267–276.

[164] J. van der Valk, K. Bieback, C. Buta, et al., "Fetal bovine serum (FBS): Past - present - future", *ALTEX* **2018**, *35*, 99–118.

[165] X. Zheng, H. Baker, W. S. Hancock, et al., "Proteomic analysis for the assessment of different lots of fetal bovine serum as a raw material for cell culture. Part IV. Application of proteomics to the manufacture of biological drugs", *Biotechnol. Prog.* **2006**, *22*, 1294–1300.

[166] W. Yang, H. Xue, W. Li, et al., "Pursuing "zero" protein adsorption of poly(carboxybetaine) from undiluted blood serum and plasma", *Langmuir* **2009**, *25*, 11911–11916.

[167] P. J. Price, E. A. Gregory, "Relationship between in vitro growth promotion and biophysical and biochemical properties of the serum supplement", *In Vitro* **1982**, *18*, 576–584.

[168] V. T. M. dos Santos, A. Mizukami, M. D. Orellana, et al., "Characterization of human AB serum for mesenchymal stromal cell expansion", *Transfus. Med. Hemother.* **2017**, *44*, 11–21.

[169] G. Vidarsson, G. Dekkers, T. Rispens, "IgG subclasses and allotypes: From structure to effector functions", *Front. Immunol.* **2014**, *5*, 520.

[170] K. C. Chan, D. A. Lucas, D. Hise, et al., "Analysis of the human serum proteome", *Clin. Proteom.* **2004**, *1*, 101–225.

[171] K. Nakanishi, T. Sakiyama, K. Imamura, "On the adsorption of proteins on solid surfaces, a common but very complicated phenomenon", *J. Biosci. Bioeng.* **2001**, *91*, 233–244.

[172] M. Rabe, D. Verdes, S. Seeger, "Understanding protein adsorption phenomena at solid surfaces", *Adv. Colloid Interface Sci.* **2011**, *162*, 87–106.

[173] N. Bellassai, A. Marti, G. Spoto, et al., "Low-fouling, mixed-charge poly-L-lysine polymers with anionic oligopeptide side-chains", *J. Mater. Chem. B* **2018**, *6*, 7662–7673.

[174] Q. Yang, C. Kaul, M. Ulbricht, "Anti-nonspecific protein adsorption properties of biomimetic glycocalyx-like glycopolymer layers: Effects of glycopolymer chain density and protein size", *Langmuir* **2010**, *26*, 5746–5752.

[175] M. Kurowska, A. Eickenscheidt, D.-L. Guevara-Solarte, et al., "A simultaneously antimicrobial, protein-repellent, and cell-compatible polyzwitterion network", *Biomacromolecules* **2017**, *18*, 1373–1386.

[176] A. Myles, D. Haberlin, L. Esteban-Tejeda, et al., "Bioinspired aryldiazonium carbohydrate coatings: Reduced adhesion of foulants at polymer and stainless steel surfaces in a marine environment", *ACS Sustain. Chem. Eng.* **2018**, *6*, 1141–1151.

[177] I. Banerjee, R. C. Pangule, R. S. Kane, "Antifouling coatings: Recent developments in the design of surfaces that prevent fouling by proteins, bacteria, and marine organisms", *Adv. Mater.* **2011**, *23*, 690–718.

[178] A. Hucknall, S. Rangarajan, A. Chilkoti, "In pursuit of zero: Polymer brushes that resist the adsorption of proteins", *Adv. Mater.* **2009**, *21*, 2441–2446.

[179] A. Gessner, A. Lieske, B.-R. Paulke, et al., "Functional groups on polystyrene model nanoparticles: Influence on protein adsorption", *J. Biomed. Mater. Res. A* **2003**, *65*, 319–326.

[180] K. M. Hansson, S. Tosatti, J. Isaksson, et al., "Whole blood coagulation on protein adsorption-resistant PEG and peptide functionalised PEG-coated titanium surfaces", *Biomaterials* **2005**, *26*, 861–872.

[181] W. Norde, "My voyage of discovery to proteins in flatland ...and beyond", *Colloids Surf. B* **2008**, *61*, 1–9.

[182] H. Sugiyama, T. Hagiwara, H. Watanabe, et al., "Effects of ionic substances on the adsorption of egg white proteins to a stainless steel surface", *Biosci. Biotechnol. Biochem.* **2012**, *76*, 467–472.

[183] M. Bellion, L. Santen, H. Mantz, et al., "Protein adsorption on tailored substrates: Long-range forces and conformational changes", *J. Phys. Condens. Matter* **2008**, *20*, 404226.

[184] M. Kabiri, L. D. Unsworth, "Application of isothermal titration calorimetry for characterizing thermodynamic parameters of biomolecular interactions: Peptide self-assembly and protein adsorption case studies", *Biomacromolecules* **2014**, *15*, 3463–3473.

[185] D. L. Elbert, J. A. Hubbell, "Surface treatments of polymers for biocompatibility", *Annu. Rev. Mater. Sci.* **1996**, *26*, 365–394.

[186] C. Blaszykowski, S. Sheikh, M. Thompson, "Biocompatibility and antifouling: Is there really a link?", *Trends Biotechnol.* **2014**, *32*, 61–62.

[187] Q. Wei, T. Becherer, S. Angioletti-Uberti, et al., "Protein interactions with polymer coatings and biomaterials", *Angew. Chem. Int. Ed.* **2014**, *53*, 8004–8031.

[188] A. Wörz, B. Berchtold, K. Moosmann, et al., "Protein-resistant polymer surfaces", *J. Mater. Chem.* **2012**, *22*, 19547–19561.

[189] W. Beckner, Y. He, J. Pfaendtner, "Chain flexibility in self-assembled monolayers affects protein adsorption and surface hydration: A molecular dynamics study", *J. Phys. Chem. B* **2016**, *120*, 10423–10432.

[190] S. Chen, L. Li, C. Zhao, et al., "Surface hydration: Principles and applications toward low-fouling/nonfouling biomaterials", *Polymer* **2010**, *51*, 5283–5293.

[191] N. Singh, X. Cui, T. Boland, et al., "The role of independently variable grafting density and layer thickness of polymer nanolayers on peptide adsorption and cell adhesion", *Biomaterials* **2007**, *28*, 763–771.

[192] M. C. Vyner, L. Liu, H. D. Sheardown, et al., "The effect of elastomer chain flexibility on protein adsorption", *Biomaterials* **2013**, *34*, 9287–9294.

[193] L.-C. Xu, C. A. Siedlecki, "Effects of surface wettability and contact time on protein adhesion to biomaterial surfaces", *Biomaterials* **2007**, *28*, 3273–3283.

[194] R. S. Kane, P. Deschatelets, G. M. Whitesides, "Kosmotropes form the basis of protein-resistant surfaces", *Langmuir* **2003**, *19*, 2388–2391.

[195] R. G. Chapman, E. Ostuni, S. Takayama, et al., "Surveying for surfaces that resist the adsorption of proteins", *J. Am. Chem. Soc.* **2000**, *122*, 8303–8304.

[196] R. A. Latour, "Thermodynamic perspectives on the molecular mechanisms providing protein adsorption resistance that include protein-surface interactions", *J. Biomed. Mater. Res. A* **2006**, *78*, 843–854.

[197] S. Lowe, N. M. O'Brien-Simpson, L. A. Connal, "Antibiofouling polymer interfaces: Poly(ethylene glycol) and other promising candidates", *Polym. Chem.* **2015**, *6*, 198–212.

[198] S. J. Sofia, V. Premnath, E. W. Merrill, "Poly(ethylene oxide) grafted to silicon surfaces: Grafting density and protein adsorption", *Macromolecules* **1998**, *31*, 5059–5070.

[199] S.-W. Lee, P. E. Laibinis, "Protein-resistant coatings for glass and metal oxide surfaces derived from oligo(ethylene glycol)-terminated alkyltrichlorosilanes", *Biomaterials* **1998**, *19*, 1669–1675.

[200] G. Qin, C. Cai, "Oxidative degradation of oligo(ethylene glycol)-terminated monolayers", *Chem. Commun.* **2009**, 5112–5114.

[201] S. Jiang, Z. Cao, "Ultralow-fouling, functionalizable, and hydrolyzable zwitterionic materials and their derivatives for biological applications", *Adv. Mater.* **2010**, *22*, 920–932.

[202] R. E. Holmlin, X. Chen, R. G. Chapman, et al., "Zwitterionic SAMs that resist nonspecific adsorption of protein from aqueous buffer", *Langmuir* **2001**, *17*, 2841–2850.

[203] Z. Zhang, S. Chen, S. Jiang, "Dual-functional biomimetic materials: Nonfouling poly(carboxybetaine) with active functional groups for protein immobilization", *Biomacromolecules* **2006**, *7*, 3311–3315.

[204] S. J. Dilly, M. P. Beecham, S. P. Brown, et al., "Novel tertiary amine oxide surfaces that resist nonspecific protein adsorption", *Langmuir* **2006**, *22*, 8144–8150.

[205] B. K. D. Ngo, M. A. Grunlan, "Protein resistant polymeric biomaterials", *ACS Macro Lett.* **2017**, *6*, 992–1000.

[206] C. P. Stallard, K. A. McDonnell, O. D. Onayemi, et al., "Evaluation of protein adsorption on atmospheric plasma deposited coatings exhibiting superhydrophilic to superhydrophobic properties", *Biointerphases* **2012**, *7*, 31.

[207] S. Staehlke, H. Rebl, B. Nebe, "Phenotypic stability of the human MG-63 osteoblastic cell line at different passages", *Cell Biol. Int.* **2019**, *43*, 22–32.

[208] L. Di-Silvio, N. Gurav, "Osteoblasts" in *Human Cell Culture: Volume V: Primary Mesenchymal Cells*, (Eds.: M. R. Koller, B. O. Palsson, J. R. W. Masters), Kluwer Academic Publishers, New York, NY, **2001**, pp. 221–241.

[209] E. M. Czekanska, M. J. Stoddart, J. R. Ralphs, et al., "A phenotypic comparison of osteoblast cell lines versus human primary osteoblasts for biomaterials testing", *J. Biomed. Mater. Res. A* **2014**, *102*, 2636–2643.

[210] K. Anselme, A. Ponche, M. Bigerelle, "Relative influence of surface topography and surface chemistry on cell response to bone implant materials. Part 2: Biological aspects", *Proc. Inst. Mech. Eng. H* **2010**, *224*, 1487–1507.

[211] J. Clover, M. Gowen, "Are MG-63 and HOS TE85 human osteosarcoma cell lines representative models of the osteoblastic phenotype?", *Bone* **1994**, *15*, 585–591.

[212] L. Bacakova, E. Filova, M. Parizek, et al., "Modulation of cell adhesion, proliferation and differentiation on materials designed for body implants", *Biotechnol. Adv.* **2011**, *29*, 739–767.

[213] K. Anselme, "Osteoblast adhesion on biomaterials", *Biomaterials* **2000**, *21*, 667–681.

[214] J. Rychly, B. J. Nebe, "Cell-material interaction", *BioNanoMaterials* **2013**, *14*, 153–160.

[215] W. Song, J. F. Mano, "Interactions between cells or proteins and surfaces exhibiting extreme wettabilities", *Soft Matter* **2013**, *9*, 2985–2999.

[216] S. Staehlke, A. Koertge, B. Nebe, "Intracellular calcium dynamics dependent on defined microtopographical features of titanium", *Biomaterials* **2015**, *46*, 48–57.

[217] S. Chen, Y. Guo, R. Liu, et al., "Tuning surface properties of bone biomaterials to manipulate osteoblastic cell adhesion and signaling pathways for the enhancement of early osseointegration", *Colloids Surf. B* **2018**, *164*, 58–69.

[218] E. Zimmerman, B. Geiger, L. Addadi, "Initial stages of cell-matrix adhesion can be mediated and modulated by cell-surface hyaluronan", *Biophys. J.* **2002**, *82*, 1848–1857.

[219] S. Guo, X. Zhu, M. Li, et al., "Parallel control over surface charge and wettability using polyelectrolyte architecture: Effect on protein adsorption and cell adhesion", *ACS Appl. Mater. Interfaces* **2016**, *8*, 30552–30563.

[220] N. Faucheux, R. Schweiss, K. Lützow, et al., "Self-assembled monolayers with different terminating groups as model substrates for cell adhesion studies", *Biomaterials* **2004**, *25*, 2721–2730.

[221] B. Nebe, B. Finke, F. Lüthen, et al., "Improved initial osteoblast functions on amino-functionalized titanium surfaces", *Biomol. Eng.* **2007**, *24*, 447–454.

[222] J. E. Raynor, T. A. Petrie, K. P. Fears, et al., "Saccharide polymer brushes to control protein and cell adhesion to titanium", *Biomacromolecules* **2009**, *10*, 748–755.

[223] S. VandeVondele, J. Vörös, J. A. Hubbell, "RGD-Grafted poly-L-lysine-graft-(polyethylene glycol) copolymers block non-specific protein adsorption while promoting cell adhesion", *Biotechnol. Bioeng.* **2003**, *82*, 784–790.

[224] J. F. Moulder, W. F. Stickle, P. E. Sobol, et al., *Handbook of X-ray Photoelectron Spectroscopy*, (Ed.: J. Chastain), Perkin-Elmer Corporation, Eden Prairie, MN, **1992**, pp. 9–28.

[225] S. L. McArthur, "Applications of XPS in bioengineering", *Surf. Interface Anal.* **2006**, *38*, 1380–1385.

[226] R. K. Gaur, K. C. Gupta, "A spectrophotometric method for the estimation of amino groups on polymer supports", *Anal. Biochem.* **1989**, *180*, 253–258.

[227] Sulfo-SDTB Instructions, Pierce Chemical Company, Rockford, IL, **1998**.

[228] R. E. Smith, W. R. Davis, "Spectrophotometric Determination of Amines with p-Chloranil", *Anal. Chem.* **1984**, *56*, 2345–2349.

[229] P. G. de Gennes, "Wetting: Statics and dynamics", *Rev. Mod. Phys.* **1985**, *57*, 827–863.

[230] F. Rupp, L. Scheideler, J. Geis-Gerstorfer, "Effect of heterogenic surfaces on contact angle hysteresis: Dynamic contact angle analysis in material sciences", *Chem. Eng. Technol.* **2002**, *25*, 877–882.

[231] D. Y. Kwok, A. W. Neumann, "Contact angle measurement and contact angle interpretation", *Adv. Colloid Interface Sci.* **1999**, *81*, 167–249.

[232] J. M. Schuster, C. E. Schvezov, M. R. Rosenberger, "Influence of experimental variables on the measure of contact angle in metals using the sessile drop method", *Procedia Mater. Sci.* **2015**, *8*, 742–751.

[233] I. Ahmad, C.-W. Kan, "A review on development and applications of bio-inspired superhydrophobic textiles", *Materials* **2016**, *9*, 892.

[234] C. N. C. Lam, R. Wu, D. Li, et al., "Study of the advancing and receding contact angles: Liquid sorption as a cause of contact angle hysteresis", *Adv. Colloid Interface Sci.* **2002**, *96*, 169–191.

[235] R. J. Good, "Contact angle, wetting, and adhesion: A critical review", *J. Adhes. Sci. Technol.* **1992**, *6*, 1269–1302.

[236] C. M. Weikart, M. Miyama, H. K. Yasuda, "Surface modification of conventional polymers by depositing plasma polymers of trimethylsilane and of trimethylsilane + O_2. II. Dynamic wetting properties", *J. Colloid Interface Sci.* **1999**, *211*, 28–38.

[237] R. G. Chaudhuri, S. Paria, "Dynamic contact angles on PTFE surface by aqueous surfactant solution in the absence and presence of electrolytes", *J. Colloid Interface Sci.* **2009**, *337*, 555–562.

[238] L. Wilhelmy, "Ueber die Abhängigkeit der Capillaritäts-Constanten des Alkohols von Substanz und Gestalt des benetzten festen Körpers", *Ann. Phys.* **1863**, *195*, 177–217.

[239] F. Rupp, D. Axmann, C. Ziegler, et al., "Adsorption/desorption phenomena on pure and Teflon® AF-coated titania surfaces studied by dynamic contact angle analysis", *J. Biomed. Mater. Res.* **2002**, *62*, 567–578.

[240] R. Di Mundo, F. Palumbo, "Comments regarding 'An essay on contact angle measurements'", *Plasma Process. Polym.* **2011**, *8*, 14–18.

[241] S. Shalel-Levanon, A. Marmur, "Validity and accuracy in evaluating surface tension of solids by additive approaches", *J. Colloid Interface Sci.* **2003**, *262*, 489–499.

[242] C. Della Volpe, D. Maniglio, M. Brugnara, et al., "The solid surface free energy calculation: I. In defense of the multicomponent approach", *J. Colloid Interface Sci.* **2004**, *271*, 434–453.

[243] C. Zhao, C. Yang, "Advances in electrokinetics and their applications in micro/nano fluidics", *Microfluid. Nanofluidics* **2012**, *13*, 179–203.

[244] Y. Gu, D. Li, "The ζ-potential of glass surface in contact with aqueous solutions", *J. Colloid Interface Sci.* **2000**, *226*, 328–339.

[245] M. Reischl, S. Köstler, G. Kellner, et al., "Oscillating streaming potential measurement system for macroscopic surfaces", *Rev. Sci. Instrum.* **2008**, *79*, 113902.

[246] A. V. Delgado, F. González-Caballero, R. J. Hunter, et al., "Measurement and interpretation of electrokinetic phenomena (IUPAC technical report)", *Pure Appl. Chem.* **2005**, *77*, 1753–1805.

[247] Q. Li, U. Jonas, X. S. Zhao, et al., "The forces at work in colloidal self-assembly: A review on fundamental interactions between colloidal particles", *Asia-Pac. J. Chem. Eng.* **2008**, *3*, 255–268.

[248] D. F. Evans, H. Wennerström, "Electrostatic double-layer forces are long-ranged" in *The Colloidal Domain*, John Wiley & Sons, New York, NY, **1999**, pp. 225–238.

[249] D. F. Evans, H. Wennerström, "Electrokinetic phenomena are used to determine zeta potentials of charged surfaces and particles" in *The Colloidal Domain*, John Wiley & Sons, New York, NY, **1999**, pp. 428–437.

[250] C. Werner, H. Körber, R. Zimmermann, et al., "Extended electrokinetic characterization of flat solid surfaces", *J. Colloid Interface Sci.* **1998**, *208*, 329–346.

[251] R. I. Krohn, "The colorimetric detection and quantitation of total protein", *Curr. Protoc. Cell Biol.* **2011**, *52*, A.3H.1–A.3H.28.

[252] P. K. Smith, R. I. Krohn, G. T. Hermanson, et al., "Measurement of protein using bicinchoninic acid", *Anal. Biochem.* **1985**, *150*, 76–85.

[253] P. R. Srinivas, "Introduction to protein eletrophoresis" in *Protein Electrophoresis: Methods and Protocols*, (Eds.: B. T. Kurien, R. H. Scofield), Methods in Molecular Biology 869, Springer, New York, NY, **2012**, pp. 23–28.

[254] E. Buxbaum, "Electrophoresis" in *Biophysical Chemistry of Proteins, An Introduction to Laboratory Methods*, Springer, Boston, MA, **2011**, pp. 61–95.

[255] U. K. Laemmli, "Cleavage of structural proteins during the assembly of the head of bacteriophage T4", *Nature* **1970**, *227*, 680–685.

[256] D. J. MacPhee, "Methodological considerations for improving Western blot analysis", *J. Pharmacol. Toxicol. Methods* **2010**, *61*, 171–177.

[257] R. K. Sundaram, N. Balasubramaniyan, P. Sundaram, "Protein stains and applications" in *Protein Electrophoresis: Methods and Protocols*, (Eds.: B. T. Kurien, R. H. Scofield), Methods in Molecular Biology 869, Springer, New York, NY, **2012**, pp. 451–464.

[258] H. Bartsch, C. Arndt, S. Koristka, et al., "Silver staining techniques of polyacrylamide gels" in *Protein Electrophoresis: Methods and Protocols*, (Eds.: B. T. Kurien, R. H. Scofield), Methods in Molecular Biology 869, Springer, New York, NY, **2012**, pp. 481–486.

[259] T. Mahmood, P.-C. Yang, "Western blot: Technique, theory, and trouble shooting", *N. Am. J. Med. Sci.* **2012**, *4*, 429–434.

[260] C. P. Moritz, "40 years Western blotting: A scientific birthday toast", *J. Proteom.* **2020**, *212*, 103575.

[261] W. N. Burnette, “"Western Blotting": Electrophoretic transfer of proteins from sodium dodecyl sulfate-polyacrylamide gels to unmodified nitrocellulose and radiographic detection with antibody and radioiodinated protein A”, *Anal. Biochem.* **1981**, *112*, 195–203.

[262] A. Alegria-Schaffer, A. Lodge, K. Vattem, “Performing and optimizing western blots with an emphasis on chemiluminescent detection” in *Guide to Protein Purification, 2nd Edition*, (Eds.: R. R. Burgess, M. P. Detscher), Methods in Enzymology 463, Elsevier, Amsterdam, **2009**, pp. 573–599.

[263] A. Canette, R. Briandet, “Microscopy: Confocal laser scanning microscopy” in *Encyclopedia of Food Microbiology: Second Edition*, (Eds.: C. A. Batt, M. L. Tortorello), Reference Module in Food Science, Elsevier, **2014**, pp. 676–683.

[264] S. W. Paddock, “Principles and practices of laser scanning confocal microscopy”, *Mol. Biotechnol.* **2000**, *16*, 127–149.

[265] U. Resch-Genger, M. Grabolle, S. Cavaliere-Jaricot, et al., “Quantum dots versus organic dyes as fluorescent labels”, *Nat. Methods* **2008**, *5*, 763–775.

[266] B. N. Giepmans, S. R. Adams, M. H. Ellisman, et al., “The fluorescent toolbox for assessing protein location and function”, *Science* **2006**, *312*, 217–224.

[267] M. C. Jamur, C. Oliver, “Permeabilization of cell membranes” in *Immunocytochemical Methods and Protocols*, (Eds.: C. Oliver, M. C. Jamur), Methods in Molecular Biology 588, Springer, New York, NY, **2010**, pp. 63–66.

[268] J. Kapuscinski, “DAPI: A DNA-specific fluorescent probe”, *Biotech. Histochem.* **1995**, *70*, 220–233.

[269] E. Wulf, A. Deboben, F. A. Bautz, et al., “Fluorescent phallotoxin, a tool for the visualization of cellular actin”, *Proc. Natl. Acad. Sci. USA* **1979**, *76*, 4498–4502.

[270] B. J. Belin, L. M. Goins, R. D. Mullins, “Comparative analysis of tools for live cell imaging of actin network architecture”, *Bioarchitecture* **2014**, *4*, 189–202.

[271] Q. Liu, J. Ding, F. K. Mante, et al., “The role of surface functional groups in calcium phosphate nucleation on titanium foil: A self-assembled monolayer technique”, *Biomaterials* **2002**, *23*, 3103–3111.

[272] J.-J. Shyue, M. R. De Guire, T. Nakanishi, et al., “Acid-base properties and zeta potentials of self-assembled monolayers obtained via in situ transformations”, *Langmuir* **2004**, *20*, 8693–8698.

[273] J. Lehnfeld, M. Gruening, M. Kronseder, et al., "Comparison of protein-repellent behavior of linear versus dendrimer-structured surface-immobilized polymers", *Langmuir* **2020**, *36*, 5880–5890.

[274] A. Genest, D. Portinha, E. Fleury, et al., "The aza-Michael reaction as an alternative strategy to generate advanced silicon-based (macro)molecules and materials", *Prog. Polym. Sci.* **2017**, *72*, 61–110.

[275] B. C. Ranu, S. Banerjee, "Significant rate acceleration of the aza-Michael reaction in water", *Tetrahedron Lett.* **2007**, *48*, 141–143.

[276] D. Bernier, U. K. Wefelscheid, S. Woodward, "Properties, preparation and synthetic uses of amine N-oxides. An update", *Org. Prep. Proced. Int.* **2009**, *41*, 173–210.

[277] N. N. Schwartz, J. H. Blumbergs, "Epoxidations with m-chloroperbenzoic acid", *J. Org. Chem.* **1964**, *29*, 1976–1979.

[278] J. C. Craig, K. K. Purushothaman, "An improved preparation of tertiary amine N-oxides", *J. Org. Chem.* **1970**, *35*, 1721–1722.

[279] S. Prakash, T. M. Long, J. C. Selby, et al., ""Click" modification of silica surfaces and glass microfluidic channels", *Anal. Chem.* **2007**, *79*, 1661–1667.

[280] F. Himo, T. Lovell, R. Hilgraf, et al., "Copper(I)-catalyzed synthesis of azoles. DFT study predicts unprecedented reactivity and intermediates", *J. Am. Chem. Soc.* **2005**, *127*, 210–216.

[281] S. E. Blondelle, R. A. Houghten, "Comparison of 55% TFA/CH_2Cl_2 and 100% TFA for Boc group removal during solid-phase peptide synthesis", *Int. J. Pept. Protein Res.* **1993**, *41*, 522–527.

[282] D. M. Shendage, R. Fröhlich, G. Haufe, "Highly efficient stereoconservative amidation and deamidation of α-amino acids", *Org. Lett.* **2004**, *6*, 3675–3678.

[283] S. Thamadilok, K.-S. Choi, L. Ruhl, et al., "Human and nonhuman primate lineage-specific footprints in the salivary proteome", *Mol. Biol. Evol.* **2019**, *37*, 395–405.

[284] S.-M. Heo, K.-S. Choi, L. A. Kazim, et al., "Host defense proteins derived from human saliva bind to Staphylococcus aureus", *Infect. Immun.* **2013**, *81*, 1364–1373.

[285] G. Socrates, *Infrared and Raman Characteristic Group Frequencies: Tables and Charts*, 3rd ed., John Wiley & Sons, Chichester, **2004**.

[286] D. Janssen, R. De Palma, S. Verlaak, et al., "Static solvent contact angle measurements, surface free energy and wettability determination of various self-assembled monolayers on silicon dioxide", *Thin Solid Films* **2006**, *515*, 1433–1438.

[287] R. J. Collins, C. N. Sukenik, "Sulfonate-functionalized, siloxane-anchored, self-assembled monolayers", *Langmuir* **1995**, *11*, 2322–2324.

[288] A. Heise, H. Menzel, H. Yim, et al., "Grafting of polypeptides on solid substrates by initiation of N-carboxyanhydride polymerization by amino-terminated self-assembled monolayers", *Langmuir* **1997**, *13*, 723–728.

[289] R. Müller, A. Eidt, K.-A. Hiller, et al., "Influences of protein films on antibacterial or bacteria-repellent surface coatings in a model system using silicon wafers", *Biomaterials* **2009**, *30*, 4921–4929.

[290] D. Y. Kwok, "The usefulness of the Lifshitz-van der Waals/acid-base approach for surface tension components and interfacial tensions", *Colloids Surf. A* **1999**, *156*, 191–200.

[291] S. H. Behrens, D. G. Grier, "The charge of glass and silica surfaces", *J. Chem. Phys.* **2001**, *115*, 6716–6721.

[292] Y.-H. M. Chan, R. Schweiss, C. Werner, et al., "Electrokinetic characterization of oligo- and poly(ethylene glycol)-terminated self-assembled monolayers on gold and glass surfaces", *Langmuir* **2003**, *19*, 7380–7385.

[293] S. S. Cheng, D. A. Scherson, C. N. Sukenik, "In situ attenuated total reflectance Fourier transform infrared spectroscopy of carboxylate-bearing, siloxane-anchored, self-assembled monolayers: A study of carboxylate reactivity and acid-base properties", *Langmuir* **1995**, *11*, 1190–1195.

[294] E. W. Moore, "Ionized calcium in normal serum, ultrafiltrates, and whole blood determined by ion-exchange electrodes", *J. Clin. Invest.* **1970**, *49*, 318–334.

[295] R. L. Schoch, G. Emilsson, A. B. Dahlin, et al., "Protein exclusion is preserved by temperature sensitive PEG brushes", *Polymer* **2017**, *132*, 362–367.

[296] D. Leckband, S. Sheth, A. Halperin, "Grafted poly(ethylene oxide) brushes as nonfouling surface coatings", *J. Biomater. Sci. Polym. Ed.* **1999**, *10*, 1125–1147.

[297] N. V. Efremova, S. R. Sheth, D. E. Leckband, "Protein-induced changes in poly(ethylene glycol) brushes: Molecular weight and temperature dependence", *Langmuir* **2001**, *17*, 7628–7636.

[298] L. Li, S. Chen, S. Jiang, "Protein interactions with oligo(ethylene glycol) (OEG) self-assembled monolayers: OEG stability, surface packing density and protein adsorption", *J. Biomater. Sci. Polym. Ed.* **2007**, *18*, 1415–1427.

[299] C. von Baeckmann, H. Kählig, M. Lindén, et al., "Irreversible adsorption of serum proteins onto nanoparticles", *Part. Part. Syst. Charact.* **2020**, *38*, 2000273.

[300] Y. L. Jeyachandran, E. Mielczarski, B. Rai, et al., "Quantitative and qualitative evaluation of adsorption/desorption of bovine serum albumin on hydrophilic and hydrophobic surfaces", *Langmuir* **2009**, *25*, 11614–11620.

[301] D. Sarkar, D. K. Chattoraj, "Kinetics of desorption of proteins from the surface of protein-coated alumina by various desorbing reagents", *J. Colloid Interface Sci.* **1996**, *178*, 606–613.

[302] H. Elwing, A. Askendal, I. Lundström, "Desorption of fibrinogen and γ-globulin from solid surfaces induced by a nonionic detergent", *J. Colloid Interface Sci.* **1989**, *128*, 296–300.

[303] A. Sethuraman, M. Han, R. S. Kane, et al., "Effect of surface wettability on the adhesion of proteins", *Langmuir* **2004**, *20*, 7779–7788.

[304] G. B. Sigal, M. Mrksich, G. M. Whitesides, "Effect of surface wettability on the adsorption of proteins and detergents", *J. Am. Chem. Soc.* **1998**, *120*, 3464–3473.

[305] C. Rodriguez Emmenegger, E. Brynda, T. Riedel, et al., "Interaction of blood plasma with antifouling surfaces", *Langmuir* **2009**, *25*, 6328–6333.

[306] L. Lindh, T. Arnebrant, P.-E. Isberg, et al., "Concentration dependence of adsorption from human whole resting saliva at solid/liquid interfaces: An ellipsometric study", *Biofouling* **1999**, *14*, 189–196.

[307] N. Vassilakos, T. Arnebrant, P.-O. Glantz, "Adsorption of whole saliva onto hydrophilic and hydrophobic solid surfaces: Influence of concentration, ionic strength and pH", *Eur. J. Oral Sci.* **1992**, *100*, 346–353.

[308] R. M. Visalakshan, M. N. MacGregor, S. Sasidharan, et al., "Biomaterial surface hydrophobicity-mediated serum protein adsorption and immune responses", *ACS Appl. Mater. Interfaces* **2019**, *11*, 27615–27623.

[309] A. Michiardi, C. Aparicio, B. D. Ratner, et al., "The influence of surface energy on competitive protein adsorption on oxidized NiTi surfaces", *Biomaterials* **2007**, *28*, 586–594.

[310] L. De Bartolo, A. Gugliuzza, S. Morelli, et al., "Novel PEEK-WC membranes with low plasma protein affinity related to surface free energy parameters", *J. Mater. Sci. Mater. Med.* **2004**, *15*, 877–883.

[311] J. Comelles, M. Estévez, E. Martínez, et al., "The role of surface energy of technical polymers in serum protein adsorption and MG-63 cells adhesion", *Nanomedicine* **2010**, *6*, 44–51.

[312] S. Patil, A. Sandberg, E. Heckert, et al., "Protein adsorption and cellular uptake of cerium oxide nanoparticles as a function of zeta potential", *Biomaterials* **2007**, *28*, 4600–4607.

[313] M. Lück, B.-R. Paulke, W. Schröder, et al., "Analysis of plasma protein adsorption on polymeric nanoparticles with different surface characteristics", *J. Biomed. Mater. Res.* **1998**, *39*, 478–485.

[314] A. El-Ghannam, E. Hamazawy, A. Yehia, "Effect of thermal treatment on bioactive glass microstructure, corrosion behavior, ζ potential, and protein adsorption", *J. Biomed. Mater. Res.* **2001**, *55*, 387–395.

[315] J. L. Dalsin, L. Lin, S. Tosatti, et al., "Protein resistance of titanium oxide surfaces modified by biologically inspired mPEG-DOPA", *Langmuir* **2005**, *21*, 640–646.

[316] F. Meder, T. Daberkow, L. Treccani, et al., "Protein adsorption on colloidal alumina particles functionalized with amino, carboxyl, sulfonate and phosphate groups", *Acta Biomater.* **2012**, *8*, 1221–1229.

[317] M. Kim, M. Sasaki, K. Saito, et al., "Protein adsorption characteristics of a sulfonic-acid-group-containing nonwoven fabric", *Biotechnol. Prog.* **1998**, *14*, 661–663.

[318] S. Ayyaru, Y.-H. Ahn, "Application of sulfonic acid group functionalized graphene oxide to improve hydrophilicity, permeability, and antifouling of PVDF nanocomposite ultrafiltration membranes", *J. Membr. Sci.* **2017**, *525*, 210–219.

[319] A. Hasan, G. Waibhaw, L. M. Pandey, "Conformational and organizational insights into serum proteins during competitive adsorption on self-assembled monolayers", *Langmuir* **2018**, *34*, 8178–8194.

[320] M. C. L. Martins, B. D. Ratner, M. A. Barbosa, "Protein adsorption on mixtures of hydroxyl- and methyl-terminated alkanethiols self-assembled monolayers", *J. Biomed. Mater. Res. A* **2003**, *67*, 158–171.

[321] C. F. Wertz, M. M. Santore, "Effect of surface hydrophobicity on adsorption and relaxation kinetics of albumin and fibrinogen: Single-species and competitive behavior", *Langmuir* **2001**, *17*, 3006–3016.

[322] R. C. Krieg, Y. Dong, K. Schwamborn, et al., "Protein quantification and its tolerance for different interfering reagents using the BCA-method with regard to 2D SDS PAGE", *J. Biochem. Biophys. Methods* **2005**, *65*, 13–19.

[323] J. Cortés-Ríos, A. M. Zárate, J. D. Figueroa, et al., "Protein quantification by bicinchoninic acid (BCA) assay follows complex kinetics and can be performed at short incubation times", *Anal. Biochem.* **2020**, *608*, 113904.

[324] V. Kumar, J. Pulpytel, H. Rauscher, et al., "Fluorocarbon coatings via plasma enhanced chemical vapor deposition of 1H,1H,2H,2H-perfluorodecyl acrylate - 2, morphology, wettability and antifouling characterization", *Plasma Process. Polym.* **2010**, *7*, 926–938.

[325] Z. Wang, H. Zuilhof, "Self-healing superhydrophobic fluoropolymer brushes as highly protein-repellent coatings", *Langmuir* **2016**, *32*, 6310–6318.

[326] L. Lindh, W. Aroonsang, J. Sotres, et al., "Salivary pellicles", *Monogr. Oral Sci.* **2014**, *24*, 30–39.

[327] M. Martínez-Hernández, V. I. García-Pérez, A. Almaguer-Flores, "Potential of salivary proteins to reduce oral bacterial colonization on titanium implant surfaces", *Mater. Lett.* **2019**, *252*, 120–122.

[328] W. Aroonsang, J. Sotres, Z. El-Schich, et al., "Influence of substratum hydrophobicity on salivary pellicles: organization or composition?", *Biofouling* **2014**, *30*, 1123–1132.

[329] L. Lindh, P.-O. Glantz, N. Strömberg, et al., "On the adsorption of human acidic proline-rich proteins (PRP-1 and PRP-3) and statherin at solid/liquid interfaces", *Biofouling* **2002**, *18*, 87–94.

[330] C.-M. Huang, "Comparative proteomic analysis of human whole saliva", *Arch. Oral Biol.* **2004**, *49*, 951–962.

[331] A. Bennick, "Salivary proline-rich proteins", *Mol. Cell. Biochem.* **1982**, *45*, 83–99.

[332] A. Walz, S. Odenbreit, K. Stühler, et al., "Identification of glycoprotein receptors within the human salivary proteome for the lectin-like BabA and SabA adhesins of Helicobacter pylori by fluorescence-based 2-D bacterial overlay", *Proteomics* **2009**, *9*, 1582–1592.

[333] J. Schaller, S. Gerber, U. Kämpfer, et al., "The immune system" in *Human Blood Plasma Proteins: Structure and Function*, John Wiley & Sons, Chichester, **2008**, pp. 195–229.

[334] M. A. Kerr, "The structure and function of human IgA", *Biochem. J.* **1990**, *271*, 285–296.

[335] V. Silin, H. Weetall, D. J. Vanderah, "SPR studies of the nonspecific adsorption kinetics of human IgG and BSA on gold surfaces modified by self-sssembled monolayers (SAMs)", *J. Colloid Interface Sci.* **1997**, *185*, 94–103.

[336] B. Lassen, K. Holmberg, C. Brink, et al., "Binding of salivary proteins and oral bacteria to hydrophobic and hydrophilic surfaces in vivo and in vitro", *Colloid Polym. Sci.* **1994**, *272*, 1143–1150.

[337] X. Wang, Y. Wang, H. Xu, et al., "Dynamic adsorption of monoclonal antibody layers on hydrophilic silica surface: A combined study by spectroscopic ellipsometry and AFM", *J. Colloid Interface Sci.* **2008**, *323*, 18–25.

[338] T. Taniguchi, D. Duracher, T. Delair, et al., "Adsorption/desorption behavior and covalent grafting of an antibody onto cationic amino-functionalized poly(styrene-N-isopropylacrylamide) core-shell latex particles", *Colloids Surf. B* **2003**, *29*, 53–65.

[339] R. J. Mairs, J. A. Beeley, "Isoelectric focusing of human salivary secretory-IgA", *Arch. Oral Biol.* **1987**, *32*, 873–877.

[340] T. Takeuchi, T. Matsushima, T. Sugimura, "Separation of human α-amylase isozymes by electro-focusing and their immunological properties", *Clin. Chim. Acta* **1975**, *60*, 207–213.

[341] L. A. Bobek, H. Tsai, A. R. Biesbrock, et al., "Molecular cloning, sequence, and specificity of expression of the gene encoding the low molecular weight human salivary mucin (MUC7)", *J. Biol. Chem.* **1993**, *268*, 20563–20569.

[342] L. Shi, K. D. Caldwell, "Mucin adsorption to hydrophobic surfaces", *J. Colloid Interface Sci.* **2000**, *224*, 372–381.

[343] L. Lindh, P.-O. Glantz, I. Carlstedt, et al., "Adsorption of MUC5B and the role of mucins in early salivary film formation", *Colloids Surf. B* **2002**, *25*, 139–146.

[344] A. J. M. Ligtenberg, N. G. Karlsson, E. C. I. Veerman, "Deleted in malignant brain tumors-1 protein (DMBT1): A pattern recognition receptor with multiple binding sites", *Int. J. Mol. Sci.* **2010**, *11*, 5212–5233.

[345] J. Madsen, J. Mollenhauer, U. Holmskov, "Gp-340/DMBT1 in mucosal innate immunity", *Innate Immun.* **2010**, *16*, 160–167.

[346] C.-G. Liu, M.-C. Zhu, Z.-N. Chen, "Preparation and purification of F(ab')$_2$ fragment from anti hepatoma mouse IgG$_1$ mAb", *World J. Gastroenterol.* **1999**, *5*, 522–524.

[347] R. Pankov, K. M. Yamada, "Fibronectin at a glance", *J. Cell Sci.* **2002**, *115*, 3861–3863.

[348] J. Schaller, S. Gerber, U. Kämpfer, et al., "Blood coagulation and fibrinolysis" in *Human Blood Plasma Proteins: Structure and Function*, John Wiley & Sons, Chichester, **2008**, pp. 89–150.

[349] B. J. Boughton, A. W. Simpson, "The biochemical and functional heterogeneity of circulating human plasma fibronectin", *Biochem. Biophys. Res. Commun.* **1984**, *119*, 1174–1180.

[350] R. M. Shelton, A. C. Rasmussen, J. E. Davies, "Protein adsorption at the interface between charged polymer substrata and migrating osteoblasts", *Biomaterials* **1988**, *9*, 24–29.

[351] B. G. Keselowsky, D. M. Collard, A. J. García, "Surface chemistry modulates fibronectin conformation and directs integrin binding and specificity to control cell adhesion", *J. Biomed. Mater. Res. A* **2003**, *66*, 247–259.

[352] D. Kohavi, A. Klinger, D. Steinberg, et al., "Adsorption of salivary proteins onto prosthetic titanium components", *J. Prosthet. Dent.* **1995**, *74*, 531–534.

[353] S.-J. Lee, H.-S. Kho, S.-W. Lee, et al., "Experimental salivary pellicles on the surface of orthodontic materials", *Am. J. Orthod. Dentofac. Orthop.* **2001**, *119*, 59–66.

[354] R. V. Soares, T. Lin, C. C. Siqueira, et al., "Salivary micelles: Identification of complexes containing MG2, sIgA, lactoferrin, amylase, glycosylated proline-rich protein and lysozyme", *Arch. Oral Biol.* **2004**, *49*, 337–343.

[355] A. Sarkar, F. Xu, S. Lee, "Human saliva and model saliva at bulk to adsorbed phases – similarities and differences", *Adv. Colloid Interface Sci.* **2019**, *273*, 102034.

[356] L. Vroman, A. L. Adams, "Adsorption of proteins out of plasma and solutions in narrow spaces", *J. Colloid Interface Sci.* **1986**, *111*, 391–402.

[357] T. Sterzenbach, R. Helbig, C. Hannig, et al., "Bioadhesion in the oral cavity and approaches for biofilm management by surface modifications", *Clin. Oral Investig.* **2020**, *24*, 4237–4260.

[358] F. J. Bikker, N. Cukkemane, K. Nazmi, et al., "Identification of the hydroxyapatite-binding domain of salivary agglutinin", *Eur. J. Oral Sci.* **2013**, *121*, 7–12.

[359] M. Hesse, H. Meier, B. Zeeh, *Spektroskopische Methoden in der organischen Chemie*, 7th ed., Georg Thieme Verlag, Stuttgart, **2005**, pp. 74–241.

[360] C. Zhang, N. Luo, D. E. Hirt, "Surface grafting polyethylene glycol (PEG) onto poly(ethylene-co-acrylic acid) films", *Langmuir* **2006**, *22*, 6851–6857.

[361] K. Lim, R. R. Y. Chua, R. Saravanan, et al., "Immobilization studies of an engineered arginine-tryptophan-rich peptide on a silicone surface with antimicrobial and antibiofilm activity", *ACS Appl. Mater. Interfaces* **2013**, *5*, 6412–6422.

[362] W. He, G. C. McConnell, T. M. Schneider, et al., "A novel anti-inflammatory surface for neural electrodes", *Adv. Mater.* **2007**, *19*, 3529–3533.

[363] F. Brotzel, Y. C. Chu, H. Mayr, "Nucleophilicities of primary and secondary amines in water", *J. Org. Chem.* **2007**, *72*, 3679–3688.

[364] I. Szleifer, "Statistical thermodynamics of polymers near surfaces", *Curr. Opin. Colloid Interface Sci.* **1996**, *1*, 416–423.

[365] H. Sugimura, A. Hozumi, T. Kameyama, et al., "Organosilane self-assembled monolayers formed at the vapour/solid interface", *Surf. Interface Anal.* **2002**, *34*, 550–554.

[366] M. Kobayashi, Y. Terayama, H. Yamaguchi, et al., "Wettability and antifouling behavior on the surfaces of superhydrophilic polymer brushes", *Langmuir* **2012**, *28*, 7212–7222.

[367] S. R. Holmes-Farley, C. D. Bain, G. M. Whitesides, "Wetting of functionalized polyethylene film having ionizable organic acids and bases at the polymer-water interface: Relations between functional group polarity, extent of ionization, and contact angle with water", *Langmuir* **1988**, *4*, 921–937.

[368] P. B. Welzel, C. Rauwolf, O. Yudin, et al., "Influence of aqueous electrolytes on the wetting behavior of hydrophobic solid polymers - Low-rate dynamic liquid/fluid contact angle measurements using axisymmetric drop shape analysis", *J. Colloid Interface Sci.* **2002**, *251*, 101–108.

[369] M. Sulpizi, M.-P. Gaigeot, M. Sprik, "The silica-water interface: How the silanols determine the surface acidity and modulate the water properties", *J. Chem. Theory Comput.* **2012**, *8*, 1037–1047.

[370] S. Salimpour Abkenar, R. M. A. Malek, F. Mazaheri, "Salt-free dyeing isotherms of cotton fabric grafted with PPI dendrimers", *Cellulose* **2015**, *22*, 897–910.

[371] E. S. Hamborg, G. F. Versteeg, "Dissociation constants and thermodynamic properties of amines and alkanolamines from (293 to 353) K", *J. Chem. Eng. Data* **2009**, *54*, 1318–1328.

[372] M. M. Ouberai, K. Xu, M. E. Welland, "Effect of the interplay between protein and surface on the properties of adsorbed protein layers", *Biomaterials* **2014**, *35*, 6157–6163.

[373] M. Berglin, E. Pinori, A. Sellborn, et al., "Fibrinogen adsorption and conformational change on model polymers: Novel aspects of mutual molecular rearrangement", *Langmuir* **2009**, *25*, 5602–5608.

[374] M. A. Carignano, I. Szleifer, "Prevention of protein adsorption by flexible and rigid chain molecules", *Colloids Surf. B* **2000**, *18*, 169–182.

[375] H. Mayr, A. R. Ofial, "Do general nucleophilicity scales exist?", *J. Phys. Org. Chem.* **2008**, *21*, 584–595.

[376] A. Isidro-Llobet, M. Álvarez, F. Albericio, "Amino acid-protecting groups", *Chem. Rev.* **2009**, *109*, 2455–2504.

[377] T. M. Chapman, "Models for polyurethane hydrolysis under moderately acidic conditions : A comparative study of hydrolysis rates of urethanes, ureas, and amides", *J. Polym. Sci. A Polym. Chem.* **1989**, *27*, 1993–2005.

[378] S. H. Hilal, S. W. Karickhoff, L. A. Carreira, et al., "Estimation of carboxylic acid ester hydrolysis rate constants", *QSAR Comb. Sci.* **2004**, *22*, 917–925.

[379] S.-B. Yeh, C.-S. Chen, W.-Y. Chen, et al., "Modification of silicone elastomer with zwitterionic silane for durable antifouling properties", *Langmuir* **2014**, *30*, 11386–11393.

[380] C.-J. Huang, Y.-C. Chang, "In situ surface tailoring with zwitterionic carboxybetaine moieties on self-assembled thin film for antifouling biointerfaces", *Materials* **2014**, *7*, 130–142.

[381] J. A. Kleingartner, H. Lee, M. F. Rubner, et al., "Exploring the kinetics of switchable polymer surfaces with dynamic tensiometry", *Soft Matter* **2013**, *9*, 6080–6090.

[382] L. Wu, J. Jasinski, S. Krishnan, "Carboxybetaine, sulfobetaine, and cationic block copolymer coatings: A comparison of the surface properties and antibiofouling behavior", *J. Appl. Polym. Sci.* **2012**, *124*, 2154–2170.

[383] C.-H. Shen, J.-C. Lin, "Solvent and concentration effects on the surface characteristics and platelet compatibility of zwitterionic sulfobetaine-terminated self-assembled monolayers", *Colloids Surf. B* **2013**, *101*, 376–383.

[384] M. Gruening, S. Neuber, P. Nestler, et al., "Enhancement of intracellular calcium ion mobilization by moderately but not highly positive material surface charges", *Front. Bioeng. Biotechnol.* **2020**, *8*, 1016.

[385] T. S. Meiron, A. Marmur, I. S. Saguy, "Contact angle measurement on rough surfaces", *J. Colloid Interface Sci.* **2004**, *274*, 637–644.

[386] H. Rangwalla, A. D. Schwab, B. Yurdumakan, et al., "Molecular structure of an alkyl-side-chain polymer-water interface: Origins of contact angle hysteresis", *Langmuir* **2004**, *20*, 8625–8633.

[387] Y. C. Jung, B. Bhushan, "Contact angle, adhesion and friction properties of micro-and nanopatterned polymers for superhydrophobicity", *Nanotechnology* **2006**, *17*, 4970–4980.

[388] H. J. Busscher, A. W. J. van Pelt, P. de Boer, et al., "The effect of surface roughening of polymers on measured contact angles of liquids", *Colloids and Surf.* **1984**, *9*, 319–331.

[389] S. Roessler, R. Zimmermann, D. Scharnweber, et al., "Characterization of oxide layers on Ti6Al4V and titanium by streaming potential and streaming current measurements", *Colloids Surf. B* **2002**, *26*, 387–395.

[390] R. Bizios, "Mini-review: Osteoblasts: An in vitro model of bone-implant interactions", *Biotechnol. Bioeng.* **1994**, *43*, 582–585.

[391] H. Rebl, B. Finke, R. Lange, et al., "Impact of plasma chemistry versus titanium surface topography on osteoblast orientation", *Acta Biomater.* **2012**, *8*, 3840–3851.

[392] L. Hao, H. Yang, C. Du, et al., "Directing the fate of human and mouse mesenchymal stem cells by hydroxyl-methyl mixed self-assembled monolayers with varying wettability", *J. Mater. Chem. B* **2014**, *2*, 4794–4801.

[393] C. Mörke, H. Rebl, B. Finke, et al., "Abrogated cell contact guidance on amino-functionalized microgrooves", *ACS Appl. Mater. Interfaces* **2017**, *9*, 10461–10471.

[394] P. van der Valk, A. W. J. van Pelt, H. J. Busscher, et al., "Interaction of fibroblasts and polymer surfaces: Relationship between surface free energy and fibroblast spreading", *J. Biomed. Mater. Res.* **1983**, *17*, 807–817.

[395] J. Y. Lim, X. Liu, E. A. Vogler, et al., "Systematic variation in osteoblast adhesion and phenotype with substratum surface characteristics", *J. Biomed. Mater. Res. A* **2004**, *68*, 504–512.

[396] S. Staehlke, H. Rebl, B. Finke, et al., "Enhanced calcium ion mobilization in osteoblasts on amino group containing plasma polymer nanolayer", *Cell Biosci.* **2018**, *8*, 22.

[397] M. Cohen, D. Joester, B. Geiger, et al., "Spatial and temporal sequence of events in cell adhesion: From molecular recognition to focal adhesion assembly", *ChemBioChem* **2004**, *5*, 1393–1399.

[398] H. Rebl, B. Finke, J. Schmidt, et al., "Accelerated cell-surface interlocking on plasma polymer-modified porous ceramics", *Mater. Sci. Eng. C* **2016**, *69*, 1116–1124.

[399] S. Guo, M. Y. Kwek, Z. Q. Toh, et al., "Tailoring polyelectrolyte architecture to promote cell growth and inhibit bacterial adhesion", *ACS Appl. Mater. Interfaces* **2018**, *10*, 7882–7891.

[400] M. Gruening, S. Neuber, K. Fricke, et al., "Cell-material interaction - Spreading course correlates with surface charge", *Am. J. Biomed. Sci. Res.* **2020**, *9*.

[401] A. Kikuchi, H. Taira, T. Tsuruta, et al., "Adsorbed serum protein mediated adhesion and growth behavior of bovine aortic endothelial cells on polyamine graft copolymer surfaces", *J. Biomater. Sci. Polym. Ed.* **1997**, *8*, 77–90.

[402] E. G. Hayman, M. D. Pierschbacher, S. Suzuki, et al., "Vitronectin - A major cell attachment-promoting protein in fetal bovine serum", *Exp. Cell Res.* **1985**, *160*, 245–258.

[403] Y. Arima, H. Iwata, "Preferential adsorption of cell adhesive proteins from complex media on self-assembled monolayers and its effect on subsequent cell adhesion", *Acta Biomater.* **2015**, *26*, 72–81.

[404] M. Dawson, W. F. Dryden, "The toxicity of spermine and spermidine to cells in culture", *Biochem. Pharmacol.* **1969**, *18*, 1307–1313.

[405] D. A. Averill-Bates, E. Agostinelli, E. Przybytkowski, et al., "Cytotoxicity and kinetic analysis of purified bovine serum amine oxidase in the presence of spermine in chinese hamster ovary cells", *Arch. Biochem. Biophys.* **1993**, *300*, 75–79.

[406] V. G. Brunton, M. H. Grant, H. M. Wallace, "Spermine toxicity in BHK-21/C13 cells in the presence of bovine serum: The effect of aminoguanidine", *Toxicol. In Vitro* **1994**, *8*, 337–341.

[407] A. Janaszewska, K. Maczyńska, G. Matuszko, et al., "Cytotoxicity of PAMAM, PPI and maltose modified PPI dendrimers in Chinese hamster ovary (CHO) and human ovarian carcinoma (SKOV3) cells", *New J. Chem.* **2012**, *36*, 428–437.

[408] A. Mecke, I. J. Majoros, A. K. Patri, et al., "Lipid bilayer disruption by polycationic polymers: The roles of size and chemical functional group", *Langmuir* **2005**, *21*, 10348–10354.

[409] J. Hernandez-Montelongo, E. G. Lucchesi, V. F. Nascimento, et al., "Antibacterial and non-cytotoxic ultra-thin polyethylenimine film", *Mater. Sci. Eng. C* **2017**, *71*, 718–724.

[410] C. Brunot, L. Ponsonnet, C. Lagneau, et al., "Cytotoxicity of polyethyleneimine (PEI), precursor base layer of polyelectrolyte multilayer films", *Biomaterials* **2007**, *28*, 632–640.

[411] Z.-M. Liu, S.-Y. Lee, S. Sarun, et al., "Immobilization of poly (ethylene imine) on poly (L-lactide) promotes MG63 cell proliferation and function", *J. Mater. Sci. Mater. Med.* **2009**, *20*, 2317–2326.

List of Publications

Publications

Terminal chemical functions of polyamidoamine dendrimer surfaces and its impact on bone cell growth
Susanne Staehlke, Jutta Lehnfeld, Andreas Schneider, J. Barbara Nebe, Rainer Müller
Materials Science & Engineering C **2019**, *101*, 190-203

Comparison of Protein-Repellent Behavior of Linear versus Dendrimer-Structured Surface-Immobilized Polymers
Jutta Lehnfeld, Martina Gruening, Matthias Kronseder, Rainer Mueller
Langmuir **2020**, *36*, 5880-5890

Enhancement of Intracellular Calcium Ion Mobilization by Moderately but Not Highly Positive Material Surface Charges
Martina Gruening, Sven Neuber, Peter Nestler, Jutta Lehnfeld, Manuela Dubs, Katja Fricke, Matthias Schnabelrauch, Christiane A. Helm, Rainer Müller, Susanne Staehlke, J. Barbara Nebe
Frontiers in Bioengineering and Biotechnology **2020**, *8*, 1016.

Saliva and Serum Protein Adsorption on Chemically Modified Silica Surfaces
Jutta Lehnfeld, Yegor Dukashin, Janet Mark, Gregory D. White, Stephanie Wu, Verena Katzur, Rainer Müller, Stefan Ruhl
Journal of Dental Research **2021**, DOI: 10.1177/00220345211022273.

Conference Contributions

Development of Protein-Resistant Surface Functionalizations for Biomaterials
Jutta Lehnfeld, Rainer Müller
13^{th} Zsigmondy Colloquium
Saarbrücken, Germany, April 5^{th}–7^{th} 2017

Development of Protein-Resistant Surface Functionalizations for Biomaterials
Jutta Lehnfeld, Jonas Blahnik, Rainer Müller
Jahrestagung der Deutschen Gesellschaft für Biomaterialien
Würzburg, Germany, November 9th–11th 2017

Influence of buffer pH and composition on wettability of modified surfaces
Jutta Lehnfeld, Verena Huber, Rainer Müller
14th Zsigmondy Colloquium
Mainz, Germany, April 9th–11th 2018

New strategies for novel cell-adhesive and protein-repellent surface functionalizations
Jutta Lehnfeld, Susanne Stählke, J. Barbara Nebe, Rainer Müller
29th European Conference on Biomaterials
Maastricht, Netherlands, September 9th–13th 2018

Material surface charges and their influence on cell physiology
Martina Gruening, Jutta Lehnfeld, Rainer Mueller, Katja Fricke, Sven Neuber, Christiane Helm, Manuela Dubs, Matthias Schnabelrauch, Barbara Nebe
6th International Symposium Interface Biology of Implants
Rostock, Germany, May 8th–10th 2019

Impact of nanoscale surface roughness combined with hydrophilic coatings carrying positive or negative charges on cell adhesion
Susanne Staehlke, Jutta Lehnfeld, Martina Gruening, J. Barbara Nebe, Rainer Müller
6th International Symposium Interface Biology of Implants
Rostock, Germany, May 8th–10th 2019

Intracellular calcium-ion mobilization on charged titanium surface modifications
Martina Gruening, Jutta Lehnfeld, Thomas Distler, Katja Fricke, Manuela Dubs, Christian Völkner, Rainer Müller, Matthias Schnabelrauch, Aldo R. Boccaccini, Sylvia Speller, Barbara Nebe
30th European Conference on Biomaterials
Dresden, Germany, September 9th–13th 2019

Declaration/Eidesstattliche Erklärung

Ich, Jutta Lehnfeld, erkläre hiermit an Eides statt, dass ich die vorliegende Arbeit ohne unzulässige Hilfe Dritter und ohne Benutzung anderer als der angegebenen Hilfsmittel angefertigt habe; die aus anderen Quellen direkt oder indirekt übernommenen Daten und Konzepte sind unter Angabe des Literaturzitats gekennzeichnet.

Daten, die im Rahmen einer Kooperation entstanden sind, aber durch andere Personen ermittelt wurden, sind an entsprechender Stelle eindeutig gekennzeichnet. Bei der Gewinnung von Daten sowie der Auswahl und Auswertung folgenden Materials haben mir die nachstehend aufgeführten Personen in der jeweils beschriebenen Weise unentgeltlich geholfen:

1.	Dr. Matthias Kronseder	XPS-Messungen
2.	Martina Grüning	Zeta-Potential mittels Strömungsstrommessungen
3.	Dr. Susanne Stählke	Zeta-Potential mittels Strömungsstrommessungen, Zellexperimente

Weitere Personen waren an der inhaltlich-materiellen Herstellung der vorliegenden Arbeit nicht beteiligt. Insbesondere habe ich hierfür nicht die entgeltliche Hilfe eines Promotionsberaters oder anderer Personen in Anspruch genommen. Niemand hat von mir weder unmittelbar noch mittelbar geldwerte Leistungen für Arbeiten erhalten, die im Zusammenhang mit dem Inhalt der vorgelegten Dissertation stehen.

Die Arbeit wurde bisher weder im In- noch im Ausland in gleicher oder ähnlicher Form einer anderen Prüfungsbehörde vorgelegt.

Ich versichere an Eides statt, dass ich nach bestem Wissen die reine Wahrheit gesagt und nichts verschwiegen habe.
Vor Aufnahme der obigen Versicherung an Eides statt wurde ich über die Bedeutung der eidesstattlichen Versicherung und die strafrechtlichen Folgen einer unrichtigen oder unvollständigen eidesstattlichen Versicherung belehrt.

Regensburg, den 22.3.2021

_____

Jutta Lehnfeld